Collateral Sensitivity Associated with Multidrug-Resistance Protein 5 in Triple-Negative Breast Cancer

Ji He

A thesis submitted to
the Faculty of Health and Environment Sciences
Auckland University of Technology
in fulfillment of the requirements for the Degree of
Doctor of Philosophy (PhD)

December 2021

School of Applied Sciences

Auckland, New Zealand.

Collateral Sensitivity Associated with Multidrug-Resistance Protein 5 in Triple-Negative Breast Cancer

Approved by:

Supervisors: Dr. Yan Li (Primary Supervisor)

Dr. Dongxu Liu (Secondary Supervisor)

Table of Contents

List of Figures

List of Tables

Attestation of Authorship

I hereby declare that this submission is my own work and that, to the best of my knowledge and belief, it contains no material previously published or written by another person (except where explicitly defined in the acknowledgements), nor material which to a substantial extent has been submitted for the award of any other degree or diploma of a university or other institution of higher learning.

Signed

Name Ji He

Date 30th November/ 2021.

Acknowledgements

At the outset, I am extremely indebted to my primary supervisor Dr. Yan Li who provides me with the opportunity to devote myself to this incredibly fantastic PhD project and helps me with thoughtful ideas and suggestions when difficulties were encountered. His marvellous patience, guidance, language, knowledge, and encouragement always impress me from start to finish. I would also like to thank Dr Li for his continuous support and encouragement with all the conferences and research publications.

Secondly, I am genuinely grateful to my secondary supervisor Dr. Dong-Xu Liu for his help and concern, as well as the wonderful SPAG5 studies. I sincerely thank him for his patience with me, inspiration, and immense knowledge. Also, I would like to thank Dr. Dong-Xu Liu for his constant support and encouragement with all the conferences and research publications.

Thirdly, I would like to convey my gratitude to Dr. Jun Lu and Dr. Fabrice Merien, who constantly contribute to the research environments during my PhD work.

Fourthly, I would like to express my sincere appreciation to all those who gave me a helping hand and a listening ear in the past four years. I would like to say thanks to my colleagues and fellow students, Kelvin, Riya, Piyush, Cindy, Stacey and Vivi, as well as all the technicians and staff working in the faculty of health and environmental sciences. Their practical guidance, invaluable assistance, and professional techniques always impress me during the PhD journey.

Finally, I would like to express thanks to my parents for their endless and robust supports.

Abstract

The multidrug resistance (MDR)-induced chemo- and targeted-therapeutic failure remains a pivotal obstacle to effective treatment against triple-negative breast cancer (TNBC). Our recent publications reviewed that the clinical trials that target ATP-Binding Cassette (ABC) transporters to reverse drug resistance have been disappointing despite the positive *in vitro* evidence. However, ABC transporters-associated collateral sensitivity (CS) is poorly understood and contributes to a promising novel therapeutic strategy to overcome MDR in breast cancer. In this study, we investigated olaparib accumulation and sensitivity in ABCC5-overexpressing HEK293 (HEK-MRP5) and *ABCC5* gene knockout (KO) TNBC cell models. The potential upstream regulators of ABCC5 were also studied in the respective gene KO cell model. Overexpression of ABCC5 in HEK-MRP5 and TNBC cells (endogenously in MDA-MB-231 and BT549 cells) was associated with increased olaparib sensitivity. This vulnerability was not reversed by a model ABCC5 inhibitor benzbromarone. The low ABCC5 expression level in isogenic parental HEK293 and KO TNBC cells was associated with an olaparib-resistant phenotype. Molecular docking studies suggested non-covalent olaparib-ABCC5 interactions with high binding affinity. In conclusion, olaparib exerted selective CS on ABCC5-expressing *BRAC1* wildtype TNBC cell lines (MDA-MB-231 and BT549) and these results may broaden the clinical indications of olaparib and/or lead to the novel combination therapies to resensitise tumour MDR in patients with TNBC.

Chapter 1. General Introduction

1.1 Breast Cancer

1.1.1 Breast Cancer Status in New Zealand and Worldwide

Cancer is a group of diseases associated with abnormal growth and spread of anomalistic cells (Tacar, Sriamornsak, & Dass, 2013). The initiation and development of cancer always rely on a series of complicated events, such as mutations at tumour suppressor genes, proto-oncogenes, and other genes involved in regulating cell differentiation and growth (Tacar et al., 2013). Cancer has become the second leading cause of death globally, and was responsible for an estimated 18.1 million new cases and 9.6 million deaths in 2018 (World Health Organization, 2018). Breast cancer accounts for nearly one-third of all cancers in women, and the incidence of breast cancer is continuously increasing worldwide. Breast cancer is the second common cancer and the fifth common cause of cancer death worldwide (World Health Organization, 2018). Similarly, in New Zealand, breast cancer is the second common type of cancer and the fourth leading cause of cancer death. One in nine New Zealand women suffers from breast cancer during their lifetime, leading to the highest breast cancer incidence in the world. According to the latest release of statistics, in 2016, 3323 new breast cancer cases were registered (New Zealand Ministry of Health, 2016b), and 641 patients died of it in 2013 (New Zealand Ministry of Health, 2016a). Worldwide, the problem was just as serious, as breast cancer was the most frequent cancer after lung cancer, with an estimated 2.09 million new cases and 627,000 deaths in 2018 (World Health Organization, 2018).

1.1.2 Breast Cancer Subtypes

Clinically, breast cancer is routinely categorized into diverse subtypes, revealing distinct prognostic and therapeutic implications. In general, the expression of oestrogen receptor (ER), progesterone receptor (PR), amplification of human epidermal growth factor receptor 2 (HER2)/Neu and Ki-67 was evaluated in breast cancer. These parameters allow classification of breast tumours as hormone receptor-positive tumours, HER2/Neu amplified tumours, and those tumours which do not express ER, PR, and do not have HER2/Neu amplification (Jhan & Andrechek, 2017). The latter group is referred to as triple-negative breast cancer (TNBC), which lacks these three molecular markers (Brenton, Carey, Ahmed, & Caldas, 2005). There are four main immunohistochemistry-based subtypes of breast cancer according to the expression of the markers mentioned above (Table 1.1) (Jhan & Andrechek, 2017).

Table 1.1 Immunohistochemistry Profile of Breast Cancer Subtypes.

	Hormone-receptor	HER2	Ki-67 level
Luminal A	ER+ and/or PR+	-	low
Luminal B	ER+ and/or PR+	+/-	high
HER2-enriched	ER- and PR-	+	
Basal-like/triple-negative	ER- and PR-	-	

Data collected from Jhan and Andrechek (2017); Tang and Tse (2016).

According to the expression of the markers above, many of the ER- and/or PR-positive breast tumours have been classified into the commonly observed luminal A and luminal B subtypes (Jhan & Andrechek, 2017). Luminal A breast cancers account for about 30 to 40% of all breast cancers, which are hormone receptor-positive (i.e., ER and/or PR positive), HER2 negative, and with low levels of Ki-67 expression (Jhan & Andrechek, 2017; Tang & Tse, 2016). Luminal A breast cancers are considered low-grade, tend to

grow slowly and have a favourable prognosis. Luminal B breast cancers account for about 20 to 30% of all breast cancers which are hormone receptor-positive (i.e., ER and/or PR positive), and either HER2 positive or HER2 negative with high level of Ki-67 (Jhan & Andrechek, 2017; Tang & Tse, 2016). Luminal B breast cancers generally grow slightly faster than luminal A breast cancers with a somewhat worse prognosis. Luminal A and B subtypes can be differentiated by the expression level of Ki-67 (X. Zhu et al., 2020). Ki-67 is a protein proposed to measure cell proliferation and located in the nucleus of cells in the given phases of the cell cycle, except the G0 quiescent state (X. Zhu et al., 2020). High levels of Ki-67 always indicate breast tumours with more tenacious proliferation and poor prognosis (X. Zhu et al., 2020). The subclassification of luminal breast cancers into luminal A and B subtypes are just based on the cut point of Ki-67 at 14% (X. Zhu et al., 2020). In luminal breast cancer, Ki-67 below 14% is regarded as luminal A subtype, while Ki-67 above 14% is luminal B subtype. Tumours with HER2 amplification and/or overexpression are classified into the HER2-positive subtype (Jhan & Andrechek, 2017). This subtype account for 12 to 20% of all breast cancers (Tang & Tse, 2016). HER2-enriched breast cancers are hormone-receptor negative (i.e., ER and PR negative) and HER2 positive. HER2-enriched breast cancers tend to grow faster than luminal cancers and can have a worse prognosis. Still, they are often successfully treated with targeted therapies aiming at the HER2 protein, such as trastuzumab and pertuzumab (Jhan & Andrechek, 2017).

Triple-negative/basal-like breast cancer (TNBC) represents tumours without ER, PR and HER2 expression (Jhan & Andrechek, 2017). This type of cancer is more common in women with *BRCA1* gene mutations, and over 80% of breast cancers among patients with a hereditary *BRCA1* mutation are TNBCs. It is also more common among younger and African-American women (Andreopoulou, Kelly, & McDaid, 2017; Jhan &

Andrechek, 2017). TNBC is more biologically aggressive than other breast cancer subtypes and takes up approximately 10 - 15% of all breast cancers (Tang & Tse, 2016). The patients diagnosed with TNBC routinely have a poor outcome, a high risk of distant recurrence, and a high frequency of visceral and central nervous metastases compared to other breast cancer subtypes (Andreopoulou et al., 2017). Triple-negative tumours lack the expression of ER, PR and HER2. The absence of these biomarkers results in the limit of treatment options amongst TNBC patients and the worst prognosis compared to patients suffering from other subtypes of breast cancer as they fail to respond to endocrine and anti-HER2 therapies.

1.2 Current Treatment of Breast Cancer

With the development of various treatment regimens, the overall survival rate of breast cancer patients has increased over the past decades. Breast cancer prognosis includes the factors such as histological features (histological type, histological grade, and lymphovascular invasion), lymph node status, tumour size, steroid hormone receptor status, and age (X. Zhu et al., 2020). Detection of this disease at an earlier stage and appropriate administration of systemic therapy in conjunction with conservative surgery and radiation have improved survival and decreased the morbidity and mortality of breast cancer patients (Lal, Mahajan, Chen, & Chowbay, 2010). Systemic treatment of breast cancer includes cytotoxic-, hormonal-, and immuno-therapeutic agents, which are utilized in adjuvant, neoadjuvant and metastatic settings (Yu & Hung, 2009). Neoadjuvant therapy is aimed at tumour downstaging, allowing for either mastectomy in the case of inoperable disease or breast conservation surgery. Adjuvant chemotherapy is used to eradicate micrometastatic disease after primary tumour

resection (Lal et al., 2010). Chemotherapy is a significant modality in the management of breast cancer patients complemented by radiotherapy and surgery. Adjuvant chemotherapy anthracycline-based regimens incorporating taxanes have been shown to significantly improve disease-free survival (DFS) and overall survival (OS) rates in high-risk, early-stage breast cancer patients (De Laurentiis et al., 2008; Peto & Group, 2007). It has been a preferred option for hormone receptor-negative patients with metastatic breast cancer (MBC) (Kataja & Castiglione, 2008). Given that the benefit from specific treatment and the adverse effect to individual patients vary dramatically in different tumour types, treatment options and host characteristics, the individualization of treatment based on the molecular variations within breast cancer is becoming important.

The expression of biomarkers is one of the significant factors for the selection of treatment strategy. About 70% of breast cancers are ER-positive, with ER being a major contributor to their development and an ideal target eligible for endocrine therapy (e.g., antioestrogen treatment tamoxifen) (Tang & Tse, 2016). Tamoxifen can compete with oestrogen and block ER, thus preventing oestrogen binding to ER and impeding the following signalling pathways related to tumour progress (Shagufta & Ahmad, 2018). PR is primarily mediated by oestrogen and is expressed in about 55 to 65% of all breast cancers. PR negative breast cancer subtypes are correlated with more aggressive behaviour and decreased response to endocrine therapy (Tang & Tse, 2016). About 20 to 30% of breast cancers exhibit *HER2* gene amplification and/or protein overexpression. These breast cancers are linked to the second poorest prognosis and good sensitivity to targeted therapies aiming at the HER2 protein, such as monoclonal antibody trastuzumab (Vu & Claret, 2012). Trastuzumab can bind to HER2 and trigger the internalization and degradation of this receptor. As an antibody, the binding of

trastuzumab to HER2 can attract immune cells to tumour sites that causes cancer cell demise. Trastuzumab can also interfere with the dimerization of HER2 and inactivate the downstream signalling pathways related to tumour progress (Vu & Claret, 2012).

About 10 to 15% of breast cancers are TNBC (Tang & Tse, 2016). Because of the lack of targeted therapies (e.g., endocrine and anti-HER2 therapies), primary treatment for TNBC patients remains chemotherapy. Fortunately, TNBC tumours generally have the best response to chemotherapy compared with other breast cancer subtypes. TNBCs have the most pathologic complete response rate (pCR) to chemotherapy at around 22% among breast cancer subtypes. At present, the cytotoxic chemotherapies for TNBC include anti-tubulins, anthracyclines, alkylating agents, antimetabolites, and platinums (Andreopoulou et al., 2017). Current frontline adjuvant and neoadjuvant regimens for TNBC typically include an anthracycline (doxorubicin or epirubicin) plus an alkylating agent (cyclophosphamide), given either concurrently with a taxane (docetaxel) or sequentially before or after a taxane (docetaxel or paclitaxel) (Andreopoulou et al., 2017). However, patients without complete response to chemotherapy still account for approximately 80% of TNBC. The recurrence and metastasis rate in TNBC patients was also higher than non-TNBC, leading to a worse survival rate, particularly in the first three years (Liedtke et al., 2008). The prognosis and survival rate for this malignant cancer subtype is poor, owing to the development of drug resistance to current chemotherapies and resultant metastasis (Anders & Carey, 2009). The patients may have a response to those regimens initially, but the response is not sustained due to the altered chemosensitivity of tumours. The development of drug resistance is a frequent problem in the management of breast cancer. Many patients' tumours are resistant to the therapeutic agents by the time of disease recurrence, leading to the average 5-year survival rate of patients with stage 0 or stage I, stage II, stage III, and MBC at 100%,

93%, 72% and 22% respectively (American Cancer Society, 2013). These data underscore drug resistance as a dominant impact of the survival of breast cancer patients after breast mastectomy, metastasis or recurrence. Once metastasis or drug resistance develops, the treatment option is very limited, and the possibility of a cure is practically non-existent.

1.2.1 Doxorubicin

Doxorubicin (DOX) is a metabolite of *Streptomyces peucetius* var. *caesius*, referred to as the anthracycline and antitumor antibiotic family of medications. It was developed as a chemotherapeutic agent in the 1970's that is used against solid tumours in the treatment of a wide range of cancers, including breast cancer, lung cancer, ovarian cancer, gastric cancer, thyroid cancer, Kaposi's sarcoma, lymphoma, bladder cancer, multiple myeloma, and acute lymphocytic leukaemia (Cortés-Funes & Coronado, 2007; Weiss, 1992). The structure of doxorubicin is shown in Figure 1.1.

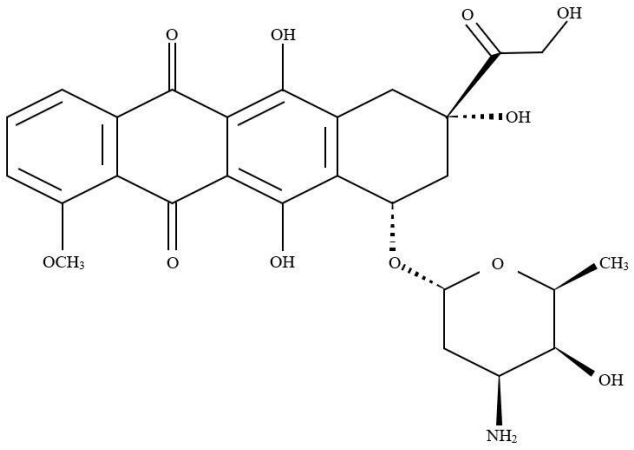

Figure 1.1 Chemical Structure of Doxorubicin.

1.2.1.1 Clinical Implication

The recommended dosage schedule of doxorubicin is 60 to 75 mg/m^2 body surface area, as a single intravenous injection administered at 21-day intervals. Patients with inadequate marrow reserves due to old age, prior therapy, or neoplastic marrow infiltration are supposed to receive a lower dose. An alternative dose schedule is 25 to 30 mg/m^2 on each of three successive days, repeated every three to four weeks. Doxorubicin has a recommended lifetime cumulative dose limit of 550 mg/m^2 body surface area. It has been administered as an intra-arterial infusion for one to three days at doses of 45 to 100 mg/m^2 (Zetsche et al., 2015).

While providing a cure in selected cases, doxorubicin causes toxicity to most major organs. Common side effects include cardiotoxicity, hair loss, loss of appetite, diarrhoea, tiredness, sore mouth and throat, and liver changes (Cortés-Funes & Coronado, 2007; Weiss, 1992). Cardiotoxicity is the most common side effect induced by doxorubicin that threatens patients' lives. Several potential treatment options have been developed to control doxorubicin-mediated cardiotoxicity, such as lowering the dosage of doxorubicin, combined therapies with cardioprotective agents (e.g., dexrazoxane) (Octavia et al., 2012), and through regulation of cardiac circular RNA expression (Gupta et al., 2018).

1.2.1.2 Mechanism of Action

A number of mechanisms have been proposed with regard to the mode of action by which doxorubicin acts in cancer cells, such as topoisomerase II poisoning, DNA adduct formation, oxidative stress, and ceramide overproduction. Topoisomerases are highly conserved enzymes in virtually all forms of life, which regulate DNA topology

to facilitate DNA replication, transcription, and other nuclear processes. Topoisomerase II is an ATP-dependent enzyme that includes two isoforms in humans, topoisomerase IIα and topoisomerase IIβ. The enzyme binds DNA supercoils and entangled DNA, breaks both strands of one DNA duplex, passes the other duplex through the resulting gap and reseals the break. This process contributes to the release of torsional stress during biological processes such as DNA replication and transcription (F. Yang, Teves, Kemp, & Henikoff, 2014).

Additionally, topoisomerase II is of significance for decatenation of DNA during mitosis, and deficiency in this enzyme results in cell death by preventing normal cytokinesis (F. Yang et al., 2014). The therapeutic effect of doxorubicin is just based on topoisomerase II poisoning (F. Yang et al., 2014). The intercalation of doxorubicin into the base pairs of the DNA's double helix *in vitro* is related to several crystal structures of complexes of DNA, resulting in DNA breaks and interference with DNA synthesis (Howerton, Nagpal, & Dean Williams, 2003; Lipscomb et al., 1994). Doxorubicin enters the cell *via* diffusion due to its higher affinity to bind to the cytoplasm's proteasome (Tacar et al., 2013). Translocation of doxorubicin into the nucleus is thought to occur *via* binding to proteasomes (Kiyomiya, Matsuo, & Kurebe, 2001). A doxorubicin proteasome complex is then translocated through the nuclear pore into the nucleus. Doxorubicin has a higher affinity for nuclear DNA over the proteasome it is attached to, allowing the dissociation of doxorubicin itself from the proteasome and bind to DNA (Tacar et al., 2013). The DNA-DOX interaction can inhibit the progression of topoisomerase II (TOP2), an enzyme functioning in supercoils relax in DNA for transcription (Bodley et al., 1989; Tewey, Rowe, Yang, Halligan, & Liu, 1984). Doxorubicin stabilizes the TOP2 complex after breaking the DNA chain for replication, preventing the DNA double helix from being resealed and

thereby stopping the replication process (Tacar et al., 2013). Apart from binding to nucleus DNA, doxorubicin is found to intercalate with mitochondrial DNA as well (Ashley & Poulton, 2009).

Evidence suggests that doxorubicin-induced topoisomerase II poisoning is unlikely to be the only mechanism regulating cancer cell death. As a DNA intercalator, doxorubicin prefers to intercalate into the sites containing adjacent GC base pairs, probably due to specific hydrogen-bond formation between doxorubicin and guanine. The formation of doxorubicin-DNA adducts is found to trigger DNA damage response and cell death through a topoisomerase II-independent mechanism (Tacar et al., 2013). These doxorubicin-DNA adducts can be detected at clinically relevant drug concentrations, suggesting their formation during chemotherapy. The stabilization of interaction between doxorubicin and DNA depends on a covalent bond mediated by cellular formaldehyde generated by free radical reactions from carbon sources, such as lipids and spermine. Formaldehyde mediates the covalent binding of guanine on one strand of DNA to doxorubicin and a hydrogen bond between doxorubicin and guanine on the opposing strand (Tacar et al., 2013; F. Yang et al., 2014). The accumulation of doxorubicin-DNA adducts may lead to increased effectiveness of doxorubicin in sensitive tumour cells. The higher levels of formaldehyde relating to doxorubicin-DNA adducts formation can be detected in doxorubicin-sensitive tumour cells compared to resistant and normal cells (Tacar et al., 2013; F. Yang et al., 2014). Thus, compounds, such as pivaloyloxymethyl butyrate (AN-9), butyroyloxymethyl-diethylphosphate (AN-7) and hexamethylenetetramine (HMTA), that release formaldehyde upon hydrolysis have been developed and utilized in combination with doxorubicin as a new approach to improve the anticancer activity of the drug (Tacar et al., 2013). However, DNA adduct formation is unlikely to be the primary mechanism of doxorubicin action

since clinical doses only generate 4.4 ± 1.0 adducts/10^7 base pair DNA, accounting for a small fraction of the total doxorubicin (Tacar et al., 2013).

Doxorubicin is also known to promote the generation of free radicals, damaging DNA and contributing to cell death. The quinone structure of doxorubicin can undergo a one-electron reduction by several oxidoreductases to form a DOX-semiquinone radical, contributing to its cytotoxicity (Minotti, 1989; Rossi, 2013). Semiquinone is an unstable metabolite, which is converted back to doxorubicin in a process that releases reactive oxygen species (ROS). ROS can induce lipid peroxidation and membrane damage, DNA damage, oxidative stress, and apoptotic pathways (Thorn et al., 2011). In addition, evidence suggests that doxorubicin enhances nucleosome turnover around promoters due to its intercalation property. These alterations in the nucleosome assembly are thought to influence mechanisms of cell demise during chemotherapy (F. Yang, Kemp, & Henikoff, 2013). Doxorubicin also plays a role in additional cellular processes, including ceramide metabolism (Y. Y. Liu, Hill, & Li, 2013) and cell cycle arrest (B. W. Chen et al., 2015). Ceramide is a lipid molecule consisting of a sphingosine and a fatty acid that is involved in a variety of cellular processes, including growth arrest, apoptosis, and senescence (F. Yang et al., 2014). Ceramide overproduction might specifically sensitize cancer cells to doxorubicin treatment.

Furthermore, doxorubicin is also associated with autophagy, being cytoprotective as a response to DNA damage. Constantly genotoxic stress can cause the hyperactivation of PARP1 (poly-ADP ribose polymerase 1), which in turn depletes both NAD+ (nicotinamide adenine dinucleotide) and ATP. Cells then experience energy failure and ultimately cell death. Normally, the cell death caused by doxorubicin always relies on the hyperactivation of PARP1-induced autophagy and necrosis. Doxorubicin at moderately high concentrations is unable to induce cell death in PARP1-deficient cells.

This event shows that the critical premise of doxorubicin-induced cell death is the collapse of cellular energy due to PARP1 hyperactivation. Thus, doxorubicin-mediated hyperactivation of PARP1 can cause cellular energy collapse and thus trigger autophagy and necrosis, ultimately resulting in apoptosis. However, on the other hand, PARP1 activation can repair the DNA lesions caused by doxorubicin treatment. As a result, PARP1 requires a balance between energy crisis and DNA damage, which depends on the dose of doxorubicin administered and PARP1 activation (Tacar et al., 2013).

1.2.1.3 Molecular Signals Activated by Doxorubicin

Doxorubicin is found to promote the generation of free radicals. The activation of AMP-activated protein kinase (AMPK) is just related to activated ROS-dependent liver kinase (LKB1). AMPK is a protein kinase acting as an intracellular energy sensor. It can reserve cellular energy and regulate cell survival and death under pathological stress (e.g., osmotic, hypoxia or oxidative stress). The AMPK-induced apoptosis is modulated by multiple downstream targets, such as c-Jun N-terminal kinase (JNK), p53 and mTORC1. It is thought that doxorubicin induces the activation of ROS-dependent LKB1 *via* the generation of ROS. The AMPK is then activated by its upstream regulator ROS-dependent LKB1. Ultimately, p53 is activated by AMPK, which initiates apoptosis (Tacar et al., 2013).

Doxorubicin also plays a role in the BCL-2/BAX apoptosis pathway. BCL-2 is known for its antiapoptotic properties, whereas BAX usually functions in pro-apoptosis. The balance between these two proteins is critical for a cell as to whether it enters apoptosis or survives. Doxorubicin is shown to down-regulate BCL-2 expression levels *via* p53 pathways. The shift in ratio between BCL-2 and BAX proteins is an important event

that determines the survival of a cell. The decrease of BCL-2 ultimately causes cell apoptosis during doxorubicin treatment (Tacar et al., 2013).

1.2.1.4 Pharmacokinetic Properties of Doxorubicin

Doxorubicin is approximately 50-80% bound to plasma proteins, and has a volume of distribution (V_d) ranging from 500 to 800 L/M^2 (Lal et al., 2010). Doxorubicin is found to undergo a triphasic plasma clearance after intravenous injection (Tacar et al., 2013). The terminal half-life of doxorubicin is 24-36 hours. Like most drugs, doxorubicin enters the cell through passive diffusion, generally accumulating to intracellular concentrations that are 10- to 500-fold greater than the extracellular compartments. The lipophilic characteristics and DNA intercalating/binding properties of doxorubicin make it penetrating tissues rapidly. However, doxorubicin cannot pass through the blood-brain barrier despite its high penetrating ability. The doxorubicin located in the nuclear compartments always exceeds the cell cytoplasm by 50-fold. Specifically, the amount of doxorubicin within the nucleus can achieve 340 μM at saturation, which means that one molecule of doxorubicin is intercalated at every five base pairs of DNA. The free intracellular doxorubicin left (0.2% of total intracellular drug) can also distribute heterogeneously in organelles, such as Golgi apparatus, lysosomes and mitochondria. The concentration of doxorubicin in the bone marrow and white blood cells is 200 to 500 times higher than in the plasm. Doxorubicin is found to accumulate mainly in the liver due to its role in metabolism. The biotransformation of doxorubicin in the body occurs primarily in the liver. The metabolising enzymes aldo-keto reductase and ubiquitous cytoplasmic carbonyl reductase are needed for the stereo-specific reduction of ketone of the C-13 yielding doxorubicinol molecule. The metabolism of doxorubicin and doxorubicinol requires a range of reactions, including hydrolytic

glycosidic and reductive cleavage, O-sulfation, O-demethylation and O-glucuronidation. The sugar components of both doxorubicin and doxorubicinol are eliminated when the glycosidic bonds of the sugar undergo acid-catalysed hydrolysis. The hydrolysis of the glycosidic bond causes doxorubicinone to be derived from doxorubicin and doxorubicinolone from doxorubicinol. A semi-quinone intermediate and subsequent protonation of the C7-aglycone radical removes the C7-linked daunosamine sugar group to produce 7-deoxydoxorubicinone from doxorubicin and 7-deoxydoxurubicinolone from doxorubicinol. For the excretion of 7-deoxyaglycones, they need to first undergo demethylation to conjugate with sulfonic or glucuronic acid (Lal et al., 2010; Tacar et al., 2013).

Plasma clearance of doxorubicin is normally in the range of 324-809 mL/min/m^2 and is predominantly mediated by the hepatobiliary pathway. Half of the excreted drugs is in the bile, usually being excreted within 5 to 7 days of treatment, compared to that of 5-12% of the drug in the patients' urine during the same time period, with 3% of the drug found in the urine in the form of doxorubicinol. After 24 hours, 10-20% of the drug is excreted in faeces, and 50% after 150 hours. The systemic clearance is dramatically reduced in obese women. The plasma concentration shows levels of doxorubicinol rapidly increasing and depleting parallel to doxorubicin levels following a bolus injection of doxorubicin. If the level of drug infusion continues for an extended period of time, the concentration of doxorubicinol will eventually transcend over doxorubicin (Lal et al., 2010; Tacar et al., 2013).

1.2.1.5 Doxorubicin Resistance

Multiple mechanisms can cause resistance to doxorubicin. The ABC (ATP-binding

cassette) transporters that pump out intracellular doxorubicin and its metabolites seem to be the most direct factor, such as ABCB1, ABCC1 and ABCG2. Apart from ABC transporters, the unique properties of some other proteins or agents can also influence doxorubicin resistance. The high mobility group box 1 protein (HMGB1) is a regulator of nuclear events (e.g., DNA replication and repair) and both selective and nonselective autophagy. Evidence shows that inhibition of both autophagy and HMGB1 increases cell sensitivity to doxorubicin both *in vivo* and *in vitro* (Huang et al., 2012). Ceramide, a cellular lipid messenger, is able to increase doxorubicin resistance in cells. Doxorubicin enhances ceramide expression levels by either activating the enzymes responsible for ceramide synthesis (e.g., glucosylceramide synthase (GCS)) or activating sphingomyelinase. By enhancing ceramide glycosylation, the endowing cellular stress by doxorubicin leads to the evolution of the cells to become cellular resistant to the drug (Y. Y. Liu et al., 2008). Furthermore, as mentioned above, the intracellular level of formaldehyde is also related to resistance to doxorubicin through mediating the formation of doxorubicin-DNA adducts (F. Yang et al., 2014). The amplification of *TOP2A* genes is proposed as a biomarker for doxorubicin response (Thorn et al., 2011). The TOP2 expression levels are found to determine the efficacy of doxorubicin treatment (Burgess et al., 2008).

1.2.2 Olaparib

Olaparib is a recently approved poly-ADP ribose polymerase (PARP) inhibitor to treat *BRCA*-mutated breast, ovarian and pancreatic cancers. It provides a targeted treatment alternative to cytotoxic chemotherapy in patients with germline mutations in *BRCA1/2* tumour suppressor genes (g*BRCA*m), HER2-negative breast cancers. Since initial

approval in December 2014, olaparib and other PARP inhibitors have shown their efficacy in treating advanced ovarian cancer. On January 8, 2018, the US Food and Drug Administration (FDA) granted regular approval of olaparib (Lynparza) for patients with g*BRCA*m, HER2-negative metastatic breast cancer (Caulfield, Davis, & Byers, 2019). The structure of olaparib is shown in Figure 1.2.

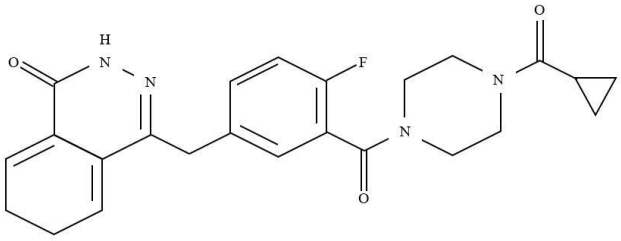

Figure 1.2. Chemical Structure of Olaparib.

1.2.2.1 Clinical Implication

Olaparib is the first treatment approved specifically for *BRCA* mutation carriers with HER2-negative metastatic breast cancer and previous treatment with chemotherapy in the neoadjuvant, adjuvant, or metastatic setting. It causes death in BRCA-deficient cells while sparing healthy cells. For patients with hormone receptor-positive breast cancers, olaparib should be administered after appropriate endocrine therapy or when the disease is deemed inappropriate for endocrine therapy (Caulfield et al., 2019).

Olaparib has been available as a capsule formulation since 2014. The poor solubility of olaparib required a heavy pill burden (16 capsules/day) in patients (Heo & Dhillon, 2018). To overcome this dosing limitation, a tablet formulation of olaparib with enhanced bioavailability has been developed. Olaparib is available for breast cancer patients as 100 mg and 150 mg oral tablets with the brand name Lynparza, which can be administered with or without food and should be swallowed whole. An oral intake

of 300 mg of olaparib tablets twice daily (12 hours apart) is recommended to be continued until disease progression or unacceptable toxicity (Paul & Montoya, 2020). The absorption of olaparib typically reaches a peak concentration ranging between 4.7 and 9.1 mcg/mL after an average of 1.5 hours, and the mean terminal half-life is 14.9 hours. The consumption of a high-fat meal with olaparib can result in drug absorption at a slowed rate but with no significant influence on the total absorption (Caulfield et al., 2019). The dose of olaparib can be adjusted according to the use of concomitant medication, renal and hepatic function, and toxicity, as shown in Table 1.2. Olaparib is extensively metabolised in the liver *via* the action of CYP3A4 enzymes, primarily through oxidation reactions with subsequent glucuronide or sulphate conjugation. Metabolites of olaparib are ultimately excreted through both urine (44%) and faeces (42%). Although over 20 metabolites are found in plasma, urine and faeces, the major circulating metabolites are represented by the mono-oxygenated form and the piperazin-3-ol form (Caulfield et al., 2019; Heo & Dhillon, 2018). Patients should be evaluated for drug interactions prior to start olaparib treatment. The concomitant use with moderate or strong SYP3A4 inducers, grapefruit juice and Seville oranges should be avoided. Because SYP3A4 can reduce efficacy of olaparib, whereas grapefruit juice and Seville oranges may increase olaparib plasma concentrations. The most commonly reported side effects include cough, constipation, dysgeusia, peripheral deem, back pain, dizziness, headache, urinary tract infection, dyspnoea, and rash. Myelodysplastic syndrome/Acute Myeloid Leukaemia (MDS/AML) was reported in 2% of patients with deleterious or suspected deleterious g*BRCA*m advanced cancers. Pneumonitis occurred in less than 1% of patients. The consumption of olaparib was found to be teratogenic and causes embryo-foetal toxicity in rats, which should be avoided during pregnancy (Paul & Montoya, 2020).

Table 1.2. Recommended Dose of Adjustment for Olaparib (Tablet Formulation). Abbr., AML: acute myeloid leukaemia; CrCl: creatinine clearance; ESRD: end-stage renal disease; MDS: myelodysplastic syndrome.

Potential cause for dose adjustment	Recommendations
Concomitant medication	
Moderate CYP3A4 inhibitors (e.g., ciprofloxacin, crizotinib, darunavir/ritonavir, diltiazem, erythromycin, fluconazole, fosamprenavir, imatinib, verapamil)	Reduce dose to 150mg by mouth twice daily
Strong CYP3A4 inhibitors (e.g., itraconazole, telithromycin, clarithromycin, ketoconazole, voriconazole, nefazodone, posaconazole, ritonavir, lopinavir/ritonavir)	Reduce dose to 100mg by mouth twice daily
Strong CYP3A4 inducers (e.g., phenytoin, rifampicin, carbamazepine, St. John's wort)	Potential for reduced efficacy; use should be avoided
Renal impairment	
CrCl 51-81 mL/min	No adjustment necessary; monitor for toxicity
CrCl 31-50 mL/min	Reduce dose to 200mg by mouth twice daily
CrCl < 30 mL/min or ESRD	Has not been studied in this population; no current recommendations
Hepatic impairment	
Mild to moderate impairment (Child-Pugh Class A and B)	No dose adjustment
Severe impairment (Child-Pugh Class C)	Has not been studied in this population; no current recommendations
Toxicity	
First occurrence	Reduce dose to 200mg by mouth twice daily
Second occurrence	Reduce dose to 100mg by mouth twice daily
	Discontinue permanently
Confirmed pneumonitis	Discontinue permanently
Confirmed secondary AML/MDS	

Data collected from Caulfield et al. (2019).

1.2.2.2 Mechanism of Action

As a hallmark of cancers, inadequate DNA repair pathways-induced genomic instability is closely related to the initiation and progression of cancers. The viability of cancer cells highly depends on some specific DNA damage repair pathways in order to eliminate the impact of DNA damage. Thus, these essential repair pathways represent ideal targets for cancer treatment (Yi et al., 2019). In normal cells, cell survival relies on DNA repair pathways (i.e., DNA single-strand break (SSB) repair pathways or

double-strand break (DSB) repair pathways) to maintain homeostasis and genomic stability. SSB repair pathways include mismatch repair (MMR), nucleotide excision repair (NER), and base excision repair (BER), while DSB repair pathways include homologous recombination (HR) and nonhomologous end-joining (NHEJ). DSB is considered to be more threatening to cells than SSB (Yi et al., 2019). BRCA1/2 are essential for the repair of double-strand breaks (DSBs) through homologous recombination (HR) (Heo & Dhillon, 2018). In the presence of BRCA1/2, cells could faithfully repair DSB damages by HR. However, a total of 19.5% of TNBC patients have been shown to carry *BRCA1/2* mutations (Jhan & Andrechek, 2017). Mutations of *BRCA1/2* genes result in defective DNA repair ability, making cells relying on less accurate repair mechanisms NHEJ pathways. NHEJ is characterized by its rapid and error-prone direct ligation (Yi et al., 2019). Thus, the genomic instability induced by the lack of BRCA1/2 and HR and the adoption of NHEJ can collectively lead to the accumulation of DSBs and an increased risk of developing cancers (Caulfield et al., 2019). These genetic mutations can significantly increase the risk of cancer initiation and progression. Specifically, germline mutations in *BRCA1/2* tumour suppressor genes result in the lifetime risk of developing breast cancer in *BRCA1* and *BRCA2* mutation carriers at 72% and 68%, respectively, compared to 12% in noncarriers (Caulfield et al., 2019). Thus, for HR deficient tumour cells, due to the low fidelity of NHEJ, intact SSB repair pathways are the vital prerequisites for cell survival.

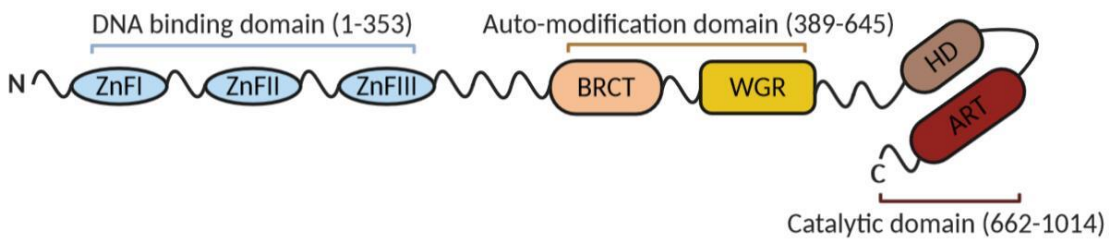

Figure 1.3. The Structure of PARP1. The seven main domains of PARP1 include three zinc-finger domains (ZnFI, ZnFII and ZnFIII) in the DNA binding domain, the BRCT domain in the auto-modification domain, and the pADPr accepting WGR domain, located centrally. The C-terminus has two catalytic domains: ART and HD domains. **Abbr.,** ART: ADP-ribosyltransferase domain; BRCT: BRCA C-terminus-like domain; C: C-terminus; HD: helical domain; N: N-terminus; WGR: tryptophan-/glycine-/arginine-rich domain. Redrawn from Min and Im (2020); Yi et al. (2019). *Created with BioRender.com.*

Poly (ADP-ribose) polymerases (PARPs) are a group of 17 enzymes in mammals activated by DNA single-strand breaks (SSBs) that participate in various cellular processes *via* covalently transferring poly (ADP-ribose) residues to target substrates by ADP-ribosyltransferase using nicotinamide adenine dinucleotide (NAD+) (also termed as PARylation) (Min & Im, 2020; Yi et al., 2019). PARP1 was the first family member identified and is mostly correlated with DNA damage repair, which generates nearly 90% of poly (ADP-ribose) chains after DNA damage event (Yi et al., 2019). It can rapidly recognize and repair multiple types of DNA damage, including SSBs, through mediating BER repair pathways (Yi et al., 2019). In addition to DNA damage repair, PARP1 plays a significant role in a wide spectrum of cellular processes due to its various substrates involved in transcriptional regulation, apoptotic cell death, chromatin decondensation, inflammation, and cell cycle regulation (Min & Im, 2020). PARP1 has a molecular weight of 113 kDa and contains seven independent domains. The DNA binding domain consists of three zinc finger-related domains, ZnFI, ZnFII and ZnFIII, at the N-terminus (residues 1-353), responsible for the recognition and interaction with

damaged DNA sites through allosteric activation. The auto-modification domain between residues 373 to 662 contains a BRCA C-terminus-like (BRCT) domain serving sites of auto-ADP ribosylation and functioning in protein-protein interaction, and a tryptophan-/glycine-/arginine-rich domain (WGR domain) which roles in activating DNA damage repair by interaction with ZnFI, ZnFII and the catalytic domain. The C-terminus (residues 662-1014) is the catalytic domain, including an ADP-ribosyltransferase (ART) domain and a helical domain (HD). The ART domain is an NAD+ acceptor site, while the HD domain inhibits the binding of PARP1 and β-nicotinamide adenine dinucleotide (β-NAD) to DNA (Figure 1.3) (Min & Im, 2020). In the non-DNA binding status, HD suppresses the binding between ART in PARP1 and its cofactor β-NAD. Once DNA SSB occurs, the DNA binding domain in PARP1 could recognize and bind to SSB. The ADP-ribosylation is covalently bound to the carbonyl group of the acidic residues of the PARP1 and target proteins *via* ester bonds which promotes the recruitment of DNA repair effectors and chromatin remodelling. Then the auto-inhibitory function of HD is abrogated, resulting in the activation of the catalytic function of ART. This catalytic activity contributes to the formation of poly ADP-ribose (PAR) chains in PARP by cleaving the glycosidic bond between nicotinamide and ribose of NAD+. NAD+ provides ADP-ribose residues to PARP1 which is the components of negative PAR chain. The binding of ADP-ribosylation to the target proteins *via* 2',1'-O-glycosidic bond helps PARP1 recruit a series of target proteins through PAR chains, such as DNA glycosylase 8-oxoguanine glycosylase 1 (OGG1), X-ray repair cross-complementing protein 1 (XRCC1), DNA polymerase (DNAP) β, DNA ligase III, proliferating cell nuclear antigen (PCNA), aprataxin, and condensing I. Typically, the XRCC1 binds directly to the PAR chain to be recruited to the DNA damage site. After the re-connection of damaged DNA, the PAR generation is increased

by sequestering poly (ADP-ribose) glycohydrolase (PARG) from the interaction with PARP1 and PARG. This auto-PARylation on PARP1 protein triggers the dissociation of PARP1 from DNA chains and restores the auto-inhibitory status of PARP1 (Figure 1.4) (Min & Im, 2020; Yi et al., 2019).

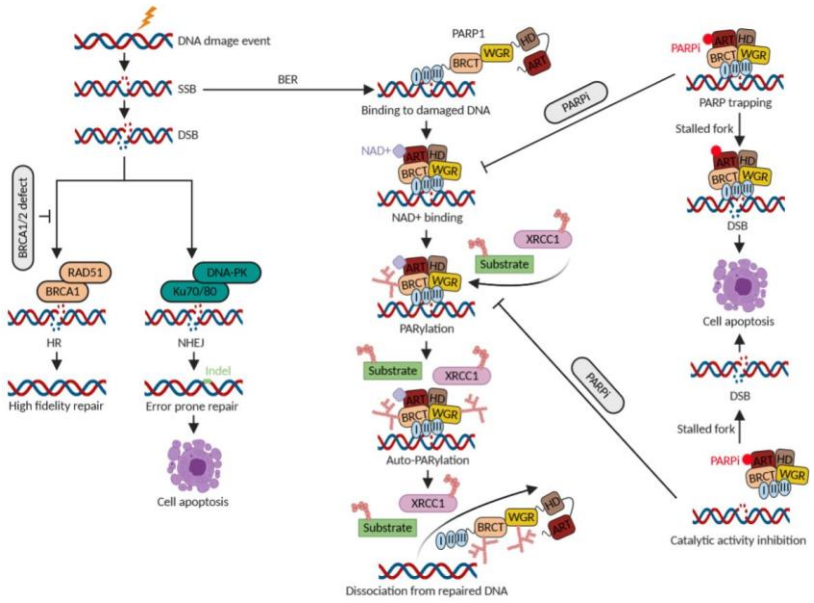

Figure 1.4. Mechanisms of PARP and PARP Inhibition in the DNA damage response. In BRCA1/2 defect cells, DSB could only be repaired by error-prone NHEJ pathways, leading to chromosomal rearrangements that are harmful to cell viability. Once DNA SSB occurs, PARP1 could recognize and interact with SSB through its zinc finger-related domains. The auto-inhibitory function of HD is abrogated, and the catalytic function of ART is activated. DNA repair-related proteins (e.g., XRCC1) are thus recruited by PARP1 and bound to the PAR chains by the catalytic activity of ART using NAD+ as a substrate. Then the auto-PARylation on PARP1 protein triggers the dissociation of PARP1 from DNA chains and restores the auto-inhibitory status of PARP1. In the presence of PARP inhibitors, PARP inhibitors can competitively bind to the pocket instead of NAD+. As a result, PARP1 is trapped in the DNA, and the enzymatic activity of PARP1 for the recruitment of repair proteins is blocked. These blocked SSB repair pathways can thus cause cell apoptosis in BRCA1/2 deficient cells. **Abbr.,** ART: ADP-ribosyltransferase domain; BER: base excision repair; BRCA1/2: breast cancer gene 1 and 2; BRCT: BRCA C-terminus-like domain; C: C-terminus; DSB: double-strand break; HD: helical domain; HR: homologous recombination; N: N-terminus; NAD+: nicotinamide adenine dinucleotide; NHEJ: nonhomologous end joining; PARP1: poly (ADP-ribose) polymerase 1; PARPi: PARP inhibitor; SSB: single-strand break; WGR: tryptophan-/glycine-/arginine-rich domain; XRCC1: X-ray repair cross-complementing protein 1. Redrawn from Min and Im (2020); Yi et al. (2019). *Created with BioRender.com.*

Inhibition of PARP not only causes the trapping of the PARP-DNA complex at replication forks but also inhibits the catalytic activity of ART in PARP1 (Figure 1.4). Thus, the SSB repair pathways are blocked by PARPi. In the absence of HR and SSB related repair, cells rely on the error-prone NHEJ repair pathways. The accumulation of SSBs leads to DSBs and ultimately cell apoptosis if the DNA lesions are not re-connected by appropriate repair mechanisms. Thus, cancer cells with g*BRCA*m-induced deficiency in DNA repair pathways are thought to be more sensitive to the PARPi, as cells without those functional proteins are unable to maintain genomic stability, leading to synthetic lethality, a process whereby the functional depletion of two genes that singly may not have a deleterious effect, leading to cell death (Caulfield et al., 2019; Heo & Dhillon, 2018).

Some nicotinamide analogues are found to competitively inhibit the binding of β-NAD to ART and enhance the cytotoxicity of DNA damaging agents. A number of PARPis are developed on the basis of the structure of nicotinamide analogues, such as olaparib, rucaparib, niraparib and talazoparib (Yi et al., 2019). As the first-in-class PARP inhibitor for cancer therapy, olaparib just relies on the exploitation of the defective DNA damage repair mechanism due to mutations and epigenetic changes of homologous recombination genes, including *BRCA1/2* (He, Green, Li, Chan, & Liu, 2020).

1.2.2.3 Pharmacokinetic Properties of Olaparib

The new tablet formulation of olaparib exhibits enhanced bioavailability compared to the previous capsule formulation (Heo & Dhillon, 2018). Phase I trial in patients with advanced solid tumours showed that a single dose of 250 mg olaparib tablets has higher

systemic exposure (i.e., peak plasma concentration (C_{max}) and area under the plasma concentration-time curve (AUC)) compared to a single dose of 400 mg olaparib capsules (Mateo et al., 2016). Moreover, a population pharmacokinetic analysis also demonstrated that olaparib AUC at a steady-state following multiple-dose of olaparib tablets (300 mg twice daily) was 77% higher than multiple-dose of olaparib capsules (400 mg twice daily) (Heo & Dhillon, 2018).

Olaparib could be rapidly adsorbed, and C_{max} typically peaked within 1.5 h (t_{max}). Olaparib AUC increased in a dose-proportional manner, while C_{max} increased slightly less than dose-proportional across a dose range of 25-450 mg. After twice-daily multiple dosing of 300 mg olaparib tablets, the accumulation ratio of olaparib at a steady-state was 1.8 (Heo & Dhillon, 2018). In patients with refractory advanced solid tumours, consumption of 300 mg olaparib tablets with a high-fat diet reduced the rate of absorption (delayed t_{max} by 2.5 h) and C_{max} by about 21% but only slightly affected olaparib absorption (increased AUC by about 8%). Olaparib tablets can thus be taken with or without food (Plummer et al., 2015).

In vitro, plasma binding of olaparib was approximately 82% in a dose-dependent manner as decreased protein binding at higher concentrations. The mean apparent volume of distribution following a single dose of 300 mg olaparib tablets was 158 L (Heo & Dhillon, 2018). With the catalysis of CYP3A4 enzymes, olaparib was extensively metabolised in the liver *via* oxidation to produce a number of metabolites undergoing subsequent glucuronide or sulphate conjugation. Following a single dose of olaparib tablets, 44% of the dose was recovered in the urine, and 42% was recovered in the faeces over seven days after administration (Caulfield et al., 2019; Heo & Dhillon, 2018). After a single dose of 300 mg olaparib tablets, the mean elimination half-life was 14.9 hours, and the apparent plasma clearance was 7.4 L/h. The pharmacokinetics

of olaparib showed a time-dependent manner following multiple dosing (steady-state clearance decreased by 15%) (Heo & Dhillon, 2018). Over 20 metabolites of olaparib were found in plasma, urine and faeces. The majority of them were represented by the mono-oxygenated and piperazin-3-ol forms (Caulfield et al., 2019; Heo & Dhillon, 2018). As shown in Table 1.2, it is not required to adjust the dosage of olaparib in patients with mild or moderate hepatic impairment (Child-Pugh Class A and B) or in patients with mild renal impairment (CrCl 51-81 mL/min). However, a lower initial olaparib dosage of 200 mg twice daily is recommended in patients with moderate renal impairment (CrCl 31-50 mL/min) due to the increased olaparib exposure by 44%. Further study is needed to explore the use of olaparib in patients with severe renal impairment (CrCl < 30 mL/min or ESRD) or severe hepatic impairment (Child-Pugh Class C) (Caulfield et al., 2019; Heo & Dhillon, 2018). Given the potential drug interactions, the use of olaparib combined with other therapeutic agents should be evaluated before starting olaparib treatment. As mentioned above, olaparib is metabolised by CYP3A4. Agents that relate to CYP3A4 activity may change olaparib exposure. Consequently, concomitant administration of olaparib with strong (e.g., itraconazole, telithromycin, clarithromycin, ketoconazole, voriconazole, nefazodone, posaconazole, ritonavir, lopinavir/ritonavir) or moderate (e.g., ciprofloxacin, crizotinib, darunavir/ritonavir, diltiazem, erythromycin, fluconazole, fosamprenavir, imatinib, verapamil) inhibitors of CYP3A should be avoided. When using olaparib in combination with CYP3A inhibitors is unavoidable, a reduction in olaparib dosage is strongly recommended to make the toxicity controllable. The coadministration of olaparib with strong (e.g., phenytoin, rifampicin, carbamazepine, St. John's wort) or moderate (e.g., efavirenz and rifabutin) CYP3A inducers is also not recommended because these agents may decrease the exposure of olaparib (Caulfield et al., 2019; Heo

& Dhillon, 2018).

Interestingly, *in vitro* studies indicate that olaparib may play a role in mediating CYP3A4, UGT1A1, and the membrane transporters ABCB1, ABCG2, OATP1B1, OCT1, OCT2, OAT3, MATE1 and MATE2 (McCormick & Swaisland, 2017; McCormick, Swaisland, Reddy, Learoyd, & Scarfe, 2018). Exposure of cancer cells to olaparib may decrease the uptake of substrates of OATP1B1, OCT1, OCT2, OAT3, MATE1 and MATE2, and enhance the cellular accumulation of substrates of ABCB1 and ABCG2, such as doxorubicin (Table 1.4). Hence, apart from monitoring substrates of CYP3A, appropriate monitoring is also advised when olaparib is used in combination with the substrates of ABCB1 and ABCG2.

1.2.2.4 Olaparib Resistance

Resistance to PARPis remains a key barrier to the long-term survival and treatment options for patients (Dziadkowiec, Gasiorowska, Nowak-Markwitz, & Jankowska, 2016). The mechanisms that render resistance to PARPis are controversial. It is believed that five main aspects are included. Firstly, a reversion mutation in the *BRCA1/2* genes is a potential reason for restoring the HR repair ability of cells. The cells with restored HR function can neutralize the DNA damage caused by PARPis. Secondly, a decrease in NHEJ may confer resistance to PARPis. The synthetic lethality relies on the error-prone NHEJ repair, which can cause genomic instability. Thirdly, decreased levels, activity or enzymatic action of PARP1 available for inhibition may restrict the effectiveness of PARPis. Fourthly, the upregulation of efflux transporters may pump out more PARPis, resulting in a decrease in the accumulation of intracellular PARPis. Lastly, an increase in the activity of DNA repair proteins such as RAD51 may result in

resistance to PARPis by restoring the DNA lesions caused by PARPis (Dziadkowiec et al., 2016). For instance, sperm-associated antigen 5 (SPAG5) is found to correlate with PARP resistance. It can typically up-regulate the expression of HR-related DNA repair proteins such as RAD51, BRCA1 and BRCA2 and shorten the S-phase duration in which olaparib-provoked DNA lesions occur (He et al., 2020).

1.2.2.5 Combination with Conventional Chemotherapy

According to the mechanism of action of PARPis mentioned above, they not only cause cytotoxicity by suppressing the recruitment of DNA repair proteins but also trap PARP by inducing stalling or collapsing of the replication fork of the PARP-DNA complex (Min & Im, 2020). On the basis of the mechanisms, activity of cytotoxicity and the regulation of PARylation, PARPis are thought to have different synergies in combinations with different chemoagents. PARPis are found to sensitize tumours to topoisomerase I inhibitors, topotecan and camptothecin. Topoisomerase I inhibitor can induce SSBs through the endonuclease activity of TOP1 and lead to DNA damage by trapping TOP1cc covalently bonded with TOP1 at the DNA 3' end. PARPi enhances this effect by sustaining the trapping of TOP1cc by inhibiting the recruitment of target proteins (Min & Im, 2020). Moreover, olaparib plays a role in mediating CYP3A4, UGT1A1, and the membrane transporters ABCB1, ABCG2, OATP1B1, OCT1, OCT2, OAT3, MATE1 and MATE2 (McCormick & Swaisland, 2017; McCormick et al., 2018). Exposure of cancer cells to olaparib may decrease the uptake of substrates of OATP1B1, OCT1, OCT2, OAT3, MATE1 and MATE2, and enhance the cellular accumulation of the substrates of ABCB1 and ABCG2, such as doxorubicin. On the other hand, as aforementioned, doxorubicin as a topoisomerase II inhibitor, its cytotoxic effect is also based on DNA damage by inhibiting the resealing of DNA helix. PARPis prevent

PARP1 from repairing DNA lesions caused by doxorubicin treatment. This dose-dependent synergistic effect was examined in this study.

1.3 Chemoresistance of Cancer

1.3.1 Multidrug-Resistance

The chemoresistance of cancer cells is primarily attributed to a trait termed multidrug resistance (MDR). The resistance of tumour to one drug or drug combination can trigger cross-resistance to other structurally or mechanistically unrelated chemotherapeutic compounds (Gerlach, Kartner, Bell, & Ling, 1986; Pastan & Gottesman, 1987). This may explain why multidrug combination regimens with distinct targets do not exhibit the expected better effectiveness. In current clinical settings, MDR remains a significant impediment to successful chemotherapy, leading to relapse and progression of most malignant tumours. The mechanisms of action mediating the development of MDR appear to be quite complicated, including but not limited to increased drug efflux from the cell, decreased drug uptake into the cell, alterations in drug metabolism, mutations of drug targets, and inactivation of death signalling pathways (Figure 1.5) (Holohan, Van Schaeybroeck, Longley, & Johnston, 2013). These mechanisms can generally be divided into two broad groups: intrinsic or acquired (Holohan et al., 2013). Consequently, MDR is either originally present in many tumours (intrinsic resistance) or may develop as chemotherapy continues (acquired resistance). Accordingly, the toxicity of chemotherapy to cancerous tissues might be limited at the very start of the administration and even become worse after successive rounds of treatment.

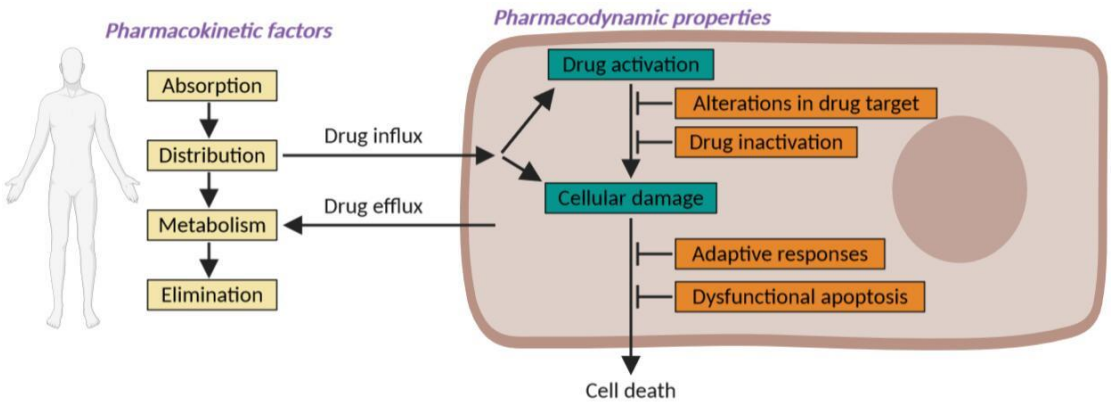

Figure 1.5. General Principles of Drug Resistance. Pharmacokinetic factors such as absorption, distribution, metabolism and elimination determine the fate of administered drugs. They are analysed to examine how an organism affects a drug from drug administration to the amount that reaches the tumour, ultimately to the point at which it is completely eliminated from the body. Pharmacodynamic properties show how the drug affects the organism. They are used to examine the effect of a drug on cancer cells. Redrawn from Holohan et al. (2013). *Created with BioRender.com.*

1.3.2 ABC Transporters Related Multidrug-Resistance

With the pivotal breakthrough in uncovering the mystery of MDR in 1976 (Juliano & Ling, 1976), membrane proteins have been correlated with drug resistance. For decades, one of the most common causes of MDR has been implicated in altered expression of the ABC (ATP-binding cassette) transporters, some of which efflux numerous chemotherapeutic compounds from the intracellular matrix (Bosch & Croop, 1996; Dean, Hamon, & Chimini, 2001). ABC transporters such as the extensively studied multidrug resistance protein 1 (MDR1; aka., P-glycoprotein, P-gp, and ABCB1), MDR-associated protein 1 (MRP1; aka., ABCC1), and breast cancer resistance protein (BCRP; aka., ABCG2) enable cancer cells to elude “hazardous substances” by extruding them out of the intracellular environment. This process is known as drug efflux (Dean et al., 2001; Gottesman, Fojo, & Bates, 2002). All the three well-documented transmembrane proteins above possess broadly overlapping substrate specificity in regulating flux across the plasma membrane and lead to transient or even incomplete response to

anticancer pharmaceuticals (Gottesman et al., 2002).

In humans, 48 genes encoding ABC transporter superfamily have been identified and phylogenetically divided into seven subfamilies (i.e., ABC subfamily A to G) based on their sequence homology and domain organization (Ambudkar, Kimchi-Sarfaty, Sauna, & Gottesman, 2003; Szakács, Paterson, Ludwig, Booth-Genthe, & Gottesman, 2006). ABC transporters, the largest family of transmembrane proteins, compose a complicated translocation system responsible for the unidirectional movement of diverse compounds across the phospholipid bilayer of cellular membranes (Ween, Armstrong, Oehler, & Ricciardelli, 2015). These ABC transporters are present in almost all forms of life that are typified by a characteristic role in regulating cellular levels of hormones, lipids, ions, xenobiotics and other small molecules (Hollenstein, Dawson, & Locher, 2007; Robert W Robey et al., 2018), in addition to their various physiological roles in regulating intracellular organelles such as the mitochondrion, lysosome, endoplasmic reticulum and Golgi apparatus (Robert W Robey et al., 2018). A consequence of these protective roles is that some ABC transporters have the ability to pump anticancer agents across lipid bilayers. In fact, only 20 or so ABC transporters are supposed to be associated with the drug-resistance phenotype (Ween et al., 2015). These ABC transporters exhibit partially mutual substrate specificity because they are found to share sequence and structural homology (Gottesman et al., 2002; Ito, Olsen, Qiu, Deeley, & Cole, 2001). Despite the well-established knowledge in the substrates and key roles for most of these transporters, their influence on clinical MDR has been controversial (Robert W Robey et al., 2018). A greater understanding of ABC transporters will theoretically be conducive to bridge the gap.

1.4 The Role of ABCC5 in Breast Cancer

Many molecular characteristics of TNBC has been proposed to be associated with patients' response to treatment. For example, the alteration of the expression of tumour suppressor gene *BRCA1* due to promoter methylation and p53 mutations was found to correlate with a good response to cisplatin treatment (Silver et al., 2010). Likewise, high expression of a surface enzyme CD73 was linked to resistance to doxorubicin in TNBC patients (Loi et al., 2013). However, with the increased understanding of ABCC5, more characteristics of breast cancer have been implicated in this membrane protein.

MRP5 (MDR-associated protein 5; aka., ABCC5) is classified into the ABCC subfamily, one of the largest subfamilies of the ABC transporters. It is characterized as an organic anion pump that can transport organic conjugates, anionic tripeptide glutathione (GSH), and nucleoside monophosphate analogues (P. Borst, Evers, Kool, & Wijnholds, 2000; Jan Wijnholds et al., 2000). The human ABCC5 gene is located on chromosome 3q27, which consists of 29 exons and spans over 98 kb (Table 1.3). It encodes a 1437 amino acid polypeptide with a molecular weight of 190 kDa (Lal et al., 2010). *ABCC5* mRNA is present in almost all tissues at low levels, suggesting that ABCC5 is ubiquitously present (Marcel Kool et al., 1997). However, ABCC5 is found relatively elevated in the brain capillary endothelial cells, pyramidal neurons and astrocytes, as well as in smooth muscle cells (SMCs) of various tissues in the human genitourinary system (Slot, Molinski, & Cole, 2011). ABCC5 can be localized to both apical and basolateral membranes (Deeley, Westlake, & Cole, 2006). No known diseases are associated with mutations in *ABCC5* (Slot et al., 2011). Consistent with ABCC4 mentioned in section 1.5.5, the structure of ABCC5 (Figure 1.6) lacks the additional N-terminal spanning domain.

Table 1.3. Details of *ABCC5* gene.

Gene name	*ABCC5*
No. of base pair	98007
Location	Chromosome 3q27.1
Gene map	https://www.ncbi.nlm.nih.gov/genome/gdv/browser/gene/?id=10057

ABCC5 expression was found to up-regulate in hepatocellular carcinoma, nasopharyngeal carcinoma, pancreatic ductal adenocarcinoma, ovarian cancer and breast cancer (Ween et al., 2015). ABCC5 has been reported to confer resistance to a number of chemodrugs such as methotrexate, 5-fluorouracil and doxorubicin, as shown in Table 1.4. Its expression was up-regulated in post-treatment (neoadjuvant chemotherapy) breast tumours compared with non-neoplastic tissues (Hlaváč et al., 2013). A significantly higher expression of ABCC5 was observed in the residual disease group in breast cancer patients who underwent sequential weekly neoadjuvant chemotherapy paclitaxel/FEC (5-fluorouracil, epirubicin and cyclophosphamide) (S. Park et al., 2006). The *ABCC5* mRNA and ABCC5 protein levels were elevated in doxorubicin-resistant lung cancer cells (Yoshida et al., 2001). ABCC5 overexpression in breast cancer stem cells has been suggested to result in chemotherapeutic resistance to the front-line drug doxorubicin in breast cancers (Y. Zhu et al., 2011). The expression of ABCC5 protein in BT-ICs (breast tumour-initiating cells) has been linked to the microRNA miR-128. The ectopic expression of miR-128 could sensitize BT-ICs to doxorubicin by reducing ABCC5 expression (Y. Zhu et al., 2011). ABCC5 could confer resistance to 5-FU (5-fluorouracil) by mediating the cellular efflux of its cytotoxic active monophosphate metabolite, 5-dUMP, rather than the parental drug itself (Pratt et al., 2005). The genotypic influence of the ABCC5 polymorphisms on the gene expression and pharmacokinetics of chemodrug substrates is not well defined (Lal et

al., 2010). The *ABCC5* g.+*7161G>A* (rs1533682) and *ABCC5* g.-*1679T>A* polymorphisms have been reported to significantly influence the pharmacokinetics of doxorubicin and doxorubicinol, respectively in Asian breast cancer patients (Lal et al., 2017).

Apart from chemoresistance-related functions, ABCC5 is found to regulate cell proliferation and metastasis in breast cancers. ABCC5 may promote cell proliferation and suppress apoptosis in breast cancer cells by the efflux of cGMP. This secondary messenger relays external signals to downstream protein kinases, ultimately inactivating protein kinase G (PKG), which is able to suppress cell proliferation. But ABCC5 shows no advantages for breast cancer proliferation and survival in end-stage bone metastases (Mourskaia et al., 2012). Both mRNA and protein levels of ABCC5 were up-regulated in metastatic skeletal breast cancer and related to osteoclast formation and breast cancer metastasis to bone (Mourskaia et al., 2012). The substrate of ABCC5 may either promote osteoclastogenesis directly or stimulate this process indirectly through an intermediate cell type present in the bone microenvironment. The locally elevated level of cGMP that ABCC5 pumps out can further increase the migration ability of osteoclast.

1.5 Other ABC Transporters-Mediated Chemoresistance in Breast Cancer

1.5.1 ABCB1

The first identified ABC transporter was MDR1 (multidrug resistance protein 1; aka., P-glycoprotein, P-gp and ABCB1), which is distributed in nearly all tissues at low

levels (Ambudkar et al., 1999; C.-H. Choi, 2005) but is found overexpressed in many tumours (Thomas & Coley, 2003). P-gp was initially isolated by Juliano and Ling (1976) from the plasma membranes of Chinese hamster ovary cells, and it was referred to as "P-glycoprotein" due to its ability to reduce drug permeability in resistant cells. The gene encoding this transporter in an animal model and the human homologue was subsequently identified in the respective study (Gros, CROoP, Roninson, Varshavsky, & Housman, 1986; Roninson et al., 1986; Ueda et al., 1986). From then on, the human gene encoding P-gp was termed and classified as ABC subfamily B member 1 (*ABCB1*) (Roninson et al., 1986; Ueda et al., 1986). ABCB1 is mainly expressed in various apical membranes of epithelial cells within human body, including gastrointestinal tract, pancreatic ductules, liver and kidney (Thiebaut et al., 1987), as well as in endothelial cells of the blood-brain barrier (BBB) (Carlos Cordon-Cardo et al., 1989). This distribution highlights its role in protecting the body from xenobiotics and other natural product toxins. Given that the entire wall of the small blood capillaries in the brain is covered by endothelial cells (tight junctions), the compounds that cannot diffuse between cells have to cross endothelial cells into the surrounding brain tissues. The presence of ABCB1 in the endothelial cells can typically pump the entered substrates back into the blood, protecting the brain tissues from xenotoxins (Carlos Cordon-Cardo et al., 1989). The functions of ABCB1 expressed in blood-testis and blood-nerve barrier are completely analogous to those in BBB (Carlos Cordon-Cardo et al., 1989). The expression of ABCB1 in apical membranes of mucosal cells is thought to pump toxins across the apical surface into the intestinal lumen, forming a first line of defence (Thiebaut et al., 1987). In the placenta, ABCB1 is found localized on the apical syncytiotrophoblast surface, protecting the foetus from toxic cationic xenobiotics (C Cordon-Cardo et al., 1990). The ABCB1 present in the apical membranes of

hepatocytes serves to transport toxins into the bile and from the intestinal epithelium into the intestinal lumen (Schinkel et al., 1997). The extruded compounds would eventually leave the body along with faeces, thus resulting in the purification and detoxification of plasma.

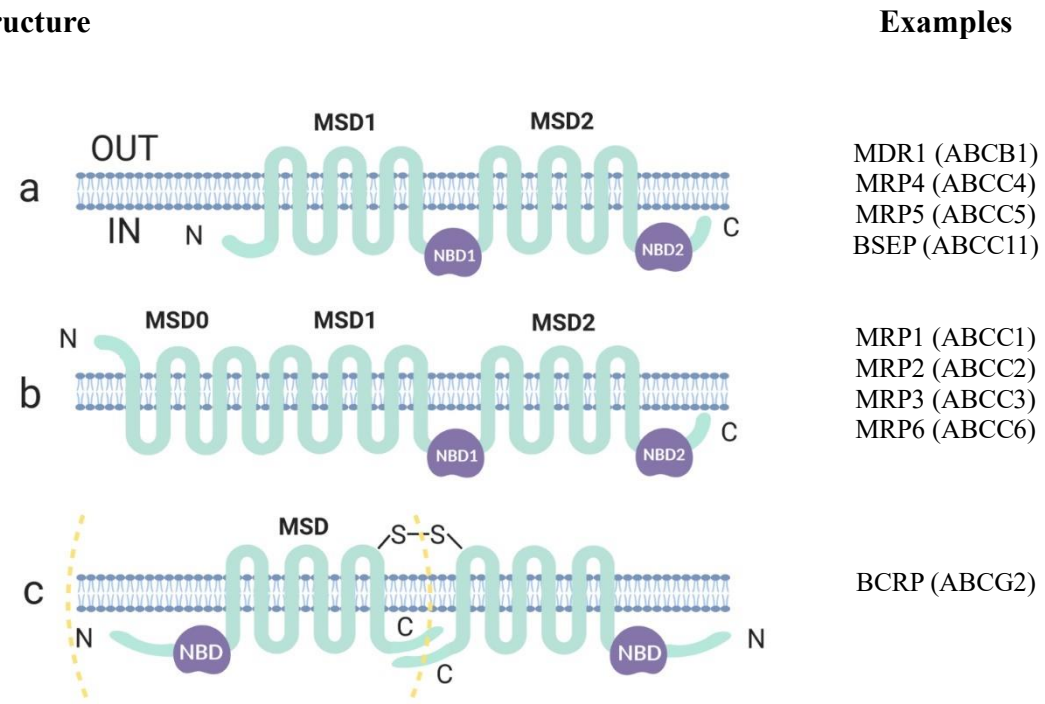

Figure 1.6. The basic structure of ABC transporters. The three different structures of ABC transporters known to render drug resistance. **a.** ABC transporters such as ABCB1 and ABCC4 possess12 transmembrane regions and two ATP-binding sites. **b.** ABCC1, 2, 3 and 6 are similar in structures that they have two ATP-binding regions. Compared with ABCB1, they have an amino-terminal end extension containing five transmembrane regions, with a total of 17 transmembrane regions. **c.** ABCG2 "half-transporter" and ABCG2 homodimer. The "half-transporter" ABCG2 just contains six transmembrane regions and one ATP-binding site. This kind of transporter is thought to function as either a homodimer or a heterodimer. **Abbr.,** ATP: Adenosine Triphosphate; BCRP: Breast cancer resistance protein; BSEP: Bile salt export pump; C: C-terminus (COOH); MDR: Multidrug resistance protein; MRP: MDR-associated protein; MSD: membrane-spanning domains (aka., transmembrane domain, TMD); N: N-terminus (NH_2); NBD: nucleotide-binding domain. Redrawn from Piet Borst, Evers, Kool, and Wijnholds (1999); L. Chen, Manautou, Rasmussen, and Zhong (2019); Gottesman et al. (2002); Schinkel and Jonker (2012); Slot et al. (2011). *Created with BioRender.com.*

Current evidence supports a topology model that ABCB1 has two intracellular ATP-binding sites and 12 transmembrane segments with the highly *N*-glycosylated first extracellular loop (Figure 1.6) (C.-j. Chen et al., 1986). These regions and sites structurally form four domains, including two cytoplasmic nucleotide-binding domains (NBDs) and two transmembrane domains (TMDs) (Figure 1.7). Current knowledge suggests that NBDs are highly conserved domains that are structurally and functionally similar throughout families. NBD proteins are connected with each other in a head-to-tail model to form a "sandwich dimer" that consists of two composite nucleotide-binding sites (NBSs), allowing ATP to bind to the ATP-binding sites where ATP hydrolyse (Slot et al., 2011). TMDs, however, are highly heterogeneous, enabling transporters to recognize and translocate a broad spectrum of substrates across membranes with the energy of ATP hydrolysis, irrespective of the prevailing concentration gradient (Dean et al., 2001). In order to bind and transport plenty of engaged substrates, basal ATP hydrolysis drives continuously conformational changes of ABC transporters (Esser et al., 2017). To be more specific, an intracellular molecule binds to a high-affinity conformation of the TMDs, followed by the binding of ATP to the NBDs. These binding events stimulate the ATPase activity of ABCB1, causing ATP hydrolysis and the generation of conformational changes from which the molecule is released. The altered conformation can be restored by the energy of ATP hydrolysis at the second ATP binding site. The transporter then once again assumes its high-affinity conformation, allowing the repeat of the excretory process (Esser et al., 2017; Johnson & Chen, 2017; Taylor et al., 2017).

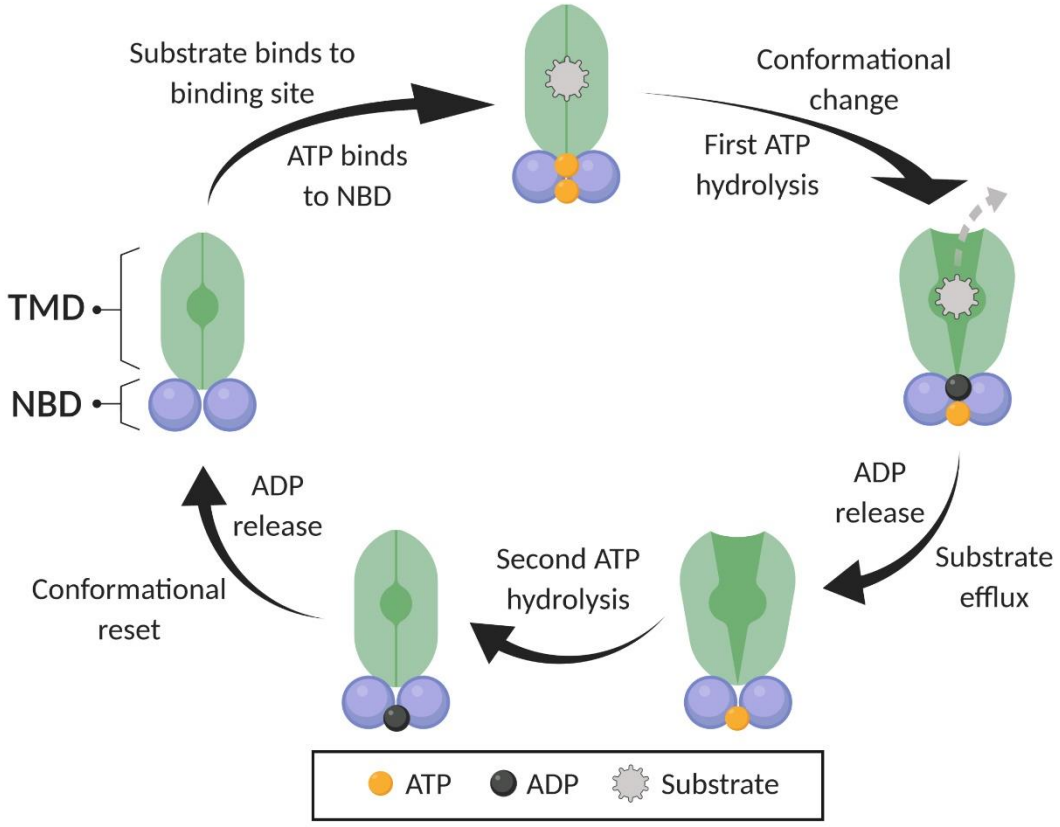

Figure 1.7. Schematic representation of the proposed pumping action of ABCB1 and possibly other ABC transporters. The substrate of ABCB1 binds to the binding pocket in the TMDs, and ATP binds to the two ATP-binding sites in the NBDs. Then the first ATP hydrolysis provides energy for the generation of a conformational change from which the substrate is released. This is followed by the hydrolysis of the second ATP, which resets the altered conformation, allowing repetition of the efflux process. **Abbr.,** ADP: Adenosine diphosphate; ATP: Adenosine Triphosphate; NBD: nucleotide-binding domain; TMD: transmembrane domain. Redrawn from Deeley et al. (2006); Khunweeraphong, Stockner, and Kuchler (2017); Robert W Robey et al. (2018). *Created with BioRender.com.*

The overexpression of ABCB1 has been correlated with chemoresistance in many cancers such as kidney, colon, adrenal, pancreas, liver and breast cancers (Thomas & Coley, 2003; Trock, Leonessa, & Clarke, 1997). ABCB1 is capable of transporting hydrophobic substrates that are either neutral or positively charged (Ambudkar et al., 1999). The hydrophobic property of ABCB1 substrates probably enables themselves passively diffuse across membranes at a reasonable rate (Schinkel & Jonker, 2012). The

substrates (Table 1.4) are normally organic molecules ranging in size from less than 200 Da to almost 1900 Da, containing diverse cytotoxic chemotherapeutic compounds such as anthracyclines and taxanes (Ambudkar et al., 1999; Schinkel & Jonker, 2012). To complicate matters, these regimens have been widely used in treating breast cancer (Moreno-Aspitia & Perez, 2009). The presence of active ABCB1 can typically interfere with the net penetration of those therapeutic compounds into tissues in a pharmacological model (Schinkel & Jonker, 2012). For instance, evidence shows that ABCB1 activity could restrict the oral bioavailability of substrate drugs by impeding the translocation of drugs from the intestinal lumen into the bloodstream (Alex Sparreboom et al., 1997). Recent studies have demonstrated that even some molecularly targeted drugs (e.g., imatinib, erlotinib, sunitinib and nilotinib) can also be handled by ABCB1 and ABCG2 (Shukla, Chen, & Ambudkar, 2012). In addition, naturally occurring genetic variants (aka., single nucleotide polymorphisms; SNPs) of ABCB1 have been proposed to influence the function and expression of this transporter, thus causing variations in intestinal absorption, elimination, and penetration of drugs into the cells. The interindividual variability in the pharmacokinetics and the pharmacodynamics of many drugs related to ABCB1 is a result of this phenomenon (Ambudkar et al., 2003; Mickley et al., 1998).

Table 1.4. Cytotoxic substrates (anticancer drugs) of ABC transporters.

Names	Substrates	References
ABCB1	Doxorubicin, Epirubicin, Docetaxel, Paclitaxel, 5-Fluorouracil, Actinomycin D, Bisantrene, Dasatinib, Daunorubicin, Digoxin, Etoposide/VP-16, Homoharringtonine, Irinotecan, Mitoxantrone, Teniposide, Topotecan, Vinblastine, Vincristine, Vindesine, Vinorelbine, Methotrexate, Mithramycin Mitomycin C	(Ambudkar et al., 1999; Schinkel & Jonker, 2012; Ween et al., 2015)
ABCC1	Doxorubicin, Epirubicin, Daunorubicin, Eribulin, Chlorambucil, Idarubicin, Etoposide/VP-16, Glucuronide, Teniposide, Vincristine, Vinblastine, Vinorelbine, Topotecan, Irinotecan/SN-38, Mitoxantrone, saquinavir, Arsenite, Trivalent antimony, Imatinib, Melphalan, Methotrexate, SN-38	(Schinkel & Jonker, 2012; Ween et al., 2015)
ABCC2	Doxorubicin, Epirubicin, Paclitaxel, Carboplatin, Cisplatin, Etoposide/VP-16, Irinotecan, Irinotecan/CPT-11, Methotrexate, Mitoxantrone, saquinavir, SN-38, Sulfinpyrazone, Topotecan, Vinblastine, Vincristine	(A. T. Nies & Keppler, 2007; Ween et al., 2015)
ABCC3	Methotrexate, Etoposide/VP-16, Teniposide, Vincristine	(P. Borst, de Wolf, & van de Wetering, 2007; Ween et al., 2015)
ABCC4	Methotrexate, 5-Fluorouracil, 6-mercaptopurine, 6-thioguanine, Bisantrene, Irinotecan/CPT11, Nucleoside monophosphates, Topotecan, Vinblastine, SN-38	(P. Borst et al., 2007; Russel, Koenderink, & Masereeuw, 2008; Ween et al., 2015)
ABCC5	Doxorubicin, Gemcitabine, Methotrexate, 5-Fluorouracil, 6-mercaptopurine, 6-thioguanine, Bisantrene, Mitoxantrone, Nucleoside monophosphates	(P. Borst et al., 2007; Ween et al., 2015)
ABCG2	Doxorubicin, Epirubicin, Methotrexate, Bisantrene, Dasatinib, Daunorubicin, Flavopiridol, Irinotecan/CPT-11, Mitoxantrone, Nilotinib, SN-38, topotecan, Tyrosine Kinase inhibitors	(Q. Mao & Unadkat, 2015; R. W. Robey, Polgar, Deeken, To, & Bates, 2007; Ween et al., 2015)

ABCB1 has been reported to frequently express in lymph node metastases of breast cancer patients (Zochbauer-Muller et al., 2001). Trock et al. (1997) conducted a meta-analysis of 31 studies from 1989-1996 to examine ABCB1 expression in breast cancer and found that 41% of breast tumours expressed this protein. A series of imaging studies *in vivo* using ^{99m}Tc-sestamibi (technetium-99m sestamibi; aka., Cardiolite), a substrate recognized by ABCB1, identified that ABCB1 activity is enhanced in breast carcinomas

(Del Vecchio et al., 1997; Kao et al., 2001; Sun et al., 2000). The incidence of ABCB1 expression was higher in patients receiving cytotoxic chemotherapy, and its expression in breast tumours was associated with treatment failure and a poor response to chemotherapy (Trock et al., 1997). Mechetner et al. (1998) found that the expression of ABCB1 was strongly correlated with doxorubicin and Taxol resistance in clinical specimens of breast carcinoma. It was also found to render eribulin resistance on MCF7 and MDA-MB-231 breast cancer cells (Oba, Izumi, & Ito, 2016). ABCB1 was significantly overexpressed at the protein level in paclitaxel-resistance SKBR3 and MCF7 breast cancer cells, and silencing of the *ABCB1* gene partially resensitized those cells (Nemcova-Furstova et al., 2016). The SNPs rs1045642, rs1128503 and rs2032582 in *ABCB1* were found to play a role in altered pharmacokinetics of doxorubicin in Asian breast cancer patients (Lal et al., 2008). The *ABCB1* SNPs rs1045642 and rs2032582 were implicated in age at breast cancer diagnosis and tumour size, respectively (Al-Eitan, Rababa'h, Alghamdi, & Khasawneh, 2019).

1.5.2 ABCC1

Initially, with the discovery of ABCB1, cancer drug resistance was supposed to arise from ABCB1 expression alone. However, the response failure of many cancers to drugs that are not ABCB1 substrates made researchers realize other factors might be involved, and attention turned to search for other drug efflux pumps, leading to the discovery of multidrug-resistance-associated protein 1.

MRP1 (MDR-associated protein 1; aka., ABCC1) encoded by *ABCC1* was the first identified member in the ABC transporter C family that is assigned classifications from ABCC1 to 12 (S. Cole et al., 1992; Kruh & Belinsky, 2003). ABCC1 is present in the

basolateral side of epithelial membranes within a wide range of tissues such as the testis and kidney (Deeley et al., 2006; Evers et al., 1996). It is involved in ATP-dependent efflux of xenobiotics across the cell membrane and could pump drugs into the body rather than into bile, urine or gut for disposal (Piet Borst et al., 1999). Unlike ABCB1, ABCC1 in mucosal cells does not pump toxins directly back to the intestinal lumen. Its localization to basolateral membranes of mucosal cells determines its responsibility for transporting toxins into the interstitium or the bloodstream (Evers et al., 1996). The metabolic waste products of CSF (blood-cerebrospinal-fluid barrier) are pumped into the blood due to the presence of ABCC1 in the basolateral membrane of the choroid plexus (Rao et al., 1999). ABCC1 is also found localized to the basolateral surface of Sertoli cells, where it can protect sperm within the testicular tubules (Gottesman et al., 2002). In the placenta, ABCC1 may be responsible for protecting foetal blood from toxic organic anions and pumping glutathione/glutathione metabolites into the maternal circulation (St-Pierre et al., 2000). Although ABCC1 is capable of exporting an array of important physiological metabolites, no known human diseases are linked with a lack of functional ABCC1 (Slot et al., 2011). The structure of ABCC1 (Figure 1.6) is similar to ABCB1, with the exception that they have an amino-terminal end extension containing five transmembrane regions (Gottesman et al., 2002). The total 17 transmembrane regions of ABCC1 constitute three membrane-spanning domains (MSDs; aka., transmembrane domains, TMDs), MSD0, MSD1 and MSD2 (Slot et al., 2011).

The overexpression of ABCC1 has been linked with chemoresistance in many cancers such as oesophageal carcinoma, leukaemias, prostate and lung cancers (Kees Nooter et al., 1995; Triller, Korošec, Kern, Košnik, & Debeljak, 2006; Zalcberg et al., 2000). In contrast to ABCB1, ABCC1 stands out for its function as a co-transporter of

amphipathic organic anions (Deeley et al., 2006). It is capable of recognizing and transporting hydrophobic drugs, organic anions, and organic anions that are conjugated or complexed to the anionic tripeptide glutathione (GSH) (e.g., inflammatory mediator leukotriene C4 (LTC_4), an arachidonic acid derivative conjugated to glutathione), to glucuronic acid (e.g., oestradiol glucuronide), or to sulphate (e.g., oestrone sulphate) (Evers et al., 1996; Leier et al., 1994; Loe, Almquist, Cole, & Deeley, 1996; Müller et al., 1994), or in some cases such as for vincristine, co-transports unconjugated glutathione (Table 1.4) (Loe, Deeley, & Cole, 1998; Rappa, Lorico, Flavell, & Sartorelli, 1997). GSH is a cellular antioxidant with many functions, including a critical role in protecting cells from the deleterious effects of oxidative stress, which is a crucial contributor to cancer (Ames, Shigenaga, & Hagen, 1993; Slot et al., 2011). GSH also contributes to the formation of hydrophilic GSH conjugates in Phase II xenobiotic metabolism, which is then translocated by ABCC1 (Slot et al., 2011). Compared with ABCB1, ABCC1 is able to confer resistance to anthracyclines (e.g., doxorubicin and epirubicin), the front-line treatments for breast cancer, however, taxanes (e.g., docetaxel and paclitaxel), the essential substrates of ABCB1 are not mediated by ABCC1 (S. P. Cole et al., 1994; Kruh & Belinsky, 2003). Intriguingly, ABCC1 from primates (e.g., humans and macaque) can transport anthracycline drugs (e.g., doxorubicin) and oestradiol glucuronide. In non-primates cases, however, ABCC1 from rat, mouse, dog or cow that has amino acid sequence similarity > 90% to that of primates is unable to export those substrates (Slot et al., 2011). Expression of ABCC1 was significantly lower in breast cancer samples prior to chemotherapy than those with exposure to chemotherapy (Trock et al., 1997). It was found to have a higher expression level in lymph node metastases than in corresponding primary tumours (Zochbauer-Muller et al., 2001). Its expression was significantly increased in grade III invasive breast ductal

carcinoma tissue, as well as in BT474, MCF7, T47D, MDA-MB-231 and HCC1806 breast cancer cells (Balaji, Udupa, Chamallamudi, Gupta, & Rangarajan, 2016). ABCC1 overexpression has also been correlated with tumour size in breast cancer (Fletcher, Haber, Henderson, & Norris, 2010). K Nooter et al. (1997) reported that overexpression of ABCC1 may be associated with chemotherapy failure in breast cancer and with shorter RFS (relapse-free) and OS (overall survival). This finding was proved by a subsequent study that *ABCC1* was up-regulated and present potential modifier of progression and response to the chemotherapy of breast carcinoma among 68 breast cancer patients treated by neoadjuvant chemotherapy (Hlaváč et al., 2013). Three common SNPs in *ABCC1* (i.e., variant rs246221, rs4148350 and rs45511201 alleles) have been associated with an elevated risk of haematological toxicity in breast cancer patients receiving 5-fluorouracil, epirubicin and cyclophosphamide chemotherapy (Vulsteke et al., 2013).

1.5.3 ABCC2

MRP2 (MDR-associated protein 2; aka., ABCC2) is also known as canalicular multi-specific organic anion transporter (cMOAT) (P. Borst et al., 2000). It was first cloned from rat liver in 1996 (Büchler et al., 1996). ABCC2 is found to function as an efflux pump that can excrete conjugated endogenous and xenobiotic substances, which is localized to the apical membrane of various polarized cells (Keppler & Konig, 1997; Konig, Nies, Cui, Leier, & Keppler, 1999). These polarized cells are present in polarized human tissues such as the kidney, small intestine, colon, gallbladder, bronchi and placenta (A. T. Nies & Keppler, 2007). The localization of ABCC2 to the apical surface of hepatocytes reflects its ability to transport bilirubin-glucuronide and other

organic anions into bile (König, Nies, Cui, Leier, & Keppler, 1999). It was also thought to play a role in the detoxification of alkylating agents in the apical epithelium of the liver and kidney (Smitherman, Townsend, Kute, & Morrow, 2004). The sequence variants inducing the absence of functionally active ABCC2 protein from the canalicular membrane of hepatocytes can result in Dubin-Johnson syndrome in humans (A. T. Nies & Keppler, 2007). The structure of ABCC2 (Figure 1.6) is consistent with ABCC1, including two NBDs and three MSDs, namely MSD0, MSD1 and MSD2 (Slot et al., 2011).

ABCC2 is present in many tumours, including renal, hepatocellular, ovarian, lung gastric, breast and colorectal carcinomas (A. T. Nies & Keppler, 2007). Like ABCC1, the substrate specificity of ABCC2 is broad, including a similar range of organic anions and anionic conjugates as ABCC1 (e.g., GSH conjugates and oestradiol glucuronide) (P. Borst et al., 2000; A. T. Nies & Keppler, 2007). The ABCC2 proteins in the liver, kidney and intestine are thought to influence the oral bioavailability of drugs, xenotoxins and their metabolites (A. T. Nies & Keppler, 2007). Recent studies demonstrated that ABCC2 limits oxaliplatin accumulation and responses both *in vitro* in colorectal and pancreatic cancer cell lines (Caco-2 and PANC-1) (Biswas et al., 2019) and in an animal model of human gastrointestinal cancer (Myint et al., 2019). Unlike ABCC1, ABCC2 can export both anthracyclines (e.g., doxorubicin and epirubicin) and taxanes (e.g., paclitaxel) (Ween et al., 2015), the first-line drugs in treating breast cancer (Moreno-Aspitia & Perez, 2009). Although ABCC2 was found to be expressed in a number of breast cancer cell lines (e.g., MCF7 and BT20), its expression showed no difference after anthracycline treatment (Faneyte, Kristel, & van de Vijver, 2004). But it was associated with acquired resistance to tamoxifen (TAM) in human breast cancer MCF7 cells (H. K. Choi, Yang, Roh, Han, & Kang, 2007). The rs3740065 SNP in

ABCC2 was significantly related to recurrence-free survival of the patients receiving tamoxifen monotherapy (Kiyotani et al., 2010). *ABCC2* SNP rs2273697 was in connection to age at breast cancer diagnosis and oestrogen receptor status for genotype association (Al-Eitan et al., 2019). The ABCC2 expression in the nuclear membrane was associated with a less advanced differentiation of neoplastic cells (most probably stem cells) and poor clinical outcomes (Maciejczyk et al., 2012).

1.5.4 ABCC3

MRP3 (MDR-associated protein 3; aka., ABCC3) has the highest degree of sequence similarity to ABCC1 (58%) (P. Borst et al., 2007). However, compared with ABCC1, ABCC3 possesses a very different and more limited substrate profile (Table 1.4) (Slot et al., 2011). ABCC3 is typified by a role in exporting organic anion, nucleosides, and organic conjugates that are conjugated to GSH, sulphate or glucuronate (P. Borst et al., 2007; P. Borst et al., 2000). However, unlike ABCC1 and 2, the efflux of anticancer drug etoposide mediated by ABCC3 appears unrelated to GSH, and the transport of intracellular GSH is not dependent on ABCC3 (M. Kool et al., 1999; Zelcer, Saeki, Reid, Beijnen, & Borst, 2001). Like ABCC1, ABCC3 is localized to the basolateral membrane in polarized epithelial cells. Its expression has been confirmed in many tissues, including liver, kidney, intestine, adrenals, pancreas, gallbladder and spleen (G. L. Scheffer et al., 2002). ABCC3 expressed on the basolateral surface of hepatocytes can pump organic anions from the liver back into the bloodstream (George L Scheffer et al., 2000). However, the actual expression of ABCC3 in the human liver is varied among individuals. This variation could be partly caused by a single nucleotide polymorphism in the promotor region of *ABCC3* that diminishes the binding of nuclear

factors (Lang et al., 2004). ABCC3 serves as a "backup" system for detoxification of toxic metabolites in the liver when ABCC2-mediated efflux is impaired in a rat model (Donner & Keppler, 2001). Consistent with animal trials, *ABCC3* in the human liver is highly inducible, which is elevated in patients with Dubin-Johnson syndrome whose bile flow is blocked (cholestasis) and functional ABCC2 is absent (P. Borst et al., 2007). Similar to ABCC1, no known human diseases are associated with mutations in the human *ABCC3* gene (Slot et al., 2011). The structure of ABCC3 (Figure 1.6) is consistent with ABCC1, including two NBDs and three MSDs, namely MSD0, MSD1 and MSD2.

ABCC3 conferring low resistance levels to many anticancer drugs such as etoposide, teniposide and vincristine has been found in different transfected cell lines (M. Kool et al., 1999; Zelcer et al., 2001; Zeng, Bain, Belinsky, & Kruh, 1999). This might partly be due to the overlap of ABCC3 substrate specificity with other ABC transporters (Zelcer et al., 2001). *ABCC3* expression is increased in many cancers, including lung cancer, cervical cancer, hepatocellular carcinoma, pancreatic cancer, and breast cancer (Ween et al., 2015). *ABCC3* was significantly elevated in relapse and late-stage ovarian cancers (Auner et al., 2010; Sedlakova et al., 2012). *ABCC3* gene was frequently coamplified with *HER2* oncogene (Partanen et al., 2012). ABCC3 expression was significantly increased in Adriamycin resistant MCF7/AdVp3000 cells, and silencing of *ABCC3* reduced Adriamycin resistance (Y. Liu, Peng, & Zhang, 2005). No increase in ABCC3 expression could be detected after anthracycline treatment in a number of breast cancer cell lines such as MCF7 and BT20 (Faneyte et al., 2004). However, a recent study suggested that the ABCC3 expression was significantly increased in grade III invasive breast ductal carcinoma tissue, as well as in BT474, MCF7, T47D, MDA-MB-231 and HCC1806 breast cancer cells (Balaji et al., 2016). Its overexpression in

transfected MDA-MB-231 and BT474 cells rendered resistance to doxorubicin, and knockdown of *ABCC3* reversed this resistance, indicating its role in therapy-induced resistance in breast cancer (Balaji et al., 2016).

1.5.5 ABCC4

MRP4 (MDR-associated protein 4; aka., ABCC4) was first cloned in 1996 (Allikmets, Gerrard, Hutchinson, & Dean, 1996). It is capable of carrying cellular signalling molecules, including cyclic nucleotides, eicosanoid, urate, and conjugated steroids (Russel et al., 2008), as well as bile salts (Rius, Hummel-Eisenbeiss, Hofmann, & Keppler, 2006). The signalling molecules (e.g., cyclic nucleotides and eicosanoid) are of importance for cellular communication (Russel et al., 2008). The bile salts (e.g., taurocholate, cholate and glycocholate) are co-transported with GSH by ABCC4 (Rius et al., 2006). ABCC4 is typified by a characteristic localization as it can be apically and/or basolaterally expressed in polarized cells (K. Lee, Klein-Szanto, & Kruh, 2000; Rius, Nies, Hummel-Eisenbeiss, Jedlitschky, & Keppler, 2003; Y. Zhang, Schuetz, Elmquist, & Miller, 2004). This localization indicates the dual functions of ABCC4 that it can play a role in both effluxes of substrates into blood and urine and translocation of substrates towards adjacent cells into the extracellular matrix or stroma (Slot et al., 2011). Immunostaining localizes the ABCC4 to many tissues, including prostate, kidney, liver, erythrocytes, adrenal gland, platelets, brain and pancreas in humans (P. Borst et al., 2007; Slot et al., 2011). Its expression in the luminal side of brain capillary endothelium and the basolateral membrane of the choroid plexus epithelium and the astrocytes may be associated with the barrier function at BBB and CSF (Leggas et al., 2004; A. Nies et al., 2004). In human liver, ABCC4 has been proposed to efflux bile

salts into bile by co-transport with GSH during impaired bile salt secretion (Rius et al., 2003). The defective expression of platelet ABCC4 may contribute to selective defect in adenine nucleotide-storage (Jedlitschky et al., 2010). Unlike ABCC1, 2 and 3, the structure of ABCC4 (Figure 1.6) is similar to ABCB1 with two NBDs and two MSDs, namely MSD1 and MSD2.

ABCC4 is related to chemoresistance to many anticancer agents such as thiopurine analogues, methotrexate and topotecan (Slot et al., 2011). *ABCC4* expression is increased in many cancers such as hepatocellular carcinoma, breast cancer, melanoma and lung cancer, while ABCC4 transporter is elevated in oesophageal and prostate cancer (Ween et al., 2015). *ABCC4* expression has been linked with cell growth in many cancers, including prostate tumours, lung cancer, pancreatic cancer, and gastric cancer (L. Chen et al., 2014; Ho et al., 2008; Z. Zhang, Wang, Shen, Peng, & Zheng, 2012; Zhao et al., 2014). Norris et al. (2005) observed that ABCC4 could confer resistance *in vitro* to the topoisomerase I poison irinotecan/CPT-11 and its active metabolite SN-38 (Table 1.4) and high ABCC4 expression might correlate with poor clinical outcomes in patients with primary neuroblastoma. *ABCC4* expression was found up-regulated in post-treatment breast tumours compared with non-neoplastic tissues (Hlaváč et al., 2013). Its expression was found to correlate with ACSL-4 (Acyl-CoA synthetase-4), an enzyme participating in arachidonic acid metabolism, *via* mTOR pathway in MCF7 and MDA-MB-231 cells (Orlando et al., 2019).

1.5.6 ABCG2

BCRP (breast cancer resistance protein; aka., ABCG2) encoded by *ABCG2* is a half ABC transporter and plays its role in drug mediation on the premise of forming either

a homodimer or an oligomer (Gottesman et al., 2002; Sarkadi, Homolya, Szakács, & Váradi, 2006). It was first identified as an ATP-dependent xenobiotic transporter in an anthracycline selected breast cancer cell line (MCF-7/AdrVp) (Doyle et al., 1998). ABCG2 has a significant overlap with ABCB1 and ABCC1 in tissue distribution and substrate specificity. The expression of ABCG2 can be found in stem cells, the apical surface of epithelial cells of the gastrointestinal tract, endothelial cells of the BBB, as well as excretory tissues including liver (i.e., canalicular membrane of hepatocytes), placenta (i.e., placental syncytiotrophoblast cells) and kidney (i.e., proximal tubular cells) (Cooray, Blackmore, Maskell, & Barrand, 2002; Maliepaard et al., 2001; Zhou et al., 2001). Its localization implies its role in limiting absorption, mediation distribution, and facilitating biliary and renal elimination of drugs or xenobiotics (Q. Mao & Unadkat, 2015). For example, the strongly induced ABCG2 in the mammary glands of mice, cows and humans can facilitate the active secretion of clinically and toxicologically substrates (e.g., topotecan) into breast milk (J. W. Jonker et al., 2005). The expression of ABCG2 in specific compartments such as the brain and the placenta can protect the body from xenobiotics and toxic endogenous compounds (Cooray et al., 2002; Johan W Jonker et al., 2000). Inhibition of ABCG2 could increase the oral bioavailability of topotecan in cancer patients from 40 to 97% (Kruijtzer et al., 2002). Furthermore, the reduced activity of ABCG2 has been implicated in the development of gout (O. M. Woodward et al., 2009) and Alzheimer's disease (Xiong et al., 2009). Normally, most observed ABCG2 SNPs are thought to influence mRNA expression or cause a transporter protein with low or absent function (Natarajan, Xie, Baer, & Ross, 2012). For example, the *ABCG2* SNP with a nonsynonymous variant in *ABCG2* at nucleotide 421, substituting lysine for glutamine on position 141 at exon 5, has been suggested to increase the oral bioavailability of topotecan compared with the wild-type

allele (A. Sparreboom et al., 2005). The structure of ABCG2 is different from most other ABC transporters (Figure 1.6). Two features make it a unique transporter that could function as either a homodimer or a heterodimer. First, ABCG2 is a "half-transporter" with only one NBD and MSD, including six transmembrane regions (Q. Mao & Unadkat, 2015). Second, the domains in ABCG2 are arranged in an "NBD-MSD" order, which is opposite to that of other transporters (Q. Mao & Unadkat, 2015). The pumping action of a symmetric homodimer of ABCG2 is similar to ABCB1. The central cavity recognizes and traps cargo. The conformational change of the central cavity allows the release of cargo to the extracellular matrix (Khunweeraphong et al., 2017).

ABCG2 expression is up-regulated in a vast range of cancers, including acute myeloid leukaemia (AML), nasopharyngeal carcinoma, pancreatic ductal adenocarcinoma, breast cancer, adenoid cystic carcinoma, oesophageal cancer, ovarian cancer and tongue cancer (Fletcher, Williams, Henderson, Norris, & Haber, 2016; Ween et al., 2015). The various substrates of ABCG2 (Table 1.4) contain cytotoxic anticancer agents, toxins and carcinogens found in food and some endogenous compounds (Doyle & Ross, 2003; Schinkel & Jonker, 2012). The anticancer drugs mediated by ABCG2 include doxorubicin, daunorubicin, methotrexate, mitoxantrone, topotecan, irinotecan and flavopiridol (Q. Mao & Unadkat, 2015). High levels of ABCG2 expression has been linked to poor clinical outcomes in AML, as previously reviewed (Fletcher et al., 2016). Doyle et al. (1998) observed that ABCG2 expression in human breast cancer cells (MCF-7/AdrVp) could cause chemoresistance by enhancing the efflux of agents such as mitoxantrone, doxorubicin, and daunorubicin. This finding was proved by a subsequent study that ABCG2 has increased around 3000 fold in Adriamycin resistant MCF7/AdVp3000 cells (Y. Liu et al., 2005). Burger et al. (2003) reported that ABCG2

mRNA expression is negatively correlated with response rate and progression-free survival (PFS) in advanced breast cancer patients who received anthracycline-based chemotherapy. The response rate to anthracycline-based regimens in patients of the ABCG2-high subgroup could decrease by 40% to 33% compared with that in patients of the ABCG2-low subgroup at 73% (Burger et al., 2003). ABCG2 expression has been proposed to correlate with HER2 expression by statistical analysis of breast tumour specimens from 196 patients (Xiang et al., 2011). The rs2231137 AA genotype was associated with elevated response to anthracycline-based chemotherapy in ER^+/PR^+ breast cancer patients (H. Wu et al., 2015). The AA genotype of rs2231142 correlated with a higher risk of breast cancer progression in Kurdish patients (Ghafouri et al., 2016). The rs2231137 GA/AA, rs2231143 AA genotypes, and haplotypes rs2231137 A-rs2231142 C or rs2231137 G-rs2231142 A were significantly associated with breast cancer risk in Chinese patients (H. Wu et al., 2015). The rs2231142 AA genotype was associated with elevated response to anthracycline-based chemotherapy in both Kurdish and Chinese breast cancer patients (Ghafouri et al., 2016; H. Wu et al., 2015). The SNP rs2231142 in *ABCG2* was also strongly correlated with axillary lymph node status in Jordanian breast cancer patients (Al-Eitan et al., 2019).

1.5.7 Other ABC Transporter Subfamilies

ABCA Family

The members of ABC transporter A family are mainly expressed in cells of the central nervous and haematopoietic system (Fletcher et al., 2010). ABCA transporters are predominantly responsible for lipid trafficking between cellular compartments and homeostasis (Fletcher et al., 2010). In breast cancer patients, the upregulation of *ABCA1*

and *12* has been associated with poor treatment response (Sarah Park et al., 2006). ABCA4 is significantly increased in Adriamycin resistant MCF7/AdVp3000 cells (Y. Liu et al., 2005). A subsequent study with regard to 68 breast cancer patients found that *ABCA2, 3, 7, 12* were up-regulated in post-treatment tumours compared with non-neoplastic tissues, and *ABCA12* and *ABCA13* were found to present potential modifiers of progression and response to the chemotherapy of breast carcinoma (Hlaváč et al., 2013). However, *ABCA5, 6, 8, 9, 10* were significantly down-regulated in post-treatment breast tumours (Hlaváč et al., 2013). ABCA1 substrates include cisplatin; ABCA2 substrates include methotrexate; ABCA3 substrates include doxorubicin, paclitaxel, cisplatin and methotrexate (Ween et al., 2015). These drugs are currently in use or used to be breast cancer treatments.

ABCB Family (2-11)

The members of ABC transporter B family are known for their role in peptide transport (Fletcher et al., 2010). *ABCB6* has been significantly increased in residual breast cancers after chemotherapy (Sarah Park et al., 2006). *ABCB2, 3, 8, 9, 10* were up-regulated in post-treatment tumours compared with non-neoplastic tissues among 68 breast cancer patients, while *ABCB1, 5, 11* were down-regulated in post-treatment breast tissues (Hlaváč et al., 2013). However, Ji Yeon, Seon-Ah, Yun-Sik, and Jin Woo (2010) illustrated that ABCB5 was up-regulated in the doxorubicin treated MCF-7 cells accompanied by the drug resistance phenotype. ABCB4 substrates include paclitaxel; ABCB5 substrates include doxorubicin and 5-fluorouracil; ABCB8 substrates include doxorubicin; ABCB11 substrates include paclitaxel (Ween et al., 2015). These drugs are front-line regimens in treating breast cancer.

ABCC Family (6-12)

ABC transporter C family is one of the largest subfamilies of ABC transporters. The ABCC proteins exist in various life forms, including plants, marine organisms and unicellular eukaryotes (Slot et al., 2011). This ABC transporter subfamily transports anionic conjugates and exports uncharged hydrophobic compounds (Ween et al., 2015). Like ABCB1, ABCC4, ABCC5, ABCC11 and ABCC12 structurally consist of four domains, including two TMDs (transmembrane domain; aka., membrane-spanning domains, MSDs) and two NBDs (nucleotide-binding domains). However, ABCC1, ABCC2, ABCC3, ABCC6 and ABCC10 have five domains with an extra domain, MSD0, located at the N-terminus (Figure 1.6) (Slot et al., 2011). The NBDs of the ABCC proteins contain some sequence variations that may influence the interaction between these transporters and ATP (Slot et al., 2011). *ABCC10, 11, 12* expressions were reported to be up-regulated in post-treatment breast tumours compared with non-neoplastic tissues, and *ABCC8* was found to play a role in progression and response to the chemotherapy of breast carcinoma (Hlaváč et al., 2013). However, *ABCC6, 9* were significantly down-regulated in post-treatment breast tissues (Hlaváč et al., 2013). ABCC7 has been found significantly down-regulated in primary breast cancer samples, which is associated with the cell invasion and migration of breast cancer cells (J. T. Zhang et al., 2013). ABCC6 substrates include doxorubicin and cisplatin; ABCC10 substrates include doxorubicin, docetaxel, paclitaxel and vinorelbine; ABCC11 substrates include 5-fluorouracil, eribulin and methotrexate (Oba et al., 2016; Ween et al., 2015). These drugs are currently in use or used to be breast cancer treatments.

ABCD Family

The *ABCD* gene encodes peroxisomal half-transporters (ABCD 1-4) (Ween et al., 2015). A recent gene expression study showed that *ABCD1, 3* expressions are up-regulated in post-treatment breast tumours compared with non-neoplastic tissues, and *ABCD2* plays

a role in progression and response to the chemotherapy of breast carcinoma (Hlaváč et al., 2013). However, *ABCD2, 4* expression was significantly down-regulated in post-treatment breast tissues (Hlaváč et al., 2013).

ABCE Family

ABCE family seem to be proteins without transmembrane domain and are responsible for mRNA translation (Fletcher et al., 2010). *ABCE1*, as the only existing ABCE transporter, was up-regulated in post-treatment breast tumours compared with non-neoplastic tissues (Hlaváč et al., 2013). ABCE1 substrates include 5-fluorouracil (Ween et al., 2015), the front-line drug in treating breast cancer.

ABCF Family

ABCF family seem to have no transmembrane domain. It is considered to localize in the cytoplasm and play a role in mRNA translation (Fletcher et al., 2010). *ABCF1, 2, 3* are up-regulated in post-treatment breast tumours compared with non-neoplastic tissues (Hlaváč et al., 2013). A previous study consisting of 191 females with primary breast cancer revealed that ABCF2 expression is negatively correlated with tumour growth and distant metastasis (Ogawa et al., 2006). In patients treated with endocrine therapy, ABCF2-positive tumours had a more prolonged disease-free survival (DFS) when the tumours were estrogen receptor (ER)-negative or progesterone receptor (PR)-negative. These data suggested that ABCF2 may also play a role in the endocrine pathway, which means that apart from ER and PR status, ABCF2 is a potential predictor for response to endocrine therapy in ER- or PR-negative breast tumours (Ogawa et al., 2006).

ABCG Family

ABCG family are also half transporters that exhibit functions on the premise of forming

either homodimers or heterodimers (Ween et al., 2015). *ABCG1* expression was up-regulated in post-treatment breast tumours compared with non-neoplastic tissues (Hlaváč et al., 2013). However, *ABCG5, 8* expression was significantly down-regulated in post-treatment breast tissues (Hlaváč et al., 2013). ABCG1 substrates include doxorubicin (Ween et al., 2015), the front-line drug in treating breast cancer.

1.6 The Role of ABC Transporter in Cancer Development and Metastasis

Although suppressing ABC transporters to overcome drug resistance is central to the development of more potent chemotherapies, the relation of these pumps to cancer initiation and progression deserves special mention. Apart from the drug efflux ability, ABC transporters are possible to have more roles in cancer development. Researchers proposed several potential mechanisms by which some ABC transporters might contribute to cancer cell proliferation and metastasis. Kuss et al. (2002) reported that downregulation of ABCC1 could reduce mitotic index within the neuroblastoma tumours in a xenografted model. Similarly, Katoh, Ueno, and Takakura (2008) found that ABCB1 could positively mediate the proliferation of Colon 26 cells in vitro and suppress tumour growth in a mouse xenograft assay. However, the mechanisms whereby ABCB1 and ABCC1 exert their roles in cell proliferation is still controversial. A possible mechanism of ABCC1 regulating tumour growth is the elevated production and export of S1P (sphingosine-1-phosphate) by ABCC1. The bioactive sphingolipid mediator S1P is a secreted protein that can bind to a family of G protein-coupled receptors (S1PR1-5) to promote cell proliferation, migration, invasion, angiogenesis, and lymphangiogenesis. ABCC1 can thus mediate these features of cancers by

exporting intracellularly generated S1P out of cancer cells and contribute to this "inside-out" signalling (Yamada et al., 2018). Current research has linked *ABCC4* with cell proliferation in lung cancer cell lines (A549 and 801D), suggesting that ABCC4 might play an essential role in controlling A549 and 801D cell growth (Zhao et al., 2014). Same findings have been proposed in cell growth of pancreatic cancer cells (Panc-1 and BxPC-3) (Z. Zhang et al., 2012) and gastric cancer cells (MGC80-3) (L. Chen et al., 2014). A potential mechanism of action is that ABCC4 can negatively mediate intracellular levels of cAMP and cGMP, the second messengers that relay external signals to downstream protein kinases, thus inactivating the cAMP/PKA signalling pathway, which can suppress cell proliferation (Sassi et al., 2008). Similarly, ABCC5 may promote cell proliferation and suppress apoptosis in breast cancer cells by the efflux of cGMP, ultimately inactivating protein kinase G (PKG). But ABCC5 shows no advantages for breast cancer proliferation and survival in end-stage bone metastases (Mourskaia et al., 2012).

Metastatic breast cancer is the major cause of death, as aforementioned. Despite the fact that direct linkage between ABC transporters and breast cancer metastasis is lacking, emerging evidence suggests the potential roles of those proteins in cell invasion, motility and migration of breast cancer cell lines. Miletti-Gonzalez et al. (2005) found that interference with the expression or function of ABCB1 influences the motility and invasion of MCF7 cells. This decrease in migration has been linked to CD44 capping, a membrane receptor associated with cell adhesion, motility and metastases, which could cause CD44 to be less functional (Miletti-Gonzalez et al., 2005). Knockdown of *ABCB1* by siRNA also reduced migration of human melanoma cell line (M14) (Colone et al., 2008). ABCC1 can promote breast cancer metastasis through the export of S1P, as aforementioned (Yamada et al., 2018). Both mRNA and protein levels of ABCC5

were up-regulated in breast cancer skeletal metastases and related to osteoclast formation and breast cancer metastasis to bone (Mourskaia et al., 2012). The substrate of ABCC5 may either promote osteoclastogenesis directly or stimulate this process indirectly through an intermediate cell type present in the bone microenvironment. The locally elevated level of cGMP, which ABCC5 pumps out, can further increase the migration ability of osteoclast. J. T. Zhang et al. (2013) demonstrated that expression of ABCC7 is a potential prognostic indicator in breast cancer and could effectively suppress epithelial-to-mesenchymal transition (EMT). This process is closely related to cancer development and metastatic progression through mediating the breakdown of cell-cell junctions and loss of epithelial polarity. Inhibition of ABCC7 function could enhance cell migration and invasion in MCF-7 breast cancer cells. At the same time, ectopic overexpression of ABCC7 could down-regulate EMT markers and suppress cell invasion and migration in highly metastatic MDA-231 breast cancer cells (J. T. Zhang et al., 2013). They further found that the EMT-suppressing effect of ABCC7 is associated with the ability of ABCC7 to inhibit NFκB targeting urokinase-type plasminogen activator (uPA), which is involved in the regulation of EMT (J. T. Zhang et al., 2013). A similar function has been found by Xie et al. (2013) that ABCC7 expression also plays a role in suppressing cell proliferation, cell invasion and migration of prostate cancer cells. Z. Chen et al. (2010) have linked ABCG2 to cell cycle progression in MCF7/MX cells. Knockdown of ABCG2 remarkably suppressed proliferation of MCF7/MX cells *via* G0/G1 phase arrest (Z. Chen et al., 2010). The *in vivo* studies have also indicated a potential link between ABC transporters and metastasis. ABCC1 has been reported to show a higher staining intensity in lymph node metastases of breast cancer patients than in their corresponding primary tumours (Zochbauer-Muller et al., 2001).

Apart from the role of ABC transporters in metastasis, disruption of the ABC transporters gene also alters tumorigenesis in mouse cancer models. Disruption of the *ABCB1* gene has been implicated in decreasing intestinal polyps and tumour incidence (Mochida et al., 2003). Disruption of the *ABCC1* gene has been linked to reduced tumour incidence and increased tumour latency in mouse models (Henderson et al., 2011). However, the lack of the *ABCG2* gene shortened tumour latency in another study (Zander et al., 2012).

1.7 Inhibition of ABC Transporters to Optimize Chemotherapy

Given the profound impact of ABC transporters on various anticancer drugs in pharmacokinetic profile, it is of great interest to search for efficacious inhibitors. Many agents have been reported as modulators in counteracting ABC transporter induced MDR. For example, Bugde et al. (2017) reviewed the mechanisms and the clinical trials of first- (e.g., verapamil, cyclosporine A, and quinine), second- (e.g., valspodar, dofequidar, and biricodar) and third-generation (e.g., elacridar, laniquidar, zosuquidar, and tariquidar) of ABCB1 inhibitors. The large majority of these agents in reversing MDR are typically limited by either unacceptable toxicity or poor clinical trial results. Because apart from tumour cells, ABCB1 can be expressed by healthy cells and play significant protective roles in barrier organs and tissues (Carlos Cordon-Cardo et al., 1989). Simply suppressing these functions may result in the side effects outweighing any effect on chemoresistance. It is even more difficult to find ideal molecule inhibitors for ABCC1 than for ABCC1 due to the poor penetration of ABCC1 substrates into cells. Furthermore, systemic inhibition of ABC transporter activity is thought to interfere with

vital immune functions and with the efficacy of anti-cancer immune responses, since ABC transporters expressing on immune cells could influence the development and functionality of T-cells and dendritic cells through regulating the secretion of immune regulatory molecules that are associated with intracellular signalling mediating cell differentiation and migration (van de Ven, Scheffer, Scheper, & de Gruijl, 2009). Although the development of traditional ABC transporter inhibitors seems to hit a bottleneck, some synthetically modified natural compounds such as Ningalin analogues, tetrandrine derivatives, and sesquiterpenes derivatives, for example, have been reported to help reverse MDR *in vitro* by inhibiting ABCB1 in different cancer cell lines with high potency and low toxicity (Dantzic et al., 2018). Some currently used drugs for other diseases also show inhibitory effects to given ABC transporters. For example, the uricosuric medication sulfinpyrazone and benzbromarone could inhibit ABCC5 activity (Jan Wijnholds et al., 2000). Metformin is used to improve insulin sensitivity in patients with Type 2 Diabetes Mellitus (DM2). It has been linked to the resensitization of ABCB1 and ABCG2 induced drug resistance in breast cancer cell lines (MCF7, T47D, BT-20 and MDA-MB-231) (Davies et al., 2017). Sulbactam is used for treating dermatological, gynecological, and intraabdominal infections. It could down-regulate the mRNA levels of ABCB1, ABCB5, ABCB8, ABCB10, ABCC1, ABCC2, ABCC3, ABCC4, ABCC5 and ABCG2 that are thought to render resistance to doxorubicin in MDA-MB-231 breast cancer cells, and ABCB1, ABCB5, ABCB8, ABCB10, ABCC1, ABCC2, ABCC3, ABCC5, ABCC10 and ABCG2 in MDA-MB-468 breast cancer cells (Wen, Su, Liou, Lin, & Lee, 2018).

Alternatively, a wide spectrum of biological factors has been linked with alterations in the expression and/or function of ABC transporters. For example, the expression of ABCG2 in MDA-MB-231 breast cancer cells could be increased by KISS1/KISS1R

signalling *via* survivin and AKT-dependent pathways (Blake et al., 2017). Its expression was also positively regulated by ACSL4 (Acyl-CoA synthetase-4), an enzyme related to arachidonic acid metabolism, via mTOR pathway in MCF7 and MDA-MB-231 cells (Orlando et al., 2019). The expression of ABCG2 in MCF7 breast cancer cells could be negatively regulated by p53 through NFκB, a powerful transcription activator (X. Wang et al., 2010). The pro-inflammatory cytokines interleukin-1β (IL-1β), interleukin-6 (IL-6) and tumour necrosis factor-α (TNF-α) have been implicated in ABCG2 expression and function in MCF7 cells (Mosaffa, Lage, Afshari, & Behravan, 2009). IL-1β and TNF-α increased ABCG2 mRNA and protein expression and its activity in MCF7 cells. IL-6 treated cells showed a higher expression level of ABCG2 protein without any influence on mRNA and function. In MCF7 mitoxantrone-resistant derivative MCF7/MX cells, both IL-1β and TNF-α increased ABCG2-mediated efflux but had no effects on mRNA levels. IL-6 showed no influence on ABCG2 protein and mRNA expression in MCF7/MX cells (Mosaffa et al., 2009). In contrast, these pro-inflammatory cytokines were found to reduce ABCG2 mRNA and protein expression and its function in human brain capillary endothelial cells (hCMEC/D3 cell line) (Poller, Drewe, Krahenbuhl, Huwyler, & Gutmann, 2010). X. Wu et al. (2013) proposed that progesterone/nuclear progestin receptor (nPRs) complex could reduce ABCG2 mRNA expression *via* binding to PRE (progesterone response element) in *ABCG2* promoter in human breast cancer T47D cells (PR^+) compared with MDA-MB-231 (PR^-) as a negative control. This suppression of ABCG2 expression was reversed by a progesterone inhibitor (RU-486), and the T47D cells (PR^+) treated with progesterone showed an elevated sensitivity to mitoxantrone which is a substrate of ABCG2 (X. Wu et al., 2013). J. Li et al. (2001) reported that nomegestrol (NOM), a derivation of progestogens, could reverse MDR in MCF7 breast cancer cell line that is resistant to

Adriamycin by reducing mRNA and protein expression of ABCB1 and glutathione S-transferase Pi (GSTπ), and thus increasing the sensitivity of MCF7/ADR cells to Adriamycin. In other investigations, however, the estrogen 17β-estradiol (E_2) was found to up-regulate mRNA and protein expression of ABCG2 *via* the combined binding of ER to p65, an NFκB family member, to the estrogen response element (ERE) and NFκB response element (NFκBRE) respectively in MCF7 cells (Pradhan, Bembinster, Baumgarten, & Frasor, 2010). W. Li et al. (2013) demonstrated that ERβ (estrogen receptor β) up-regulated ABCG2 expression in the presence of 17β-estradiol (E_2) through the interaction between ERβ/E_2 complex and ERE (estrogen response element). With the development of delivery technologies such as nanoparticle carriers (Slastnikova, Ulasov, Rosenkranz, & Sobolev, 2018), the use of antibodies or inhibitors against those intracellular or extracellular regulators of ABC transporters may thus represent a novel strategy to overcome MDR in breast cancer.

1.8 ABC Transporter-Related Collateral Sensitivity

ABC transporters expressed in the plasma membrane are mediators of MDR through pumping out a wide spectrum of chemotherapeutics irrespective of the concentration gradient (Bosch & Croop, 1996; Dean et al., 2001). Thus, the extensive expression of ABC transporters lowered intracellular concentrations of chemotherapeutics to subtherapeutic levels and led to tumour resistance in a wide range of cancers (Ween et al., 2015). However, some ABC transporters are found to play an opposing role in cancer chemoresistance, instead of increasing the survival of cancer cells in the presence of therapeutic agents, through a phenomenon termed collateral sensitivity (CS). The term CS was first proposed in a study by Szybalski and Bryson in 1952 to

describe the hypersensitivity of drug-resistant *Escherichia coli* to other unrelated agents (Szybalski & Bryson, 1952). CS is a type of synthetic lethality in which the genetic alterations accrued that confer resistance to one agent sensitizes the cells to a second agent (Hall, Handley, & Gottesman, 2009). CS thus makes the identified compounds selectively killing MDR cells irrespective of the existence of other MDR mechanisms in cancer cells. As such, apart from CS, the genetic alterations may also lead to unpredictable cross-resistance depending on the gene expression alterations induced during adaptation (Hall et al., 2009). CS can be evaluated most easily *in vitro* by comparing a drug's cytotoxicity (IC50) between the parental line and its resistant sub-line (Hall et al., 2009). The IC_{50} of a drug is normally higher in the MDR line than the parental line, and therefore yield a resistance ratio of > 1 (RR, determined by $RR = \frac{\text{IC50}-\text{resistant line}}{\text{IC50}-\text{parental line}}$). Conversely, a CS agent will show greater efficacy against the MDR line than the parental line, and therefore the RR will be < 1. In the case of both CS and cross-resistance, at least a two-fold effect is probably required to be considered of significance (Hall et al., 2009). The potential mechanisms by which CS agents selectively kill MDA cells include production of ROS *via* futile hydrolysis of ATP, exploitation of energetic sensitivities, extrusion of endogenous substrates which are essential for cell survival, and perturbation of the plasma membrane (Pluchino, Hall, Goldsborough, Callaghan, & Gottesman, 2012).

ROS generation as a hypothesis for CS is based on observations that numerous CS agents are substrates of ABCB1, facilitating ATPase activity and substrate translocation from the intracellular to the extracellular environment. Once back in the extracellular environment, substrates are thought to enter the cells through passive diffusion and repeat the extrusion cycle, a process known as futile cycling, leading to elevated

amounts of cellular ATP hydrolysis (Pluchino et al., 2012). As a result, the increased cellular ATP hydrolysis induces oxidative stress in cells due to either an increase in ROS production from increased oxidative phosphorylation or a depletion in antioxidant defences such as glutathione. The inefficiencies in oxidative phosphorylation result in a reduction of dioxygen to superoxide (O_2^-), which reacts with H_2O_2 to produce hydroxyl radicals (·OH) (Hall et al., 2009). Ultimately, MDR cells initiate apoptosis when the ROS accumulation reaches a certain level (Pluchino et al., 2012). Karwatsky, Lincoln, and Georges (2003) noted that verapamil induces apoptotic cell death in MDR CH^RC5 cells accompanied by elevated levels of ROS and diminished glutathione levels and that CS can be abrogated when ABCB1 function is inhibited by ABCB1 inhibitor PSC833. The *in vivo* circumstance of futile hydrolysis of ATP is unclear since the substrates of ABC transporters in the extracellular environment can be rapidly removed by the circulatory system, compared to the constant exposure to drugs in culture medium *in vitro*. Apart from the ROS generation hypothesis, several compounds that are not ABCB1 substrates have been identified as MDR-selective. This is probably due to the increased sensitivity of ABCB1-expressing cells to changes in energy utilization. Agents that interfere with pathways such as glycolysis or oxidative phosphorylation may thus preferentially kill MDR cells. For example, ABCB1-expressing cells are more prone to be killed by the glycolysis antimetabolite 2-deoxy-D-glucose and the electron transport chain inhibitors rotenone and antimycin A. However, the ability of such compounds to significantly influence cellular ATP stores in MDR cells is not well defined (Pluchino et al., 2012). Furthermore, ABCB1 as a transporter of exogenous xenobiotics is also involved in the translocation of endogenous substrates. Thus, a CS agent may not regulate cytotoxicity directly but somewhat indirectly by stimulating or facilitating the efflux of an endogenous essential molecule or by sensitizing cells to the

loss of a vital metabolite which is an ABCB1 substrate (Pluchino et al., 2012). Some CS agents are also found to induce membrane perturbation to a greater extent in ABCB1-expressing cell lines (Pluchino et al., 2012). This phenomenon links CS agents to the changes in structure and fluidity of the membrane. A significant reduction in lipid structural order (i.e., membrane fluidity) was observed in the colchicine resistant B30 cell line with the treatment of CS agents pentazocine and verapamil. In addition, the hydrophobic nature of verapamil, pentazocine, pethidine and naloxone and their ability to intercalate into the lipid bilayer could cause leakage of the polar fluorescent dye 6-CF through the cell membrane (Pluchino et al., 2012).

However, apart from the underlying mechanisms mentioned above, CS agents are likely to act their roles through alternative mechanisms such as enhanced uptake by ABCB1-expressing cells or altered intracellular drug trafficking (Pluchino et al., 2012). The validation of CS agents against MDR cells should not be limited to ABCB1-expressing cells but include those expressing other transporters such as the ABC transporter C subfamily (Hall et al., 2009). It seems that a unified mechanism that can account for all CS is non-existent, and more work remains to uncover the mechanism of action of agents related to CS. The development of CS agents is quite promising because adjuvant administration of CS agents may help prevent MDR during traditional chemotherapeutic regimens. The use of CS agents may also resensitise resistant tumours to commonly employed therapeutics through selective elimination of MDR cells in a heterogeneous tumour population. Given that MDR is able to induce relapse and progression of most malignant tumours and remains a significant impediment to successful chemotherapy, the exploitation of MDR by CS compounds provides a novel strategy against MDR tumours.

1.9 Hypothesis and Amis of Thesis

Triple-negative breast cancer is one of the leading causes of death worldwide, especially in New Zealand; over 3,000 new cases and more than 650 deaths are reported annually (New Zealand Ministry of Health, 2016a). However, treatment for TNBC patients is currently limited due to the development of resistance to chemotherapies and stimulated metastases. It has become clear that ABC transporters could directly pump out chemodrugs to render chemoresistance in cancer development and progression. Their overexpression is thus associated with poor clinical outcomes of cancer patients and serves as a convincing predictor for patients' response to chemotherapy in given cancer types. Accumulating evidence also defines the role of some ABC transporters in cancer cell proliferation, invasion, and migration. These have suggested that ABC transporters may independently regulate many dominant features of cancers and represent a promising target to overcome chemoresistance, progression and metastasis of cancers. ABCC5 has been up-regulated in post-treatment (neoadjuvant chemotherapy) breast tumours compared with non-neoplastic tissues (Hlaváč et al., 2013). Its expression is related to not only doxorubicin resistance but also breast cancer skeletal metastases (Mourskaia et al., 2012; Y. Zhu et al., 2011). However, with doxorubicin as a current front-line drug for breast cancer and olaparib as a recently approved PARPi, very few studies have directly addressed the role of ABCC5 in the efficacy of olaparib and olaparib/doxorubicin combination in breast cancers. Hence, the current study tested the hypothesis that ABCC5 transports doxorubicin and olaparib in breast cancers, thereby control the amount of these drugs accumulated in cells and reduce their sensitivity to these drugs. This study further tested the role of ABCC5 in breast cancer metastases in an *ABCC5* gene knockout breast cancer cell model.

In this thesis, firstly, the association of ABCC5 and breast cancer outcomes, the expression status of ABCC5 in breast cancer, and co-expression of *ABCC5* in breast cancer were examined using Oncomine datasets. It was crucial to determine whether ABCC5 exists in the interested breast cancer cells and affects breast cancer patients' clinical outcomes.

The thesis then studied the role of ABCC5 in the potency of doxorubicin and olaparib in ABCC5-overexpressing HEK293 cells (HEK-MRP5) and its isogenic control cell line (HEK-P). HEK293 cells are referred to as human embryonic kidney cells, with cellular structure and functions comparable to *in vivo* circumstances. This cell model includes an ABCC5-overexpressing line (HEK-MRP5) and an isogenic parental line (HEK-P), in which the functional expression of ABCC5 was examined by measuring the cellular accumulation of a typical fluorescent substrate 2′,7′-Bis(2-carboxyethyl)-5(6)-carboxyfluorescein (BCECF). The isogenic HEK293 cell pair was used as a "clean system" to determine the role of ABCC5 in doxorubicin and olaparib sensitivity. Published data regarding the role of ABCC5 in the translocation of doxorubicin were well defined. A number of studies have reported that doxorubicin is a substrate of ABCC5, as reviewed by Ween et al. (2015). But no studies were done to examine the relation between ABCC5 and olaparib. Cellular accumulation of doxorubicin and BCECF was determined and the effect of olaparib and/or doxorubicin on cell viability measured by using MTT assay.

Lastly, this thesis examined the role of ABCC5 in determining the potency of doxorubicin, olaparib and doxorubicin/olaparib combination and in clonogenicity in a panel of *ABCC5* gene knockout human breast cancer cell lines. Stable breast cancer cell lines with *ABCC5* deleted were generated using sgRNA guided CRISPR-associated Cas9 nuclease (CRISPR-Cas9) gene-editing technology, followed by limiting dilution,

cell uptake study, PCR, sequencing and flow cytometric analysis of surface staining of ABCC5 protein. These stable cell lines were then used in *in vitro* assays to investigate the effects of altered ABCC5 levels on cell sensitivity to selected drugs. Functional expression of ABCC5 was assessed by 1) measuring the cellular accumulation of a typical fluorescent substrate BCECF; and 2) determining the anti-proliferation effects of doxorubicin, olaparib and doxorubicin/olaparib combination in control and *ABCC5* knockout cells. A pharmacological study was performed to fully investigate the impact of selected drugs on tumour sensitivities through assays, including cell proliferation (i.e., MTT assays) and clonogenicity of breast cancer cells (i.e., colony formation assays).

Chapter 2. Material and Methods

2.1 Chemicals

The chemical compounds, reagents, buffers, solutions, consumables, and kits used in this study, together with their suppliers and catalogue numbers, were listed below in Table 2.1. All the instruments used in this study were provided by the Applied Sciences Laboratory in Auckland University of Technology (AUT).

Table 2.1 The chemical compounds, reagents, buffers, solutions, consumables, and kits used in this study with their suppliers.

Chemicals	Suppliers	Catalogue No.
Acid-Phenol: Chloroform, pH 4.5 (with IAA, 125:24:1)	Invitrogen, NZ	AM9720
Agarose RA™	VWR Life Science, US	N605-500G
Alexa Fluor® 488 Annexin V/Dead Cell Apoptosis Kit	Invitrogen, NZ	V13241
Anti-Kiss1 receptor antibody	Abcam, NZ	ab137483
Anti-Mouse IgG (whole molecule) – Peroxidase antibody produced in rabbit	Sigma-Aldrich, NZ	A9044-2ML
BCECF-AM (2′,7′-Bis(2-carboxyethyl)-5(6)-carboxyfluorescein acetoxymethyl ester)	ThermoFisher Scientific, NZ	B8806-1MG
Beckman Coulter Blue Test Tube (12X75 mm)	Beckman Coulter, CA	2523749
Benzbromarone	Sigma-Aldrich, NZ	B5774-1G
Bovine serum albumin (BSA) (powder)	AUT Chemistry Lab	-
Collagen Coating Solution	Sigma-Aldrich, NZ	125-50
cOmplete™, Mini, EDTA-free Protease Inhibitor Cocktail	Sigma-Aldrich, NZ	4693159001
Crystal Violet	Sigma-Aldrich, NZ	C6158-100G
CutSmart™ Buffer	Biolabs, NZ	B7204S
DC Protein Assay Reagents Package	BIO-RAD, NZ	5000116
DEPC-treated water	Bioline, USA	BIO-38030
Donkey Anti-Mouse IgG (H+L) Highly Cross-Adsorbed Secondary Antibody, HRP	ThermoFisher Scientific, NZ	A16017
Apoptosis Kit with Annexin V Alexa Fluor™ 488 & Propidium Iodide (PI)	ThermoFisher Scientific, NZ	V13241
DMSO (dimethyl sulfoxide) (99.7%)	ThermoFisher Scientific, NZ	FSBBP231-1
Dithiothreitol (DTT)	BIO-RAD, NZ	1610610
Doxorubicin Hydrochloride	Abcam, NZ	Ab120629
EcoR1	Biolabs, NZ	B0101S
Ethanol absolute	ThermoFisher Scientific, NZ	AJA214-20L
Foetal Bovine Serum (FBS)	Medi'Ray, NZ	MG-FBS0820-500ML
GeneArt™ Genomic Cleavage Detection Kit	Life Technologies, NZ	A24372
Geneticin™ Selective Antibiotic (G418 Sulfate)	ThermoFisher Scientific, NZ	11811031
Goat Anti-Rabbit IgG H&L (DyLight® 488)	Abcam, NZ	ab150077
Goat anti-Rabbit IgG (H+L) Secondary Antibody, HRP	ThermoFisher Scientific, NZ	65-6120

Goat Anti-Rat IgG H&L (Alexa Fluor® 488)	Abcam, NZ	ab96887
Goat Anti-Rat IgG (H+L) Secondary Antibody, HRP	Invitrogen, NZ	62-9520
Greiner high and medium binding 96 black well plate	Sigma-Aldrich, NZ	M5061
Hanks' Balanced Salt Solution (HBSS) (1X)	ThermoFisher Scientific, NZ	14175095
Hexadimethrine bromide	Sigma-Aldrich, NZ	H9268
Isopropanol, Optima™ LC/MS Grade	Fisher Chemical™	A4614
L-Glutamine	Life Technologies, NZ	20530081
LightCycler® EvoScript RNA SYBR® Green I Master	Roche Diagnostics N.Z., Ltd.	07800134001
Lipofectamine™ CRISPRMAX™ Cas9 Transfection Reagent	ThermoFisher Scientific, NZ	CMAX00003
Lipofectamine™ RNAiMAX reagent	Invitrogen, NZ	13778
Laemmli Sample Buffer (4X)	BIO-RAD, NZ	1610747
LB agar	Life Technologies, NZ	22700-025
Memcode™ Reversible Protein Stain Kit	ThermoFisher Scientific, NZ	24585
Mem-PER™ Plus Membrane Protein Extraction Kit	ThermoFisher Scientific, NZ	89842
Methanol	Sigma-Aldrich, NZ	34860
Milli-Q water	AUT Chemistry Lab	-
Mini-PROTEAN® TGX™ Precast Gel (10%)	BIO-RAD, NZ	4561034
MISSION® pLKO.1-puro Non-Mammalian shRNA Control Transduction Particles	Sigma-Aldrich, NZ	SHC002V
Monoclonal Anti-β-Actin Antibody Produced in Mouse	Sigma-Aldrich, NZ	A2228
MRP5 Monoclonal Antibody (M5I-1)	Invitrogen, NZ	MA1-35683
MTT (3-(4,5-dimethylthiazol-2-yl)-2,5-diphenyltetrazolium bromide)	Sigma-Aldrich, NZ	M2128-1G
Nail Polish	Mode Cosmetics	-
Normal Goat Serum	Invitrogen, NZ	PCN5000
Not1	Biolabs, NZ	R3189
Olaparib	Sapphire Bioscience, AUS	S1060
Opti-MEM™ I Reduced Serum Medium	ThermoFisher Scientific, NZ	31985070
Paraformaldehyde	Sigma-Aldrich, NZ	P6148-500G
Pemetrexed	Juno Pharmaceuticals NZ Ltd	-
Penicillin-Streptomycin (10000 U/mL)	Life Technologies, NZ	15140122
Phosphate buffer saline (PBS) pH7.4 (10X)	ThermoFisher Scientific, NZ	70011044
Plasmid	OriGene Technology, Inc	-
Precision Plus Protein™ Kaleidoscope™ Standards	BIO-RAD, NZ	1610375
Primers	Integrated DNA Technologies / ThermoFisher Scientific, NZ	-
ProLong™ Diamond Antifade Mountant with DAPI	Invitrogen, NZ	P36962
Purified BSA 100X	Biolabs, NZ	B9001S
Puromycin Dihydrochlarid	ThermoFisher Scientific, NZ	A1113803
PVDF (polyvinylidene fluoride) membrane	Life Technologies, NZ	22860
Rat IgG2α Isotype Control	ThermoFisher Scientific, NZ	PA5-33214
Recovery™ Cell Culture Freezing Medium	Life Technologies, NZ	12648010
RIPA Lysis and Extraction Buffer	ThermoFisher Scientific, NZ	89901
RPMI-1640 Medium, no glutamine	Life Technologies, NZ	21870092
RPMI-1640 Medium, no glutamine, no phenol red	ThermoFisher Scientific, NZ	32404014
QIAamp DNA Mini Kit	QIAGEN, Germany	51306
QIAGEN Plasmid Maxi Kit	QIAGEN, Germany	12165
QIAquick® Gel Extraction Kit	QIAGEN, Germany	28704
Saponin	Sigma-Aldrich, NZ	47036-50G-F
SDS (Sodium dodecyl sulphate)	AUT Chemistry Lab	-
sgRNA (*ABCC5*)	Integrated DNA Technologies	Hs.Cas9.ABCC5.1.AC
sgRNA (*ABCC5*) set1	ThermoFisher Scientific, NZ	CRISPR826999_CR
sgRNA (*ABCC5*) set2	ThermoFisher Scientific, NZ	CRISPR826959_CR
sgRNA (*ABCC5*) set3	ThermoFisher Scientific, NZ	CRISPR827002_CR
shRNA lentiviral particle	Sigma-Aldrich, NZ	TRCN0000060307
Sodium azide	AUT Chemistry Lab	-
Sodium Chloride (NaCl) (ReagentPlus®, ≥99%)	Sigma-Aldrich, NZ	793566-1KG
Sodium Bicarbonate ($NaCO_3$) (ReagentPlus®,	Sigma-Aldrich, NZ	S8875-500G

≥99.5%)		
SPAG5 Mouse Monoclonal Antibody (Clone ID: OTI3F10)	OriGene Technology, Inc	TA810452
Stealth siRNAs for ABCC5 set1	Invitrogen, NZ	HSS173353
Stealth siRNAs for ABCC5 set2	Invitrogen, NZ	HSS115284
Stealth siRNAs for ABCC5 set3	Invitrogen, NZ	HSS173354
SuperSignal™ West Pico PLUS Chemiluminescent Substrate	ThermoFisher Scientific, NZ	34578
SYBR™ Gold Nucleic Acid Gel Stain (10000X)	ThermoFisher Scientific, NZ	S11494
TaKaRa PCR Amplification Kit	TaKaRa Bio USA, Inc.	R011
Target2™ PTFE Syringe Filters	ThermoFisher Scientific, NZ	F2500-3
TBE Buffer (Tris-borate-EDTA) (10X)	ThermoFisher Scientific, NZ	B52
Terumo Syringe 1ml-27g x ½"	NZSafetyBlackwoods	6003636
TrackIt™ 100 bp DNA Ladder (100 bp-2,000 bp)	Life Technologies, NZ	10488058
Trans-Blot® Turbo™ 5X Transfer buffer	BIO-RAD, NZ	-
Tris-EDTA Buffer Solution (TE buffer)	Sigma-Aldrich, NZ	93283-100ML
Tris/Glysine/SDS Buffer (10X) (Running buffer)	BIO-RAD, NZ	1610772
TRIzol™ Reagent	Invitrogen, NZ	15596018
Trypan Blue Solution, 0.4%	ThermoFisher Scientific, NZ	15250061
TrueCut Cas9 Protein V2	ThermoFisher Scientific, NZ	A36499
TrypLE™ express	ThermoFisher Scientific, NZ	12604021
Trizma® Base (Tris-base)	Sigma-Aldrich, NZ	T1503-1KG
Tris-HCl Buffer (0.5 M, pH6.8)	BIO-RAD, NZ	1610799
Triton™ X-100	Sigma-Aldrich, NZ	T8787-250ML
TurboFect Transfection Reagent	ThermoFisher Scientific, NZ	R0531
Tween 20 Solution (10%)	BIO-RAD, NZ	1610781
1 µ-Slide 8 well ibiTreat Microscopy Chamber	ibidi Technologies	80806

MTT powder was dissolved in 1X PBS at a concentration of 12 mM. MTT solution was appropriately filtered and stored at 4 °C for up to 2 weeks.

Benzbromarone powder (Sigma-Aldrich, NZ) was dissolved in DMSO at a concentration of 200 mM and stored at -20 °C.

Pemetrexed powder (Juno Pharmaceuticals NZ Ltd) was dissolved in 1X PBS at a concentration of 200 mM and stored at -20 °C.

Doxorubicin powder (Abcam, NZ) was dissolved in *Milli-Q* water at a concentration of 40 mM and stored at -20 °C.

Olaparib powder (Sapphire Bioscience, AUS) was dissolved in DMSO at a concentration of 50 mM and stored at -20 °C.

2.2 Cell Lines and Cell Culture

2.2.1 HEK293 (Human Embryonic Kidney-293) Cell Lines

The parental HEK293 (HEK-P) and ABCC5-overexpressing HEK293 cells (HEK-MRP5) were kindly provided by Dr. Yan Li. The consistent expression of ABCC5 in HEK-MRP5 cells was confirmed using cell uptake study (section 2.7.2.1) every 1 to 2 months.

2.2.2 Human Breast Cancer Cell Lines

The breast cancer cell lines, MDA-MB-231 (ATCC® HTB-26™), BT549 (ATCC® HTB-122 ™), MCF7 (ATCC® HTB-22™), T47D (ATCC® HTB-133™) and SKBR3 (ATCC® HTB-30™) were purchased from ATCC (Cryosite Ltd, NSW, AU).

2.2.3 Cell Culture

Cell lines including HEK293, MDA-MB-231, MCF7, T47D, SKBR3 and BT549 were grown in RPMI-1640 medium supplemented with 10% FBS, 1% penicillin-streptomycin, and 1% L-glutamine. Cells were cultured as general cell culture protocol at 37 °C supplied with 5% carbon dioxide in a humidified incubator (Forma™ Series II 3110 Water-Jacketed CO_2 Incubator; Thermo Fisher Scientific, Inc). Cells were routinely passaged at around 90% confluence and discarded when they achieved either passage number of 30 or a culture period of 3 months.

PBS, TrypLE™ and complete medium (CM) were pre-warmed in a water bath. The old culture medium was discarded carefully with the aid of a pipette. The cells were then washed with 3 mL (T25 flask) or 5 mL (T75 flask) of sterile pre-warmed PBS, followed

by detachment by adding 1 mL (T25 flask) or 2 mL (T75 flask) of TrypLE™ into the culture flask. The flask was kept in an incubator for 0.5 to 5 min depending on cell type (i.e., HEK293 cells for 0.5 min, MDA-MB-231 and BT549 cells for 2 min, MCF7 and SKBR3 cells for 3 min, and T47D for 5 min). An aliquot of 2 mL (T25 flask) or 4 ml (T75 flask) of CM was then added into the culture flask to stop trypsinization. The cells were gently suspended and transferred to a 15 ml centrifuge tube and centrifuged at 200 × *g* for 5 min. The supernatant was carefully removed, and the cell pellet was resuspended by using 1 mL of CM. In order to maintain these cell lines, about 5 to 10% of the cell suspension was transferred to a new cell culture flask with 6 mL (T25 flask) or 15 mL (T75 flask) of fresh CM.

2.2.4 Freezing Cells

For optimum results, cells were in the mid-log phase of growth with > 90% viability at the time of freezing. The cell lines used in this study were frozen using commercial freezing medium (Recovery™ Cell Culture Freezing Medium) and cryopreserved in -80 ℃ freezer (Model: 5905; ThermoFisher Scientific, Inc) as common stock, and master stock of each cell line was stored in a proper liquid nitrogen tank (Taylor Wharton HC35 Cryogenic Refrigerator With 11-in). A self-prepared freezing medium, as shown in Table 2.2, was used when the commercial one was out of stock.

Table 2.2 Recipe of self-prepared freezing medium.

RPMI-1640 medium	70%
FBS	20%
Filtered DMSO	10%

Freezing medium was thawed and pre-warmed in a water bath. Cells were detached, centrifuged and resuspended as the method shown in section 2.2.3. The viable cells were counted and calculated using the method in section 2.2.6. The cells were then spun down, and the supernatant was carefully removed. The cell pellet was resuspended with a proper volume of ice-cold freezing medium to reach a certain ratio of 1×10^6 cells in 1 mL of freezing medium. An aliquot of 1 mL cell suspension containing 1×10^6 cells was dispensed into a new cryovial. The cryovial was immediately placed and kept in a -80 °C freezer for short term storage. Otherwise, after 24 hours, the cryovials were transferred into a liquid nitrogen tank for long term storage.

2.2.5 Thawing Cells

CM was pre-warmed in a water bath. The cryovial containing frozen cells was taken out from -80℃ freezer (Model: 5905; ThermoFisher Scientific, Inc) or liquid nitrogen tank (Taylor Wharton HC35 Cryogenic Refrigerator With 11-in) and immediately placed into a 37 ℃ water bath. The cells were thawed quickly (< 1 minute) by gently swirling the cryovial in the 37 ℃ water bath until there was just a tiny bit of ice left. The cells were then transferred dropwise to a 15 mL centrifuge tube containing 9 mL of pre-warmed CM, and centrifuged at 200 × *g* for 5 min. The supernatant was carefully removed, and the cell pellet was resuspended with 1 mL of CM. The cell suspension was transferred to a new cell culture flask with 6 mL (T25 flask) or 15 mL (T75 flask) of fresh CM.

2.2.6 Cell Counting

Cells were detached, centrifuged, and resuspended as the method shown in section 2.2.3.

10 µL of cell suspension was mixed with 10 µL of 0.4 % Trypan Blue Solution on a piece of parafilm. An up to 40 µL of 0.4 % Trypan Blue Solution was added when the cell density was high. 10 µL of the mixture was then added to a haemocytometer (Neubauer Improved; BOECO Germany) until the chamber under the coverslip was filled. After counting the cells in 4 square areas (Figure 2.1), the total number of cells in 1 ml culture medium was calculated by the following equation.

$$\text{Number of cells/ml} = \text{Average number of cells per square} \times N \times 10^4$$

N = The proportion of 10 µL cell suspension dilution from Trypan Blue Solution (e.g., N = 2 when10 µL of cell suspension was mixed with 10 µL of Trypan Blue Solution; N = 5 when 10 µL of cell suspension was mixed with 40 µL of Trypan Blue Solution)

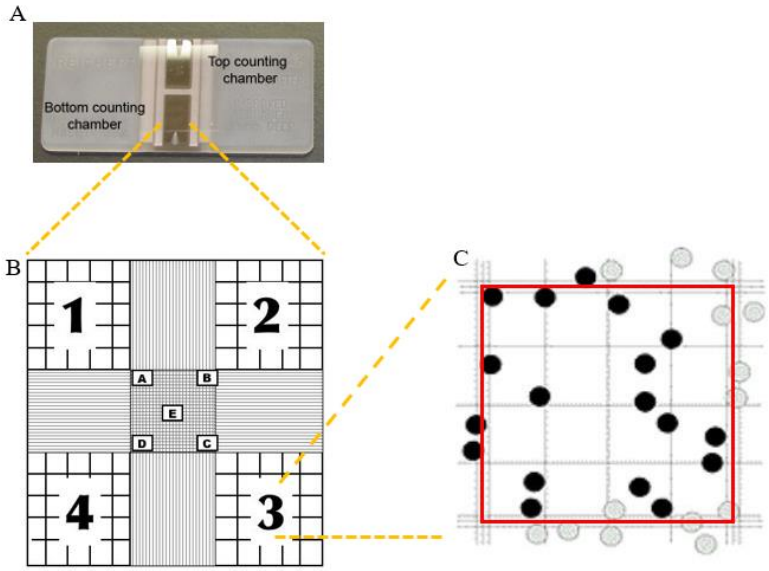

Figure 2.1 Cell counting using a haemocytometer. ***A.*** Schematic representation of a haemocytometer. ***B.*** The four counting squares of a haemocytometer. Each of the four squares is 1 square millimetre in size and represents a total volume of 0.1 mm^3 or 10^{-4} mL. ***C.*** Counting cell numbers in the red counting square. Include the cells that mount on the left and top borders and ignore those that mount on the right and bottom. The dark dots represent the cells that should be counted, and the grey ones represent those that should not be counted. The viable cells are not stained by Trypan Blue Solution, while the dead ones get stained and show a blue colour.

2.3 CRISPR-Cas9 Gene Editing Technology

2.3.1 Ribonucleoprotein-Based Transfection

In this study, a CRISPR-Cas9-based method was used to knock out the ABCC5 gene in MDA-MB-231, BT549 and MCF7 human breast cancer cell lines. A specific sgRNA was designed in complex with Cas9 protein forming ribonucleoprotein (RNP), which was delivered into cells through endocytosis. The specific chromatin region was identified by sgRNA and cleaved by Cas9 protein. The DSBs were reconnected by the error-prone nonhomologous end-joining DNA repair route (NHEJ), and the formation of frameshift might thus lead to *ABCC5* gene deletion.

Cells were seeded into a 12-well plate at a density of 1×10^5 cells/well (nearly 38% confluence) in CM 24-hr prior to transfection. *ABCC5*-sgRNA, TrueCut™ Cas9 Protein v2 and Lipofectamine™ Cas9 Plus™ reagent were gently mixed with Opti-MEM™ I reduced serum medium in a fresh and RNAse-free microcentrifuge tube (tube 1) according to the manufacturer's instruction (Lipofectamine™ CRISPRMAX™ Cas9 Transfection Reagent) (Table 2.3). *ABCC5*-sgRNA (IDT technology) target genomic sequence was "AGATCCACACAACCCTTCGC" (genomic loci: exon5 183987840-183987860). A 1:3 molar ratio of TrueCut™ Cas9 to sgRNA was used in this study, which was found to give the highest gene editing efficiency in our previous work. In order to examine the influence of sgRNA and Cas9 protein on ABCC5 expression, two control groups were added in this study, as shown in Table 2.3.

Table 2.3 Preparation of tube 1.

Tube 1	Reagent	Volume
RNA only control group	Opti-MEM™ I reduced serum medium	150 µL
	ABCC5-sgRNA	45 pmol
Cas9 only control group	Opti-MEM™ I reduced serum medium	150 µL
	TrueCut™ Cas9 Protein v2	15 pmol
	Lipofectamine™ Cas9 Plus™ reagent	5 µL
Knockout group	Opti-MEM™ I reduced serum medium	150 µL
	TrueCut™ Cas9 Protein v2	15 pmol
	ABCC5-sgRNA	45 pmol
	Lipofectamine™ Cas9 Plus™ reagent	5 µL

Three microlitre of Lipofectamine™ CRISPRMAX™ reagent was diluted in 50 µL of Opti-MEM™ I reduced serum medium (tube 2) followed by a 1 min incubation at room temperature. The diluted Lipofectamine™ CRISPRMAX™ reagent in tube 2 was then added into tube 1. The transfection complex was mixed thoroughly and incubated for 15 min at room temperature, and then added to the adherent cells. The medium containing transfection complex was removed after 48-hr incubation and replaced with fresh CM. The transfected cells were validated and screened as the methods shown in section 2.4.

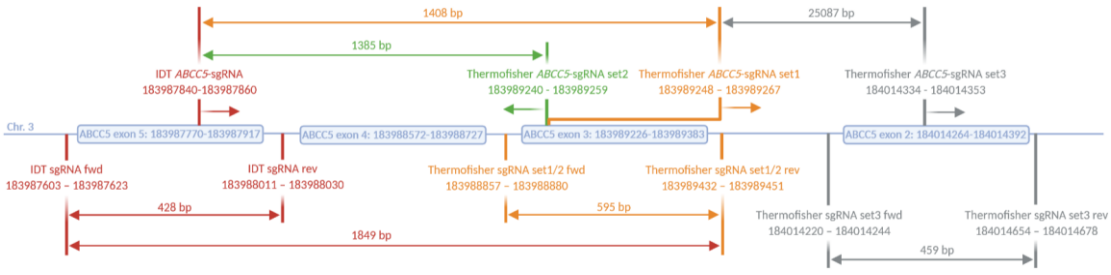

Figure 2.2 *ABCC5* sgRNAs and primers used in this study. *Created with BioRender.com.*

A 2nd round of knockout using a combination of IDT *ABCC5*-sgRNA plus Thermofisher

ABCC5-sgRNA set1 (“TCAGAGCACTCAAGCCATGA”; genomic loci: exon3 183989248 – 183989267) or IDT *ABCC5*-sgRNA plus Thermofisher *ABCC5*-sgRNA set2 (“TGAGTGCTCTGAAGCCCATC”; genomic loci: exon3 183989240 - 183989259) was done in order to delete WT allele when only heterozygous KO clones were isolated (Figure 2.2). Thermofisher *ABCC5*-sgRNA set3 (“ACACTTCTATACCCAGGACT”; genomic loci: exon2 184014334 - 184014353) was not adopted due to its distant genomic loci from other sgRNAs (Figure 2.2). The recipe of tube 1 for 2nd round of knockout is shown in Table 2.4. A DNA fragment of around 1408 (IDT *ABCC5*-sgRNA + Thermofisher *ABCC5*-sgRNA set1) / 1385 bp (IDT *ABCC5*-sgRNA + Thermofisher *ABCC5*-sgRNA set2) was knocked out.

Table 2.4 Preparation of tube 1 for 2nd round of knockout.

Tube 1	Reagent	Volume
2nd round of Knockout	Opti-MEM™ I reduced serum medium	150 μL
	TrueCut™ Cas9 Protein v2	15 pmol
	IDT *ABCC5*-sgRNA	22.5 pmol
	Thermofisher *ABCC5*-sgRNA set1 or set2	22.5 pmol
	Lipofectamine™ Cas9 Plus™ reagent	5 μL

2.3.2 Plasmid-Based Transfection

2.3.2.1 Heat Shock Bacterial Transformation

The plasmids (pCasG-SPAG5-gRNA1, pCasG-SPAG5-gRNA2, pUC-SPAG5 donor Luciferase-puro, pUC-SPAG5 donor GFP-neo and pCMV6-Entry-SPAG5-Myc-Flag) used in this study were designed and purchased from OriGene Technology, Inc. Heat shock bacterial transformation was employed to amplify the plasmids used for *SPAG5* gene knockout and knockin. JM109 competent cells (100 μL) were incubated on ice for 30 min prior to transformation, followed by exposure to 2 – 5 ng plasmid DNA on ice for 30 min. Heat shock transformation of JM109 competent cells required the cells

undergoing a heat-pulse (0 ℃ - 43 ℃) plus a cold-shock (43 ℃ - 0 ℃). The heat-pulse leads to a decrease in cell membrane fluidity, allowing the import of plasmid DNA into cells. A subsequent cold-shock restores the fluidity of the cell membrane, thus preventing the efflux of plasmid DNA. The JM109 competent cells that acquired ampicillin-resistant gene were then kept in ice water for 2 min and immediately streaked on an LB agar plate containing 40 mL LB broth with ampicillin at a concentration of (50 μL/mL). LB agar plate containing JM109 competent cells was incubated overnight at 37 ℃. Single-cell colonies were picked up with the aid of pipette tips and inoculated into 10 mL of LB medium containing 50 μL/mL ampicillin. The cells were allowed to grow for approximately 8 hours at 37°C with vigorous shaking at 200 RPM until the medium became turbid. The starter culture LB medium was then transferred to 1000 mL of LB medium containing 100 μL/mL ampicillin and incubated at 37 ℃ for 12 to 16 hours with vigorous shaking at 200 RPM until the medium was completely turbid. The LB medium containing transformed JM109 competent cells were proceeded to the extraction of plasmid intermediately or stored at – 20 ℃.

2.3.2.2 Extraction and Purification of Plasmid

The plasmid DNA from transformed JM109 competent cells were extracted and purified by using QIAGEN Plasmid Maxi Kit (QIAGEN, Germany) according to the manufacturer's instruction. The JM109 competent cells obtained from section 2.3.2.1 were centrifuged at 6000 × *g* for 15 min at 4 ℃. The bacterial pellet was resuspended in 10 mL Buffer P1 containing RNase A (100 μg/ml) and LyseBlue (1:1000). Buffer P2 was then added and mixed thoroughly to lyse the cells at room temperature (15–25°C) for 5 min. The lysate was neutralized by adding acidic potassium acetate Buffer 3, followed by incubation on ice for 20 min. The lysate was centrifuged at 20000 × *g* for

30 min at 4 ℃. The supernatant containing plasmid DNA was promptly removed and centrifuged again at 20000 × *g* for 30 min at 4 ℃. The supernatant containing plasmid DNA was applied to pre-equilibrated QIAGEN-tip 500 that was washed with Buffer QBT and emptied by gravity flow. The supernatant was allowed to enter the resin by gravity flow, and the plasmid DNA was supposed to attach to the resin. The QIAGEN-tip was washed twice with 30 mL Buffer QC, which moved through the QIAGEN-tip by gravity flow. The plasmid DNA was then eluted using 15 mL Buffer QF and precipitated by adding 10.5 mL isopropanol, followed by centrifugation at 15000 × *g* for 30 min at 4 ℃. The plasmid DNA pellet was washed with 5 mL of 70% ethanol and centrifuged at 15000 × *g* for 10 min. The supernatant was carefully removed, and the pellet was air-dried for 5 – 10 min and redissolved in 0.5 mL TE buffer. The purified plasmid DNA concentration was measured using the NanoDrop® ND-1000 UV spectrophotometer (NanoDrop Products, USA). The purity was determined by the A260/A280 and A260/A230 ratios. An A260/A280 ratio between 1.8 and 2.0 and an A260/A230 ratio higher than 2.3 were considered as relatively pure dsDNA.

2.3.2.3 Restriction Enzyme Digestion

To check the quality of amplified plasmid DNA, restriction enzyme digestion was employed to cleave the pre-designed cleavage sites in the plasmid. The cleaved bands were separated and visualized by subsequent agarose gel electrophoresis. 12 μL of plasmid DNA was mixed with 2 μL of CutSmart™ Buffer, 0.2 μL Purified BSA 100X, and 0.2 μL EcoR1 or Not1 enzyme. The mixture was brought to a final volume of 20 μL with *Milli-Q* water. The digestion was done at 37 ℃ for 1 hour, followed by agarose gel analysis as the method shown in section 2.4.3.

2.3.2.4 Transfection

In this study, a CRISPR-Cas9-based method was used for the knockout of SPAG5 gene in BT549, T47D, SKBR3 and MCF7 human breast cancer cell lines. A specific plasmid containing sequence encoding gRNA and Cas9 protein and a donor plasmid were delivered into cells through endocytosis. The specific chromatin region was cleaved by Cas9 protein. The DSBs were repaired by the homology-directed repair DNA repair route (HDR) with the integration of donor sequence.

Cells were seeded into a 6-well plate at a density of 3 - 5 × 10^5 cells/well (nearly 70% confluence) in CM 24-hr prior to transfection. The plasmid containing gRNA sequence, donor plasmid and TurboFect Transfection Reagent were gently mixed with Opti-MEM™ I reduced serum medium in a fresh and RNAse-free microcentrifuge tube according to the manufacturer's instruction (OriGene Technology, Inc) (Table 2.5). The transfection complex was mixed thoroughly and incubated for 15 min at room temperature, and then added to the adherent cells.

Table 2.5 Preparation of transfection reagents.

Reagent	Volume
Opti-MEM™ I reduced serum medium	250 μL
gRNA	1 μg
Donor DNA	1 μg
TurboFect Transfection Reagent	6 μL

SPAG5-gRNA target sequence was "CCTTCGCCCCAGACGGTAAG" for gRNA1 and "AGATCTCCCGCTTACCGTCT" for gRNA2. The medium containing the transfection complex was removed after 36-hr incubation. The transfected cells were

then dispensed into Petri dishes with fresh CM containing 0.4% puromycin, as shown in section 2.5.

If no homozygous knockout cells could be isolated, the second round of *SPAG5* gene knockout was done using the same gRNAs and another donor plasmid containing neomycin-resistant sequence in the heterozygous clones with WT alleles. Two different types of donor plasmids, linear neomycin-resistant DNA segment and traditional plasmid, were used in the 2nd round KO (Figure 2.3). The former one could be integrated into the cleavage site in either forward or reverse direction. Cells were thus selected using CM containing geneticin (dissolved in *MilliQ*-water) at a concentration of 400 μg/mL.

2.4 Screening and Validation of *ABCC5* Gene Knockout Clones

2.4.1 PCR (Polymerase Chain Reaction) Amplification

2.4.1.1 Reconstitution of Primer

Upon receipt, dried oligos were reconstituted in TE buffer for long term storage and stored at -20 °C. Before opening, the tube containing oligos was centrifuged for 1 min at low speed (maximum RCF 4,000 × *g*) to collect the contents at the bottom of the tube. An appropriate volume of TE buffer was then added into the tube with the aid of a pipette to prepare 100 μM (100 pmol/μL) stock solutions. The tube was briefly vortexed and centrifuged at low speed (maximum RCF 4,000 × *g*) for 2 min, followed by a 15 min incubation at room temperature to rehydrate the oligos. The tube was briefly vortexed and centrifuged at low speed (maximum RCF 4,000 × *g*) for 2 min again to ensure that all the contents were resuspended and collected at the bottom. The

resuspended oligos were appropriately aliquoted and stored at -20 °C.

2.4.1.2 Extraction of DNA

Cells were harvested and counted at around 90% confluence as the method in section 2.2.6. A total of 1 × 10^6 cells was centrifuged at 200 × *g* for 5 min at 4 ℃. The supernatant was carefully removed, and the cell pellet was lysed by 50 µL of Cell Lysis Buffer together with 2 µL of Protein Degrader in a PCR tube according to the manufacturer's instruction (GeneArt™ Genomic Cleavage Detection Kit). The cell lysate was then placed in Mastercycler® Pro (Eppendorf AG). The programme is listed below in Table 2.6. The cell lysate was immediately proceeded to PCR amplification or stored at -20 ℃.

Table 2.6 Thermal cycler programme for cell lysis.

Temperature	Time
68 ℃	15 min
95 ℃	10 min
4 ℃	Hold

2.4.1.3 PCR Amplification

Cells were grown in a cell culture flask with the culture conditions mentioned above until around 90% confluence. Then, cells were trypsinized, centrifuged and resuspended as the method shown in section 2.2.3. Extraction of DNA was done using the GeneArt™ Genomic Cleavage Detection Kit according to the method in section 2.4.1.2. After that, the cell lysate was mixed with primers, AmpliTaq Gold 360® Master Mix, and water in a PCR tube according to the manufacturer's instruction (GeneArt™ Genomic Cleavage Detection Kit). A positive control template provided in the kit was

done in order to validate the manipulations. The primer constructs used in this study are listed in Table 2.8. The PCR reaction was conducted with the conditions listed in Table 2.7 using LightCycler® 480 Real-Time PCR System (Roche Molecular Systems, Inc).

Table 2.7 PCR amplification thermal cycler conditions.

Stage	Temperature	Time	Cycles
Enzyme activation	95 ℃	10 min	1 X
Denature	95 ℃	30 sec	
Anneal	60 ℃	30 sec	40 X
Extend	72 ℃	30 sec	
Final extension	72 ℃	7 min	1 X
Hold	4 ℃	∞	1 X

The extension time was adjusted with the size of the amplicon (60 seconds for each kb). For example, a 30 sec extension time was applied in each cycle to amplify the PCR product of 428 bp in size. To verify the length of amplicon, agarose gel analysis was employed after PCR amplification as the method mentioned in section 2.4.3. After the PCR reaction, samples were immediately proceeded to agarose gel analysis, enzyme digestion or stored at –20°C.

Table 2.8 Primer constructs used in PCR amplification of ABCC5 gene.

Primer	Constructs
IDT Forward primer	5’- TTC CAG CTG TTG CCA AAA TCC -3’
IDT Reverse primer	5’- GAG ACT TGT GTG AGT GGT GG -3’
PCR Amplicon	428 bp
Thermofisher set1 Forward primer	5’- CCT GAA TGT TCT AAA ACG GCT TTG -3’
Thermofisher set1 Reverse primer	5’- TCA GTT CCG TTT GCC TCT CG -3’
PCR Amplicon	595 bp

2.4.2 Genomic Cleavage Detection Assay

GeneArt™ Genomic Cleavage Detection Kit was employed in this study to examine the formation of indels. Loci, where the TrueCut™ Cas9 Protein v2 – induced DSB occurred, were amplified by PCR (section 2.4.1.3). The amplicons were denatured and re-annealed to produce mismatches as strands with an indel re-annealed strands with no indel or a different indel. The mismatches were subsequently detected and cleaved by Detection Enzyme, followed by gel electrophoresis and band densitometry in order to analyse the cleaved bands.

The amplicons with or without indels were randomly re-annealed to form heterogeneous DNA duplexes before enzyme digestion. The PCR product was combined with 10X Detection Reaction Buffer and nuclease-free water according to the manufacturer's instruction (GeneArt™ Genomic Cleavage Detection Kit). The mixture was then placed in LightCycler® 480 Real-Time PCR System (Roche Molecular Systems, Inc) and underwent the re-annealing programme as shown in Table 2.9.

Table 2.9 Re-annealing programme.

Stage	Temperature	Time	Temperature/Time
1	95 °C	10 min	-
2	95 – 85 °C	-	-2 °C/s
3	85 °C	1 min	-
4	85 – 75 °C	-	-0.3 °C/s
5	75 °C	1 min	-
6	75 – 65 °C	-	-0.3 °C/s
7	65 °C	1 min	-
8	65 – 55 °C	-	-0.3 °C/s
9	55 °C	1 min	-
10	55 – 45 °C	-	-0.3 °C/s
11	45 °C	1 min	-
12	45- 35 °C	-	-0.3 °C/s
13	35 °C	1 min	-
14	35 – 25 °C	-	-0.3 °C/s
15	25 °C	1 min	-
16	25 – 4 °C	-	-0.3 °C/s
17	4 °C	∞	-

The re-annealed PCR product was immediately proceeded to enzyme digestion by which the existence of mismatches in DNA duplexes was identified. The re-annealed PCR product was mixed with the Detection Enzyme according to the manufacturer's instruction (GeneArt™ Genomic Cleavage Detection Kit). The re-annealed PCR product together with Detection Enzyme was then transferred to Mastercycler® Pro (Eppendorf AG) and incubated for 30 min at 42 ℃. The heteroduplex DNA containing mismatched indel was cleaved by the Detection Enzyme, allowing for quantification of gene editing efficiency using agarose gel analysis (section 2.4.3).

2.4.3 Agarose Gel Analysis

The accuracy of PCR product, enzyme digestion and cleavage efficiency were identified using agarose gel analysis. 2% agarose gel solution (0.5 cm gel thickness: 1g agarose powder in 50 mL 1X TBE buffer; 1 cm gel thickness: 2g agarose powder in 100 mL 1X TBE buffer) was microwaved until completely clear and poured into the gel tray in casting position with a proper comb. The agarose gel was allowed to cool down until solidified. After that, the comb was removed, the gel tray was turned to running position, and the buffer chamber of the gel tank (Owl™ EasyCast™ B1 Mini Gel Electrophoresis Systems; ThermoFisher Scientific, Inc) was filled with 1X TBE buffer. 10 μL of each sample was mixed with 2 μL of loading buffer provided in TrackIt™ 100 bp DNA Ladder kit and loaded into agarose gel. A DNA ladder (TrackIt™ 100 bp DNA Ladder) was loaded in parallel as a sizing standard. The gel tank was connected to BioVolt™ 300V Power Supply (Select BioProducts). The gel electrophoresis programme was listed in Table 2.10.

Table 2.10 Agarose gel electrophoresis programme.

Stage	Voltage	Time
Step 1	50 V	10 min
Step 2	100 V	1.5 hrs

After electrophoresis, the agarose gel was completely immersed in 1X SYBR™ Gold Nucleic Acid Gel Stain for 30 min at room temperature or overnight at 4 ℃. The agarose gel was then visualized by using a UV transilluminator (SamrtView Pro 1100 Imager System, UVCI-1100; MS Major Science). The size of the PCR product and quantification of gene editing efficiency were done using ImageJ software. The cleavage efficiency of *ABCC5* gene was calculated using the following equation.

$$\text{Cleavage Efficiency} = 1 - [(1 - \text{fraction cleaved})^{0.5}]$$

Fraction Cleaved = sum of cleaved band intensities / (sum of the cleaved and parental band intensities)

Then, the percent of homozygous knockout in pooled cell population in both *ABCC5* gene alleles was calculated using the following equation.

$$\text{Both alleles knocked out \%} = \text{cleavage efficiency} \times \text{cleavage efficiency}$$

If the probability of an indel resulting in frameshift was 2/3, the chance of having a homozygous KO was then calculated using the following equation.

$$\text{Homozygous KO \%} = (\text{cleavage efficiency} \times \text{cleavage efficiency}) \times (66\% \times 66\%)$$

2.4.4 Limiting Dilution Cloning (LDC)

After determination of gene knockout efficiency, the pooled cell population was

proceeded to limiting dilution cloning to isolate the homozygous knockout monoclonal cells. The cells were seeded into 96-well plates at a density of 0.8 cells/well. This seeding strategy ensured that some wells received a single cell and minimized the likelihood of receiving more than one cell. Given that an individual cell could be challenging to find, one of the corner wells in each 96-well plate was seeded with approximately 1000 cells for focusing the microscope later when scanning the plate for individual cells. Cells were then observed and monitored every 3 - 4 days for cell growth. The culture medium was replaced on a weekly basis. The knockout clones were screened out using Spark® Multimode Microplate Reader-based cell uptake study (section2.7.2.2), immunocytochemistry (section 2.10) and cell surface staining assay (section 2.7.1) at a protein level and further validated with genomic cleavage detection assay (section 2.4.2) and Sanger sequencing assay (section 2.4.6) at a gene level.

2.4.5 Purification of PCR Amplicons

The purification of PCR products from knockout single-cell clones was done by using QIAquick® Gel Extraction Kit. After gel electrophoresis (section 2.4.3), the DNA (band) was excised from the agarose gel with a scalpel. 1 volume of gel slice (100 mg gel ~ 100 µL) was mixed with 3 volumes of Buffer QG and incubated at 50 ℃ for 10 min until the gel slice had completely dissolved. The sample was then mixed with 1 gel volume isopropanol and applied to the QIAquick column and centrifuged at 17900 × *g* for 1 min. The flow-through was discarded. The sample in the QIAquick column was further washed with 750 µL Buffer PE and incubated for 5 min at room temperature, followed by centrifugation at 17900 × *g* for 1 min. The flow-through was discarded. The QIAquick column was placed into a 1.5 mL centrifuge tube. 50 µL buffer EB

(10mM Tris-HCl, pH 8.5) was added to the centre of the QIAquick membrane in order to elute DNA. The column was allowed to stand for 1 min and centrifuged at 17900 × *g* for 1 min. The purified DNA was immediately proceeded to sequencing or stored at –20°C.

2.4.6 Sanger Sequencing Assay

In order to detect the homozygosity and nucleotide order of knockout clones, the purified PCR products from single knockout cell clones (section 2.4.5) together with negative controls were sent to Massey University for Sanger Sequencing Service. The concentration of DNA was estimated by comparing with the fluorescence intensity of TrackIt™ 100 bp DNA Ladder, of which the concentration was known in agarose gel analysis (section 2.4.3). The samples were prepared by mixing 4 pmol of *ABCC5*-sgRNA reverse primer and 12 ng of DNA sample (2.5 ng/100 bp) with an appropriate volume of nuclease-free water to achieve a final volume of 20 μL. The mixture was then posted to Massey University immediately for PCR amplicon sequencing.

2.5 Screening and Validation of *SPAG5* Gene Knockout Clones

The pooled knockout cell population obtained from section 2.3.2.4 was proceeded to antibiotic selection immediately to isolate knockout monoclonal cells. Cells were split into 2-8 Petri dishes. CM with 0.4 μg/mL of puromycin (puromycin dissolved in *MilliQ*-water) was then applied to cells to dilute out wild type cells. CM with 0.4 μg/mL of puromycin was changed every 2 to 3 days, and cells were treated with puromycin for 2

to 4 weeks until single-cell colonies could be observed. The colonies were picked up and seeded in a 96-well plate with the aid of pipettor tips and a microscope. Once most of the colonies achieved around 90% confluence, the cells on the 96-well plate were subcultured into two 96-well plates. One plate was proceeded to genetic validation of KO clones, while the other was kept culturing in an incubator.

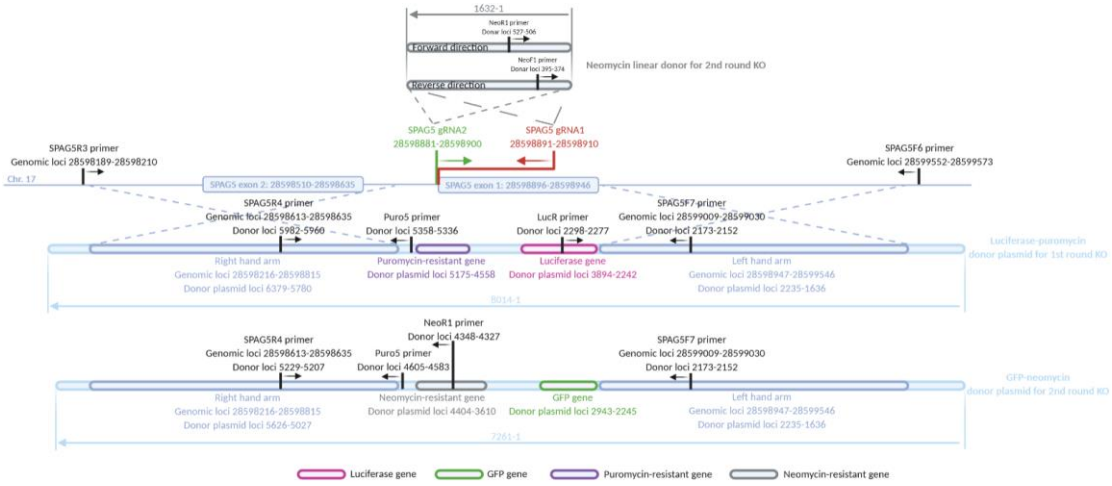

Figure 2.3 *SPAG5* gRNAs and primers used in this study. *Created with BioRender.com.*

To screen the single-cell clones on 96-well plates, the genomic DNA of cells was extracted using a self-prepared cell lysis buffer and heated up in a thermal cycler, as shown in Table 2.11 and Table 2.12. 5 µL of the extracts was proceeded to PCR amplification as the method shown in section 2.4.1.3 using TaKaRa PCR Amplification Kit according to the manufacturer's instruction.

Table 2.11 Recipe of self-prepared cell lysis buffer for DNA extraction.

Cell lysis buffer for DNA extraction	
TE buffer	38 μL/well
Tween 20	0.1%
Protease K	2 μL/well

Table 2.12 Thermal cycler programme for cell lysis.

Temperature	Time
56 ℃	15 min
95 ℃	10 min
4 ℃	Hold

Alternatively, the genomic DNA of cells was extracted and purified using QIAamp DNA Mini Kit (QIAGEN, Germany) according to the manufacturer's instructions. Cells were detached and harvested as the method in section 2.2.3. The cell pellet was resuspended in PBS to a final volume of 200 μL. 20 μL QIAGEN Protease K was then added to the cell suspension. Cells were lysed by mixing with 200 μL Buffer AL and pulse-vortex for 15 seconds. The lysate was incubated at 56 ℃ for 10 min, followed by the addition of 200 μL ethanol (96 – 100%). The mixture was carefully applied to the QIAamp Mini spin column without wetting the rim and centrifuged at 6000 × *g* for 1 min. 500 μL Buffer AW1 was added to the QIAamp Mini spin column and centrifuged at 6000 × *g* for 1 min. 500 μL Buffer AW2 was added to the QIAamp Mini spin column and centrifuged at 20000 × *g* for 3 min. The genomic DNA was eluted by applying 200 μL Buffer AE to the QIAamp Mini spin column that was placed in a 1.5 mL microcentrifuge tube. After 1 min incubation at room temperature (15 – 25 ℃), the QIAamp Mini spin column was centrifuged at 6000 × *g* for 1 min. The genomic DNA was collected in a microcentrifuge tube, and 250 ng of DNA was immediately proceeded to PCR amplification as the method shown in section 2.4.1.3 using TaKaRa PCR Amplification Kit according to the manufacturer's instruction or stored at -20 ℃.

The PCR products were detected by using agarose gel electrophoresis, as shown in section 2.4.3. The primer constructs used in this study are shown in Table 2.13 and Figure 2.3.

Table 2.13 Primer constructs used in PCR amplification of *SPAG5* gene and donor sequence.

Primer	Constructs
Puro 5	5'- TTGAATGGAAGGATGGAGCTAC -3'
SPAG5R3	5'- GACTGACCTTTCCGTAAGTGAC -3'
SPAG5F6	5'- GTTAGCCCAGTAAACTGGTAGC -3'
LucR	5'- GTCTTCGAGTGGGTAGAATGGC -3'
SPAG5F7	5'- AGAGCAGGTTCAAACACAGACG -3'
SPAG5R4	5'- GGAGTTCTCATAGATGGTTTTCC -3'
NeoF1	5'- TCATGCGAAACGATCCTCATCC -3'
NeoR1	5'- TTCCTCGTGCTTTACGGTATCG -3'

If no homozygous knockout cells could be isolated, the second round of *SPAG5* gene knockout was done using donor plasmid containing geneticin-resistant sequence in the clones with WT and edited alleles (Figure 2.3). Cells were thus selected using CM containing geneticin (dissolved in *MilliQ*-water) at a concentration of 400 μg/mL.

2.6 qRT-PCR Assay

2.6.1 Extraction of Total RNA

Cells were grown in monolayer in a cell culture flask with the aforementioned culture conditions until around 90% confluence. Cells were lysed with 0.5 mL (T25 flask) or 1 mL (T75 flask) of TRIzol™ Reagent and homogenized by pipetting up and down several times. The cell lysate was then transferred into an RNase-free Eppendorf tube and incubated for 5 min to permit dissociation of the nucleoproteins complex. After incubation, an aliquot of 0.1 mL (T25 flask) or 0.2 mL (T75 flask) of chloroform was added to the cell lysate and incubated for 3 min with agitation. The sample was then

centrifuged for 15 min at 12000 × *g* at 4 °C. Thus, the mixture separated into a lower red phenol-chloroform, interphase, and a colourless upper aqueous phase. The aqueous phase containing the RNA was transferred to a new Eppendorf tube. An aliquot of 0.25 mL (T25 flask) or 0.5 mL (T75 flask) of isopropanol was added to the aqueous phase and incubated for 10 min with agitation. The sample was then centrifuged for 10 min at 12000 × *g* at 4 °C. The supernatant was gently removed with the aid of a pipet. Total RNA precipitate thus formed a white gel-like pellet at the bottom of the tube. The RNA pellet was resuspended in 0.5 mL (T25 flask) or 1 mL (T75 flask) of 75% ethanol, which was diluted with DEPC-treated water. The sample was vortexed briefly and centrifuged for 5 min at 7500 × *g* at 4 °C. The supernatant was gently discarded, and the RNA pellet was allowed to air dry for 5-10 min. The RNA pellet was resuspended in 50 μL of DEPC-treated water and incubated in a water bath at 56 °C for 15 min. The sample was proceeded to downstream experiments directly or stored at -80 °C.

The concentration and quality of RNA yield were determined by using the NanoDrop® ND-1000 UV spectrophotometer (NanoDrop Products, USA). An A260/A280 ratio higher than 2 and an A260/A230 ratio between 2.1 and 2.3 were associated with relatively pure RNA.

2.6.2 One-Step qRT-PCR

The expression levels of all tested genes were measured using qRT-PCR. The RNA samples were reverse transcripted and PCR amplified by using LightCycler® EvoScript RNA SYBR® Green I Master and LightCycler® 480 Real-Time PCR System (Roche Molecular Systems, Inc). The reaction was prepared according to the manufacturer's protocol (Table 2.14). The primer constructs used in this study are listed in Table 2.15. The thermal cycling conditions are listed in Table 2.16.

Table 2.14 Reaction mix for One-Step qRT-PCR.

Reagent	Volume for 1 reaction
Master Mix (5x)	4 µL
Primer (10 µM)	1 µL/each
RNA sample	200 ng
PCR grade water	Up to 25 µL

Table 2.15 Primer constructs used in qRT-PCR.

ABCC5 (Chr. 3)				
Primer	**Constructs**			
Fwd	5'- CTCCAGATAACTCCACCAGACGG -3'			
Rev	5'- AGAGGTGACCTTTGAGAACGCA -3'			
	cds range	**Length**	**Primer range**	**Involved length**
Exon 26	183937901 - 183938060	160 bp	183938010 -	51 bp
Exon 25	183942727 - 183942916	190 bp	183942848	122 bp
				Sum: 173 bp
PARP1 (Chr. 1)				
Primer	**Constructs**			
Fwd	5'- ATCCACCTCATCGCCTTTTC -3'			
Rev	5'- GCAGAGTATGCCAAGTCCAACAG -3'			
	cds range	**Length**	**Primer range**	**Involved length**
Exon 5	226388656 - 226388755	100 bp	226388731	25 bp
Exon 4	226390410 - 226390624	215 bp	-	215 bp
Exon 3	226392199 - 226392314	116 bp	226392258	60 bp
				Sum: 300 bp
BRCA1 (Chr. 17)				
Primer	**Constructs**			
Fwd	5'- CTTGACCATTCTGCTCCGTT -3'			
Rev	5'- GCGTCCCCTCACAAATAAAT -3'			
	cds range	**Length**	**Primer range**	**Involved length**
Exon 10	43091435 - 43094860	3426 bp	43093898 -	149 bp
			43094046	Sum: 149 bp
BRCA2 (Chr. 13)				
Primer	**Constructs**			
Fwd	5'- GAAAATCAAGAAAAATCCTTAAAGGCT -3'			
Rev	5'- GTAATCGGCTCTAAAGAAACATGATG -3'			
	cds range	**Length**	**Primer range**	**Involved length**
Exon 12	32344558 - 32344653	96 bp	32344608 -	46 bp
Exon 13	32346827 - 32346896	70 bp	32346881	55 bp
				Sum: 101 bp
PD-L1/CD274 (Chr. 9)				
Primer	**Constructs**			
Fwd	5'- GGCCGAAGTCATCTGGACAA -3'			
Rev	5'- TGGAGGATGTGCCAGAGGTA -3'			
	cds range	**Length**	**Primer range**	**Involved length**
Exon 4	5462834 - 5463121	288 bp	5462925 -	197 bp
Exon 5	5465499 - 5465606	108 bp	5465521	23 bp
				Sum: 220 bp

cds: coding sequence.

Table 2.16 Thermal cycling conditions for qRT-PCR.

Stage	Temperature	Time	Cycles
Reverse transcription	60 ℃	15 min	1 X
Enzyme activation	95 ℃	10 min	1 X
Denature	95 ℃	15 sec	
Anneal	60 ℃	30 sec	45 X
Extend	72 ℃	20 sec	

The results were analysed using the comparative threshold (Ct) cycle method. The mean Ct value was determined from the amplification plots generated by LightCycler® 480 Real-Time PCR System to detect the mRNA expression of each target gene. An internal control, glyceraldehyde-3-phosphate dehydrogenase (GAPDH), was used to normalise the target gene expression using the $2^{-\Delta\Delta Ct}$ method.

2.7 Flow Cytometry-Based Assays

2.7.1 Cell Surface Staining Assay

The cell surface expression of ABCC5 protein in human breast cancer cells was confirmed by flow cytometry. Cells were harvested and counted at around 90% confluence as the method in section 2.2.6. 1×10^6 cells were resuspended with 100 μL of ice-cold PBS containing 1% paraformaldehyde (PFM; fixative) and incubated for 15 min at 4 °C to fix the membrane proteins and prevent the modulation and internalization of surface antigens which could produce a loss of fluorescence intensity. After fixation, cells were washed twice with ice-cold PBS containing 0.1% saponin and 0.1% sodium azide and centrifuged at 400 × *g* for 5 min. An aliquot of 100 μL ice-cold PBS containing 0.1% saponin was adopted to resuspend the cells and incubated for 15 min

at 4 °C to resolve and remove cholesterol and increase membrane permeabilization. Cells were then blocked with 200 μL of 5% BSA in PBS for 15 min at room temperature to prevent nonspecific binding of antibodies. After blocking, cells were washed twice with ice-cold PBS containing 0.1% saponin and 0.1% sodium azide and centrifuged at 400 × *g* for 5 min. 100 μL of MRP5 Monoclonal Antibody (M5I-1) in ice-cold diluted solution (2% BSA in PBS) was applied to cells. A Rat IgG2α Isotype Control group was added to eliminate the background staining, which could be caused by Fc receptors on target cells, nonspecific interactions with cellular proteins, carbohydrates, lipids and cell autofluorescence. Cells were allowed to stand for 60 min at 4 °C in dark. After primary antibody incubation, cells were washed twice with ice-cold PBS containing 0.1% saponin and 0.1% sodium azide and centrifuged at 400 × *g* for 5 min. Cells were then incubated with Goat Anti-Rat IgG H&L (DyLight® 488) in 100 μL ice-cold diluted solution for 60 min at 4 °C in dark. After secondary antibody incubation, cells were washed twice with ice-cold PBS containing 0.1% saponin and 0.1% sodium azide and centrifuged at 400 × *g* for 5 min. Cells were ultimately resuspended with ice-cold PBS containing 1% PFM to a final volume of 200 μL in Beckman Coulter Blue Test Tubes and immediately proceeded to flow cytometry using MoFlo™ XDP flow cytometer (Beckman Coulter, Inc., CA) or stored at 4 °C in dark for up to 24 hours. The fluorescence intensity was determined with the fluorescence emission at 525 nm using 488 nm excitation. The mean fluorescence intensity obtained from flow cytometry was analyzed by using Kaluza Analysis Software and PRISM® GraphPad 8.

2.7.2 Cell Uptake Study

2.7.2.1 Flowcytometry-Based Cell Uptake Study

The function of ABCC5 transporter in HEK293 cells and human breast cancer cells was

evaluated by cell uptake study using the non-fluorescent precursor 2′,7′-Bis(2-carboxyethyl)-5(6)-carboxyfluorescein acetoxymethyl ester (BCECF-AM). BCECF-AM could enter cells by passive diffusion and be hydrolysed by cytosolic esterase to yield an ABCC5 fluorescent substrate BCECF, which was pumped out by ABCC5. Thus, the cellular accumulation of BCECF was considered to vary inversely with the functional expression of ABCC5 and ultimately achieve a steady-state. Cell uptake study was also employed to determine the cellular accumulation of fluorescent drug doxorubicin in these cell lines.

Cells were harvested and counted at around 90% confluence as the method in section 2.2.6. 0.5×10^6 cells were resuspended with 1 mL of FBS- and phenol red-free medium (RPMI-1640 Medium, no glutamine, no phenol red) or Hanks' Balanced Salt Solution (HBSS) buffer. The accumulation of BCECF or doxorubicin was conducted by spiking cells with 0.25 μM BCECF-AM (final DMSO concentration of 0.1%) or 6 μM doxorubicin at 37 °C in a water bath. A control group of cells incubated with the same volume of DMSO or water was added to eliminate the influence of solvent on ABCC5 function. To terminate the ABCC5-mediated export of BCECF or doxorubicin, 3 mL of ice-cold PBS was added to cells, followed by centrifugation at 400 × *g* for 5 min. Cells were washed with 3 mL of ice-cold PBS again prior to reconstitution in 200 μL ice-cold PBS containing 1% PFM in Beckman Coulter Blue Test Tubes. The fluorescence intensity of BCECF was determined with the fluorescence emission at 525 nm using 488 nm excitation using MoFlo^{TM} XDP flow cytometer (Beckman Coulter, Inc., CA). The data were analysed by using Kaluza Analysis Software and PRISM® GraphPad 8.

2.7.2.2 Spark® Multimode Microplate Reader-Based Cell Uptake Study

The determination of knockout single-cell clones was done by using Spark® Multimode Microplate Reader-based cell uptake study by which the ABCC5 function was examined. An identical method as in section 2.7.2.1 was employed to expose cells to BCEECF-AM. After 2 times washing with 3 mL of ice-cold PBS, cells were resuspended and lysed using 1 mL of 0.1% Triton X-100 dissolved in PBS and incubated for 10 min at room temperature with agitation. The cell lysate was then centrifuged at 2000g for 5 min. The supernatant was loaded into a 96-well plate with flat bottom black wells (Greiner high and medium binding 96 black well plate) and determined with the fluorescence emission at 525 nm using 488 nm excitation using Spark® Multimode Microplate Reader (Tecan Trading AG). The data were further divided by the protein concentration of cell lysate, which was determined by DC protein analysis (section 2.9.2.1) to eliminate the variations in cell number. The data were analyzed by using Microsoft® Excel® and PRISM® GraphPad 8.

2.7.3 Apoptotic Analysis

The influence of olaparib on cell apoptosis was determined using Alexa Fluor® 488 Annexin V/Dead Cell Apoptosis Kit with Annexin V Alexa Fluor™ 488 & Propidium Iodide (PI). Cells were harvested and counted at around 90% confluence as the method in section 2.2.6. Cells were seeded into a 6-well plate at a density of 4×10^5 cells/well 24 hrs prior to the addition of treatment. Olaparib at a series of concentrations was then added to the wells accompanied by a control group with CM. 1×10^5 cells were detached and collected in a set of 15 mL centrifuge tubes using the method in section 2.2.6 in a 48-, 72- and 96-hr interval. Cells were washed with 1 mL of ice-cold PBS

before exposure to 100 µL of 1X annexin-binding buffer (Component C) in Beckman Coulter Blue Test Tubes. 5 µL of Alexa Fluor® 488 annexin V (Component A) and 1 µL of 100 µg/mL propidium iodide (PI) (Component B) working solution were then applied to cells. After a 15 min incubation at room temperature, 400 µL of 1X annexin-binding buffer was added to cells. Cells were kept on ice and proceeded to flow cytometry using MoFlo™ XDP flow cytometer (Beckman Coulter, Inc., CA). The stained cells were measured with the fluorescence emission at 530 nm and 575 nm using 488 nm excitation. The data were analyzed by using Kaluza Analysis Software and PRISM® GraphPad 8.

2.7.4 Cell Cycle Assay

The influence of olaparib on cell cycle was examined using cell cycle assay, which was based on the proportional intercalation of propidium iodide (PI) to double-stranded DNA base pairs with no specificity. Cells were seeded into a 6-well plate at a density of 4×10^5 cells/well 24 hrs prior to the addition of treatment. Olaparib at a series of concentrations was then added to the wells accompanied by a control group with CM. Cells were detached and collected in a set of 15 mL centrifuge tubes using the method in section 2.2.3 in a 48-, 72- and 96-hr interval. Cells were then fixed in ice-cold PBS containing 1% PFM; fixative and incubated for 30 min at 4 °C to fix the membrane proteins, followed by centrifugation at 400 × *g* for 5 min. Cells were washed twice with ice-cold PBS, followed by a 30 min incubation with 0.1% saponin dissolved in PBS to permeabilize the cell membrane. Ribonuclease and RNase were added to cells to ensure no RNA was stained. 1 µL of 100 µg/mL PI working solution was then applied to cells. After a 15 min incubation at room temperature, the fluorescence was detected with the

fluorescence emission at 575 nm using 488 nm excitation on MoFlo™ XDP flow cytometer (Beckman Coulter, Inc., CA). The data were analyzed by using Kaluza Analysis Software and PRISM® GraphPad 8.

2.8 Growth Inhibition Assay (MTT Assay)

2.8.1 Collagen Coating

Given that certain types of cells, such as HEK293 cells, required pre-coated surface to aid adherence, Collagen Coating Solution was employed to pre-coat 96-well plate before plating cells. The surface of each well on the 96-well plate was coated with 32 μL of Collagen Coating Solution for 30 min at 37 °C or 2 hrs or overnight at room temperature. The collagen coating solution was removed by aspiration in a sterile hood. The coated flask was used immediately or stored at 4°C for up to 2 weeks.

2.8.2 MTT Assay

The MTT (3-(4,5-dimethylthiazol-2-yl)-2,5-diphenyltetrazolium bromide) assay was used to measure viable cells in this study. The yellowish tetrazolium salt was reduced by mitochondrial dehydrogenase of living cells to produce water-insoluble dark blue formazan crystals, which were then dissolved in DMSO. The absorbance or optical density (OD) of the solution was measured colourimetrically using a spectrophotometer at 540 nm with a reference of 680 nm.

To evaluate the cellular sensitivity of different cell lines to chemodrugs cytotoxicity, cells were exposed to chemodrugs at different concentrations for 4 hrs, followed by determination of cell viability with MTT assay. Cells were harvested and counted at

around 90% confluence as the method in section 2.2.6. Cells were seeded into 96-well plates at a density of 2×10^3 cells/well in CM (100 μL). After 24 hrs incubation for attachment, an aliquot of 100 μL of treatment in CM at a series of concentrations were then added to each well accompanied by blank (CM only) and vehicle control (cells without treatment) groups. Cells were exposed to treatment for the designated incubation time (normally 4 hrs) at 37 ºC in an incubator. To terminate drug exposure, the CM containing chemodrugs was removed and replaced with fresh CM. Cells were then incubated for 4 extra days. After incubation, the old culture medium was replaced with 100 μL of fresh CM. 10 μL of 12mM MTT was then added to each well and incubated for approximately 4 hrs until the purple precipitate was clearly visible. Then 85 μL of supernatant was removed, and 150 μL of DMSO was added to each well to dissolve the formazan. After shaking for 5 min, the absorbance (OD value) was measured by Thermo Scientific Multiskan GO (ThermoFisher Scientific, Inc) at the wavelength of 540 nm with a reference wavelength of 680 nm. The data of experimental groups were obtained by subtracting their absorbance at 680 nm and the absorbance of blank control from their absorbance at 540 nm. The data were then presented as percent cell viability of experimental groups compared with the vehicle control group, the viability of which was taken as 100%. The IC_{50} value was statistically analyzed by using Microsoft® Excel® and PRISM® GraphPad 8. CI value of drug combination was analysed by using CompuSyn software (Chou, 2006).

2.9 Western Blotting

2.9.1 Preparation of Cell Lysate

2.9.1.1 Extraction of Intracellular Protein

For the intracellular protein such as beta-actin, the cell lysate was prepared by using the following method. Cells were cultured in CM in a T75 flask as the method in section 2.2.3. When cells achieved around 90% confluence, the old culture medium was discarded. Cells were washed twice with 5 mL of ice-cold PBS or TBS. Cells were then lysed using 1 mL of RIPA Lysis and Extraction Buffer containing 200 µL of protease inhibitor (cOmplete™, Mini, EDTA-free Protease Inhibitor Cocktail), and incubated on ice for 10 min with agitation. The protein concentration of cell lysate was measured by DC protein analysis (section 2.9.2.1). The cell lysate was proceeded immediately to DC protein analysis, sample preparation or stored at -20 ºC.

Before gel electrophoresis, 3 volumes of cell lysate were mixed 1 volume of 4X Laemmli Sample Buffer containing 10% β-mercaptoethanol. The volume of the mixture was dependent on the protein concentration of cell lysate and the size of the well. Cell lysate in sample buffer was reduced and denatured by boiling at 70 ºC for 10 min in a heating block (Multi-Block Heater; Lab-line Instruments, Inc). Cell lysate in sample buffer was then centrifuged at 14000 × *g* for 1 min. The cell lysate was proceeded to gel electrophoresis (section 2.9.3) or stored at -20 ºC.

2.9.1.2 Extraction of Membrane Protein

The protocol for extraction of intracellular protein was found to be unfit in the preparation of membrane protein. Thus, a modified Laemmli lysis buffer (Table 2.17) was used to extract membrane protein instead of RIPA Lysis and Extraction Buffer.

Sodium dodecyl sulphate (SDS) acted as both detergent and reducing agent that were able to dissolve and reduce amphiphilic protein, while detergents NP-40 and sodium deoxycholate in RIPA Lysis and Extraction Buffer were able to dissolve hydrophobic protein (membrane protein) specifically. Dithiothreitol (DTT) was a reducing agent that was used to reduce the disulphide bonds of proteins and peptides. Tris-HCl in RIPA Lysis and Extraction Buffer was used to regulate pH at around pH 7.6. NaCl in RIPA Lysis and Extraction Buffer was able to maintain the osmolarity of cell lysate.

Table 2.17 Recipe of modified Laemmli lysis buffer (1.6 mL).

Component	Amount
RIPA Lysis and Extraction Buffer	1.2 mL
4X Laemmli Sample Buffer	0.4 mL
DTT	0.016 g
SDS	0.025 g

Cells were cultured and washed as the method in section 2.9.1.1. Cells were then lysed using 1 mL of modified Laemmli lysis buffer containing 200 µL of protease inhibitor (cOmplete™, Mini, EDTA-free Protease Inhibitor Cocktail), and incubated for 10 min at room temperature with agitation. Room temperature prevented the precipitation of the high concentration of SDS used in the modified Laemmli lysis buffer. The cell lysate was then passed through 27-gauge needle (Terumo Syringe 1ml-27g x ½") at least 10 times to reduce viscosity and probably physically break the vesicles generated by small membrane fragments. The protein concentration of cell lysate was quantified by densitometric protein analysis (section 2.9.2.2) due to the existence of DTT. The cell lysate was proceeded immediately to protein densitometric analysis (section 2.9.2.2), gel electrophoresis (section 2.9.3) or stored at -20 ºC.

2.9.2 Protein Concentration Analysis

2.9.2.1 DC (Detergent Compatible) Protein Analysis

The DC protein analysis was done using the DC Protein Assay Reagents Package according to the manufacturer's instructions. 20 µL of reagent S was mixed with each mL of reagent A. 5 µL of cell lysate and a standard BSA solution ranging from 0 to 3 mg/mL were added into a clean and dry microtiter plate. 25 µL of reagent S + A was then added into each well, followed by 200 µL of reagent B. After 15 min incubation, absorbance was read at 750 nm. The data were analysed using Microsoft® Excel®. The protein concentration of cell lysate was calculated according to the linear relation between BSA standard and absorbance.

2.9.2.2 Densitometric Protein Analysis

The cell lysate (section 2.9.1.2) prepared using modified Laemmli lysis buffer was loaded to SDS-PAGE directly. After gel electrophoresis (section 2.9.3), the protein was transferred to PVDF (polyvinylidene fluoride) membrane and stained by Memcode™ Reversible Protein Stain Kit according to the manufacturer's instruction. The membrane was rinsed with *Milli-Q* water three times and placed in a suitable plastic tray, and then incubated with an appropriate volume of Memcode™ Sensitizer that could completely cover the membrane (the same volume of other reagents was used thereafter) for 2 min at room temperature with agitation. Memcode™ Reversible Stain was further added to the membrane, followed by 1 min incubation at room temperature with agitation. To eliminate the background stain, the membrane was rinsed with Memcode™ Destain three times and incubated with Destain / Methanol Solution (Memcode™ Destain 1:1 with reagent grade methanol) for 5 min at room temperature.

The membrane was then rinsed with *Milli-Q* water five times. Stained proteins appeared as turquoise-blue bands with a clear background. The membrane was then scanned using ImageQuant™ LAS 500 (Bio-Rad Laboratories, Inc). The intensity of protein stain was analysed by using ImageJ software. The protein concentration of cell lysate was calculated by comparing with the area value of total protein stain of pre-identified standard cell lysate, as shown in Figure 3.3.

After analysing protein concentration, the stain was erased by incubation membrane with Eraser / Methanol Solution (Memcode™ Stain Eraser 1:1 with reagent grade methanol) for 10 min at room temperature with agitation. The membrane was rinsed with *Milli-Q* water 5 times. The membrane was then proceeded to subsequent western blotting detection (section 2.9.4).

2.9.3 SDS-PAGE (Sodium Dodecyl Sulphate-Polyacrylamide) Gel Electrophoresis

SDS-PAGE gel electrophoresis was used to separate denatured proteins according to their molecular mass. The polypeptides could be maintained in a denatured state once treated with strong reducing agents (i.e., 2-mercaptoethanol, DTT and SDS) to remove the secondary and tertiary structure. The combination of heating and SDS was sufficient to break the many noncovalent bonds with regard to protein folds. DTT or β-mercaptoethanol could break any covalent bonds between cysteine residues. In SDS-PAGE gel electrophoresis, SDS enabled the proteins to carry negative charge. Sample proteins could move to the anode through the polyacrylamide mesh of the gel. Smaller proteins (usually measured in kilodalton, kDa) migrated faster through this mesh. These different rates of advancement (different electrophoretic mobilities) were separated into

bands within each lane. The concentration of polyacrylamide determined the gel resolution as: (i) the greater the polyacrylamide concentration, the better the resolution of lower molecular weight protein; (ii) the lower the polyacrylamide concentration, the better the resolution of higher molecular weight proteins.

Gel tank (Mini-PROTEAN® Tetra Vertical Electrophoresis Cell; Bio-Rad Laboratories, Inc) and Mini-PROTEAN® TGX™ Precast Gel (10%) was assembled according to the manufacturer's instruction. The chamber was filled with 1X running buffer (Tris/Glycine/SDS Buffer (10X)). A proper volume of cell lysate (section 2.9.1.1 and 2.9.1.2) was loaded into the gel parallel with Precision Plus Protein™ Kaleidoscope™ Standards. The lid of the gel tank was appropriately placed, and the power leads were connected to PowerPac™ HC Power Supply (Bio-Rad Laboratories, Inc). The gel electrophoresis programme is listed in Table 2.18 below.

Table 2.18 Gel electrophoresis programme.

Stage	Time
50 V	10 min
100 V	1 hour

PVDP membrane was activated by washing with 95% methanol and 1X transfer buffer (Trans-Blot® Turbo™ 5X Transfer buffer) respectively for 2 min on a rotary shaker until the membrane was translucent. The ion reservoir stacks were rinsed with 1X transfer buffer (Trans-Blot® Turbo™ 5X Transfer buffer) for 2 min with agitation. After gel electrophoresis, the gel cassette was removed. The transfer sandwich was assembled in the following order from bottom to top: bottom ion reservoir stack >> PVDF membrane >> gel >> top ion reservoir stack. The gel and PVDF membrane were carefully aligned and placed in the centre of the cassette base of the Trans-Blot®

Turbo™ Blotting System (Bio-Rad Laboratories, Inc). Any trapped air bubbles in the sandwich were expelled by using a blot roller. The cassette was then slid into one of the bays in Trans-Blot® Turbo™ Blotting System (Bio-Rad Laboratories, Inc). For ABCC5 protein detection, a HIGH MW programme for large proteins (> 150 kDa) was employed. LOW MW programme for small proteins (< 30 kDa) was employed for beta-actin detection. After the transfer of protein from gel to PVDF membrane, the transfer sandwich was disassembled. PVDF membrane was washed with TBST buffer for 5 min with agitation. The PVDF membrane was immediately proceeded to protein densitometric analysis (section 2.10.2.2) or western blotting (section 2.10.4).

2.9.4 Western Blotting

Western blotting was used to detect and identify ABCC5 protein expression in HEK293 cells and human breast cancer cells in this study, as well as beta-actin as a control. The SDS-PAGE gel was placed next to a PVDF membrane, and an electrical current caused the proteins to migrate from the gel to the membrane. The membrane was then probed by primary antibodies specific for the target of interest and visualized using fluorescent or chemiluminescent secondary antibodies.

PVDF membrane was blocked with blocking buffer (filtered 2% BSA in TBST buffer) for 1 hour at room temperature in a plastic tray with agitation to prevent non-specific antibody binding. After blocking, the PVDF membrane was incubated with MRP5 Monoclonal Antibody (M5I-1) (ABCC5) or Monoclonal Anti-β-Actin Antibody Produced in Mouse (beta-actin) diluted in 1% BSA overnight at 4 ºC. PVDF membrane was then washed three times with TBST buffer for 5 min with agitation to remove unbound primary antibodies. Goat anti-Rat IgG (H+L) Secondary Antibody, HRP

(ABCC5) or Donkey Anti-Mouse IgG (H+L) Highly Cross-Adsorbed Secondary Antibody, HRP (beta-actin) diluted in 1% BSA was applied to PVDF membrane, followed by 1-hr incubation at room temperature with agitation. After incubation, the PVDF membrane was washed 2 times with TBST buffer and 1 time with *Milli-Q* water for 5 min with agitation to remove unbound secondary antibodies. PVDF membrane was then incubated with SuperSignal™ West Pico PLUS Chemiluminescent Substrate (Stable Peroxide Solution and Luminol/Enhancer Solution at a 1:1 ratio) for 5 min at room temperature with agitation. To keep the PVDF membrane wet, it was covered by a plastic film. The chemiluminescence was determined using ImageQuant™ LAS 500 (Bio-Rad Laboratories, Inc). The intensity of protein stain was analysed by using ImageJ software.

2.9.5 Membrane Stripping for Re-Staining

The protein stain on the PVDF membrane was stripped off when multiple targets were examined, and the PVDF membrane was then re-stained with another set of primary and secondary antibodies.

The stripping buffer (Table 2.19) was pre-warmed to 50 ºC in a water bath. PVDF membrane was incubated with an appropriate volume of pre-warmed stripping buffer that could cover the membrane at 50 ºC in a water bath for up to 45 min with some agitation. PVDF membrane was then rinsed with running water tap for 2 min and washed with TBST buffer for 5 min to completely remove β-mercaptoethanol. PVDF membrane was proceeded to western blotting (section 2.9.4) from the blocking step.

Table 2.19 Recipe of stripping buffer (100 mL).

Component	Concentration	Volume
SDS	10%	20 mL
Tris-HCl, pH6.8	0.5 M	12.5 mL
Milli-Q water	-	67.5 mL
β-mercaptoethanol	0.8%	0.8 mL

2.10 Immunocytochemistry

To evaluate the ABCC5 expression in cell lines, cells were processed to immunocytochemistry to visualize the protein. Cells were harvested and counted at around 90% confluence as the method in section 2.2.6. Cells were then seeded into chamberslides (1 μ-Slide 8 well ibiTreat Microscopy Chamber) at a density of 1×10^5 cells/well in CM (400 μL). After 48 hrs incubation for attachment, the old CM was removed. Cells were gently washed twice with sterile PBS. To fix the membrane proteins and prevent the modulation and internalization of surface antigens which could produce a loss of fluorescence intensity, cells were incubated with 200 μL of ice-cold PBS containing 1% PFM (fixative) for 15 min at 4 °C. After fixation, cells were washed twice with ice-cold PBS containing 0.1% saponin and 0.1% sodium azide. An aliquot of 150 μL ice-cold PBS containing 0.1% saponin was adopted to resolve and remove cholesterol and increase membrane permeabilization. After 15 min incubation at 4 °C with saponin, cells were then blocked with 200 μL of 5% Normal Goat Serum in PBS for 30 min at room temperature to prevent nonspecific binding of antibodies. After blocking, 150 μL of MRP5 Monoclonal Antibody (M5I-1) in ice-cold diluted solution (1% Goat Serum in PBS) was directly applied to cells. A Rat IgG2α Isotype Control group was added to eliminate the background staining, which could be caused by Fc receptors on target cells, nonspecific interactions with cellular proteins, carbohydrates, lipids, and cell autofluorescence. Cells were allowed to stand for 60 min at 4 °C in dark.

After primary antibody incubation, cells were washed twice with ice-cold PBS containing 0.1% saponin and 0.1% sodium azide for 5 min. Cells were then incubated with Goat Anti-Rat IgG H&L (DyLight® 488) in 150 µL ice-cold diluted solution for 60 min at 4 °C in dark. After secondary antibody incubation, cells were washed twice with ice-cold PBS containing 0.1% saponin and 0.1% sodium azide for 5 min. After washing, the excess liquid in wells was removed, and one drop of Mounting Medium (ProLong™ Diamond Antifade Mountant with DAPI) was applied to cells. The chamberslidses were sealed with nail polish. Cells were cured for 24 hours at room temperature and were imaged using Olympus BX51 Fluorescence Microscope (Olympus Corporation, Japan) or stored at 4 °C for up to half a year. The fluorescence was determined with the fluorescence emission at 525 nm and 460 nm using 488 nm and 360 nm excitation, respectively.

2.11 Colony Formation Assay

To investigate the role of *ABCC5* gene in clonogenicity of breast cancer cells, 200 cells (WT and heterozygous KO clones) were seeded in a 6-well plate and incubated for 10 days.

To investigate the influence of olaparib on clonogenicity of breast cancer cells and *ABCC5* knockout cells, 2000 cells (WT and heterozygous KO clones) were seeded in a 96-well plate 24-hr prior to the addition of olaparib. Cells were treated with serially diluted olaparib for 4 hours, followed by 4 days incubation with fresh CM.

After incubation, CM was removed gently, and cells were rinsed with 2 mL (6-well plate) or 200 µL (96-well plate) of PBS. Cells were fixed with 1 mL (6-well plate) or 100 µL (96-well plate) of 4% PFM for 15 min at room temperature. Cells were stained

with 0.5% crystal violet solution for 15 min at room temperature. After incubation, crystal violet was rinsed off by immersing the plates in tap water. The plates were allowed to air dry for few minutes and imaged using Zeiss Primovert Compact Inverted Microscope (Carl Zeiss AG). The colonies were analysed and counted using ImageJ software.

2.12 Data Analysis

Data were presented by descriptive statistics as mean value with standard error of the mean (mean ± SD). Linear and non-linear regression were carried out using PRISM® software (GraphPad, Version 8.0). The statistical analysis was performed by a one-way or two-way analysis of variance (ANOVA) with a post-hoc test (Sidak's multiple comparison post-test) or Student's unpaired t-test by using PRISM® software (GraphPad, Version 8.0). All data analysed using ANOVAs should meet the assumptions of equal variance and homogeneity. Comparisons between two or more groups with a *P*-value of < 0.05 were considered statistically significant.

For the IC_{50} calculation, normalised mean absorbance values were obtained from independent experiments and non-linear regression analyses were applied to determine IC_{50} values of drugs using PRISM® software (GraphPad, Version 8.0). The data were fit into a nonlinear regression inhibition-response model with variable slope (three parameters), using the following equation.

$$Y = Bottom + (Top-Bottom)/(1+10^{((LogIC_{50}-X)*H)})$$

Where Bottom and Top stand for the minimum and maximum viability values determined in MTT assay, respectively; X for logarithm concentration; and H for Hill slope.

Chapter 3. Establishment of *ABCC5* Gene Knockout Breast Cancer Cell Model

3.1 Introduction

The CRISPR-Cas9 system is an established natural defence mechanism of bacteria protecting against invading pathogens encoded by nearly all archaea and approximately half of bacteria (Barrangou et al., 2007; Makarova et al., 2011; Terns & Terns, 2011). These immune systems mainly consist of the CRISPR (clustered regularly interspaced short palindromic repeat) and Cas (CRISPR-associated) genes. This genome editing strategy is superior to other technologies, including zinc finger nucleases (ZFNs) and transcription activator-like effector nucleases (TALENs), given its ease of design, cost-effectiveness, greater on-target DNA cleavage activity, multiplexing capabilities, and wide suitability for diverse cell types and organisms. These features make it a reliable and controllable gene-editing system with high specificity and efficiency (Carroll, 2014; Mali et al., 2013).

Generally, CRISPR-Cas systems have been divided into three types (I–III) across an array of bacterial and archaeal hosts. Within the three types of CRISPR-Cas systems, the type II CRISPR-Cas system is well documented and developed. The bacterial type II CRISPR-Cas system was initially constructed as a dual RNA-guided Cas endonuclease complex which could mediate site-specific DNA double-stranded breaks (DSBs) in vitro and in mammalian cells (Bhaya, Davison, & Barrangou, 2011; Terns & Terns, 2011; Wiedenheft, Sternberg, & Doudna, 2012). The combination of a 42-nucleotide CRISPR RNA (crRNA) and an 80-nucleotide transactivating crRNA

(tracrRNA) yields the dual RNA complex known to be recognized by Cas9 protein. The former directs the RNA-Cas9 protein complex to a particular site of the cellular genome with the sequence adjacent to a protospacer adjacent motif (PAM) *via* Watson–Crick pairing, whereas the latter binds to the former through the partially complementary sequence (Figure 3.1) (Jinek et al., 2012). To enhance the efficiency of double-stranded break activity, a modified single 102-nucleotide guide RNA (sgRNA) has been introduced as a fusion of crRNA and tracrRNA, simplifying the original two RNA system into simple one (Cong et al., 2013; Jinek et al., 2012; Mali et al., 2013). After the cationic lipid-mediated delivery of the RNA-Cas9 protein complex into a cell by endocytosis, the expected sequence of the cellular genome can be cleaved by this complex, allowing the generation of DSBs. Upon cleavage by Cas9, in mammalian cells, the lesion on the target locus (DSB) is repaired through one of the two major mechanisms, including mutagenic nonhomologous end-joining (NHEJ) known to re-ligate and disrupt gene by frameshift mutations where the insertion or deletion of several base-pairs (indels) appears, and homologous recombination (HDR) with the presence of an exogenous donor template for the precise insertion of a designated sequence (Carroll, 2014; Mali et al., 2013). Two forms of repair template can be leveraged to mediate the indel sequence, the single-stranded DNA oligonucleotides (ssODNs) and the conventional double-stranded DNA targeting constructs with homology arms flanking the insertion sequence. The former is associated with small edits in the genome, such as the application of single-nucleotide mutations for probing causal genetic variations. Unlike NHEJ, the activation of HDR is contingent on the cell type and state since it is normally active in dividing cells (F. Chen et al., 2011; Saleh-Gohari & Helleday, 2004). Most lesion repair outcomes are considered insertions or deletions (indels) of no more than 20 bp. Indels of larger size are rarely reported

(Kosicki, Tomberg, & Bradley, 2018). The RNA-Cas9 protein complex can be cleared rapidly within 48 hours, minimizing the chance for off-target cleavage when compared to vector systems. The Cas9 nuclease has been tested in a wide variety of suspension and adherent cell lines and has shown superior genomic cleavage efficiencies and cell survivability compared to plasmid-based CRISPR systems (F. Chen et al., 2011; Cong et al., 2013; Perez et al., 2008).

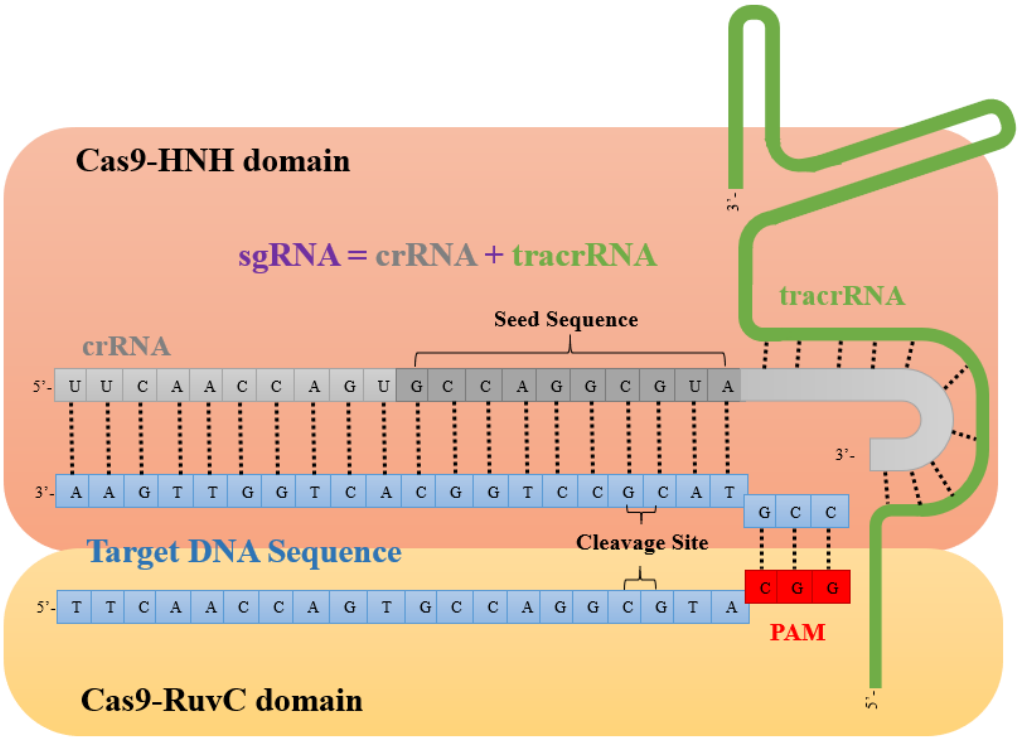

Figure 3.1. Schematic illustration of DNA recognition by CRISPR-Cas9. Cas9 protein along with sgRNA binds to its complementary target DNA adjacent to a 3'-PAM. HNH domain of Cas9 protein cleaves the complementary strand, while RuvC domain cleaves the noncomplementary strand. The 10-nt crRNA seed sequence recognizes DNA closest to the PAM sequence. The cleavage site of Cas9 protein is always 3-4 nucleotides upstream of the PAM sequence. Dashed lines between nucleotides represent direct base pairing. **Abbr., PAM:** protospacer adjacent motif.

The development of the CRISPR-Cas9 system enables researchers to carry out proof-

of-principle studies in animal models. A previous study demonstrated the ability to edit both alleles of a target gene in one generation of mice (H. Wang et al., 2013). Another study elucidated a model for delivering sgRNA *in vivo* that adeno-associated virus (AAV)-mediated gene delivery and its subsequent transcription could produce the sgRNA and Cas9 protein (S. Chen et al., 2015; Platt et al., 2014). However, the successes in animal models are still unable to dispel concerns with regard to practice, ethics, and safety in human clinical trials (Baltimore et al., 2015). The first challenge in using the CRISPR-Cas9 system as a potential therapeutic approach is the specific delivery of the Cas9 protein and sgRNA to recipient cells (F Ann Ran et al., 2015). Additionally, to which extent the potential off-target cleavage would influence the prognosis of patients restricts its therapeutic potentials (Fu et al., 2013; Patrick D Hsu et al., 2013; Kuscu, Arslan, Singh, Thorpe, & Adli, 2014; Pattanayak et al., 2013; Tsai et al., 2015). The existence of persistent nuclease activity also remains an obstacle to effectively protect *in vivo* sgRNA from hydrolysation (Patrick D Hsu et al., 2013; Lin, Staahl, Alla, & Doudna, 2014; Pattanayak et al., 2013). Previous studies reported that crRNA (CRISPR RNA) with chemical modifications showed greatly increased half-lives with the presence of ribonucleases in serum and tissues *in vivo* (Braasch et al., 2003; Chiu & Rana, 2003). Meghdad Rahdar et al. (2015) developed scrRNA (synthetic CRISPR RNA) with five 2'-*O*-Me-modified nucleotides at both the 5'- and 3'-termini with a fully substituted phosphorothioate backbone (scrRNA-PS-OME), and with cRt modifications at the 3'-end of scrRNA showing increased stability and transfection activity.

The main aim of this chapter is to establish *ABCC5* gene knockout (KO) cell lines in MDA-MB-231 and BT549 TNBC cells, as well as MCF7, a non-TNBC control group. A specific single guide (sg)RNA was designed to flank the target chromatin region. The

target DNA sequence was deleted once the simultaneous double-stranded breaks (DSB) were formed. The two distal DNA ends were reconnected by nonhomologous end-joining DNA repair route (NHEJ) (Kuscu et al., 2014; Matys et al., 2003). *ABCC5* KO cells were then isolated through limiting dilution cloning by which a monoclonal clone was established. To screen KO clones, PCR was employed to detect the gene cleavage efficiency. Primers (short DNA fragments) containing sequences complementary to the target region, along with a DNA polymerase (e.g., Taq polymerase), selectively and exponentially amplified the specific gene segment in which indels occur. The indel locus was further cleaved by Detection Enzyme, and thus two nucleotide chains in different lengths were detected. The cleavage efficiency was analysed by comparing the cleaved amplicons with the parental on a UV transilluminator (SamrtView Pro 1100 Imager System, UVCI-1100; MS Major Science). The sequence of the edited gene was determined using Sanger Sequencing Service. To check the expression of ABCC5 protein in KO clones, three distinct assays were performed. For western blotting assay, cell lysate containing sample proteins and a standard ladder were separated in a molecular weight-dependent manner and visualised by chemiluminescent antibodies. For surface staining assay and immunocytochemistry, cells were stained with fluorescent antibodies. The expression level of ABCC5 protein was in direct proportion to signal intensity. Functional expression of ABCC5 was assessed by measuring the cellular accumulation of a typical fluorescent substrate BCECF using cell uptake study (Kolber, Quinones, Gress, & Henkert, 1988). ABCC5 transporter has been reported to play a role in retarding the accumulation of BCECF by pumping them out extracellularly, leading to a relatively lower accumulation in ABCC5-rich cells.

3.2 Material and Methods

The details of the chemicals and experimental methods are shown in Chapter 2.

3.3 Results

3.3.1 Validation of Morphology of Cell Lines

To validate the MDA-MB-231 and BT549 TNBC cell lines and the non-TNBC MCF7 cell line, cell morphology was visualized by using Zeiss Primovert Compact Inverted Microscope (Carl Zeiss AG) and compared with the supplier's schematic illustration from ATCC (Cryosite Ltd, NSW, AU) (Figure 3.2).

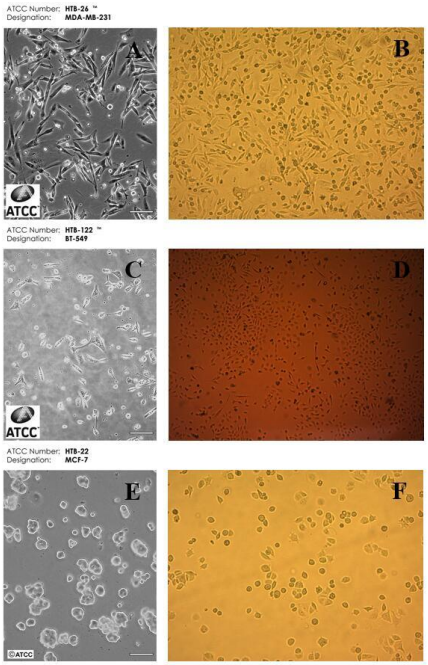

Figure 3.2 Morphology of human breast cancer cell lines used in this study. Images for MDA-MB-231 cells in Panel A, BT549 cells in Panel C and MCF7 cells in Panel E were obtained from ATCC (Cryosite Ltd, NSW, AU). Images for MDA-MB-231 cells in Panel B, BT549 cells in Panel D and MCF7 cells in Panel F were taken using Zeiss Primovert Compact Inverted Microscope (Carl Zeiss AG) and cells were cultured in Applied Sciences Laboratory in Auckland University of Technology (AUT).

3.3.2 Validation of ABCC5 and ABCC2 Functional Expression in TNBC Cells

Before investigating the ABCC5 expression in breast cancer cells using western blotting assay (section 2.9), both the total protein stain and immunoblotting assay were confirmed to be linear over a series of protein quantities. This ensured that both assays accurately measured the changes in total protein and ABCC5 expression at the range of amounts expected in subsequent experiments.

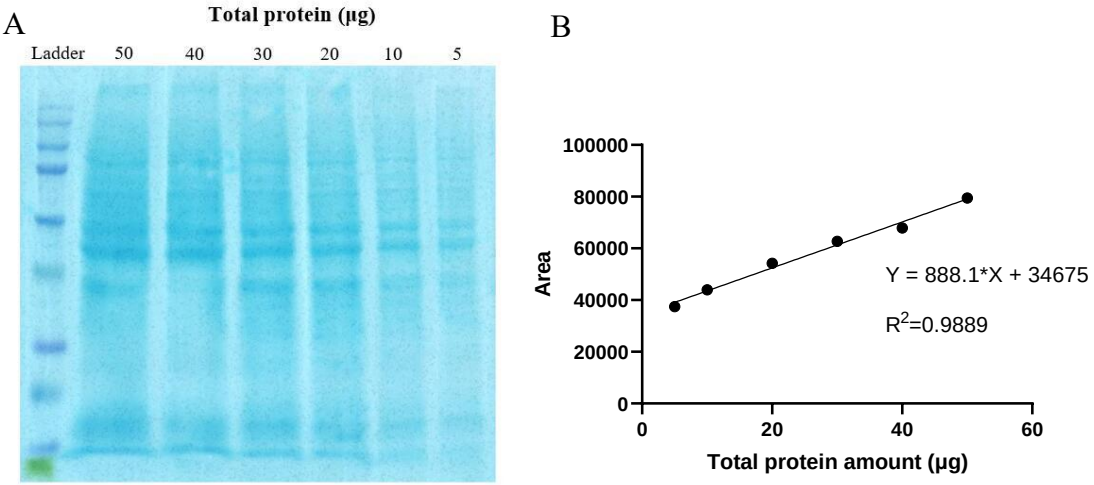

Figure 3.3 Total protein stain of serially diluted MDA-MB-231 cell lysate. A. Total protein stain. The amount of total protein loaded per well was labelled at the top of the image. **B.** A plot of area value vs. protein amount. A line of best-fit with the R^2 value of the goodness-of-fit was shown. The area values were measured using ImageJ software.

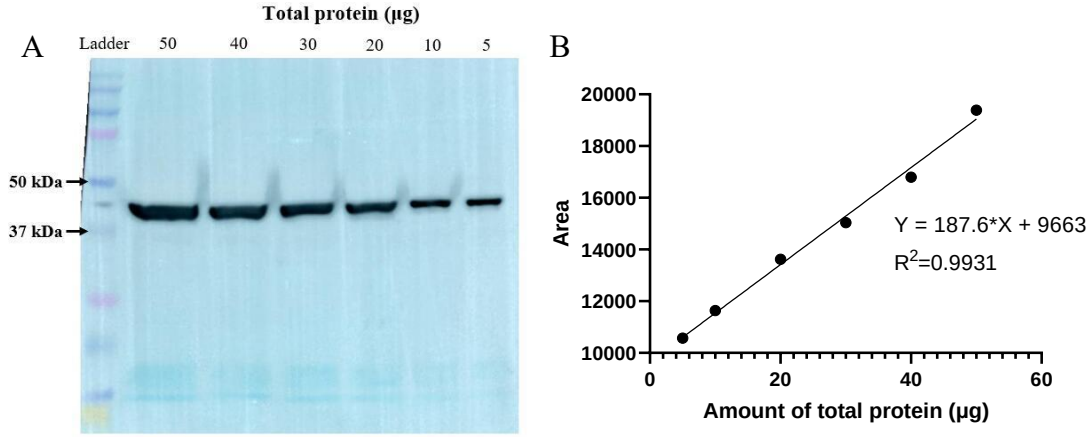

Figure 3.4 Immunoblot of serially diluted MDA-MB-231 cell lysate. A. The beta-actin (42 kDa) on the PVDF membrane was stained by Monoclonal Anti-β-Actin Antibody and Donkey Anti-Mouse IgG (H+L) Highly Cross-Adsorbed Secondary Antibody, HRP. **B.** A plot of area value vs. protein amount. A line of best-fit with the R^2 value of the goodness-of-fit was shown. The area values were measured using ImageJ software.

Figure 3.3A shows the total protein staining of serially diluted MDA-MB-231 cell lysate with protein quantities ranging from 5 to 50 µg. The area value of each lane was plotted against the loaded protein in Figure 3.3B. A best-fit line shows that the total protein band densities (area values) determined using ImageJ software was linearly increased (R^2 = 0.9889) with the protein amounts.

In Figure 3.4A, an immunoblot of beta-actin with the Monoclonal Anti-β-Actin Antibody and Donkey Anti-Mouse IgG (H+L) Highly Cross-Adsorbed Secondary Antibody is shown using serially diluted MDA-MB-231 cell lysate (5 to 50 µg). A single band with a molecular weight of around 42 kDa was detected, which corresponds to the reported size of the beta-actin (Eaton et al., 2013). The band density of beta-actin for each lane was plotted against the amounts of total protein. A line of best-fit through the points with an R^2 value of 0.9931 shows that the quantified beta-actin band density was linear over the designated protein amount range (Figure 3.4B). These results

suggest that the total protein loaded per well can range from 5 to 50 μg in the subsequent experiments, which fits nicely in the linear relation between band density and protein amounts.

The functional ABCC5 expression was then confirmed in breast cancer cells using cell surface staining assay (section 2.7.1) and flow-cytometry-based cell uptake study (section 2.7.2.1).

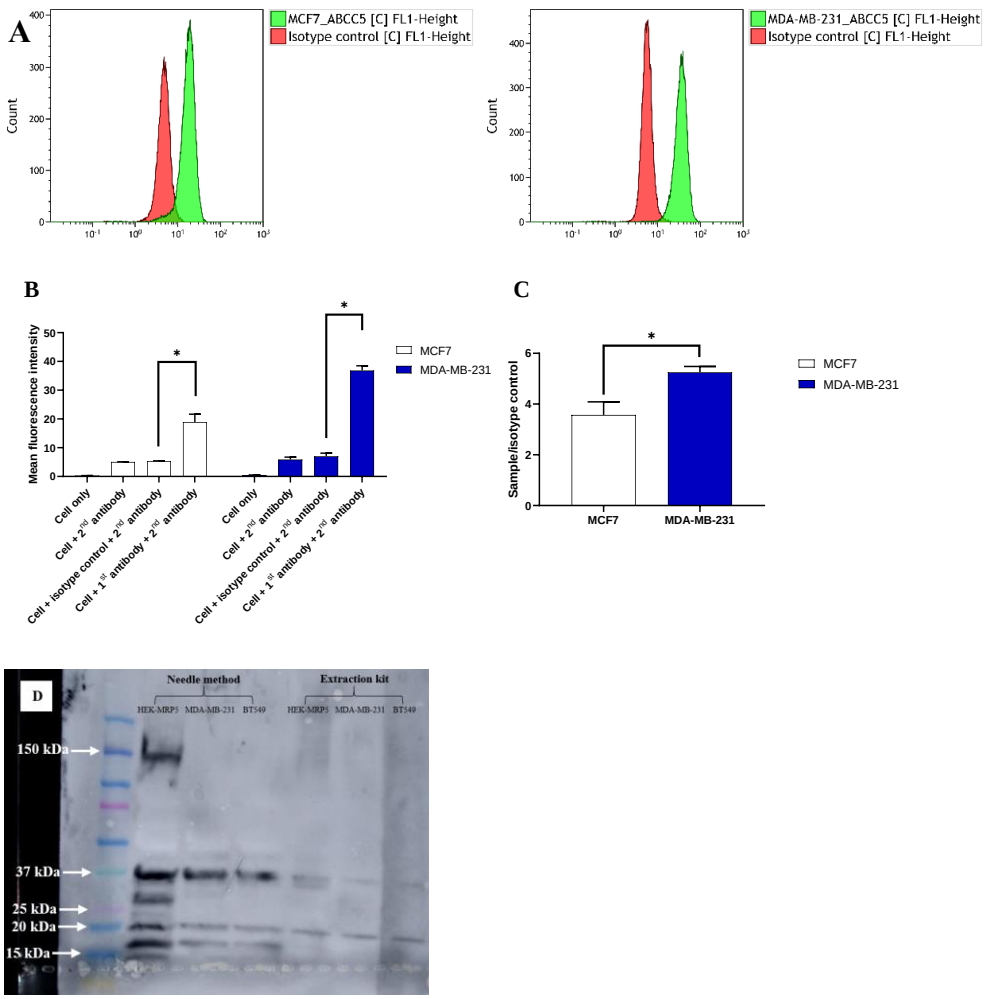

Figure 3.5 Validation of ABCC5 expression in MDA-MB-231 and MCF7 cells. A. ABCC5 protein detected in representative flow cytometry histogram of cell surface staining using the anti-ABCC5 (green) and isotype control IgG2a (red) on MCF7 and MDA-MB-231 cells. Both the primary antibody and isotype control were labelled with Alexa Fluor 488 secondary antibody. The X-axis is the fluorescence signal intensity displayed in a linear log scale. **B.** Immunostaining of MDA-MB-231 and MCF7 cells using MRP5 Monoclonal Antibody and Goat Anti-Rat IgG H&L (DyLight® 488) secondary antibody. Results were plotted as average fluorescence vs. cell type. Data were presented as mean ± SD of three independent experiments, each repeat was run in duplicates. *$P < 0.05$ significantly different from the fluorescence of the corresponding isotype control, calculated using Student unpaired t-test. **C.** Comparison of ABCC5 expression level in MDA-MB-231 and MCF7 cells. Results were plotted as fluorescence intensity of sample/fluorescence intensity of isotype control vs. cell type. Data were presented as mean ± SD of three independent experiments, each repeat was run in duplicates. *$P < 0.05$ significantly different from the fluorescence of the non-TNBC MCF7 cells, calculated using Student unpaired t-test. **D.** Immunoblot of membrane fractions from HEK-MRP5, MDA-MB-231 WT, and BT549 WT cells using MRP5 Monoclonal Antibody and Goat anti-Rabbit IgG (H+L) Secondary Antibody, HRP.

In terms of Western Blotting results, only shorter bands than expected could be detected in TNBC cell lines (Figure 3.5D). These bands were more like degraded ABCC5 protein considering the multiple bands shown in the positive control, HEK-MRP5 cells (Figure 3.5D). This degradation might appear in the protein extraction step. Thus, different extraction methods were tested, including the needle method, as shown in section 2.9.1.2, standard lysis method using RIPA buffer (section 2.9.1.1), acetone protein precipitation, and a commercial membrane protein extraction kit (Mem-PER™ Plus Membrane Protein Extraction Kit). Unfortunately, none of these methods could contribute to the expected results in TNBC cell lines. Only degraded bands could be observed in TNBC cell lines when the needle method (section 2.9.1.2) was applied, as shown in Figure 3.5D. Future studies may aim at increasing the protein concentration of samples by using an ultra-centrifuge. To examine ABCC5 expression in TNBC cell lines, alternative methods, including cell surface staining (section 2.7.1) and immunocytochemistry (section 2.10), were used in this study. Figure 3.5A and B shows immunostaining results, which demonstrate the expression level of ABCC5 in MDA-MB-231 and MCF7 cells. BT549 cells were not tested due to the breakdown of the flow cytometer. After staining with MRP5 Monoclonal Antibody and Goat Anti-Rat IgG H&L (DyLight® 488) secondary antibody in cell surface staining assay, the ABCC5 fluorescence intensity of each cell line was compared with the corresponding isotype control group (Rat IgG2α Isotype Control). This comparison eliminated the background staining due to Fc receptors on target cells, nonspecific interactions with cellular proteins, carbohydrates, lipids, and cell autofluorescence. All of the selected cell lines in this study exhibited expression of ABCC5 with a *P*-value of < 0.05 compared with isotype control. To compare the expression level of ABCC5 in these three cell lines, the fluorescence intensity of samples was divided by the fluorescence intensity of isotype

control. In Figure 3.5C, a *P*-value of < 0.05 demonstrates that the expression level of ABCC5 in MDA-MB-231 TNBC cells was significantly higher than non-TNBC MCF7 cells. The immunostaining results correspond to the cell uptake study that the ABCC5-mediated BCECF export was reversed by benzbromarone compared to the DMSO control group in MDA-MB-231 and MCF7 cells (Figure 3.6). BT549 cells were not tested due to the breakdown of the flow cytometer. The ABCC5-mediated rate-limiting effect on BCECF accumulation was suppressed by pre-incubating the cells with either 20 or 50 μM benzbromarone for 30 min. However, unlike the isogenic HEK-P and HEK-MRP5 cells, the BCECF accumulation was unable to reflect the variations of ABCC5 functional expression in different cell lines considering the different cell morphology and granularity. These results suggest that ABCC5 was functionally overexpressed in MDA-MB-231 TNBC cells compared to the non-TNBC MCF cells. The subsequent cytotoxicity studies in these cell lines are based on the ABCC5 expression and function to evaluate the role of this membrane transporter in doxorubicin and olaparib sensitivity in TNBC cells.

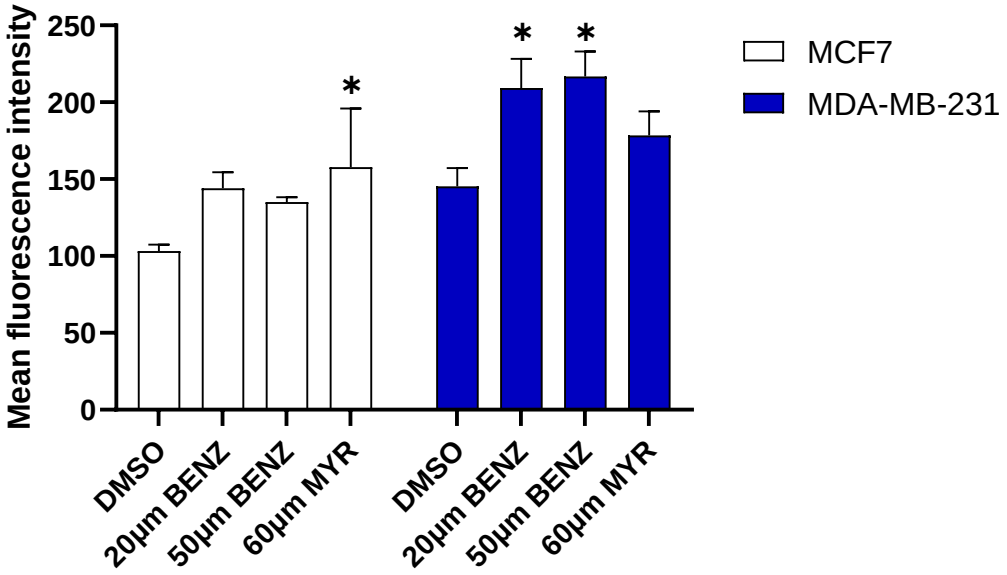

Figure 3.6 The cellular accumulation of BCECF in MDA-MB-231 and MCF7 cells after 30 min pre-incubation with 20 µM benzbromarone, 50 µM benzbromarone and 60 µM myricetin, respectively. Results were plotted as average fluorescence vs. cell type. Data were presented as mean ± SD of two independent experiments, each repeat was run in duplicates. **P*<0.05 significantly different from the BCECF accumulation in corresponding DMSO control groups, calculated using one-way ANOVA and Sidak's multiple comparison post-test to compare all treatment groups with the corresponding DMSO control group within each cell type.

To explore whether overexpression of ABC transporters is prevalent in TNBC cells, MDA-MB-231 TNBC cells and non-TNBC MCF7 cells were determined the expression of another ABC transporter ABCC2 using cell surface staining assay (section 2.7.1).

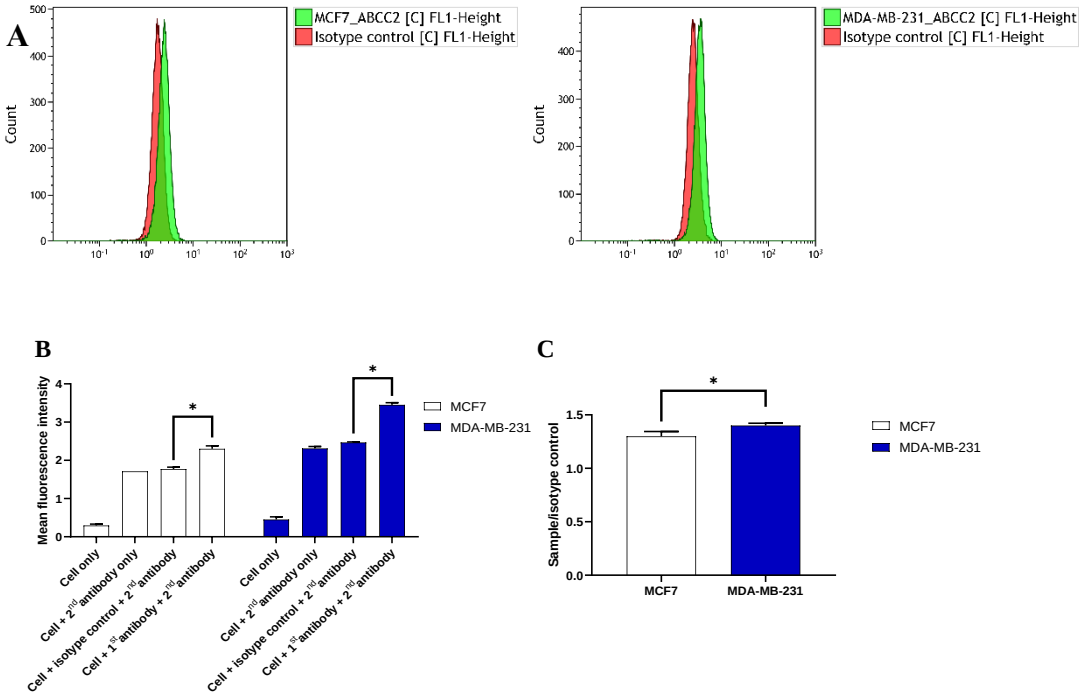

Figure 3.7 Validation of ABCC2 expression in MDA-MB-231 and MCF7 cells compared with the isotype control using cell surface staining assay. A. ABCC2 protein detected in representative flow cytometry histogram of cell surface staining using the anti-ABCC2 (green) and isotype control IgG2a (red) on MCF7 and MDA-MB-231 cells. Both the primary antibody and isotype control were labelled with Alexa Fluor 488 secondary antibody. The X-axis is the fluorescence signal intensity displayed in a linear log scale. **B.** Immunostaining of MDA-MB-231 and MCF7 cells using MRP2 Monoclonal Antibody and Goat Anti-Mouse IgG H&L secondary antibody. Results were plotted as average fluorescence vs. cell type. Data were presented as mean ± SD of triplicates. **P* < 0.05 significantly different from the fluorescence of the corresponding isotype control, calculated using Student unpaired t-test. **C.** Comparison of ABCC2 expression level in MDA-MB-231 and MCF7 cells. Results were plotted as fluorescence intensity of sample/fluorescence intensity of isotype control vs. cell type. Data were presented as mean ± SD of triplicates. **P* < 0.05 significantly different from the fluorescence of the non-TNBC MCF7 cells, calculated using Student unpaired t-test.

Both MDA-MB-231 and MCF7 cells had an expression of ABCC2 with a *P*-value of < 0.05 compared with isotype control (Figure 3.7A and B). A *P*-value of < 0.05 demonstrates that the expression level of ABCC2 in MDA-MB-231 TNBC cells was significantly higher than non-TNBC MCF7cells (Figure 3.7C). These results suggest that ABCC2 was also functionally overexpressed in MDA-MB-231 TNBC cells

compared to non-TNBC MCF7 cells. Overexpression of ABC transporters may thus be a prevalent phenotype among TNBC cell lines.

3.3.3 Establishment of *ABCC5* Gene Knockout Clones

3.3.3.1 *ABCC5* Gene Knockout Efficiency

The role of ABCC5 in doxorubicin and olaparib cellular sensitivity in MDA-MB-231, BT549 and MCF7 cells was determined using an *ABCC5* gene deletion cell model. To establish an *ABCC5* gene knockout cell line, a CRISPR-Cas9-based method was applied in these cell lines in this study. A specific sgRNA was designed in complex with Cas9 protein to form ribonucleoprotein (RNP), which was delivered into cells through endocytosis. The specific chromatin region was flanked by RNP and cleaved by Cas9 protein. The DSBs were reconnected by nonhomologous end-joining DNA repair route (NHEJ). The genomic DNA of the transfected cells were extracted and amplified to determine cleavage efficiency. The pooled population of knockout cells transfected with *ABCC5*-sgRNA (IDT technology) are supposed to have three bands, one parental band of PCR product (428 bp) and two cleaved bands (~238 bp and ~170 bp).

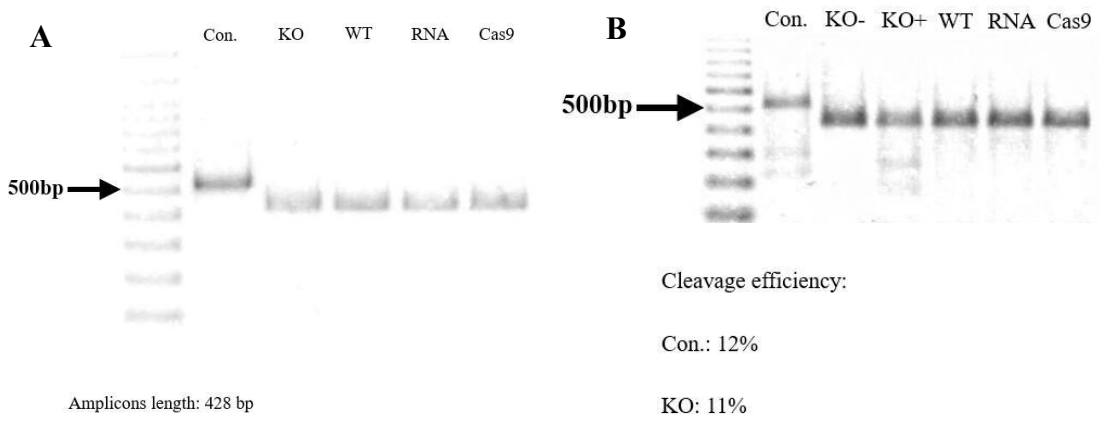

Figure 3.8 Determination of knockout efficiency in MDA-MB-231 cells. A. Gel image of PCR amplicons of MDA-MB-231 wild-type (WT) and KO cell lysate, as well as control groups. The above samples were PCR amplified using IDT-fwd and IDT-rev primers flanking the region of interest. A positive control group provided in GeneArt™ Genomic Cleavage Detection Kit was done to validate the manipulations. **B.** Enzyme digestion in MDA-MB-231 WT and KO PCR products, as well as control groups. A positive control group provided in GeneArt™ Genomic Cleavage Detection Kit was done to validate the manipulations. All the samples were treated with Detection Enzyme except for a PCR product only group as a negative control (KO-).

Figure 3.8A shows the PCR amplification using MDA-MB-231 wild-type (WT), KO and control cells demonstrating the primer-flanking region where the cleavage site existed. A positive control provided in GeneArt™ Genomic Cleavage Detection Kit was done to validate the manipulations. After genomic cleavage detection assay (section 2.4.2), KO (KO+) and positive control (Con.) groups showed cleaved bands in ~238 bp/170 bp and ~291 bp/225 bp with a cleavage efficiency of 11% and 12%, respectively (Figure 3.8B). In comparison, the negative control, RNA only, Cas9 only and KO PCR product without Detection Enzyme (KO-) groups just exhibited a parental band of PCR amplicon, indicating non-cleavage in the sequence of interest. Similar results were found in BT549 and MCF7 KO cells with a cleavage efficiency of 3% and 7%, respectively, as shown in Figure 3.9 and Figure 3.10.

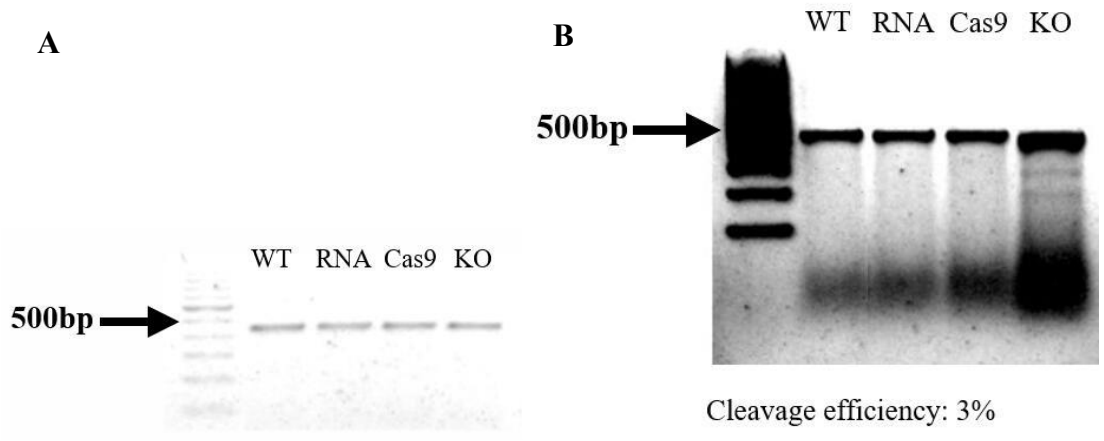

Figure 3.9 Determination of knockout efficiency in BT549 cells. A. Gel image of PCR amplicons of BT549 WT and KO cell lysate, as well as control groups. The above samples were PCR amplified using IDT-fwd and IDT-rev primers flanking the region of interest. **B.** Enzyme digestion in BT549 WT and KO PCR products, as well as control groups. All the samples were treated with Detection Enzyme.

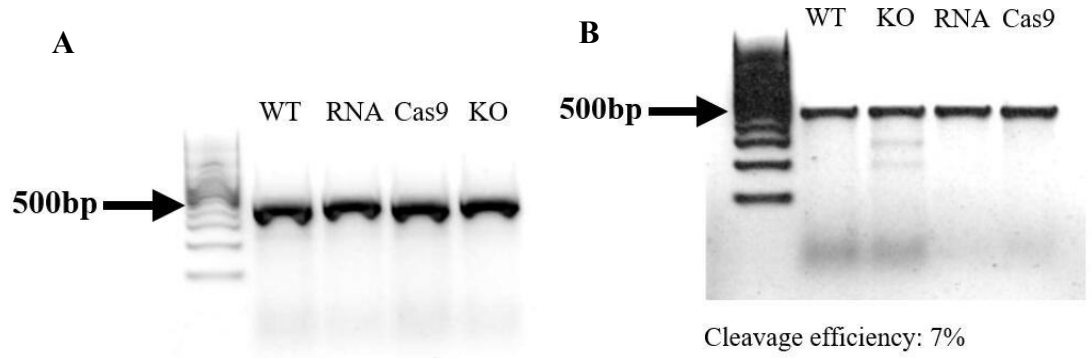

Figure 3.10 Determination of knockout efficiency in MCF7 cells. A. Gel image of PCR amplicons of MCF7 WT and KO cell lysate, as well as control groups. The above samples were PCR amplified using IDT-fwd and IDT-rev primers flanking the region of interest. **B.** Enzyme digestion in MCF7 WT and KO PCR products, as well as control groups. All the samples were treated with Detection Enzyme.

After validating ABCC5 knockout at a gene level, the functional expression of ABCC5 protein in the pooled population of KO cells was further investigated. The ABCC5-mediated rate-limiting effect on BCECF accumulation was determined using either flow-cytometry- or Spark® Multimode Microplate Reader-based cell uptake study

(section 2.7). With the decrease of ABCC5 expression, cellular BCECF accumulation is supposed to increase in pooled KO cells. However, no significant difference in BCECF accumulation was found between the pooled and WT cells in all three cell lines (Figure 3.11). This might be due to the low cleavage efficiency-induced limited proportion of KO cells in the pooled population, which could not enhance the overall fluorescence intensity.

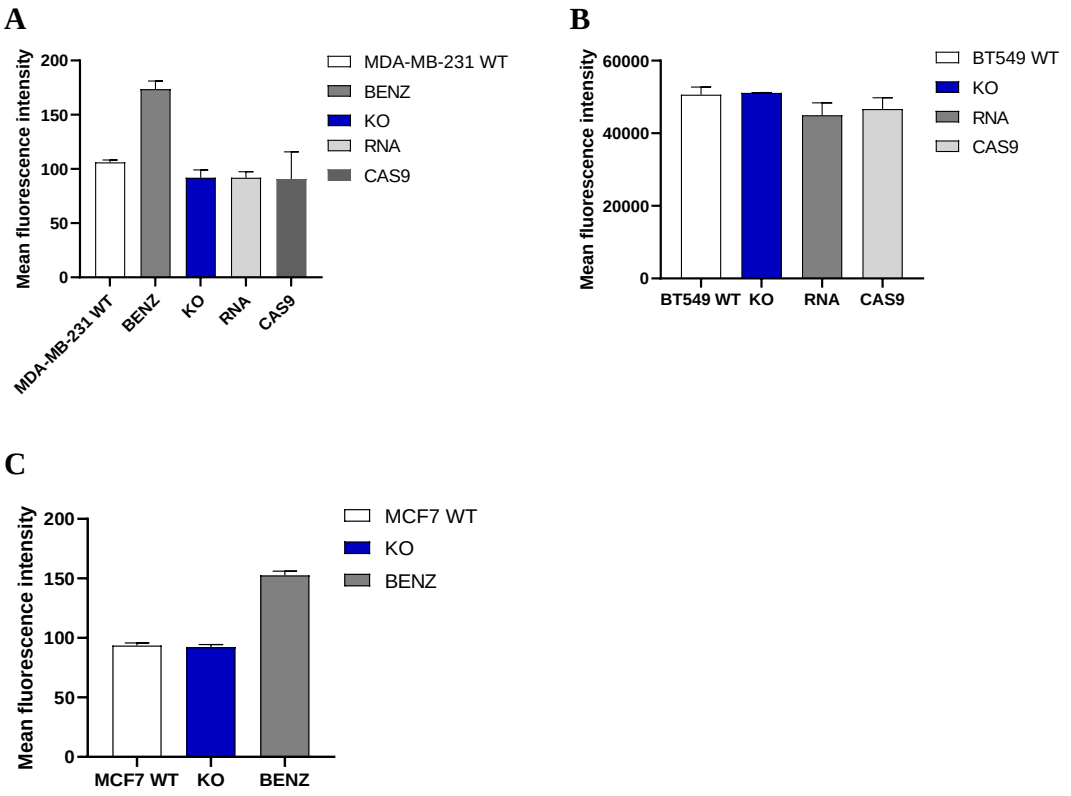

Figure 3.11 Determination of ABCC5 functional expression in the pooled population of MDA-MB-231 (A), BT549 (B) and MCF7 (C) KO cells compared with WT cells. Results were plotted as average fluorescence intensity vs. cell type. Data were presented as mean ± SD of triplicates. No difference was shown between the pooled KO population and WT cells in these three cell lines, calculated using Student's unpaired t-test.

3.3.3.2 Screening of Single Knockout Cell Clones

The knockout cells were isolated from the pooled population using limiting dilution cloning (section 2.4.4). The single knockout clones were then proceeded to Spark® Multimode Microplate Reader-based cell uptake study (section 2.7.2.2) to detect the ABCC5-mediated BCECF accumulation. To eliminate the variations in cell number, data were further normalised by dividing the protein concentration of cell lysate determined by DC protein analysis (section 2.9.2.1) into fluorescence intensity. Lack of ABCC5 expression in either homozygous or heterozygous KO clones results in a higher fluorescence intensity, which represents a higher intracellular accumulation of BCECF. The linear correlation between fluorescence reading and fluorescein with the presence of different detergents was examined using Spark® Multimode Microplate Reader-based cell uptake study (section 2.7.2.2). The tested lysis buffers did not affect the linearity of uptake study (Figure 3.12A, B, and C). Thus, the more potent lysis agent, Triton X-100, was adopted to lyse cells. The linearity of DC protein analysis (section 2.9.2.1) was further examined with the presence of 0.1% Triton X-100 as shown in Figure 3.12D.

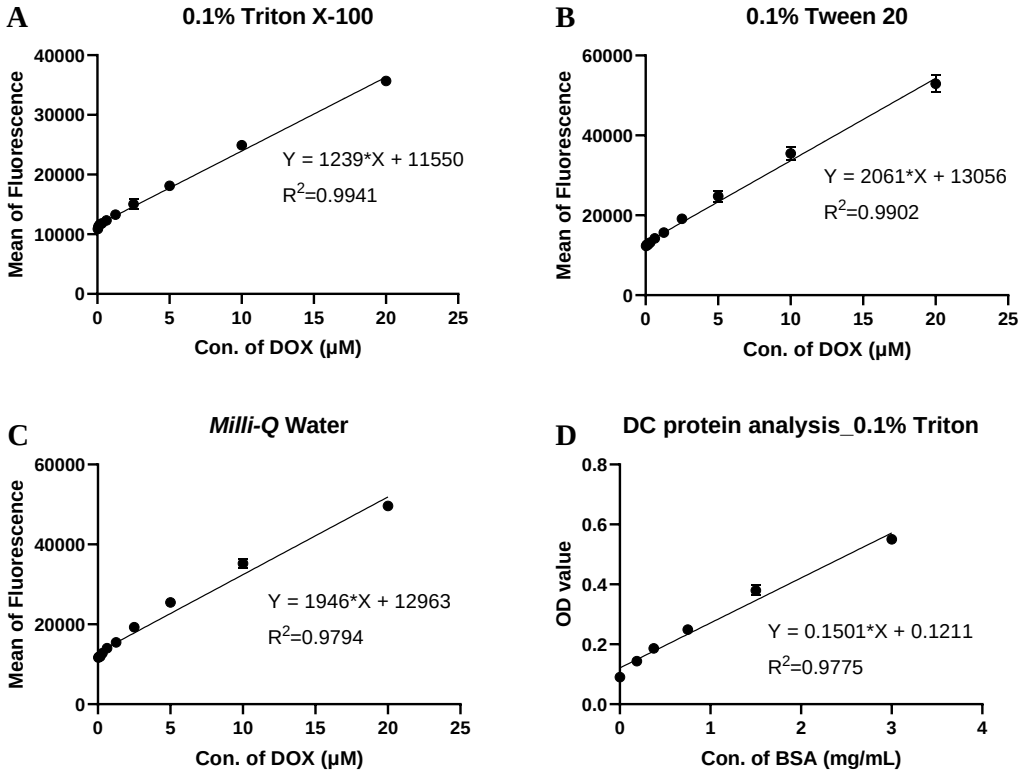

Figure 3.12 Validation of Spark® Multimode Microplate Reader-based cell uptake study and DC protein analysis. Doxorubicin was serially diluted in 0.1% Triton X-100 (**A**), 0.1% Tween 20 (**B**), and Milli-Q water (**C**), respectively. Data were presented as mean ± SD of duplicates. A line of best-fit with the R^2 value of the goodness-of-fit was shown. **D.** Linearity of absorbance (OD value) with increasing concentration of BSA in 0.1% Triton X-100. Data were presented as mean ± SD of triplicates. A line of best-fit with the R^2 value of the goodness-of-fit was shown.

Table 3.1 Screening of MDA-MB-231 single knockout cell clones. Data were presented as fluorescence intensity/protein concentration/10000. Results were compared with both DMSO-treated negative control MDA-MB-231 WT cells and positive control MDA-MB-231 cells pre-treated with 50 μM benzbromarone.

Clone NO.	**WT**	**BENZ**	**1**	**2**	**3**	**4**	**5**	**6**	**7**
Fu/mg/10000	10.392	20.732	11.592	12.958	9.556	11.560	18.402	10.912	8.705
Clone NO.	**8**	**9**	**10**	**11**	**12**	**13**	**14**	**15**	**16**
Fu/mg/10000	8.212	8.401	8.115	10.007	14.164	11.756	12.186	12.582	9.675
Clone NO.	**17**	**18**	**19**	**20**	**21**	**22**	**23**	**24**	**25**
Fu/mg/10000	8.226	10.508	10.355	9.111	9.621	9.370	11.650	9.046	13.174
Clone NO.	**26**	**27**	**28**	**29**	**30**	**31**	**32**	**33**	**34**
Fu/mg/10000	2.763	11.343	13.262	9.193	6.691	8.453	10.887	8.305	7.984
Clone NO.	**35**	**36**	**37**	**38**	**39**	**40**	**41**	**42**	**43**
Fu/mg/10000	8.195	8.402	15.402	14.100	18.229	13.256	12.971	21.770	18.665
Clone NO.	**44**	**45**	**46**	**47**	**48**	**49**	**50**	**51**	**52**
Fu/mg/10000	9.831	13.637	12.251	9.721	10.239	18.753	13.999	11.526	7.714
Clone NO.	**53**	**54**							
Fu/mg/10000	16.181	20.528							

The full data of MDA-MB-231 single knockout cell clones are shown in Table 3.1. The potential *ABCC5* gene knockout clones were labelled in red colour. The normalized fluorescence intensity ($\frac{\text{Fluorescence intensity}}{\text{Protein concentration}*10000}$) in clone 5, 12, 37, 39, 42, 43, 49, 53 and 54 were higher than WT and close to positive control cells pre-treated with 50 μM benzbromarone. To confirm the ABCC5-mediated BCECF accumulation in these clones, cells were appropriately counted and proceeded to Spark® Multimode Microplate Reader-based cell uptake study (section 2.7.2.2). In Figure 3.13, the BCECF accumulation in clone 39, 42, 43, 49, 53 and 54 was consistent with the above results. A *P*-value of < 0.05 demonstrates that clone 39, 42, 43 and 49 might be homozygous *ABCC5* gene KO clones, while clone 53 and 54 might be heterozygous *ABCC5* gene KO clones with a *P*-value of < 0.05. Clone 5, 12 and 37 were considered as WT cells.

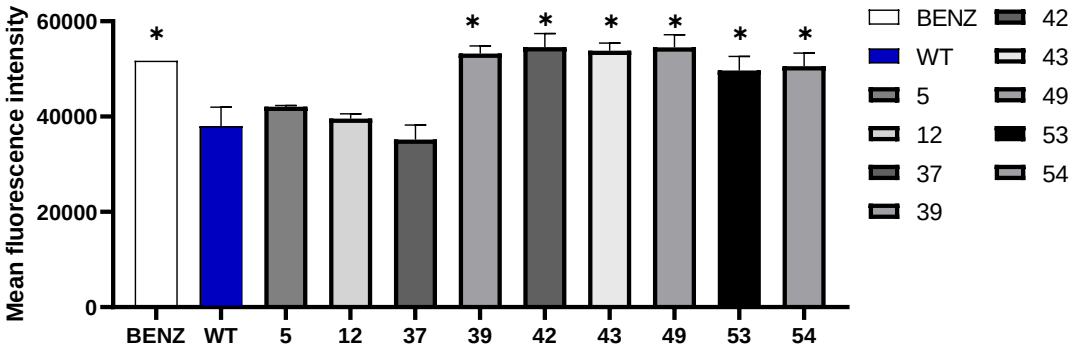

Figure 3.13 Confirmation of MDA-MB-231 single knockout cell clones. Data were presented as mean ± SD of duplicates. *$P < 0.05$ significantly different from the BCECF accumulation in negative control MDA-MB-231 WT cells treated with DMSO, calculated using one-way ANOVA and Sidak's multiple comparison post-test to compare all treatment groups with the DMSO control group.

The full data of BT549 single knockout cell clones were presented in the same manner as MDA-MB-231 KO clones, as shown in Table 3.2. The potential *ABCC5* gene knockout clones were labelled in red colour. The clones in grey colour were lost because of yeast contamination. The normalized fluorescence intensity ($\frac{\text{Fluorescence intensity}}{\text{Protein concentration} * 10000}$) in BT549 KO clone 26, 29, 30, 32, 39, 45, 46, 48, 49, 50, 53 and 60 were higher than WT and close to positive control cells pre-treated with 50 μM benzbromarone. To confirm the ABCC5-mediated BCECF accumulation in these clones, cells were counted properly and proceeded to Spark® Multimode Microplate Reader-based cell uptake study (section 2.7.2.2). In Figure 3.14, the BCECF accumulation in clone 30, 32, 39, 46, 49 and 53 was consistent with the above results. A *P*-value of < 0.05 demonstrates that clone 32, 39 and 49 might be homozygous *ABCC5* gene KO clones, while clone 30, 46 and 53 might be heterozygous *ABCC5* gene KO clones with a *P*-value of < 0.05. Clone 21, 22, 29, 40, 45, 48, 50, 52 and 54 were considered as WT cells.

Table 3.2 Screening of BT549 single knockout cell clones. Data were presented as fluorescence intensity/protein concentration/10000. Results were compared with both DMSO-treated negative control BT549 WT cells and positive control BT549 cells pre-treated with 50 μM benzbromarone.

Clone NO.	WT	BENZ	1	2	3	4	5	6	7
Fu/mg/10000	16.539	29.446	15.673	11.619	8.514	8.113	11.361	9.162	7.947
Clone NO.	8	9	10	11	12	13	14	15	16
Fu/mg/10000	8.973	43.837	13.062	11.384	6.727	6.941	9.882	10.695	12.444
Clone NO.	17	18	19	20	21	22	23	24	25
Fu/mg/10000	9.286	16.468	9.282	28.143	25.497	25.950	9.053	9.534	12.765
Clone NO.	26	27	28	29	30	31	32	33	34
Fu/mg/10000	34.491	12.587	11.391	41.844	20.117	11.149	41.683	7.904	3.776
Clone NO.	35	36	37	38	39	40	41	42	43
Fu/mg/10000	8.386	6.697	12.857	10.562	34.197	20.375	13.318	13.099	11.254
Clone NO.	44	45	46	47	48	49	50	51	52
Fu/mg/10000	14.509	20.869	45.916	15.721	17.688	29.247	26.593	14.454	28.315
Clone NO.	53	54	55	56	57	58	59	60	61
Fu/mg/10000	39.132	21.944	14.996	11.821	21.868	14.702	56.465	35.209	91.019

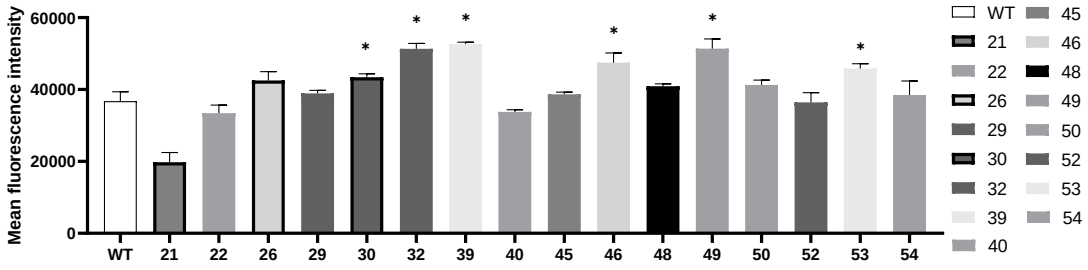

Figure 3.14 Confirmation of BT549 single knockout cell clones. Data were presented as mean ± SD of duplicates. *P < 0.05 significantly different from the BCECF accumulation in negative control BT549 WT cells treated with DMSO, calculated using one-way ANOVA and Sidak's multiple comparison post-test to compare all treatment groups with the DMSO control group.

The full data of MCF7 single knockout cell clones are shown in Table 3.3. The potential *ABCC5* gene knockout clones were labelled in red colour. The clones in grey colour

were lost because of yeast contamination. The normalized fluorescence intensity ($\frac{\text{Fluorescence intensity}}{\text{Protein concentration}*10000}$) in MCF7 KO clone 20, 23, 24 and 59 were higher than WT and close to positive control cells pre-treated with 50 μM benzbromarone. To confirm the ABCC5-mediated BCECF accumulation in these clones, cells were counted properly and proceeded to Spark® Multimode Microplate Reader-based cell uptake study (section 2.7.2.2). In Figure 3.15, the BCECF accumulation in all the clones showed no significant difference compared to WT cells, which means that all the clones may be considered as WT cells.

Table 3.3 Screening of MCF7 single knockout cell clones. Data were presented as fluorescence intensity/protein concentration/10000. Results were compared with both DMSO-treated negative control MCF7 WT cells and positive control MCF7 cells pre-treated with 50 μM benzbromarone.

Clone NO.	**WT**	**BENZ**	**1**	**2**	**3**	**4**	**5**	**6**	**7**
Fu/mg/10000	11.549	18.788	8.713	9.417	20.853	11.866	8.473	8.861	9.739
Clone NO.	**8**	**9**	**10**	**11**	**12**	**13**	**14**	**15**	**16**
Fu/mg/10000	13.751	9.081	11.396	9.893	8.903	25.904	9.928	18.668	52.522
Clone NO.	**17**	**18**	**19**	**20**	**21**	**22**	**23**	**24**	**25**
Fu/mg/10000	11.858	10.593	10.979	13.558	7.716	13.341	19.482	13.831	10.704
Clone NO.	**26**	**27**	**28**	**29**	**30**	**31**	**32**	**33**	**34**
Fu/mg/10000	9.035	10.055	12.062	9.038	12.448	11.677	8.995	10.319	7.879
Clone NO.	**35**	**36**	**37**	**38**	**39**	**40**	**41**	**42**	**43**
Fu/mg/10000	13.243	15.093	7.875	6.243	9.687	10.740	26.983	11.762	9.455
Clone NO.	**44**	**45**	**46**	**47**	**48**	**49**	**50**	**51**	**52**
Fu/mg/10000	7.326	9.909	14.175	13.951	9.282	35.988	12.819	5.843	5.232
Clone NO.	**53**	**54**	**55**	**56**	**57**	**58**	**59**	**60**	**61**
Fu/mg/10000	10.981	9.314	20.057	10.997	15.065	8.842	13.145	8.800	8.369
Clone NO.	**62**	**63**	**64**	**65**	**66**	**67**	**68**		
Fu/mg/10000	16.239	5.725	10.666	9.764	53.977	21.214	10.933		

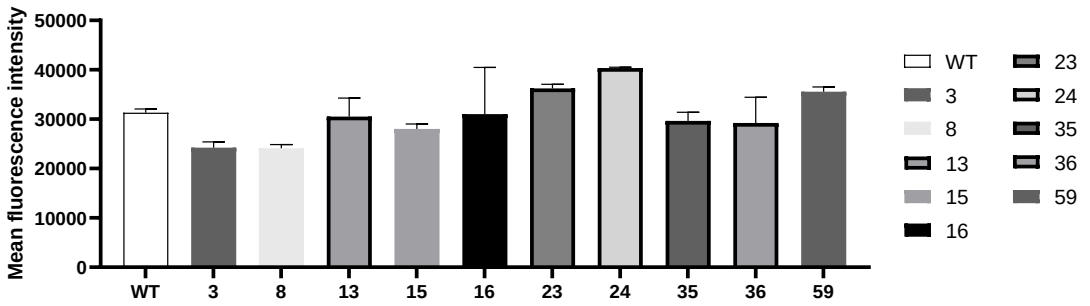

Figure 3.15 Confirmation of MCF7 single knockout cell clones. Data were presented as mean ± SD of duplicates. No significant difference from the BCECF accumulation in negative control BT549 WT cells treated with DMSO, calculated using one-way ANOVA and Sidak's multiple comparison post-test to compare all treatment groups with the DMSO control group.

3.3.3.3 PCR Amplicon Sequencing

After screening of *ABCC5* gene KO clones, the genomic DNA of these clones was PCR amplified and proceeded to Sanger Sequencing Service using IDT-rev primer (section 2.4.6) in Massey University to examine the frameshift in the target sequence.

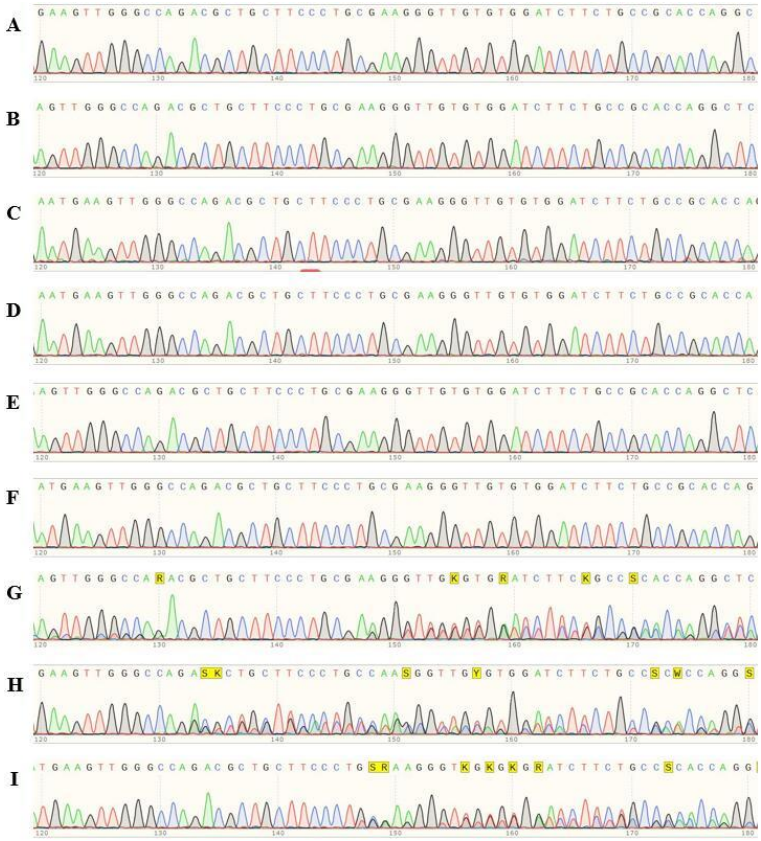

Figure 3.16 Sequencing results of MDA-MB-231 WT, negative control RNA only and Cas9 only groups, and KO single-cell clones. A. WT; **B.** RNA only; **C.** Cas9 only; **D.** Clone 39; **E.** Clone 42; **F.** Clone 43; **G.** Clone 49; **H.** Clone 53; **I.** Clone 54.

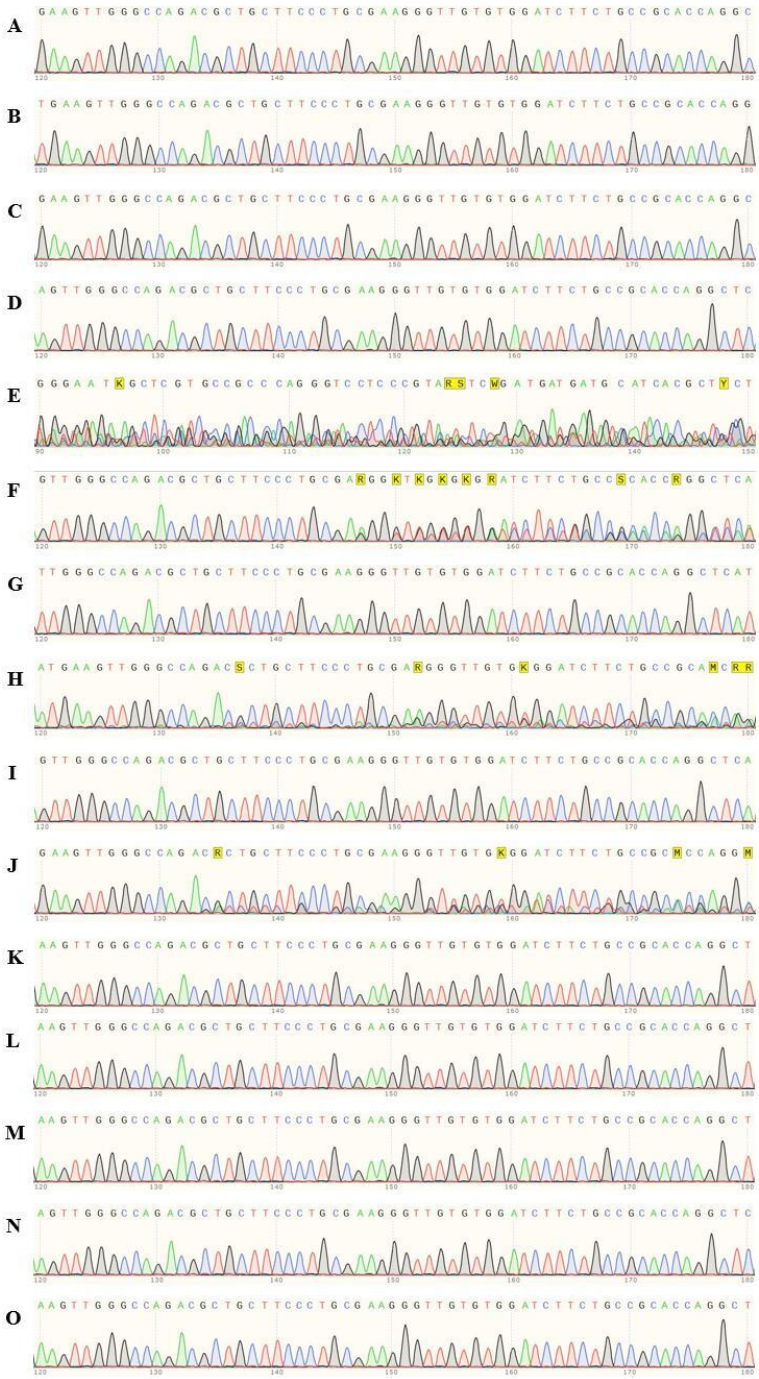

Figure 3.17 Sequencing results of BT549 WT, negative control RNA only and Cas9 only groups, and KO single-cell clones. A. WT; **B.** RNA only; **C.** Cas9 only; **D.** Clone 26; **E.** Clone 29; **F.** Clone 30; **G.** Clone 32; **H.** Clone 39; **I.** Clone 45; **J.** Clone 46; **K.** Clone 48; **L.** Clone 49; **M.** Clone 50; **N.** Clone 53; **O.** Clone 60.

Figure 3.18 Sequencing results of MCF7 WT, negative control RNA only and Cas9 only groups, and KO single-cell clones. A. WT; **B.** RNA only; **C.** Cas9 only; **D.** Clone 20; **E.** Clone 23; **F.** Clone 24; **G.** Clone 59.

In Figure 3.16A, Figure 3.17A and Figure 3.18A, the primer-flanking sequence of MDA-MB-231, BT549 and MCF7 WT cells were matched with the data from BLAST® (https://blast.ncbi.nlm.nih.gov/Blast.cgi) (Figure 0.2, Figure 0.11 and Figure 0.26 in appendix), indicating the homozygosity of non-mutated target sequence in these cell lines. The sequence of RNA only and Cas9 only groups was consistent with WT cells in all three cell lines demonstrating that sgRNA or Cas9 protein alone was unable to cleave the target site (Figure 3.16B, C, Figure 3.17B, C and Figure 3.18B, C). However, MDA-MB-231 KO clone 39, 42 and 43 (Figure 3.16D, E, F), which were initially considered as homozygous KO cells in cell uptake study (section 3.3.3.2), showed the same sequence as WT cells. A possible explanation is that other pathways relating to BCECF-AM hydrolysation or BCECF accumulation might be influenced by the agents used in transfection or by off-target effects. Clone 49, 53 and 54 were heterozygous KO clones with a WT allele and an allele containing indel (Figure 3.16G, H, I). Clone 49

had a WT allele and an allele with an "A" deletion (Table 3.4). Clone 53 had an edited allele with a 19 bp deletion after NHEJ repair (Table 3.4). A replacement of "GC" with "T" was found in the indel allele in clone 54 (Table 3.4). Similarly, BT549 KO clone 30 had a WT allele and an allele with an "A" deletion (Table 3.5). BT549 KO clone 29, 39 and 46 were mixed population rather than single-cell clones (Figure 3.17E, H, J), while the other BT549 KO clones and all of the four MCF7 KO clones were WT cells. The global alignment using BLAST® (https://blast.ncbi.nlm.nih.gov/Blast.cgi) of the primer-flanking sequence of each group compared with WT cells is shown in Figure 0.2 to Figure 0.32 in appendix.

Table 3.4 Sequence of the allele after NHEJ repair in heterozygous MDA-MB-231 KO clones.

	Sequence												
WT	GGG	CCA	GAC	GCT	GCT	TCC	CTG	CGA	AGG	GTT	GTG	TGG	AT
Clone 49	GGG	CCA	GAC	GCT	GCT	TCC	CTG	CGA	- GG	GTT	GTG	TGG	AT
Clone 53	GGG	CCA	G - -	- - -	- - -	- - -	- - -	- - -	- - G	GTT	GTG	TGG	AT
Clone 54	GGG	CCA	GAC	GCT	GCT	TCC	CTT	- GA	AGG	GTT	GTG	TGG	AT

Table 3.5 Sequence of the allele after NHEJ repair in heterozygous BT549 KO clones.

	Sequence												
WT	GGG	CCA	GAC	GCT	GCT	TCC	CTG	CGA	AGG	GTT	GTG	TGG	AT
Clone 30	GGG	CCA	GAC	GCT	GCT	TCC	CTG	CGA	-GG	GTT	GTG	TGG	AT

To confirm the existence of indels in single KO cell clones, genomic cleavage detection assay (section 2.4.2) was done using two representative clones, MDA-MB-231 KO clone 42 and 54. The former showed homozygous KO phenotype in cell uptake study and WT genotype in Sanger Sequencing assay, and the latter showed both heterozygous KO phenotype and genotype. In Figure 3.19A, no cleaved bands were detected, demonstrating that clone 42 was WT cells. In comparison, clone 54 showed two cleaved

bands with a parental band, indicating the heterozygosity of a WT allele and an allele with indel. In order to eliminate the possibility of identical indels in both alleles in clone 42 after NHEJ repair route, the PCR amplicons of clone 42 were mixed thoroughly with PCR amplicons of WT cells, followed by genomic cleavage detection assay (section 2.4.2). The addition of the WT DNA segment ensured the formation of mismatch in DNA duplex if the same indels existed in both alleles of clone 42. However, no cleaved bands were observed after enzyme digestion, which means that the primer-flanking sequence of clone 42 is identical with WT cells (Figure 3.19B). The up-regulated BCECF accumulation in clone 42 in cell uptake study (Figure 3.13) might be caused by either hyperactivation of BCECF-AM hydrolysation-related signalling or off-target effect of *ABCC5* sgRNA.

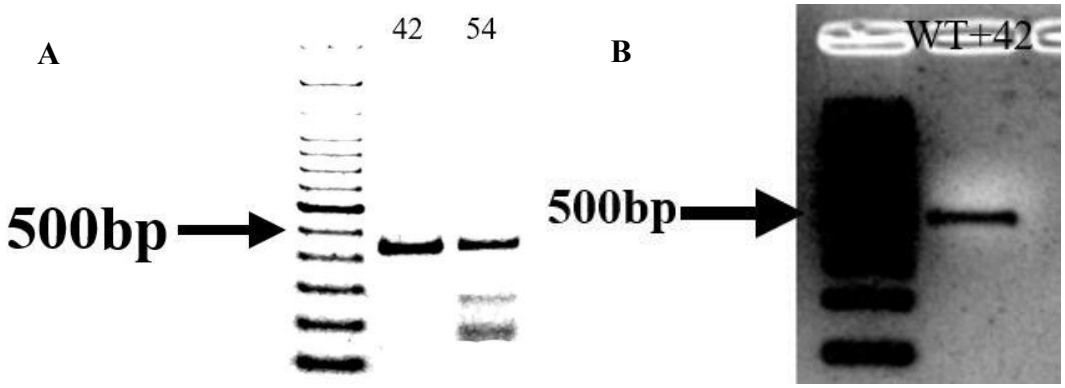

Figure 3.19 Confirmation of indels existing in two representative MDA-MB-231 single KO cell clones using genomic cleavage detection assay. A. Genomic DNA of clone 42 and 54 were PCR amplified and proceeded to genomic cleavage detection assay. B. Genomic DNA of WT cells and clone 42 was mixed thoroughly, followed by genomic cleavage detection assay.

3.3.3.4 Knockout of Wild-Type Allele in Heterozygous KO Clones

To knockout the WT allele in heterozygous KO clones, a dual-sgRNA system was

introduced in this study (section 2.3.1). Two sgRNAs with two different target sequences were used to delete a DNA fragment of around 1408 bp (IDT *ABCC5*-sgRNA + Thermofisher *ABCC5*-sgRNA set1) or 1385 bp (IDT *ABCC5*-sgRNA + Thermofisher *ABCC5*-sgRNA set2) (Figure 3.20 and Figure 3.21). Thus, two bands of 1849 bp and ~441/~464 bp in size were detected in the pooled population of KO cells when IDT forward and Thermofisher set1/2 reverse primers were used (Figure 3.20 and Figure 3.21). Theoretically, the edited allele in 1st round of KO should not be edited in 2nd round of KO due to the reuse of IDT *ABCC5*-sgRNA in 2nd round of transfection. IDT *ABCC5*-sgRNA was unable to target the edited allele in 1st round of KO due to the mismatch between the sequence of indel allele and IDT *ABCC5*-sgRNA. Therefore, the bands of 1849 bp in size might represent the WT allele and/or the edited allele in 1st round of KO in the pooled KO population.

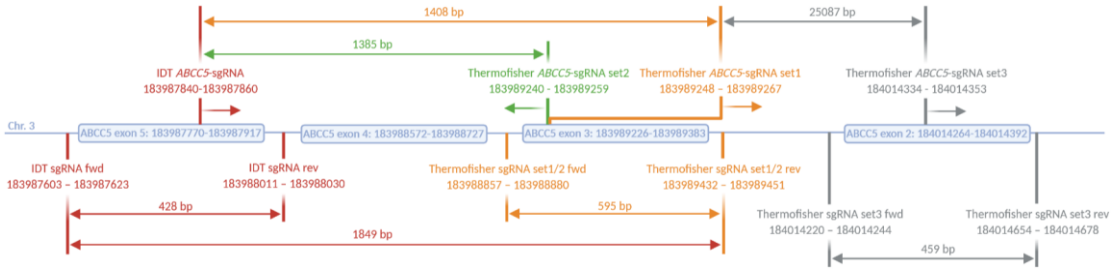

Figure 3.20 ABCC5 sgRNAs and primers used in this study. *Created with BioRender.com.*

A

```
        10         20         30         40         50
MKDIDIGKEY IIPSPGYRSV RERTSTSGTH RDREDSKFRR TRPLECQDAL
        60         70         80         90        100
ETAARAEGLS LDASMHSQLR ILDEEHPKGK YHHGLSALKP IRTTSKHQHP
       110        120        130        140        150
VDNAGLFSCM TFSWLSSLAR VAHKKGELSM EDVWSLSKHE SSDVNCRRLE
       160        170        180        190        200
RLWQEELNEV GPDAASLRRV VWIFCRTRLI LSIVCLMITQ LAGFSGPAFM
       210        220        230        240        250
VKHLLEYTQA TESNLQYSLL LVLGLLLTEI VRSWSLALTW ALNYRTGVRL
       260        270        280        290        300
RGAILTMAFK KILKLKNIKE KSLGELINIC SNDGQRMFEA AAVGSLLAGG
       310        320        330        340        350
PVVAILGMIY NVIILGPTGF LGSAVFILFY PAMMFASRLT AYFRRKCVAA
       360        370        380        390        400
TDERVQKMNE VLTYIKFIKM YAWVKAFSQS VQKIREEERR ILEKAGYFQS
       410        420        430        440        450
ITVGVAPIVV VIASVVTFSV HMTLGFDLTA AQAFTVVTVF NSMTFALKVT
       460        470        480        490        500
PFSVKSLSEA SVAVDRFKSL FLMEEVHMIK NKPASPHIKI EMKNATLAWD
       510        520        530        540        550
SSHSSIQNSP KLTPKMKKDK RASRGKKEKV RQLQRTEHQA VLAEQKGHLL
       560        570        580        590        600
LDSDERPSPE EEEGKHIHLG HLRLQRTLHS IDLEIQEGKL VGICGSVGSG
       610        620        630        640        650
KSSLISAILG QMTLLEGSIA ISGTFAYVAQ QAWILNATLR DNILFGKEYD
       660        670        680        690        700
EERYNSVLNS CCLRPDLAIL PSSDLTEIGE RGANLSGGQR QRISLARALY
       710        720        730        740        750
SDRSIYILDD PLSALDAHVG NHIFNSAIRK HLKSKTVLFV THQLQYLVDC
       760        770        780        790        800
DEVIFMKEGC ITERGTHEEL MNLNGDYATI FNNLLLGETP PVEINSKKET
       810        820        830        840        850
SGSQKKSQDK GPKTGSVKKE KAVKPEEGQL VQLEEKGQGS VPWSVYGVYI
       860        870        880        890        900
QAAGGPLAFL VIMALFMLNV GSTAFSTWWL SYWIKQGSGN TTVTRGNETS
       910        920        930        940        950
VSDSMKDNPH MQYYASIYAL SMAVMLILKA IRGVVFVKGT LRASSRLHDE
       960        970        980        990       1000
LFRRILRSPM KFFDTTPTGR ILNRFSKDMD EVDVRLPFQA EMFIQNVILV
      1010       1020       1030       1040       1050
FFCVGMIAGV FPWFLVAVGP LVILFSVLHI VSRVLIRELK RLDNITQSPF
      1060       1070       1080       1090       1100
LSHITSSIQG LATIHAYNKG QEFLHRYQEL LDDNQAPFFL FTCAMRWLAV
      1110       1120       1130       1140       1150
RLDLISIALI TTTGLMIVLM HGQIPPAYAG LAISYAVQLT GLFQFTVRLA
      1160       1170       1180       1190       1200
SETEARFTSV ERINHYIKTL SLEAPARIKN KAPSPDWPQE GEVTFENAEM
      1210       1220       1230       1240       1250
RYRENLPLVL KKVSFTIKPK EKIGIVGRTG SGKSSLGMAL FRLVELSGGC
      1260       1270       1280       1290       1300
IKIDGVRISD IGLADLRSKL SIIPQEPVLF SGTVRSNLDP FNQYTEDQIW
      1310       1320       1330       1340       1350
DALERTHMKE CIAQLPLKLE SEVMENGDNF SVGERQLLCI ARALLRHCKI
      1360       1370       1380       1390       1400
LILDEATAAM DTETDLLIQE TIREAFADCT MLTIAHRLHT VLGSDRIMVL
      1410       1420       1430
AQGQVVEFDT PSVLLSNDSS RFYAMFAAAE NKVAVKG
```

B

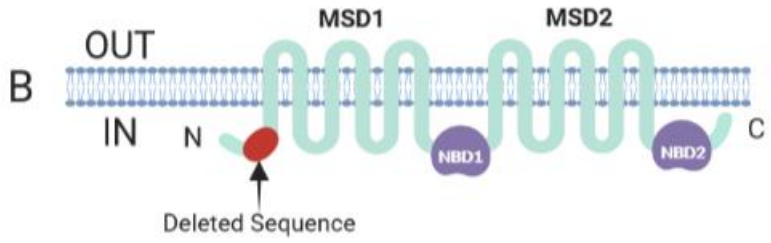

Figure 3.21 Schematic representation of the deleted amino acids of ABCC5 using a dual-sgRNA strategy. A. Amino acid sequence of ABCC5. Membrane-spanning domains (MSD) are highlighted in grey. Nucleotide-binding domains (NBD) are highlighted in purple. The amino acid sequence highlighted in yellow, green, and blue represents the deleted sequence of exon 3, 4, and 5, respectively. The antibody target sequence is bolded and underlined. Data were extracted from the UniProt database (https://www.uniprot.org/)**. B.** The loci of the deleted amino acids of ABCC5. *Created with BioRender.com.*

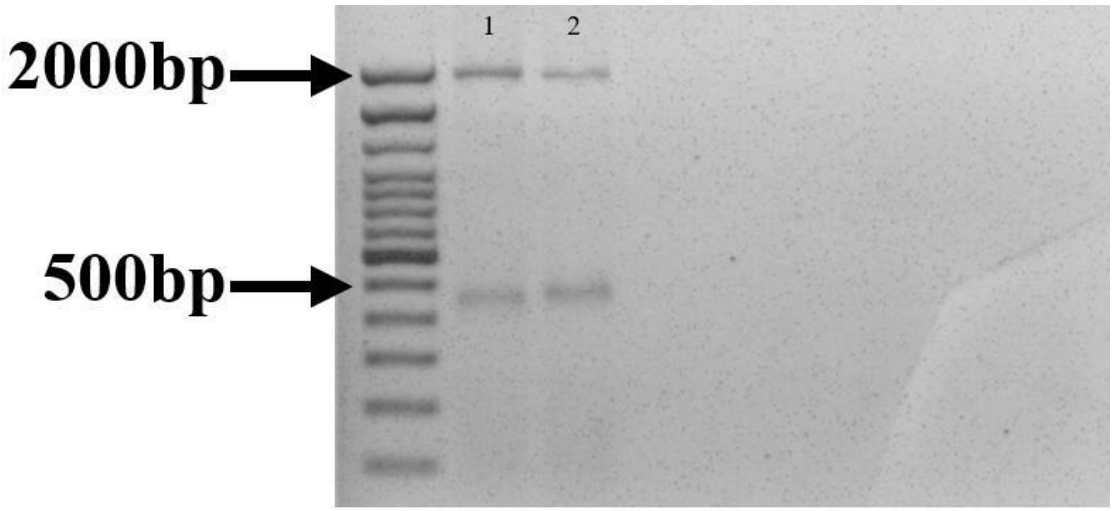

1. gRNA: IDT gRNA + Thermofisher gRNA set1; Primer: IDT-fwd + TF set1-rev
2. gRNA: IDT gRNA + Thermofisher gRNA set2; Primer: IDT-fwd + TF set1-rev

Figure 3.22 Determination of target sequence deletion after second-round KO in MDA-MB-231 KO clone 54. MDA-MB-231 KO clone 54 was transfected with either combination 1 or 2 to remove around 1408bp and 1385bp. The 1849bp and ~441/~464bp bands represent WT and edited allele in 1st round KO, and allele with target DNA fragment deletion, respectively. The above samples were PCR amplified using the same set of primers (IDT forward primer and Thermofisher set1 reverse primer) flanking the region of interest.

The pooled population of MDA-MB-231 clone 54 showed two bands in correct size after treating with sgRNA combination of either IDT *ABCC5*-sgRNA plus Thermofisher *ABCC5*-sgRNA set1 (group 1 in Figure 3.22) or IDT *ABCC5*-sgRNA plus Thermofisher *ABCC5*-sgRNA set2 (group 2 in Figure 3.22). Group 1 was further proceeded to limiting dilution. The combination of IDT *ABCC5*-sgRNA and Thermofisher *ABCC5*-sgRNA set1 was additionally used to knockout the WT allele in heterozygous BT549 clone 30 (group 2 in Figure 3.23). For MCF7 cells, this dual-sgRNA system was used in WT cells directly since no KO clones were obtained from the previous transfection (group 1 in Figure 3.23).

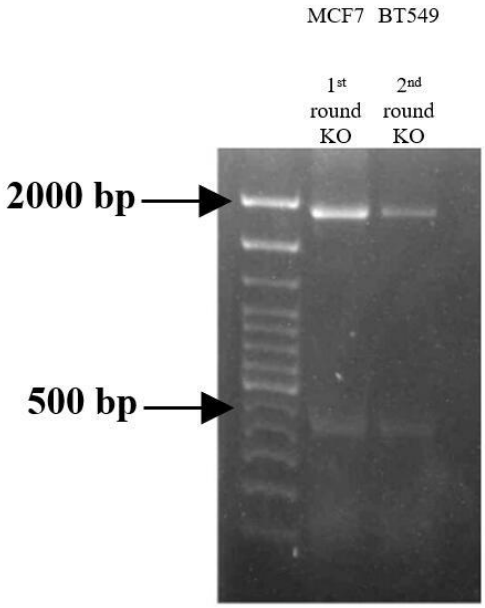

Figure 3.23 Determination of target sequence deletion in the pooled population after first and second-round KO in MCF7 WT cells and BT549 KO clone 30, respectively. BT549 KO clone 30 was transfected with a combination of IDT ABCC5 sgRNA plus Thermofisher ABCC5 sgRNA set1 in order to remove the target DNA fragment of around 1408bp. The 1849bp and ~441bp bands represent WT and edited allele in 1st round KO, and allele with target DNA fragment deletion, respectively. The above samples were PCR amplified using the same set of primers (IDT forward primer and Thermofisher set1 reverse primer) flanking the region of interest.

After limiting dilution cloning, two copies of the single cell clones were cultured in 96-well plates. One of the copies was proceeded to genomic DNA extraction, which was PCR amplified using IDT forward and Thermofisher set1/2 reverse primers. Clones showed a shorter band (~441bp), or multiple bands were screened out and further investigated. In Figure 3.24, Figure 3.25 and Figure 3.26, the positive clones of MDA-MB-231, BT549 and MCF7 cells were circled in red. The cleaved bands showed different lengths in different clones. Some clones even showed multiple bands. The 1849 bp bands representing WT and the indel allele were obtained in some clones. To examine the presence of WT allele and the expression ABCC5 protein, these clones

were all tested ABCC5 expression at both gene and protein levels.

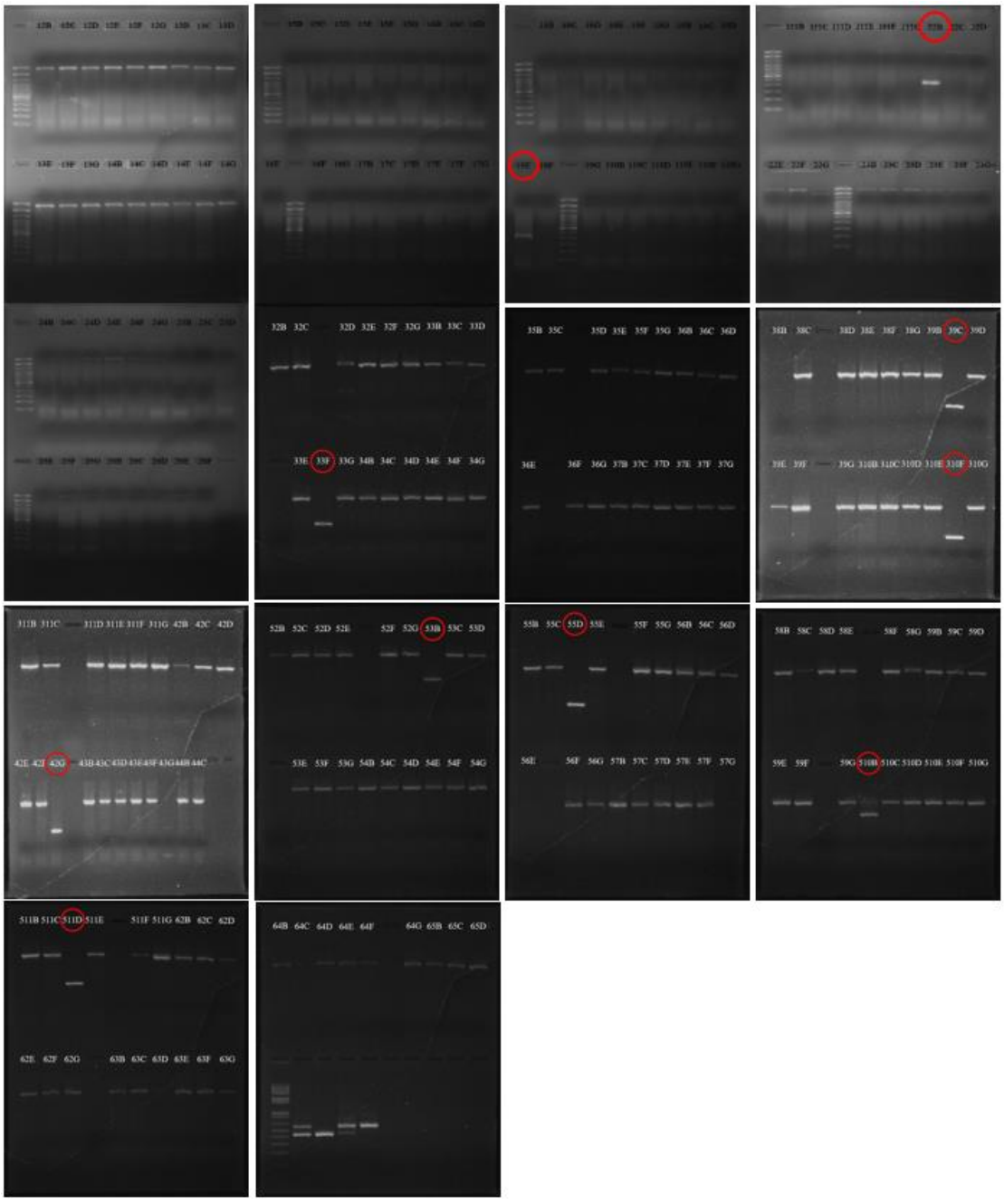

Figure 3.24 Screening of the deletion of the target sequence in the 2nd round of MDA-MB-231 single-cell clones. The 1849bp and ~441bp bands represent the WT and edited allele in 1st round KO, and allele with target DNA fragment deletion, respectively. The above samples were PCR amplified using IDT forward primer and Thermofisher set1 reverse primer flanking the region of interest.

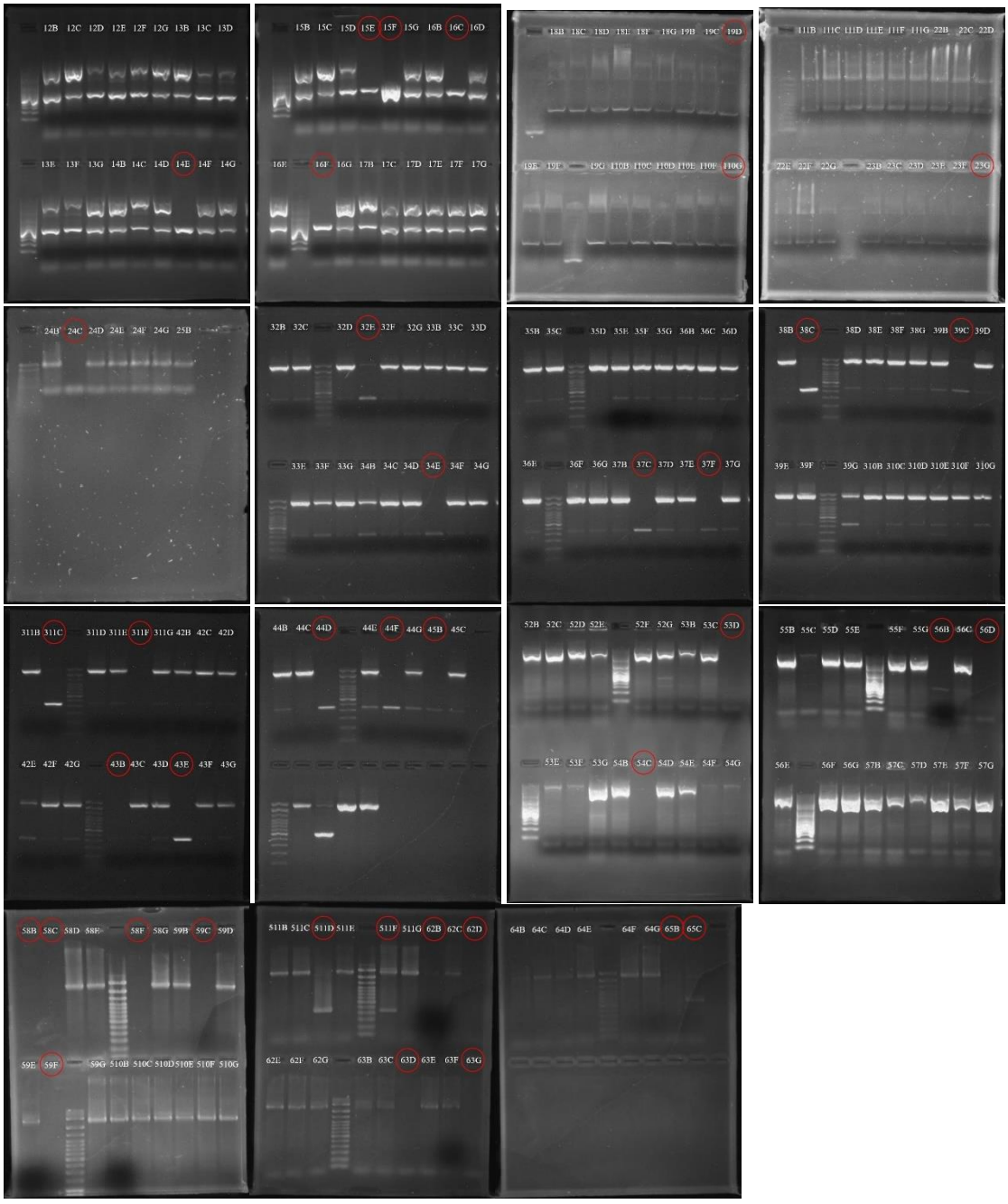

Figure 3.25 Screening of the deletion of the target sequence in the 2nd round of BT549 single-cell clones. The 1849bp and ~441bp bands represent the WT and edited allele in 1st round KO, and allele with target DNA fragment deletion, respectively. The above samples were PCR amplified using IDT forward primer and Thermofisher set1 reverse primer flanking the region of interest.

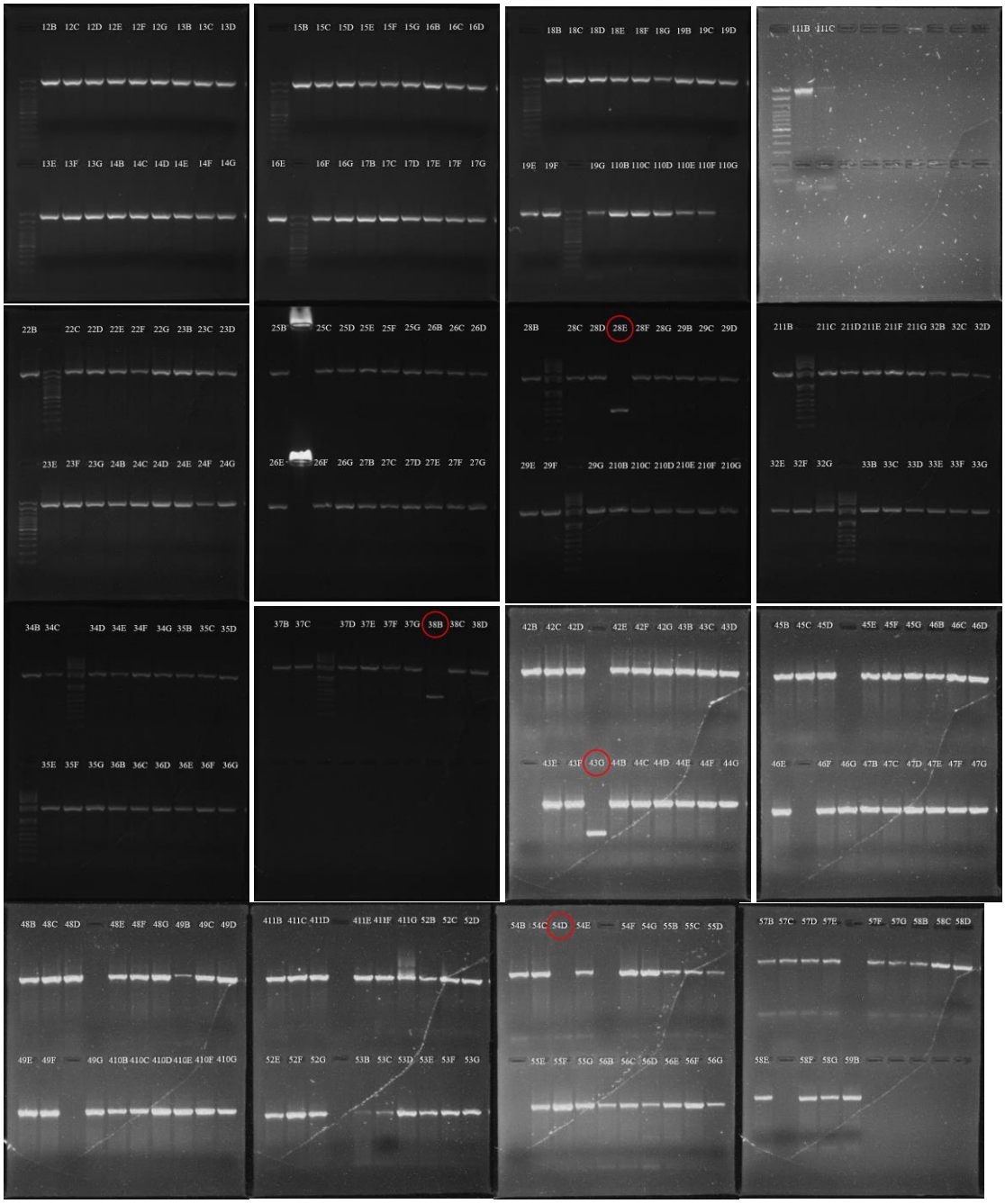

Figure 3.26 Screening of the deletion of the target sequence in MCF7 single cell clones. The 1849bp and ~441bp bands represent the WT allele and the allele with target DNA fragment deletion, respectively. The above samples were PCR amplified using IDT forward primer and Thermofisher set1 reverse primer flanking the region of interest.

3.3.3.5 Validation of Potential Homozygous KO Clones

The potential homozygous KO clones screened out in section 3.3.3.4 were subcultured in 6-well plates. Unfortunately, some of the clones were dead after successive rounds

of passage. To confirm the genotype of the potential homozygous KO clones, PCR results were repeated using the same primers (IDT forward and Thermofisher set1/2 reverse primers). Theoretically, an indel allele and an allele with 1408 bp deletion were detectable in MDA-MB-231 and BT549 KO clones. A WT allele and/or alleles with 1408 bp deletion were detectable in MCF7 clones due to the non-existence of the indel allele.

In Figure 3.27, Figure 3.28 and Figure 3.29, all of the WT cells only showed a band at 1849 bp, indicating that the primers are specific to the target loci. Some of the KO clones, such as BT549 clone 19D, 23G, 39c, 56D, 511F, 63D, and MCF7 clone 54D, showed the same band as WT cells. These clones were thus considered as WT or heterozygous cells. However, multiple faint longer bands were detected in the clones with a clear shorter band (~441 bp). To figure out the reason for this phenomenon, some representative clones were sent for sequencing.

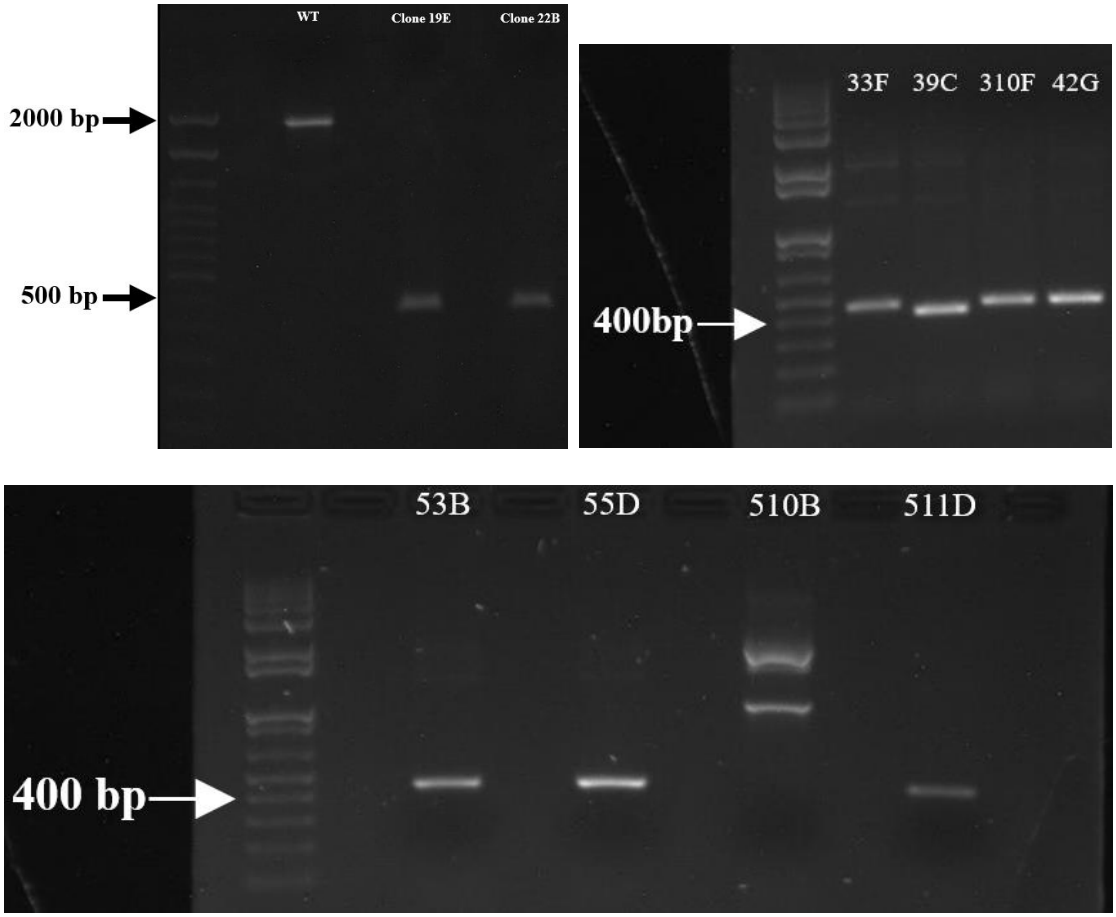

Figure 3.27 Confirmation of the deletion of target sequence in MDA-MB-231 homozygous KO clone 19E, 22B, 33F, 39C, 310F, 42G, 53B, 55D, 510B and 511D. The 1849bp and ~441bp bands represent the edited allele in 1st round KO and the allele with target DNA fragment deletion, respectively. The above samples were PCR amplified using IDT forward primer and Thermofisher set1 reverse primer flanking the region of interest.

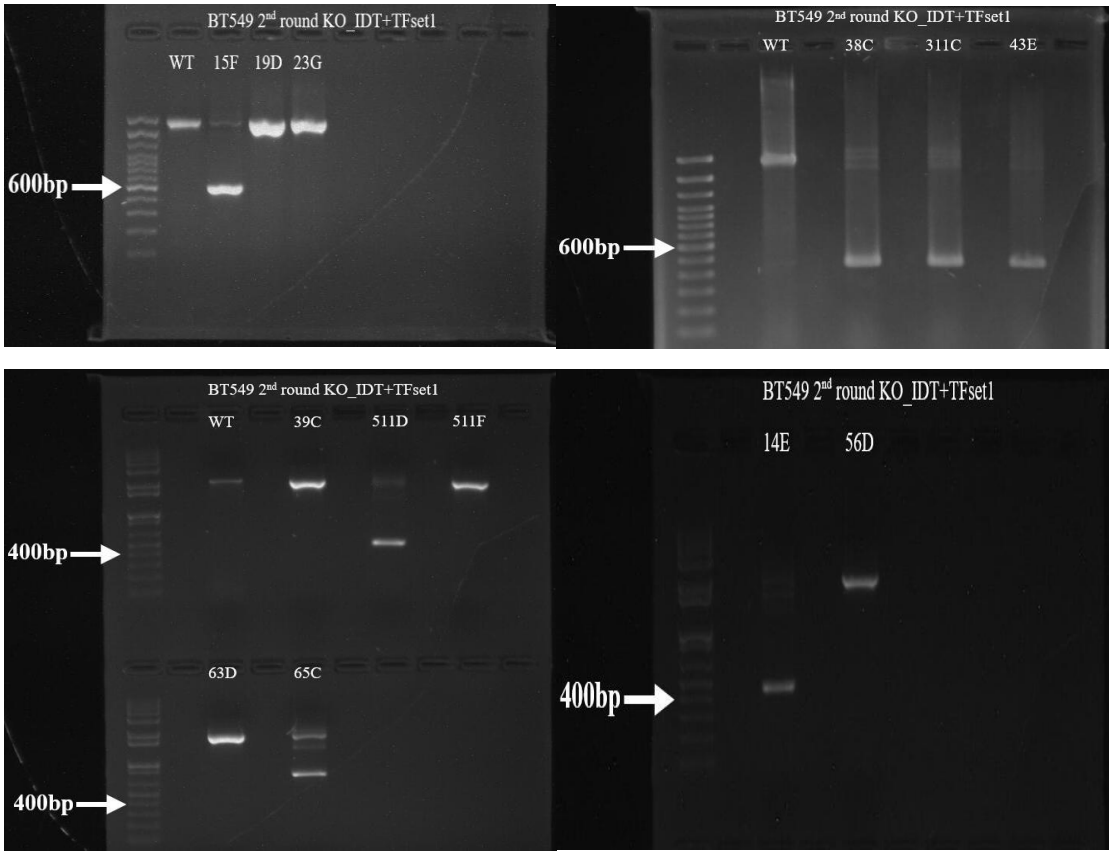

Figure 3.28 Confirmation of the deletion of the target sequence in BT549 homozygous KO clone 14E, 15F, 38C, 311C, 43E, 511D and 65C. The 1849bp and ~441bp bands represent the edited allele in 1st round KO and the allele with target DNA fragment deletion, respectively. The above samples were PCR amplified using IDT forward primer and Thermofisher set1 reverse primer flanking the region of interest.

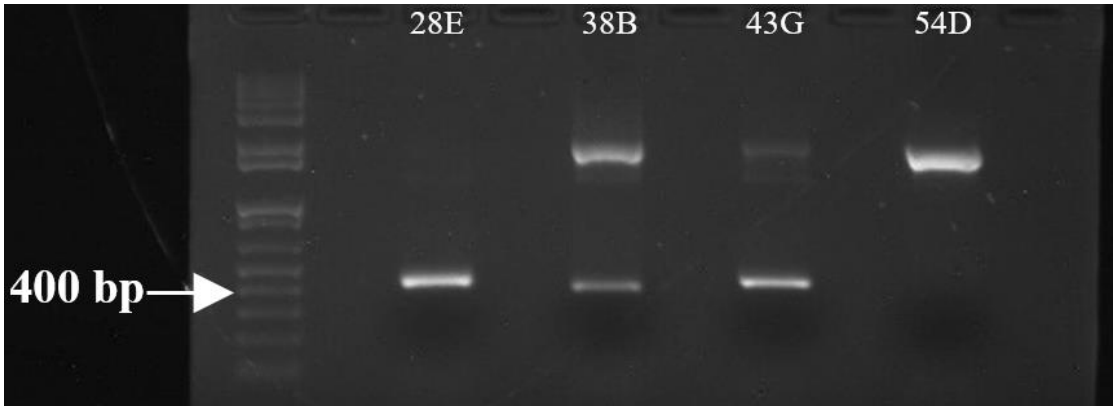

Figure 3.29 Confirmation of the deletion of the target sequence in MCF7 homozygous KO clone 28E. The 1849bp and ~441bp bands represent the edited allele in 1st round KO and the allele with target DNA fragment deletion, respectively. The above samples were PCR amplified using IDT forward primer and Thermofisher set1 reverse primer flanking the region of interest.

To confirm the above PCR results, some representative samples were sent for sequencing service using Thermofisher set1/2 reverse primer (Figure 0.33 to Figure 0.39). In terms of WT cells, the quality of sequencing results was not good (Figure 3.30). This is probably a result of the 25-consecutive thymine (T) close to the Thermofisher set1/2 reverse primer target loci, which was circled in red in Figure 3.30. Repetitive nucleotides may lead to misreading in Sanger Sequencing Service. Therefore, IDT forward primer should also be used in future studies to sequence these amplicons. The WT sequence will be then evaluated by combining the sequence upstream and downstream from the 25-consecutive thymine. In this study, sequence data from BLAST® (https://blast.ncbi.nlm.nih.gov/Blast.cgi) were used to identify the target gene modification.

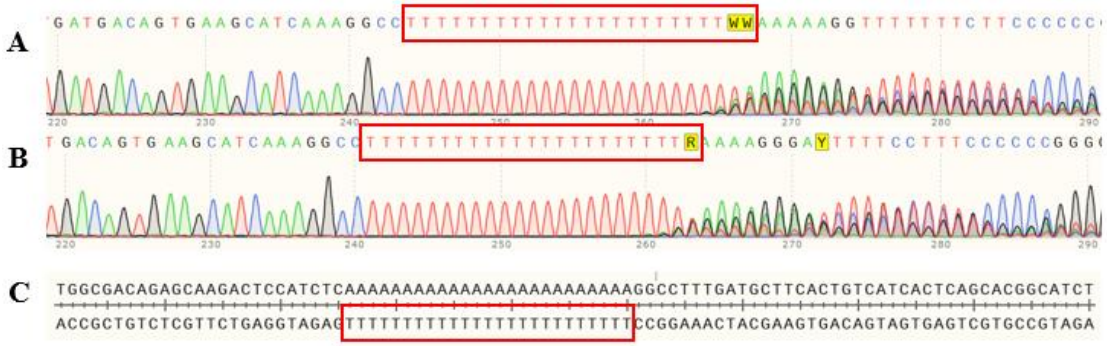

Figure 3.30 Sequencing results of MDA-MB-231 and BT549 WT cells. A. MDA-MB-231 WT; **B.** BT549 WT; **C.** Sequence data from BLAST®.

The short band of MDA-MB-231 clone 19E and 22B, and BT549 clone 38C, 311C and 43E was extracted and sent for sequencing. BT549 clone 15F was selected to sequence both the long and short bands due to the relatively clear long band compared with other

clones. In Table 3.6 and Table 3.7, the cleavage sites of both sgRNAs on the target allele were accurately located at 3-5 base pairs upstream PAM in these clones. A 1407 bp DNA segment was deleted from the target allele in MDA-MB-231 clone 19E and BT549 clone 38C, 311C and 43E. MDA-MB-231 clone 22B had a 1410 bp deletion in the target allele. Interestingly, no indel was observed in the target allele after DNA religation when a dual-sgRNA strategy was applied in all the tested clones. Since base pair insertion and/or deletion is regarded as a hallmark of NHEJ repair route, a possible explanation for this phenomenon is that only base pair deletion occurred after NHEJ repair in these clones. In terms of BT549 clone 15F, the short band exhibited a rearrangement after NHEJ repair (Figure 0.36 in appendix), while the long band showed heterogeneity (Figure 0.35 in appendix). Theoretically, the long band was supposed to be the indel allele edited in 1st round transfection. The heterogeneous sequence of the long band might thus be caused by copy number variation (CNV). Different edited alleles collectively led to the heterogeneity of the long band of BT549 clone 15F.

Table 3.6 Sequence of homozygous MDA-MB-231 KO clones.

	Sequence										
WT	ACA	ACC	CTT	CGC	AGG	-------- 1392bp --------	CTC	AAG	CCA	TGA	TGG
Clone 19E	ACA	ACC	CTT	- - -	- - -	-------- 1392bp --------	- - -	- - -	- - -	TGA	TGG
Clone 22B	ACA	ACC	C - -	- - -	- - -	-------- 1392bp --------	- - -	- - -	- - -	- GA	TGG

Table 3.7 Sequence of homozygous BT549 KO clones.

	Sequence										
WT	ACA	ACC	CTT	CGC	AGG	-------- 1392bp --------	CTC	AAG	CCA	TGA	TGG
Clone 38C	ACA	ACC	CTT	- - -	- - -	-------- 1392bp --------	- - -	- - -	- - -	TGA	TGG
Clone 311C	ACA	ACC	CTT	- - -	- - -	-------- 1392bp --------	- - -	- - -	- - -	TGA	TGG
Clone 43E	ACA	ACC	CTT	- - -	- - -	-------- 1392bp --------	- - -	- - -	- - -	TGA	TGG

To prove the above hypothesis, all of the KO clones were further PCR amplified using another two sets of primers, including IDT forward / IDT reverse and Thermofisher

set1/2 forward / Thermofisher set1/2 reverse primers (Figure 3.20), that flank the cleavage sites of IDT sgRNA and Thermofisher set1 sgRNA, respectively. In Figure 3.31 and Figure 3.32, some of the MDA-MB-231 and BT549 KO clones showed multiple bands, while some did not. These results revealed that the heterogeneity might not be prevalent among KO clones. In terms of MCF7 KO clones that were transfected with two sgRNAs directly, clone 38B and 43G showed both primers flanking regions, while clone 28B only had IDT primers flanking region (Figure 3.33). The Thermofisher primers flanking region might be deleted in MCF7 clone 28B. These results were repeated once to eliminate the potential errors in manipulation.

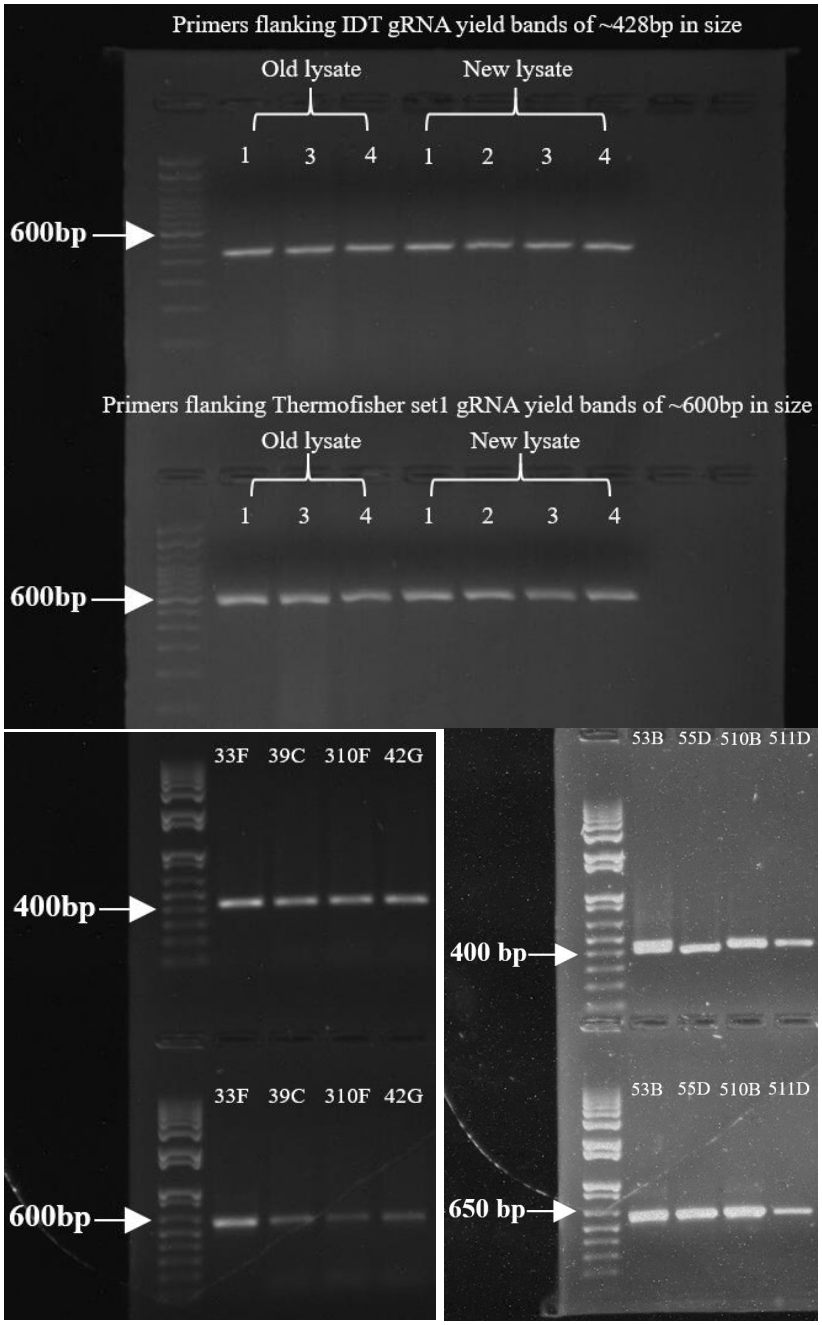

Figure 3.31 Confirmation of the deletion of the target sequence in MDA-MB-231 homozygous KO clones. 1, MDA-MB-231 WT; 2, Heterozygous c54; 3, Homozygous c19E; 4, Homozygous c22B. The above samples were PCR amplified using primers flanking IDT *ABCC5* sgRNA region (~428 bp) and Thermofisher *ABCC5* sgRNA set1 region (~600 bp), respectively.

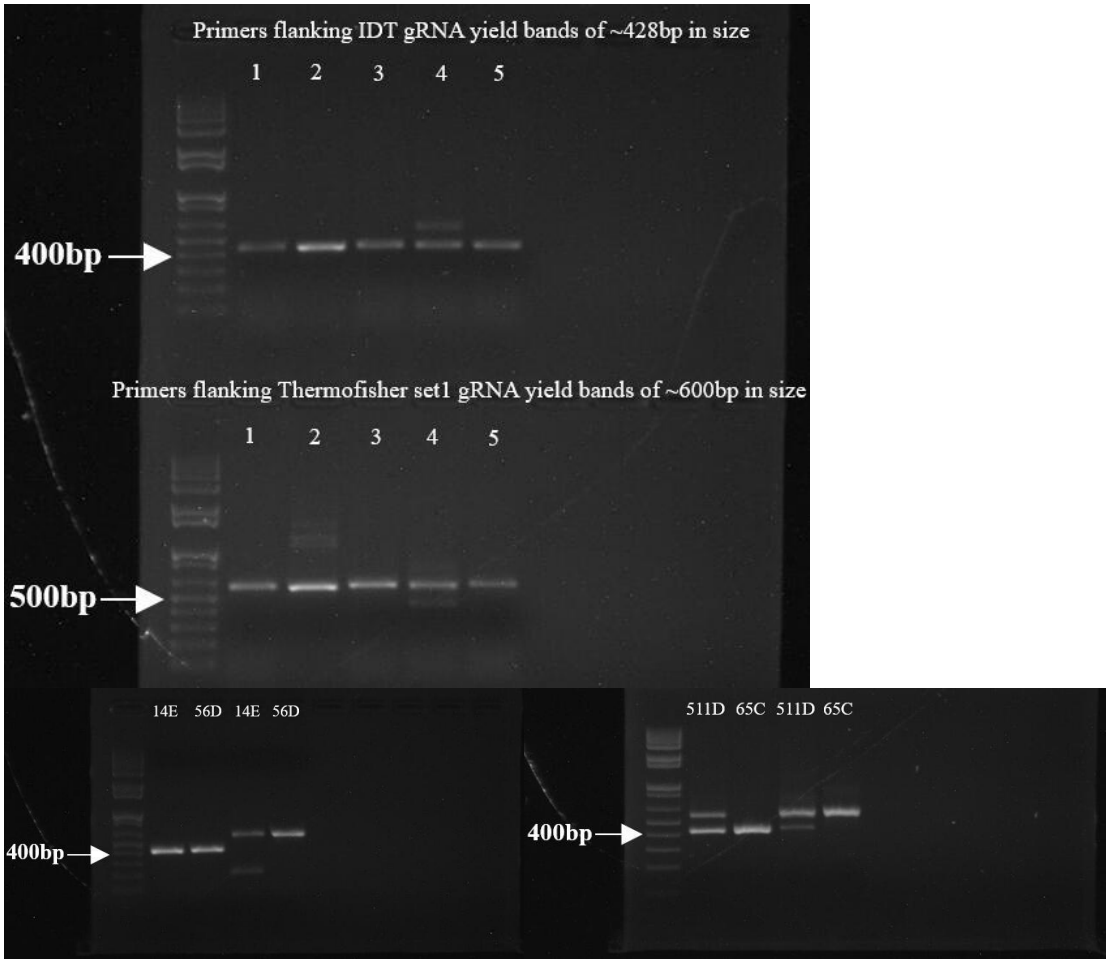

Figure 3.32 Confirmation of the deletion of the target sequence in BT549 homozygous KO clones. 1, BT549 WT; 2, Homozygous c15F; 3, Homozygous c38C; 4, Homozygous c311C; 5, Homozygous c43E. The above samples were PCR amplified using primers flanking IDT *ABCC5* sgRNA region (~428 bp) and Thermofisher *ABCC5* sgRNA set1 region (~600 bp), respectively.

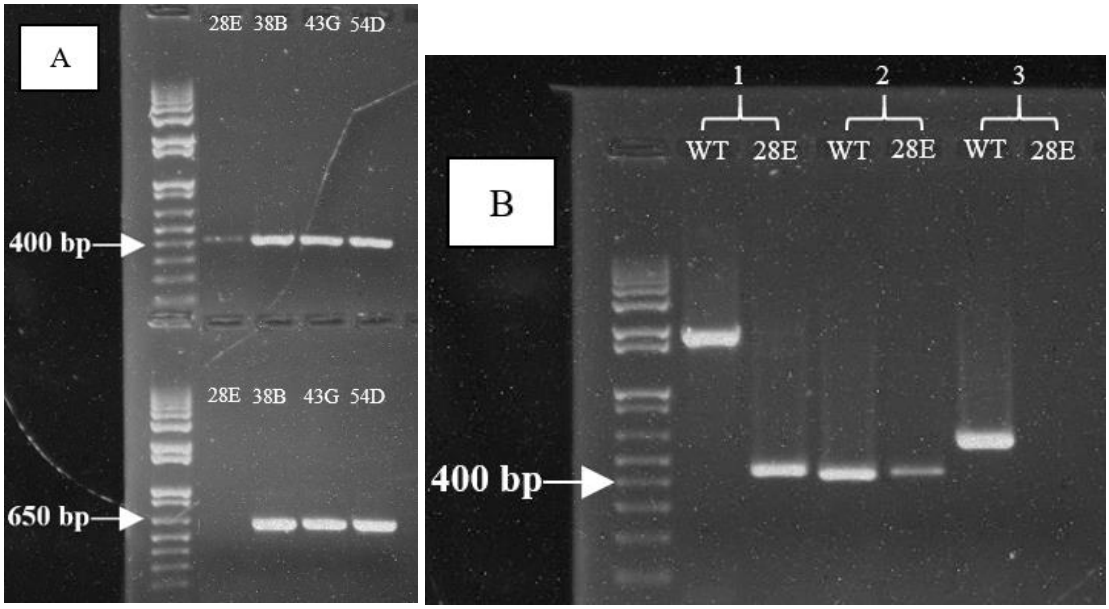

Figure 3.33 Confirmation of the deletion of the target sequence in MCF7 homozygous KO clones. A. Samples were PCR amplified using primers flanking IDT *ABCC5* sgRNA region (~428 bp) and Thermofisher *ABCC5* sgRNA set1 region (~600 bp), respectively. **B.** The repetition of A. Samples were PCR amplified using primers flanking both sgRNAs (1849 bp and ~441 bp) (1), IDT *ABCC5* sgRNA region (~428 bp) (2), and Thermofisher *ABCC5* sgRNA set1 region (~600 bp) (3), respectively.

In consideration of the high cost of testing CNV in these cell lines, such as Microarray, Next Generation Sequencing (NGS), Fluorescence In Situ Hybridization (FISH) and qPCR, all of the clones were proceeded to immunocytochemistry (section 2.10) directly to test ABCC5 protein expression. Western blotting was not adopted because ABCC5 protein from cancer cell lines could not be detected in our lab. All the WT cells and KO clones were stained with MRP5 Monoclonal Antibody and Goat Anti-Rat IgG H&L (DyLight® 488) secondary antibody. The fluorescence intensity of KO clones was compared with corresponding isotype control. PANC1 WT cells, the line tested to overexpress ABCC5 by one of our colleagues Piyush, were immunostained as a positive control (Figure 3.34). Unfortunately, although the fluorescence intensity of almost all KO clones was lower than WT cells, ABCC5 protein was still expressed in these KO clones since the fluorescence intensity was still much higher than isotype controls

(Figure 3.35, Figure 3.36 and Figure 3.37). Thus, all of the KO clones were regarded as heterozygous cells. The phenotype of these KO clones was consistent with the genotype. CNV of *ABCC5* in these clones probably led to incomplete deletion of the target sequence. The extra WT alleles enabled ABCC5 protein to express, but probably at a lower level. Interestingly, although the Themofisher set1/2 primers flanking region was deleted in MCF7 clone 28E (Figure 3.33), ABCC5 protein was not fully knocked out. This phenomenon might be caused by exon skipping or translation reinitiation (Smits et al., 2019). The truncated protein or isoforms of ABCC5 might still interact with antibodies and remain ABCC5 function.

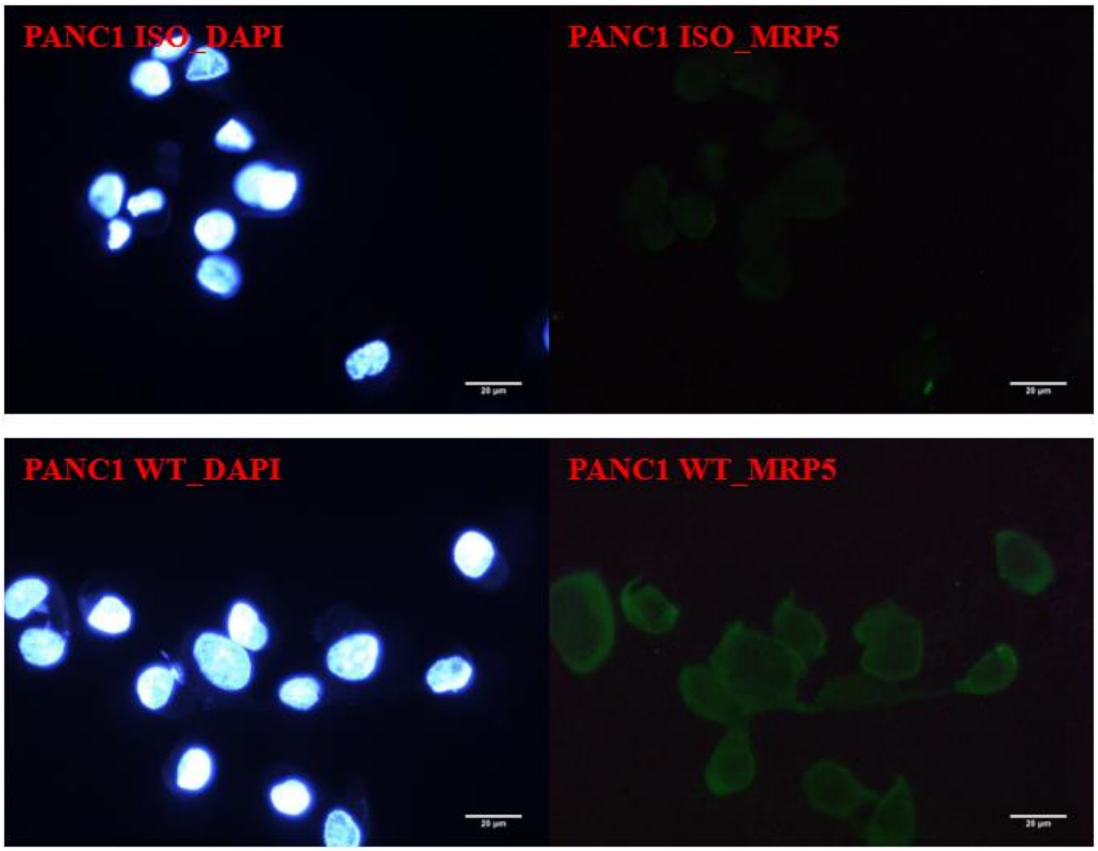

Figure 3.34 Immunocytochemistry of WT PANC1 cells. Cells were stained with DAPI, MRP5 Monoclonal Antibody and Goat Anti-Rat IgG H&L (DyLight® 488) secondary antibody. Fluorescence intensity was compared with isotype control.

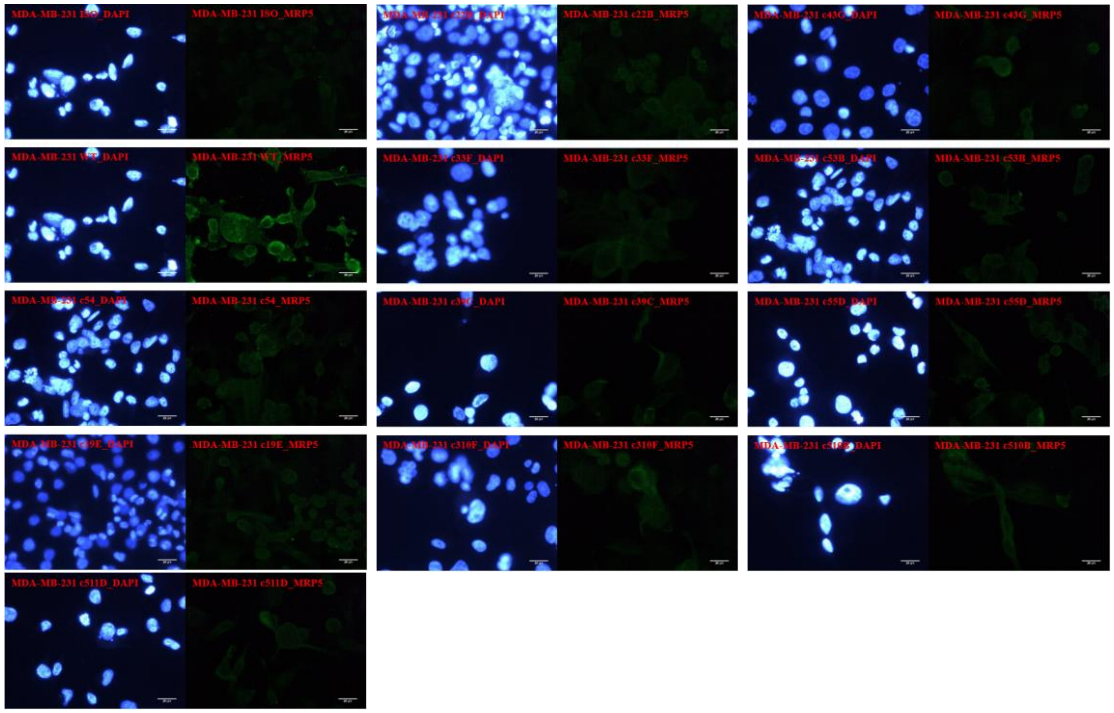

Figure 3.35 Immunocytochemistry of WT and KO clones of MDA-MB-231 cells. Cells were stained with DAPI, MRP5 Monoclonal Antibody and Goat Anti-Rat IgG H&L (DyLight® 488) secondary antibody. Fluorescence intensity was compared with isotype control.

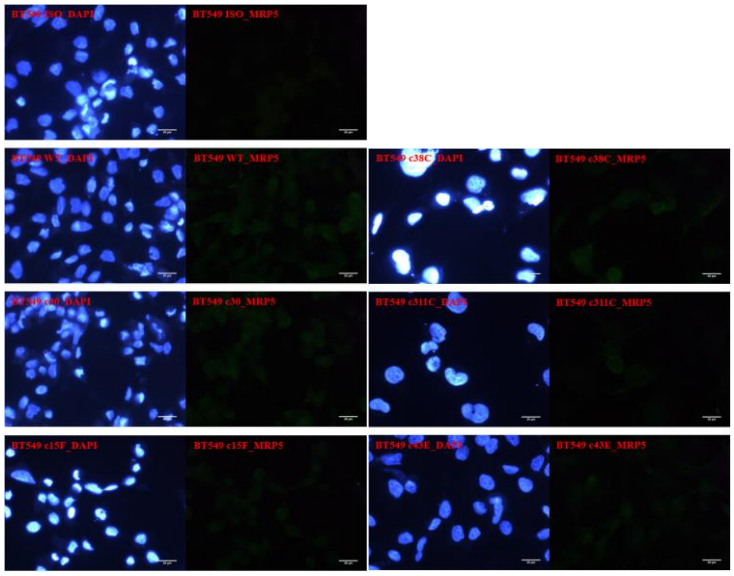

Figure 3.36 Immunocytochemistry of WT and KO clones of BT549 cells. Cells were stained with DAPI, MRP5 Monoclonal Antibody and Goat Anti-Rat IgG H&L (DyLight® 488) secondary antibody. Fluorescence intensity was compared with isotype control.

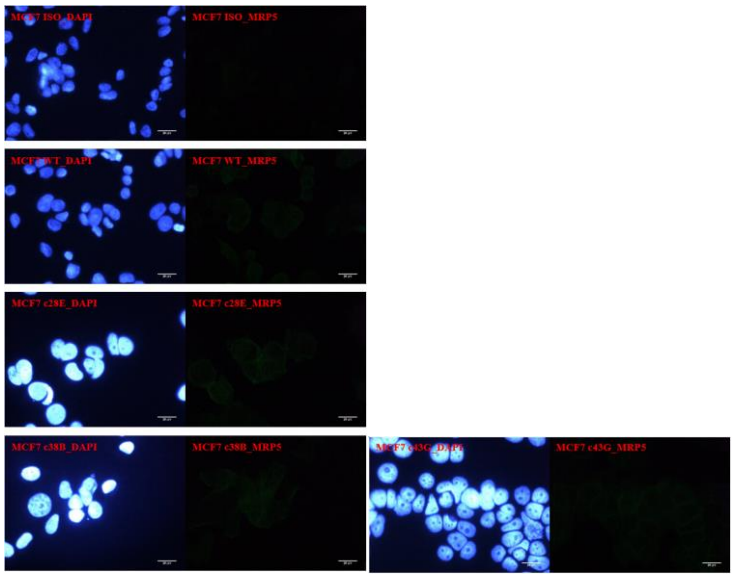

Figure 3.37 Immunocytochemistry of WT and KO clones of MCF7 cells. Cells were stained with DAPI, MRP5 Monoclonal Antibody and Goat Anti-Rat IgG H&L (DyLight® 488) secondary antibody. Fluorescence intensity was compared with isotype control.

To examine whether the lowered ABCC5 expression could induce a higher accumulation of ABCC5 substrates, some representative clones were proceeded to uptake study (section 2.7.2.2). In Figure 3.38, the MDA-MB-231 clones obtained from the 2nd round of KO showed even lower BCECF accumulation compared with clones from the 1st round of KO. This might also be a result of the off-target effect of *ABCC5*-sgRNAs. BT549 clones obtained from the 2nd round of KO showed noticeable higher BCECF accumulation compared with clones from the 1st round of KO. MCF7 clones showed a minor increase in BCECF accumulation compared with WT. This might be a result of the low expression level of ABCC5 in MCF7 cells. The clones were not further proceeded to 3rd round of transfection to delete more *ABCC5* gene copies due to lack of proper screening methods if the same sets of sgRNAs and primers were applied. Therefore, in consideration of both the potential more off-target effects induced by the

2nd round of KO and the BCECF rate-limiting effect of the clones, heterozygous MDA-MB-231 clone 49, 53 and 54, BT549 clone 30 and 311C, and MCF7 clone 28E were used for downstream functional studies.

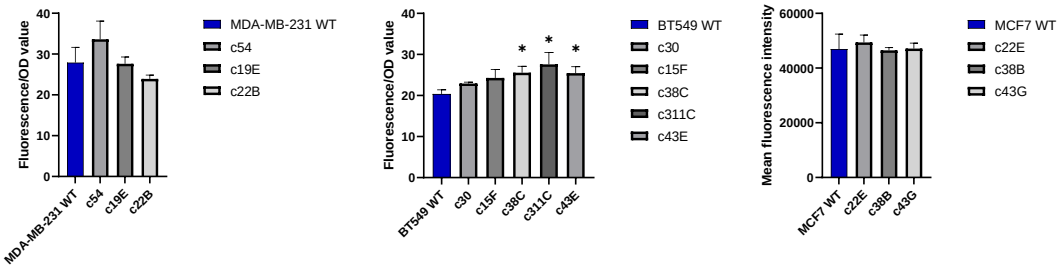

Figure 3.38 The cellular accumulation of BCECF in MDA-MB-231, BT549 and MCF7 KO clones. Results were plotted as normalized fluorescence vs. cell type. Data were presented as mean ± SD of triplicates. *P<0.05 significantly different from the BCECF accumulation in corresponding WT cells, calculated using one-way ANOVA and Sidak's multiple comparison post-test to compare all KO clones with the control groups.

3.4 Discussion

The aim of the studies presented in this chapter was to establish homozygous *ABCC5* KO breast cancer cell lines. This was accomplished by transfecting different lines with different *ABCC5*-sgRNAs or *ABCC5*-sgRNA combinations. The KO clones were screened and validated at both gene and protein levels.

Before commencing these studies, the functional expression of ABCC5 was determined in the three cell lines used in *ABCC5* gene KO studies. TNBC cell lines were found to overexpress ABCC5 as compared with the non-TNBC MCF7 cells. The cellular accumulation of ABCC5 substrate BCECF was significantly higher in ABCC5 inhibitor (i.e., benzbromarone and myricetin) treated groups than negative controls. These results

reveal the functional overexpression of ABCC5 protein in TNBC cells. *ABCC5* gene knockout studies will further examine whether ABCC5 overexpression could alter the efficacy of its substrate drugs in an extracellular translocation-dependent manner in TNBC cell lines.

To establish *ABCC5* gene knockout cell lines, a CRISPR-Cas9-based gene editing method was applied in two TNBC cell lines (i.e., MDA-MB-231 and BT549) and a non-TNBC control line, MCF7, in this study. The ribonucleoproteins (RNP) consisting of the pre-designed IDT *ABCC5*-sgRNA and Cas9 protein were delivered into cells through lipid transfection. The RNP-induced DSBs were reconnected by nonhomologous end-joining DNA repair route (NHEJ). The pooled population of all the three KO lines showed positive results in genomic cleavage detection assay with a cleavage efficiency of around 11%, 3% and 7% for MDA-MB-231, BT549 and MCF7 cells, respectively. The cleavage efficiency in this study was much lower than the results obtained by one of our colleagues Riya (nearly 50% on *ABCC2* KO Caco-2 cells; data not shown), the examples in manufacturer's instruction, and the results in other studies (Liang et al., 2015; Sakuma, Nishikawa, Kume, Chayama, & Yamamoto, 2014). After limiting dilution cloning, unfortunately, all of the MDA-MB-231 and BT549 clones were identified as heterozygous KO clones at both gene and protein levels. No positive MCF7 clones were obtained. Thus, the 2nd round of KO was conducted using a dual-sgRNA strategy to delete an 1849 bp DNA segment of the WT allele in the representative heterozygous clones. MCF7 WT cells were directly transfected with this dual-sgRNA strategy. Again, after the 2nd round of transfection, the clones were all heterozygous at both gene and protein levels. Undoubtedly, the low cleavage efficiency in this study might be partially caused by some common operational errors, such as degradation of IDT *ABCC5*-sgRNA after successive rounds of freeze-thaw cycle, loss

of bioactivity of Cas9 protein after long-term storage, and unexpected RNase contamination in transfection complex during manipulation. The use of different kinds of endonucleases (e.g., T4 endonuclease I, T4 endonuclease VII, and Surveyor) in the enzyme mismatch cleavage assay may result in underestimation of cleavage efficiency due to their various sensitivity and specificity to indels in different sizes (Mean, Pierides, Deltas, & Koptides, 2004; Vouillot, Thelie, & Pollet, 2015). However, to our understanding, the low cleavage efficiency in pooled KO population and the heterozygosity of all KO clones were more likely to derive from some more complicated reasons, including different chromatin states (i.e., heterochromatin and euchromatin), folding structure and orientation of sgRNA, *ABCC5* copy number variation (CNV), and chromosomal mosaicism.

Apart from the common parameters relating to the variability of CRISPR-Cas9 editing efficiency, such as the specific construction and composition of Cas9 protein (X. Liu et al., 2016; F. A. Ran et al., 2015), GC content, secondary structure and nucleotide preference of sgRNA (X. Liu et al., 2016; M. Rahdar et al., 2015), and primary target sequence (P. D. Hsu et al., 2013), the chromatin state also influences CRISPR-Cas9 gene editing efficiency. Chromatin state (i.e., heterochromatin and euchromatin) refers to the way DNA is modified and packaged in the nucleus. Euchromatin is considered as relatively unpacked and accessible chromatin, while heterochromatin as densely packed nucleosomes, crowed by non-histone proteins hampering accessibility (Verkuijl & Rots, 2019). The transition from compact or closed heterochromatin to relaxed or open euchromatin is mediated by a broad spectrum of macromolecular complexes and their respective catalytic activities, including methylation-demethylation, acetylation-deacetylation, and phosphorylation-dephosphorylation (Janssen, Chen, Liu, & Goncalves, 2019). The relatively unpacked euchromatin was more accessible to Cas9

protein over heterochromatin (Verkuijl & Rots, 2019). Besides, nucleosome may be another factor that influences Cas9 binding. Nucleosomes are the primary constituent of chromatin, being formed of 147 bps of DNA wrapped around a complex of eight histone proteins (Verkuijl & Rots, 2019). Functional Cas9 binding was strongly occluded by nucleosomes, in which the DNA at the centre remained almost completely resistant to cleavage compared to those near the nucleosome edge or non-nucleosome areas (Verkuijl & Rots, 2019). But these DNA became accessible during natural nucleosome remodelling and breathing, the processes mediated by remodelling enzymes, transcription, and DNA replication (Verkuijl & Rots, 2019). Targeting the sequences embedded in more relaxed chromatin structure and low nucleosome occupancy regions may thus increase the accumulation of Cas9-mediated mutagenesis. Therefore, for the KO cells in present study, the chromosomal state of the target gene and the loci of the target DNA sequence in the nucleosome might collectively induce the low cleavage efficiency. The re-cutting of smaller mutations despite sgRNA mismatches (van Overbeek et al., 2016) might further reduce the cleavage efficiency in the 2nd round of KO. Based on these findings, the impact of different chromatin states on CRISPR-Cas9-based gene editing at off-target sites is of interest and warrants in-depth investigations. Future *ABCC5* gene KO studies involving chromatin remodelling agents (e.g., programmable trans-activators, histone deacetylase inhibitors, and DNA methyltransferase inhibitors) may help improve cleavage efficiency and the possibility of obtaining homozygous clones. Similarly, siRNA-mediated inhibition against the silencing protein SuZ12 relating to heterochromatin may represent a reliable strategy to enhance Cas9 function (Daer, Cutts, Brafman, & Haynes, 2017).

Besides, sgRNA that directly base-paired to the sense strand of DNA, the template for RNA polymerase, was found to increase mutagenesis rate (Verkuijl & Rots, 2019). RNA

polymerase could displace specifically oriented Cas9 protein from DNA, freeing them and promoting additional cleavage events (Verkuijl & Rots, 2019). Meanwhile, after binding of Cas9 to PAM, the sgRNA invades into the PAM-adjacent protospacer DNA duplex and displaces the complementary strand of the protospacer, resulting in the formation of an R-loop motif immediately upstream of the PAM. The competition between the invaded sgRNA and the re-annealing of the DNA duplex contributes to a dynamic R-loop structure. This target DNA/sgRNA bound structure, i.e., R-loop structure, was found to correlate with overall Cas9 cleavage efficiency and targeting specificity (Xu, Duan, & Chen, 2017). Given that Cas9 has no energy-dependent helicase activity, the mechanism of target DNA unwinding is unknown, but probably relies upon thermally available energy. Higher free energy of sgRNA might benefit the formation of the RNA/DNA heteroduplex, and thus more efficient Cas9 activity (Y. J. Yang et al., 2017). Therefore, whether or not the different folding structures and orientation of sgRNA that targeting either sense or antisense strand of *ABCC5* gene in present study affected the cleavage efficiency and heterozygosity of KO clones remained to be investigated.

Moreover, cancer cells were characterized by two prominent features, large-scale structural rearrangements of chromosomes and abnormal numbers of chromosomes. Gene rearrangement related CNV of the target gene may remain an obstacle to gene KO studies. The term CNV refers to an intermediate-scale genetic change, operationally defined as segments greater than 1000 base pairs in length but typically less than 5 megabases, including both additional copies of sequence (duplications) and deletions. In fact, large-scale CNV involving hundreds of thousands of DNA base pairs were unexpectedly common and represented a significant source of genetic variation throughout the human genome of healthy individuals (Iafrate et al., 2004; Sebat et al.,

2004), so did cancer cells (Shao et al., 2019; Shlien & Malkin, 2009). Focal amplification in cancer cells could result in tandem duplication of a specific gene to hundreds of copies (Beroukhim et al., 2010). CNV can affect the expression of genes, alter the organization of chromatin, and/or influence the regulation of genes in the vicinity (F. Zhang, Gu, Hurles, & Lupski, 2009). Breast cancer was found to contain 200 germline CNVs overlapping with protein-coding genes among 686 samples (Kumaran et al., 2017). In the case of *ABCC5* KO cells in present study, the low cleavage efficiency and the heterozygosity of KO clones might be a result of aberrant *ABCC5* gene copy numbers, in which RNPs were insufficient to modify all the copies. Therefore, in consideration of the potential CNV of *ABCC5* in breast cancer cell lines, future attempts to KO *ABCC5* gene may start with examining CNV in these cell lines using technologies, such as Microarray, Next Generation Sequencing (NGS), Fluorescence In Situ Hybridization (FISH), Southern Blotting and qPCR. However, it is also of importance to recognize certain limitations when determining CNVs of cell cultures. For example, the recurrent CNV is mainly mediated by non-allelic homologous recombination (NAHR), which also occurs in mitosis (Gu, Zhang, & Lupski, 2008). Cancer cells in culture might thus acquire genomic CNVs that were not present in the starting material (Pollex & Hegele, 2007). This may cause variations in CNVs of a certain cell line in different labs and presumably make the research findings valueless to clinical practice. Thus, the need for a comprehensive database of CNV information from large-scale *in vitro* and *in vivo* studies is becoming increasingly urgent, since a comprehensive genomic CNV map may help scientists select research strategies, validate cell line mutations, and determine the potential role of CNVs in human diseases.

Nevertheless, the CNV of *ABCC5* gene might also occur after *ABCC5* gene KO rather than in wild-type cells. Certain gene KO cell models might involve some kind of

crosstalk between RNP-induced DSBs, gene repair routes, and gene rearrangements. Gene KO clones with Cas9-induced large-scale gene rearrangements, chromosomal translocations, gene inversions or large insertions/deletions were reported in a comprehensive study of Cas9-induced mutagenesis (Kosicki et al., 2018). K. J. Woodward et al. (2005) and J. A. Lee et al. (2006) proposed that one of the broken ends of a single DSB in one strand could invade and copy from the sister chromatid and result in duplication. The ends were then re-ligated *via* NHEJ repair route. In the case of *ABCC5* KO in present study, whether the RNP-induced DSB in one strand of *ABCC5* gene led to non-recurrent rearrangements of *ABCC5* gene between the two sister chromatids or even between homologous chromosomes was unknown. The extra copies of *ABCC5* gene made this gene detectable at both gene and protein levels. But, whether the heterozygosity of current KO clones was such a result of this phenomenon remained to be determined. Furthermore, chromosomal topologies were found to control gene-editing outcomes by changing the balance between different DNA repair pathways that are recruited during DNA lesions occur (Janssen et al., 2019). Homology-directed repair (HDR) could re-ligate DNA lesions with high fidelity using the sister chromatid or homologous chromosome as a template (Devkota, 2018; Heyer, 2015). The CNV of *ABCC5* gene generated either endogenously in wild-type cells or exogenously by RNPs might induce chromatin conformational changes. Thus, whether the RNP-induced DSB in one strand of *ABCC5* gene could be repaired precisely according to the other allele *via* repair routes other than NHEJ, such as HDR and microhomology-mediated end joining (MMEJ) repair, was of interest to be explored. A further question would be whether or not the germline *ABCC5* CNV-induced genomic structural changes, in this case, were related to NHEJ and FoSTeS (Gu et al., 2008), the genomic architecture-dependent gene rearrangement pathways, which in turns mediated *ABCC5* CNV again.

Notably, a shred of indirect evidence for these speculations about sister chromatids/homologous chromosomes crosstalk in KO cells was that the mutated gene in a given KO clone only showed a single sequence in some studies (Binda, Klaver, Berkhout, & Das, 2020; Kawamura et al., 2015), which means that all the copies of the target gene were repaired in the same manner. Given that random base-pair insertion and/or deletion is regarded as a hallmark of NHEJ repair route, different edited copies are supposed to contain different indels. In other words, diploid KO cells should have two different edited sequence, while triploid KO cells having three sequence and so on. The identical indels in different copies of the target gene in those studies, to our understanding, might be caused by crosstalk between sister chromatids or homologous chromosomes. To be exact, the DSB in the first allele was repaired by NHEJ, while the DSB in the second allele was repaired by HDR after the repair of the first allele. Moreover, Lieber, Gu, Lu, Shimazaki, and Tsai (2010) reviewed that DSBs on different chromosomes could get re-joined by NHEJ. If DNA ends from different chromosomes are joined, then a chromosomal translocation arises. Thus, for the KO clones of present study, if on-target DSB on the expected chromosome and off-target DSBs on other chromosomes occurred simultaneously, the relationship between the potential re-joining of heterologous chromosomes-induced chromosomal translocation and *ABCC5* gene expression was unknown. Whether or not this chromosomal translocation was further related to alterations in *ABCC5* CNV remained to be explored. Taken together, the above speculations only discussed DSB occurred in one allele. In case of cells containing biallelic DSBs, the presence of wild-type homologous sequence could be impossible in some cell phases if the *ABCC5* gene was diploid. In consideration of the heterozygosity of KO clones in present study, therefore, it was more likely that all the three wild-type cell lines used in this study gained germline CNV of *ABCC5*. But the

ABCC5 gene copy number, theoretically, could be further expanded after transfection, which remained to be investigated.

In addition to the gene rearrangement-dependent *ABCC5* CNVs, the potential chromosomal mosaicism of certain breast cancer cell lines is correlated with altered *ABCC5* gene copy numbers. Human cells typically contain 23 pairs of chromosomes (46 in total). Chromosomal mosaicism refers to alterations in chromosome number or structure within a given cell population (Levy, Hoffmann, McCoy, & Grati, 2021). These changes can occur during the formation of reproductive cells, in early foetal development, in any cell after birth (Levy et al., 2021), and definitely during carcinogenesis (Thompson & Compton, 2011). A typical example of aneuploid is Down syndrome (aka., trisomy 21), with which patients' somatic cells have three copies of chromosome 21 for a total of 47 chromosomes per cell (Levy et al., 2021). Mosaic aneuploidies in reproductive cells and early foetal are mainly derived from postzygotic mitotic chromosome segregation errors, postzygotic mitotic trisomy/monosomy rescue of a pre-existing aneuploid of meiotic origin, anaphase lag, unattached chromosome to spindles, tripolar spindle formation, and endoduplication or failed cytokinesis. Details of these mechanisms are reviewed in Levy et al. (2021). Ectopic chromosome numbers in cancer cells are caused by loss of mitotic fidelity. Proteins that maintain the mitotic spindle checkpoint and sister chromatid cohesion play key roles in this process, in which chromosomal instability leads to the missegregation of chromosomes during mitosis (Thompson & Compton, 2011). A specific kinetochore-microtubule (kMT) attachment error called merotely is the major source of chromosome segregation errors, which refers to the attachment of single kinetochores with microtubules emanating from more than one spindle pole. Eventually, the chromatid attached to both poles can be segregated to the same daughter cell in anaphase, resulting in formation of aneuploid

daughter cells, one with an extra copy of chromosome and the other missing a copy (Thompson & Compton, 2011). Thus, if the entire chromosome 3 or the arm of chromosome 3 in which *ABCC5* gene embedded was amplified in the breast cancer cell lines used in this study, the low cleavage efficiency and the heterozygosity of KO clones might be a result of this phenomenon. To complicate matters, the extra copies of chromosome 3 might strengthen the likelihood of the crosstalk between RNP-induced DSBs, gene repair routes, and gene rearrangements, as discussed above. Also, based on the above discussions, since the screening of KO clones in present study was limited to the immediate vicinity of the cleavage site and loss-of-function screens, there was a possibility that clones with Cas9-induced large-scale gene rearrangements, chromosomal translocations and gene inversions was misclassified as wild-type despite the fact that ABCC5 expression in these cases might not be affected. Similarly, whether the indel allele in some clones was lost due to loss of heterozygosity (LOH), a common genetic event in cancer cells (Thiagalingam et al., 2001), remained to be investigated.

In contrast to the above points of view, some other studies reported that sgRNA is insensitive to copy numbers. Yuen et al. (2017) reported that KO efficiency was largely insensitive to the copy number of the target gene but is primarily determined by the intrinsic potency of the sgRNA, which was further dependent on KO time course and the threshold level of sgRNA/Cas9 in cells. But the authors mentioned that these results could be confounded by cell-line specific factors. Thus, future KO studies may increase the amount of sgRNA and Cas9 protein and prolong the transfection time course to overcome the potential *ABCC5* CNVs.

However, MCF7 clone 28E was genetically validated as homozygous KO with deletion of Thermofisher *ABCC5*-sgRNA set1 target region, but still with ABCC5 protein expression. This made us start to think about other potential reasons that could cause

failure in generating KO cells. The production of truncated protein isoforms due to translation reinitiation or skipping of the edited exon might result in this phenomenon. Smits et al. (2019) reported that residual protein expression was found in about one third out of 193 KOs at variable levels from low to original. These truncated protein isoforms could remain cellular function and presumably involve other unknown roles (He, Fortunati, Liu, & Li, 2021). However, in MCF7 clone 28E, the amino acids encoded by the deleted DNA sequence overlaps with the target epitope sequence of the ABCC5 primary antibody. This makes the ABCC5 primary antibody used in this study theoretically unable to stain homozygous KO clones that lack the DNA sequence encoding the target epitope. Use of other ABCC5 primary antibodies targeting different epitopes, rather than the genetically deleted one, was not done, because the potential presence of truncated ABCC5 isoforms might react with those antibodies. The presence of truncated ABCC5 isoforms and the gene rearrangement mentioned above hardly explain the ABCC5 protein expression in MCF7 clone 28E. The most likely explanation is that the unmatched genotype and phenotype of clone 28E is a result of non-specific bindings of the ABCC5 primary antibody. But these non-specific bindings might be within the truncated ABCC5 isoforms, given that no cross-reactions of ABCC5 primary antibody with other proteins were found in the ABCC5-overexpressing HEK293 cell model. Thus, future *ABCC5* KO studies may recruit high-resolution mass spectrometry and protein sequencing to examine the presence of truncated ABCC5 isoforms and their exact amino acid sequence.

In conclusion, the breathtaking CRISPR-Cas9-based gene modification technology is undoubtedly an excellent genetic manipulation method for pharmacology and molecular biology studies, but the CRISPR-Cas9 system seems to be involved in multiple cellular processes and exerts a profound impact on cells. The most obvious

consequences of the CRISPR-Cas9 system are the endonuclease activity of Cas9-induced cell damage and the off-target effect of CRISPR-Cas9, as we previously reviewed (He et al., 2021). Considering the questions that arose in the current study, the mechanisms underlying the CRISPR-Cas9 system, the exact genotype of KO cells, and the potential crosstalk between CRISPR-Cas9 and other signalling networks warrant in-depth investigations. Since only heterozygous KO clones were obtained in gene KO studies, the downstream functional studies were only conducted on heterozygous KO clones.

Chapter 4. ABCC5-Induced Cell Behavioural and Pharmacological Alterations in Breast Cancer

4.1 Introduction

Acquired drug resistance prevents cancer therapies from achieving stable and complete responses. As we previously reviewed in a review article "Pleiotropic Roles of ABC Transporters in Breast Cancer" (He et al., 2021), although ABC transporters showed superior drug efflux ability in *in vitro* studies, clinical use of ABC transporter inhibitors was unable to benefit the OS and DFS in breast cancer patients. However, olaparib might be a CS agent that selectively targets ABCC5-overexpressing cells (Chapter 6). In consideration of the results obtained from the HEK293 cell model, knockout of *ABCC5* may interrupt the molecular pathways related to the ABCC5-induced olaparib sensitivity, and olaparib mixed with doxorubicin probably shows a synergistic effect in TNBC cells. Here we hypothesise that olaparib is able to selectively induce cell death in ABCC5-overexpressing TNBC cells, and this effect can be reversed in an *ABCC5* gene knockout cell model. Olaparib combined with doxorubicin may further show a synergistic effect in selectively targeting ABCC5-rich TNBC cells.

This proposed study aims to: (i) assess *ABCC5* expression and *ABCC5*-related breast cancer clinical outcomes across normal and breast cancer patients with the use of the datasets and analysis provided in the ONCOMINE platform; (ii) investigate the role of ABCC5 in doxorubicin and olaparib sensitivity in TNBC cells using *ABCC5* gene

KO cell model; (iii) identify whether ABCC5 is related to metastases in TNBC cell lines.

4.2 Material and Methods

The details of the chemicals and experimental methods are shown in Chapter 2.

4.3 Results

4.3.1 ONCOMINE Datasets

The ONCOMINE database is a platform that integrates a number of cancerous microarray datasets from cancerous samples with normal samples (Rhodes et al., 2007; Rhodes et al., 2004). The ONCOMINE analysis pipelines, including differential expression analysis, coexpression analysis, meta-analysis and cancer outlier profile analysis (COPA), collectively contribute to a user-friendly assessment tool of gene expression patterns and molecular subtypes of numerous cancers. The aim of this section was to assess ABCC5 expression and ABCC5-related breast cancer clinical outcomes across normal and breast cancer patients using the datasets and analysis provided in the ONCOMINE platform.

Log_2-median centred intensity values for the breast cancer expression of ABC transporter candidates from different datasets containing patients with different metastasis, recurrence, chemodrug response and survival status were exported from ONCOMINE. The filters were set at "Gene: *ABCC5* + Analysis Type: Cancer vs. Normal Analysis + Cancer Type: Breast Cancer" for differential expression of *ABCC5* across normal and breast cancer patients, "Gene: *ABCC5* + Cancer Type: Breast Cancer

+ Data Type: mRNA + Sample Type: Clinical Specimen + Clinical Outcome: Metastatic Event Status/Patient Treatment Response/Recurrence Status/Survival Status" for breast cancer clinical outcomes, "Gene: *ABCC5* + Analysis Type: Cancer vs. Normal Analysis + Cancer Type: Breast Cancer + Concept: *SPAG5*-HPRD Interaction Sets/*KISS1*-HPRD Interaction Sets" for coexpression of *SPAG5* or *KISS1/KISS1R* with *ABCC5*, and "Gene: *ABCC5* + Analysis Type: Coexpression Analysis + Cancer Type: Breast Cancer + Data Type: mRNA + Sample Type: Clinical Specimen" for coexpression of other proteins with *ABCC5*.

4.3.1.1 The Overexpression of ABCC5 in Breast Cancer Compared with Normal Analyses

The Gene Summary View in

Table 4.1 shows several significant analyses that had *ABCC5* as a highly ranked over- or under-expressed gene across cancer types. ABCC5 expression in cancer vs. normal analyses showed more significant overexpression analyses than significant

downregulation analyses, especially in breast and lung cancer.

Table 4.1 Disease summary for ABCC5 (ONCOMINE). Threshold was set at *P*-value < 0.05, fold change > 2, and gene rank = 10%.

Analysis Type by Cancer	Cancer vs. Normal		Cancer vs. Cancer				Outlier	
			Cancer Histology		Multi-cancer			
Bladder Cancer			2	2	2		4	1
Brain and CNS Cancer		1			1		6	10
Breast Cancer	7			1	2		21	9
Cervical Cancer	3		1	1			5	1
Colorectal Cancer	1					2	4	3
Oesophageal Cancer	1				2		5	1
Gastric Cancer		3		1			6	1
Head and Neck Cancer	1					1	9	5
Kidney Cancer	3		3	3	1		6	2
Leukaemia	2	1	3	4	1		12	13
Liver Cancer	1							3
Lung Cancer	6		13	13	2		13	2
Lymphoma	3			1		1	7	5
Melanoma					1		3	3
Myeloma							2	
Other Cancer			1	1			10	3
Ovarian Cancer							4	1
Pancreatic Cancer					1	1	1	3
Prostate Cancer	1						15	6
Sarcoma		1	2	1			4	4
Significant Unique Analysis	29	6	25	27	13	5	128	71
Total Unique Analysis	433		717		260		944	

Cell colour is determined by the best gene rank percentile for the analyses within the cell

Given that TNBC is more biologically aggressive than other breast cancer subtypes, as previously reviewed in section 1.1.2, the Finak Breast dataset from ONCOMINE, including 59 patients with invasive breast carcinoma, was selected and analysed. To further assess the differential expression of some common ABC transporters in invasive breast carcinoma compared with normal breast tissues, the Finak Breast dataset in cancer vs. normal analyses were extracted (Figure 4.1). Only ABCC5 expression showed a significant increase in invasive breast carcinoma when comparing normal and cancerous samples with a *P*-value of < 0.05. The average ABCC5 expression level upon comparing invasive breast carcinoma and normal breast tissues exhibited an up to 3.42-fold change in the Finak Breast dataset. However, ABCC1 and ABCC2 were significantly down-regulated in invasive breast carcinoma in comparison to normal breast tissues (*P*-value < 0.05). The expression of other ABC transporters such as ABCB1, ABCC3, ABCC4 and ABCG2 in invasive breast carcinoma either remained at the same level or slightly lower than normal breast tissues. Herein, we conclude that ABCC5 is overexpressed in invasive breast carcinoma compared with normal breast tissues. This overexpression might be associated with many substrate export or cellular functions since other common ABC transporters were down-regulated in invasive procedures for breast carcinoma.

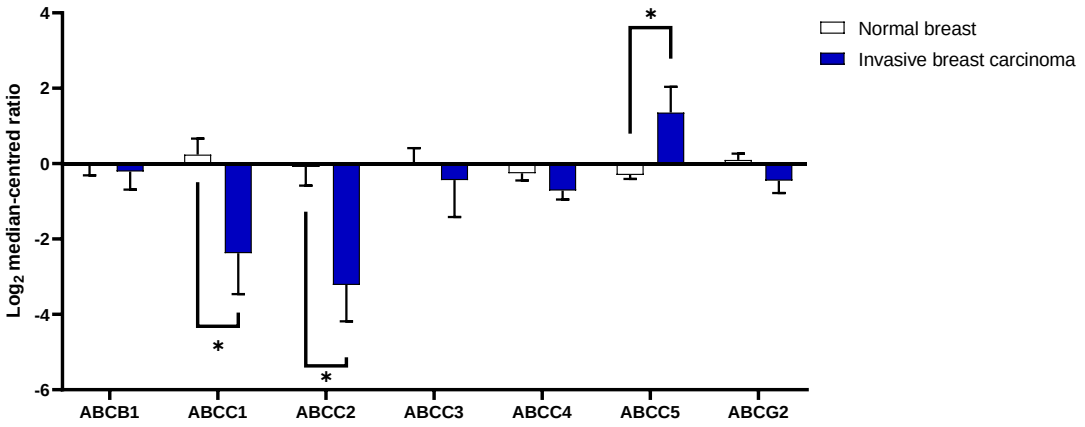

Figure 4.1 Differential expression of common ABC transporters in invasive breast carcinoma compared with normal breast tissue. Data from the Finak Breast dataset from ONCOMINE included 59 breast cancer patients who had tumour microarray gene expression analysis. Results were plotted as Log_2 median-centred ratio vs. ABC transporter type. Data were presented as mean ± SD. *$P < 0.05$ significantly different from the ABCC5 expression in normal breast tissue, calculated using two-way ANOVA and Sidak's multiple comparison post-test to compare all specimens.

4.3.1.2 The Association of ABCC5 and Breast Cancer Outcomes

The differential analysis not only compares ABCC5 expression across cancerous and normal histological samples but also compare metastases, recurrence, chemodrug response and survival of cancer patients. Figure 4.2 shows ABCC5 expression in both non-metastatic and metastatic breast cancer histological specimens at 1, 3 and 5 years, respectively. Patients with metastasis in comparison to non-metastasis at 1 year showed a significant increase in ABCC5 expression. However, this differential expression of ABCC5 was not reflected in metastatic event status at either 3 or 5 years.

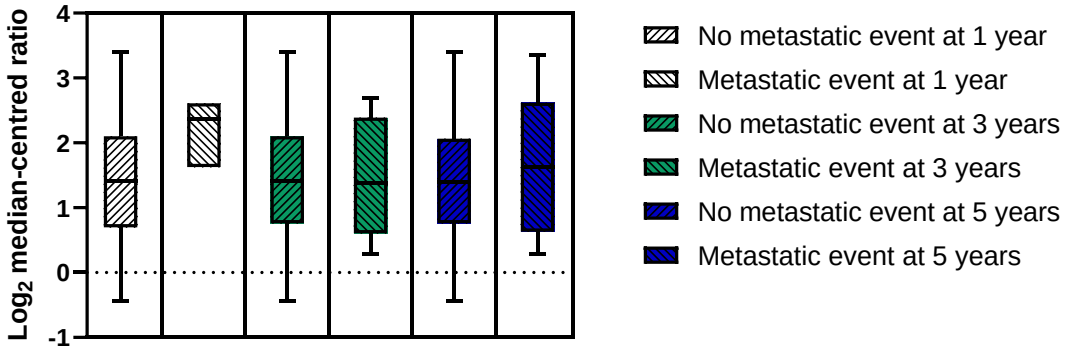

Figure 4.2 Differential expression of ABCC5 in non-metastatic and metastatic breast cancer patients at 1, 3 and 5 years. Data from the Desmedt Breast dataset from ONCOMINE included the metastatic event status of 198 breast cancer patients. Results were plotted as Log_2 median-centred ratio vs. metastatic event status. Data were presented as box and Tukey whiskers. Error bars are maximum and minimum values. Boxes and lines therein are 10 to 90th percentile values and median values.

A similar trend as the metastatic event status was found in the recurrence status of breast cancer patients at 1, 3 and 5 years (Figure 4.3). The increase in ABCC5 expression only occurred in breast cancer patients with recurrence at 1 year. In contrast, the recurrence at 3 and 5 years showed no significant difference in ABCC5 expression.

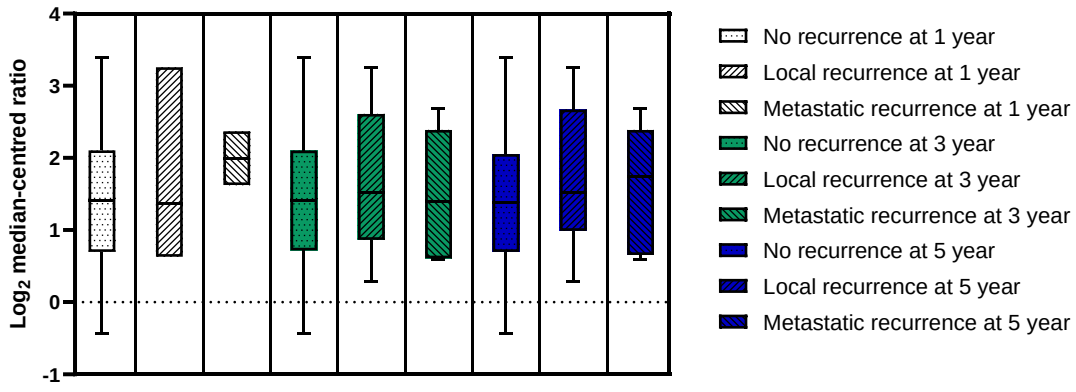

Figure 4.3 Differential expression of ABCC5 in non-recurrence, local recurrence and metastatic recurrence breast cancer patients at 1, 3 and 5 years. Data from the

Desmedt Breast dataset from ONCOMINE included the recurrence status of 198 breast cancer patients. Results were plotted as Log_2 median-centred ratio vs. recurrence status. Data were presented as box and Tukey whiskers. Error bars are maximum and minimum values. Boxes and lines therein are 10 to 90th percentile values and median values.

Apart from the weak correlation between ABCC5 expression and breast cancer metastasis and recurrence, its expression was not associated with patients' response to FAC (fluorouracil, doxorubicin/Adriamycin and cyclophosphamide) or doxorubicin/cyclophosphamide + taxane treatment (Figure 4.4).

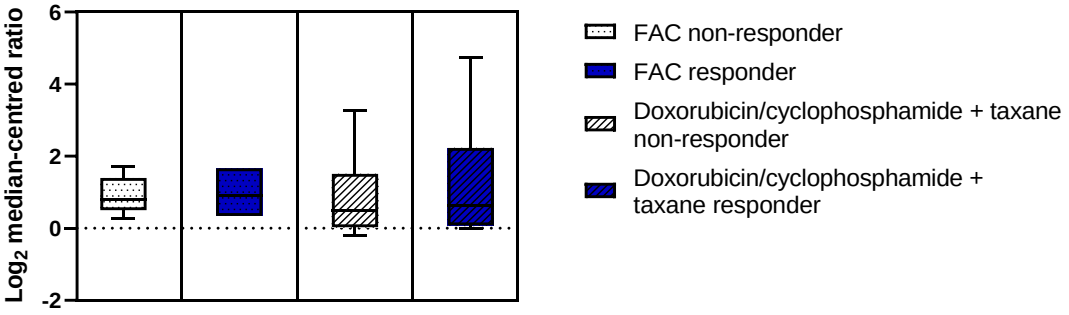

Figure 4.4 Differential expression of ABCC5 in non-responder and responder breast cancer patients. Data from the Tabchy Breast and Esserman Breast datasets from ONCOMINE included the metastatic event status of 178 and 130 breast cancer patients, respectively. Results were plotted as Log_2 median-centred ratio vs. response status. Data were presented as box and Tukey whiskers. Error bars are maximum and minimum values. Boxes and lines therein are 10 to 90th percentile values and median values.

However, the survival of breast cancer patients at 1, 3 and 5 years showed that high

expression of ABCC5 reduced the survival rate of breast cancer patients. The alive breast cancer patients at 1, 3 and 5 years all showed lower ABCC5 expression (Figure 4.5). These results suggested that although ABCC5 expression is not directly correlated with breast cancer metastasis, recurrence and chemodrug response, it exerts an impact on the overall survival of breast cancer patients.

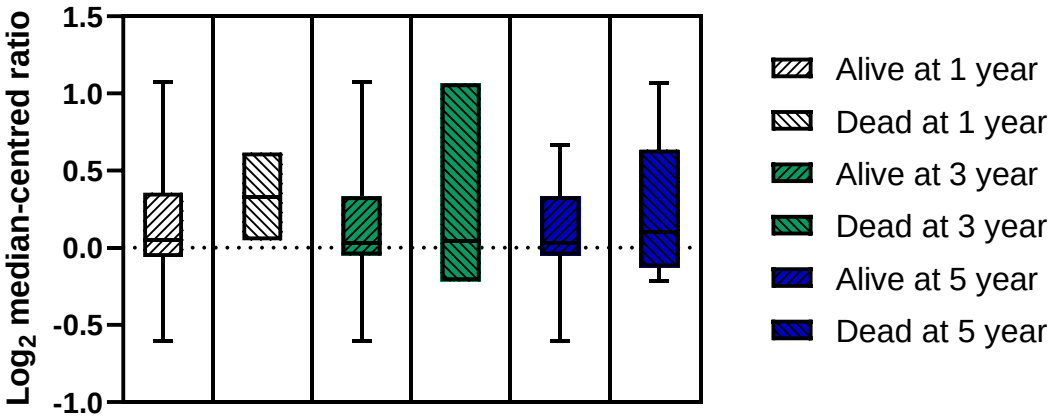

Figure 4.5 Differential expression of ABCC5 in alive and dead breast cancer patients at 1, 3 and 5 years. Data from the TCGA Breast 2 dataset from ONCOMINE included the recurrence status of 1602 breast cancer patients. Results were plotted as Log_2 median-centred ratio vs. survival status. Data were presented as box and Tukey whiskers. Error bars are maximum and minimum values. Boxes and lines therein are 10 to 90^{th} percentile values and median values.

4.3.1.3 Multi-Gene Validation: Coexpression of ABCC5 and Its Potential Upstream Regulators in Breast Cancer

To investigate the coexpression of possible targets in our hypotheses with *ABCC5*, the top two datasets Finak Breast and TCGA Breast, which showed the highest gene ranks for *ABCC5*, were selected and analysed the expression of *SPAG5*, *KISS1* and *KISS1R* in breast cancer compared with normal breast tissues. These datasets contain tumour

microarray gene expression analysis from specimens of invasive breast carcinoma, male breast carcinoma, mixed lobular and ductal breast carcinoma intraductal cribriform breast adenocarcinoma, invasive ductal breast carcinoma and mucinous breast carcinoma. The meta-analysis of Finak Breast and TCGA Breast datasets revealed that *SPAG5*, *KISS1* and *KISS1R* might be coexpressed with *ABCC5* with *P*-values of 0.005, 0.0000006 and 0.042, respectively (Table 4.2).

Table 4.2 The identified targets that are also up-regulated in *ABCC5* overexpressing datasets in breast cancer. The top two datasets Finak Breast and TCGA Breast, containing seven cancer vs. normal analyses that showed the highest gene ranks for *ABCC5*, were analysed the expression of *SPAG5*, *KISS1* and *KISS1R*. *P*-values measure whether the difference in means between breast cancer and normal breast tissues is likely to occur solely by chance, calculated using Student unpaired t-test.

Gene Symbol	*P*-value
ABCC5	0.000028
SPAG5	0.005
KISS1	0.000000956
KISS1R	0.042

Due to the broad nature of both SPAG5- and KISS1&KISS1R-mediated gene transcription and protein synthesis signalling pathways as reviewed in section 5.1, the *P*-values that indicate the significant difference in protein expression between breast cancer and normal breast tissues bolsters the evidence that there might be a correlation between SPAG5 and/or KISS1&KISS1R and ABCC5 (Table 4.2). Given the nature of membrane transporters, ABCC5 is unlikely to be a protein synthesis regulator. ABCC5 is thus a potential downstream effector regulated by SPAG5- and/or KISS1&KISS1R-related signalling pathways.

Apart from the proposed targets above, Table 4.3 shows a number of targets whose expression strongly correlated with the expression of *ABCC5* (> 0.7 correlation score).

These results suggest that *ABCC5* expression might be involved in multiple signalling pathways and could have a synergistic effect with other proteins.

Table 4.3 *ABCC5* coexpression analysis in breast cancer across 43 datasets. Threshold was set at *P*-value < 0.0001, fold change > 2, and gene rank = 10%. A coexpression correlation threshold of 0.7 was used to eliminate genes that are not highly correlated with ABCC5.

Gene Symbol	Gene Name	Correlation	Cytoband	Dataset
ABCC5	ATP-binding cassette, sub-family C (CFTR/MRP), member 5	1.000	3q27	
BCL2	B-cell CLL/lymphoma 2	0.946	18q21.33; 18q21.3	Schuetz Breast
PHF15	PHD finger protein 15	0.946	5q31.1	Schuetz Breast
PLEKHF2	pleckstrin homology domain-containing family F (with FYVE domain) member 2	0.915	8q22.1	Dairkee Breast
LOC100132214	similar to calcium-promoted Ras inactivator	0.906	7q22.1	Schuetz Breast
TMEM115	transmembrane protein 115	0.906	3p21.3	Schuetz Breast
SEL1L	sel-1 suppressor of lin-12-like (C. elegans)	0.889	14q24.3-q31	Schuetz Breast 2
ACP6	acid phosphatase 6, lysophosphatidic	0.882	1q21	Schuetz Breast
SORD	sorbitol dehydrogenase	0.882	15q15.3	Schuetz Breast
AGR2	anterior gradient homolog 2 (Xenopus laevis)	0.846	7p21.3	Schuetz Breast
C6orf211	chromosome 6 open reading frame 211	0.846	6q25.1	Schuetz Breast
CA12	carbonic anhydrase XII	0.846	15q22	Schuetz Breast
CYB561D2	cytochrome b-561 domain containing 2	0.846	3p21.3	Schuetz Breast
DHPS	deoxyhypusine synthase	0.846	19p13.2-p13.1	Schuetz Breast
FBP1	fructose-1,6-bisphosphatase 1	0.846	9q22.3	Schuetz Breast
LASS6	LAG1 homolog, ceramide synthase 6	0.846	2q24.3	Schuetz Breast
QDPR	quinoid dihydropteridine reductase	0.846	4p15.31	Schuetz Breast
SLC20A1	solute carrier family 20 (phosphate transporter), member 1	0.846	2q11-q14	Schuetz Breast
SYNGR2	synaptogyrin 2	0.846	17q25.3	Schuetz Breast
TBK1	TANK-binding kinase 1	0.846	12q14.1	Schuetz Breast
TOR1B	torsin family 1, member B (torsin B)	0.846	9q34	Schuetz Breast
YIPF6	Yip1 domain family, member 6	0.846	Xq12	Schuetz Breast
ACP5	acid phosphatase 5, tartrate resistant	0.826	19p13.3-p13.2	Schuetz Breast
APOC1	apolipoprotein C-I	0.826	19q13.2	Schuetz Breast

C5orf15	chromosome 5 open reading frame 15	0.826	5q31.1	Schuetz Breast
DALRD3	DALR anticodon binding domain containing 3	0.826	3p21.31	Schuetz Breast
DHPS	deoxyhypusine synthase	0.826	19p13.2-p13.1	Schuetz Breast
IGFBP2	insulin-like growth factor binding protein 2, 36kDa	0.826	2q33-q34	Schuetz Breast
MAN1A1	mannosidase, alpha, class 1A, member 1	0.826	6q22	Schuetz Breast
PLP2	proteolipid protein 2 (colonic epithelium-enriched)	0.826	Xp11.23	Schuetz Breast
MED13L	mediator complex subunit 13-like	0.824	12q24.21	Dairkee Breast
NAAA	N-acylethanolamine acid amidase	0.824	4q21.1	Dairkee Breast
ACSS1	acyl-CoA synthetase short-chain family member 1	0.798	20p11.23-p11.21	Dairkee Breast
CABC1	chaperone, ABC1 activity of bc1 complex homolog (S. pombe)	0.798	1q42.13	Dairkee Breast
CSAD	cysteine sulfinic acid decarboxylase	0.798	12q13.11-q14.3	Dairkee Breast
DCP2	DCP2 decapping enzyme homolog (S. cerevisiae)	0.798	5q22.2	Dairkee Breast
EPM2AIP1	EPM2A (laforin) interacting protein 1	0.798	3p22.1	Dairkee Breast
FAM134C	family with sequence similarity 134, member C	0.798	17q21.2	Dairkee Breast
MAGED2	melanoma antigen family D, 2	0.798	Xp11.2	Dairkee Breast
TRPS1	trichorhinophalangeal syndrome I	0.798	8q24.12	Dairkee Breast
ZNF552	zinc finger protein 552	0.798	19q13.43	Dairkee Breast
SLC22A15	solute carrier family 22, member 15	0.768	1p13.1	Korde Breast
ZNF212	zinc finger protein 212	0.796	7q36.1	Chang Breast
TTC37	tetratricopeptide repeat domain 37	0.766	5q15	Schuetz Breast 2
ZBTB10	zinc finger and BTB domain containing 10	0.766	8q13-q21.1	Schuetz Breast 2
BCAS4	breast carcinoma amplified sequence 4	0.765	20q13.13	Schuetz Breast
CLN3	ceroid-lipofuscinosis, neuronal 3	0.765	16p12.1	Schuetz Breast
DHX58	EXH (Asp-Glu-X-His) box polypeptide 58	0.765	17q21.2	Schuetz Breast
DMXL2	Dmx-like 2	0.765	15q21.2	Schuetz Breast
ETNK2	ethanolamine kinase 2	0.765	1q32.1	Schuetz Breast
FKBP4	FK506 binding protein 4, 59kDa	0.765	12p13.33	Schuetz Breast
GRPEL1	GrpE-like 1, mitochondrial (E. coli)	0.765	4p16	Schuetz Breast
GSTM3	glutathione S-transferase mu 3 (brain)	0.765	1p13.3	Schuetz Breast
LASS2	LAG1 homolog, ceramide synthase 2	0.765	1q21.3	Schuetz Breast
NAT1	N-acetyltransferase 1 (arylamine N-acetyltransferase)	0.765	8p23.1-p21.3	Schuetz Breast
PPT1	palmitoyl-protein thioesterase 1	0.765	1p32	Schuetz Breast
SLC39A6	solute carrier family 39 (zinc transporter), member 6	0.765	18q12.2	Schuetz Breast
SPG11	spastic paraplegia 11 (autosomal recessive)	0.765	15q14	Schuetz Breast
TSPAN31	tetraspanin 31	0.765	12q13.3	Schuetz Breast
ANKRD11	ankyrin repeat domain 11	0.755	16q24.3	Esserman Breast
ANKRD28	ankyrin repeat domain 28	0.754	3p25.1	Schuetz Breast 2
C14orf142	chromosome 14 open reading frame 142	0.754	14q32.12	Schuetz

GPHN	gephyrin	0.754	14q23.3	Breast 2 Schuetz
ICK	intestinal cell (MAK-like) kinase	0.754	6p12.1	Breast 2 Schuetz
NEK4	NIMA (never in mitosis gene a)-related kinase 4	0.754	3p21.1	Breast 2 Schuetz
DYNC112	dynein, cytoplasmic 1, intermediate chain 2	0.753	2q31.1	Breast 2 Hedenfalk
ENPP1	ectonucleotide pyrophosphatase/phosphodiesterase 1	0.753	6q22-q23	Breast Hedenfalk
C14orf43	chromosome 14 open reading frame 43	0.744	14q24.3	Breast Dairkee
C17orf62	chromosome 17 open reading frame 62	0.744	17q25.3	Breast Dairkee
ERBB3	v-erb-b2 erythroblastic leukemia viral oncogene homolog 3 (avian)	0.744	12q13	Breast Dairkee
HEXIM1	hexamethylene bis-acetamide inducible 1	0.744	17q21.31	Breast Dairkee
ISOC1	isochorismatase domain containing 1	0.744	5q22.1-q33.3	Breast Dairkee
KIAA0182	KIAA0182	0.744	16q24.1	Breast Dairkee
LIG3	ligase III, DNA, ATP-dependent	0.744	17q11.2-q12	Breast Dairkee
LOC100132288	hypothetical protein LOC100132288	0.744	21p11.2	Breast Dairkee
TSR2	TSR2, 20S rRNA accumulation, homolog (S. cerevisiae)	0.744	Xp11.22	Breast Dairkee
ITGBL1	integrin, beta-like 1 (with EGF-like repeat domains)	0.715	13q33	Breast Finak

4.3.2 ABCC5-Related Collateral Sensitivity in Breast Cancer Cells

4.3.2.1 Validation of the Decreased ABCC5 Expression in Heterozygous Knockout Clones

Prior to testing the sensitivity of heterozygous KO clones to doxorubicin and olaparib, the functional expression of ABCC5 in these clones were determined using immunocytochemistry (section 2.10) and uptake study (section 2.7.2.2). Surface staining assay (section 2.7.1) was not conducted on KO clones due to the breakdown of the flow cytometer.

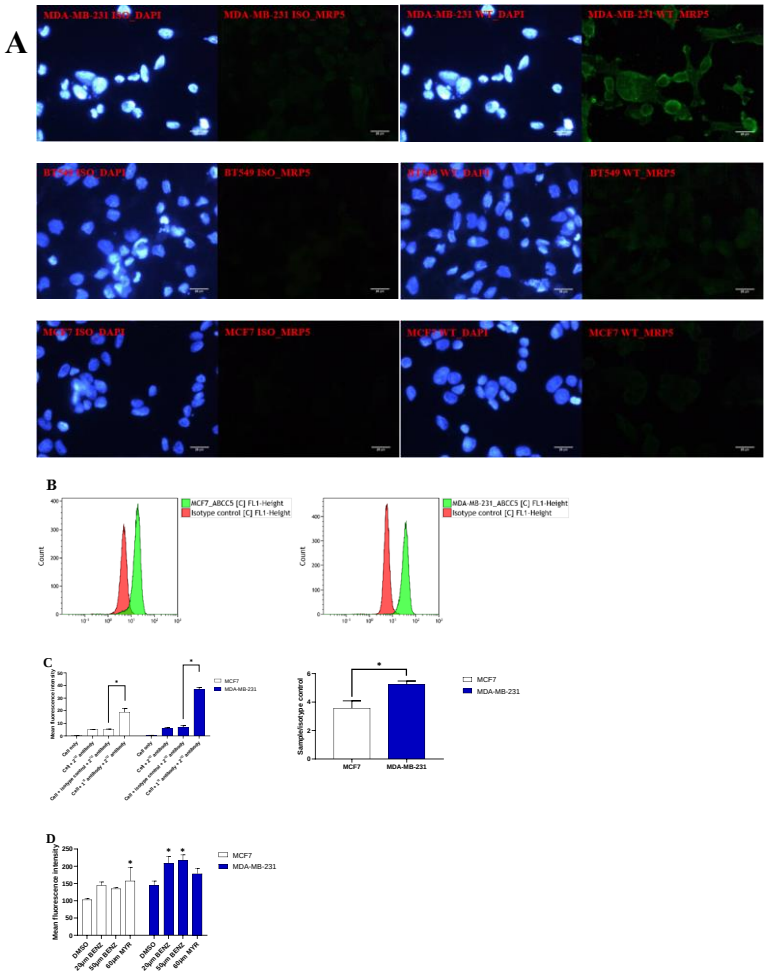

Figure 4.6 Functional expression of ABCC5 in wild-type breast cancer cells. A. Immunocytochemistry of MDA-MB-231, BT549 and MCF7 WT cells. Cells were stained with MRP5 Monoclonal Antibody and Goat Anti-Rat IgG H&L (DyLight® 488) secondary antibody. The isotype control (ISO) groups were stained with IgG2a primary antibody and Goat Anti-Rat IgG H&L (DyLight® 488) secondary antibody. **B.** ABCC5 protein detected in representative flow cytometry histogram of cell surface staining using the anti-ABCC5 (green) and isotype control IgG2a (red) on MCF7 and MDA-MB-231 cells. Both the primary antibody and isotype control were labelled with Alexa Fluor 488 secondary antibody. The X-axis is the fluorescence signal intensity displayed in a linear log scale. **C.** Cell surface staining of ABCC5 in MDA-MB-231 and MCF7 WT cells. Results were plotted as fluorescence intensity of sample/fluorescence intensity of isotype control vs. cell type. Data were presented as mean ± SD of three

independent experiments, each repeat was run in duplicates. *$P < 0.05$ significantly different from the fluorescence of the non-TNBC MCF7 cells, calculated using Student unpaired t-test. **D.** The cellular accumulation of BCECF in MDA-MB-231 and MCF7 cells after 30 min pre-incubation with ABCC5 inhibitors. Results were plotted as average fluorescence vs. cell type. Data were presented as mean ± SD of two independent experiments, each repeat was run in duplicates. *$P<0.05$ significantly different from the BCECF accumulation in corresponding DMSO control groups, calculated using one-way ANOVA and Sidak's multiple comparison post-test to compare all treatment groups with the corresponding DMSO control group for each cell line.

Figure 4.6 shows the functional expression of ABCC5 in breast cancer cells. After staining with MRP5 Monoclonal Antibody and Goat Anti-Rat IgG H&L (DyLight® 488) secondary antibody, signals indicating ABCC5 expression appeared in all the tested cell lines. Surface staining assay was not conducted on BT549 WT cells due to the breakdown of the flow cytometer. Immunostaining results correspond to the BCECF accumulation status in these cell lines. A *P*-value of < 0.05 demonstrates that the accumulated BCECF in WT cells was significantly lower than cells pre-treated with ABCC5 inhibitor benzbromarone. Immunocytochemistry and uptake studies were further adopted to examine the functional expression of ABCC5 in KO clones. ABCC5 protein expression was down-regulated in KO clones (Figure 4.7A), and the BCECF accumulation in these clones was much higher than in WT cells with a *P*-value of < 0.05 (Figure 4.7B). These results reveal that ABCC5 was functionally down-regulated in heterozygous *ABCC5* gene KO clones.

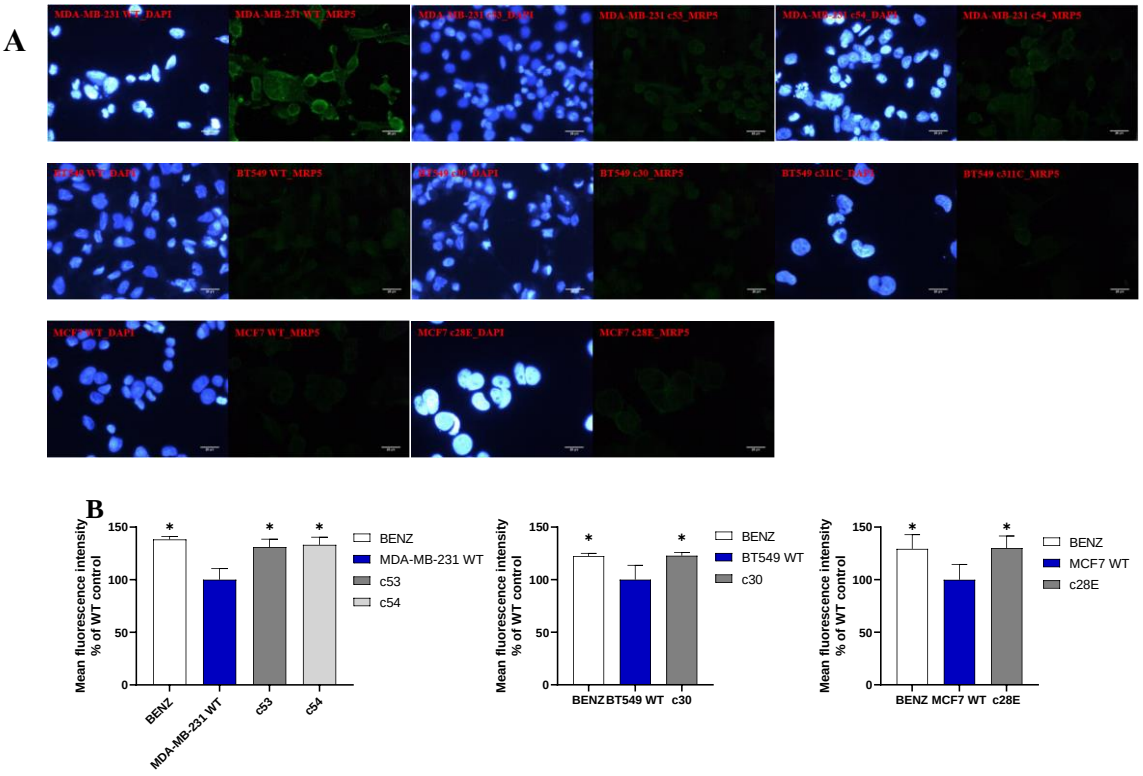

Figure 4.7 Functional expression of ABCC5 in heterozygous knockout clones. A. Immunocytochemistry of MDA-MB-231, BT549 and MCF7 KO clones. Cells were stained with MRP5 Monoclonal Antibody and Goat Anti-Rat IgG H&L (DyLight® 488) secondary antibody. The isotype control (ISO) groups were stained with IgG2a primary antibody and Goat Anti-Rat IgG H&L (DyLight® 488) secondary antibody. **B.** The cellular accumulation of BCECF in MDA-MB-231, BT549 and MCF7 KO clones. Data were presented as % of wild-type control. Results were plotted as % of wild-type control vs. cell type. Data were presented as mean ± SD of at least triplicates, respectively. **P*<0.05 significantly different from the BCECF accumulation in corresponding WT cells, calculated using one-way ANOVA and Sidak's multiple comparison post-test to compare all KO clones with the control groups.

4.3.2.2 The Sensitivity of Heterozygous *ABCC5* Knockout Clones to Doxorubicin and Olaparib

Prior to investigating the ABCC5-related drug sensitivity in breast cancer cells using MTT assay (section 2.8), the influence of different DMSO purity on absorbance readings was tested. This ensured the precision and accuracy in detecting cells at low density.

Table 4.4 The influence of relatively impure DMSO (Cat. Number: D/4121/24, Fisher Scientific) on absorbance. 100 µL complete medium (CM) was mixed with 10 µL MTT and incubated for 4 hours. After incubation, 85 µL mixture was removed. 150 µL DMSO was then added into each well and incubated for 30 min.

	DMSO only	CM+DMSO	MTT+DMSO	CM+MTT+DMSO
Mean ± SD	0.0026 ± 0.0012	0.0079 ± 0.0009	0.0469 ± 0.0041	0.2253 ± 0.0060

Table 4.5 Examination of the potential reactions between RPMI 1640 medium, FBS, L-glutamine, Pen-strep, MTT and DMSO (Cat. Number: D/4121/24, Fisher Scientific). 100 µL of RPMI 1640, FBS, L-glutamine and Pen-strep was mixed with 10 µL MTT and incubated for 4 hours, respectively. After incubation, 85 µL mixture was removed. 150 µL DMSO was then added into each well and incubated for 30 min.

	RPMI+DMSO	RPMI+MTT	RPMI+MTT+DMSO
Mean ± SD	0.0081 ± 0.0043	0.0030 ± 0.0015	0.1611 ± 0.0126
	FBS+DMSO	**FBS+MTT**	**FBS+MTT+DMSO**
Mean ± SD	0.0816 ± 0.0148	0.0041 ± 0.0017	0.3609 ± 0.0122
	L-glu+DMSO	**L-glu+MTT**	**L-glu+MTT+DMSO**
Mean ± SD	0.0019 ± 0.0001	0.0101 ± 0.0013	0.0019 ± 0.0016
	Pen-strep+DMSO	**Pen-strep+MTT**	**Pen-strep+MTT+DMSO**
Mean ± SD	0.0034 ± 0.0015	0.0085 ± 0.0004	0.0019 ± 0.0012
	DMSO only	**MTT+DMSO**	
Mean ± SD	0.0017 ± 0.000611	0.0219 ± 0.003051	

The relatively impure DMSO was found to react with CM and reduce MTT to generate an absorbance reading of around 0.2253 (Table 4.4). This value virtually represents the OD value of 2000 to 4000 cells (Figure 4.8). In comparison to the reasonable OD value of blank control in MTT assay (Table 4.6), this value is not acceptable, especially when minor variations of cell viability are detected between KO clones. To further examine

which component of CM induces the reaction with relatively impure DMSO and the reduction of MTT, RPMI 1640 medium, FBS, L-glutamine and Pen-strep were tested, respectively. FBS was found to participate in these reactions with an OD value of around 0.3609 (Table 4.5). This study did not test which contaminant in relatively impure DMSO could react with FBS. Therefore, it is of significance to use relatively pure DMSO in MTT assay to guarantee the accuracy of the results.

Table 4.6 The reasonable absorbance reading of blank control. DMSO was purchased from ThermoFisher Scientific, NZ (Cat. Number: FSBBP231-1). 100 μL complete medium (CM) was mixed with 10 μL MTT and incubated for 4 hours. After incubation, 85 μL mixture was removed. 150 μL DMSO was then added into each well and incubated for 30 min.

	CM+MTT+DMSO
Mean ± SD	0.0621 ± 0.0029

The MTT assay used to quantify total viable cell number/well was further verified for linearity at the expected range of cell numbers. A linear relationship between absorbance and cell numbers was observed for MDA-MB-231 cells ranging from 500 to 16000 with an R^2 value of 0.9956 (Figure 4.8B). However, when the cell number was expanded to 32000 cells, the linearity between OD value and cell numbers was compromised ($R^2 = 0.9602$) (Figure 4.8A). Thus, a cell number of around 16000 cells was considered maximum at the measurement of OD value. Given that HEK293 cells had an average doubling time of 24 hours (Cervera, Gutiérrez, Gòdia, & Segura, 2011) and the exposure duration of cells to chemodrugs was 4 days, a seeding density of 2000 cells/well was used in this study.

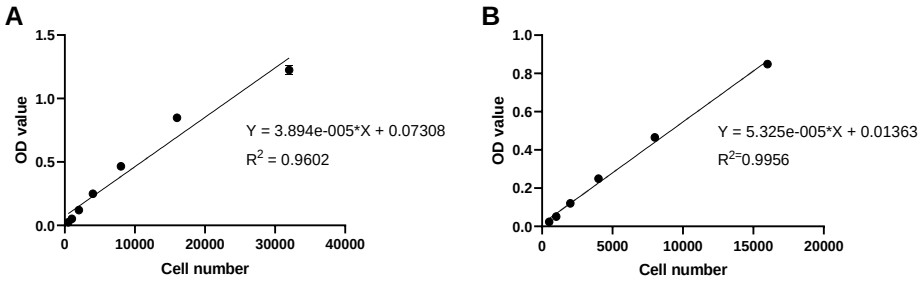

Figure 4.8 Linearity of absorbance (OD value) with increasing cell numbers of MDA-MB-231 cells. A. Cell number from 500 to 32000. **B.** Cell number from 500 to 16000. Data were presented as mean ± SD of triplicates.

Since no homozygous KO clones were obtained in the current study, the sensitivity of heterozygous KO clones to pemetrexed, doxorubicin, and olaparib were determined using MTT assay (section 2.8).

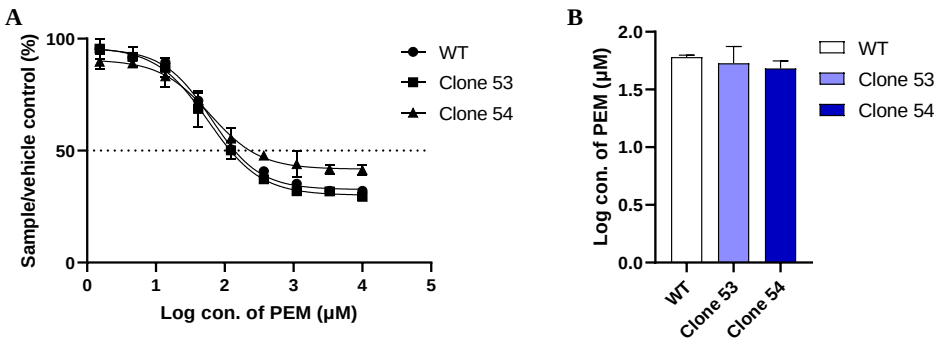

Figure 4.9 The pemetrexed-induced growth inhibition in MDA-MB-231 wild-type cells and heterozygous knockout clones. A. Growth inhibition curve. Results were plotted as % of cell viability from vehicle control vs. log concentration of pemetrexed. Data were presented as mean ± SD of two independent experiments, each repeat was run in triplicates. **B.** Comparison of IC_{50} values between MDA-MB-231 WT cells and KO clones. Results were plotted as Log IC_{50} value vs. cell type. Data were presented as mean ± SD of two independent experiments, each repeat was run in triplicates. No significant difference from the IC_{50} value of pemetrexed in MDA-MB-231 WT cells was calculated using one-way ANOVA and Sidak's multiple comparison post-test to compare all clones with WT cells.

Pemetrexed, a well-documented ABCC5 substrate antifolate chemodrug (Kobayashi et al., 2013), was employed as a positive control to study the ABCC5-related olaparib sensitivity. To compare ABCC5-mediated pemetrexed sensitivity in heterozygous MDA-MB-231 KO clones, cells were treated with pemetrexed for 4-hr, followed by 4 days incubation with CM. Unlike the MTT results of the HEK293 cell model (section 6.3.3.3), the lowered expression of ABCC5 in heterozygous MDA-MB-231 KO clones did not alter the sensitivity to pemetrexed (Figure 4.9A). IC_{50} values for pemetrexed-induced growth inhibition remained at the same level in MDA-MB-231 WT and heterozygous KO cells (Figure 4.9B). This might be due to the different dominant pemetrexed-resistance pathways in HEK293 and MDA-MB-231 cells, respectively. In other words, the lowered expression of ABCC5-induced sensitive phenotype might be compensated by other signalling pathways that could regulate pemetrexed-resistance in heterozygous MDA-MB-231 KO clones, such as the *solute carrier family 19 member 1 (SLC19A1)* (Tanino, Tsubata, Harashima, Harada, & Isobe, 2018) and Hedgehog (HH) pathway (Y. Liu, Huber, Kiefl, Tufman, & Kauffmann-Guerrero, 2020). However, another study demonstrated that ABCC5 could mediate pemetrexed-resistance in MCF7 breast cancer cells in *ABCC5* knockdown and overexpressing cell models (J. Chen et al., 2021). Taken together, the decrease of ABCC5 expression in present heterozygous KO clones might not be sufficient for significant alterations in pemetrexed sensitivity.

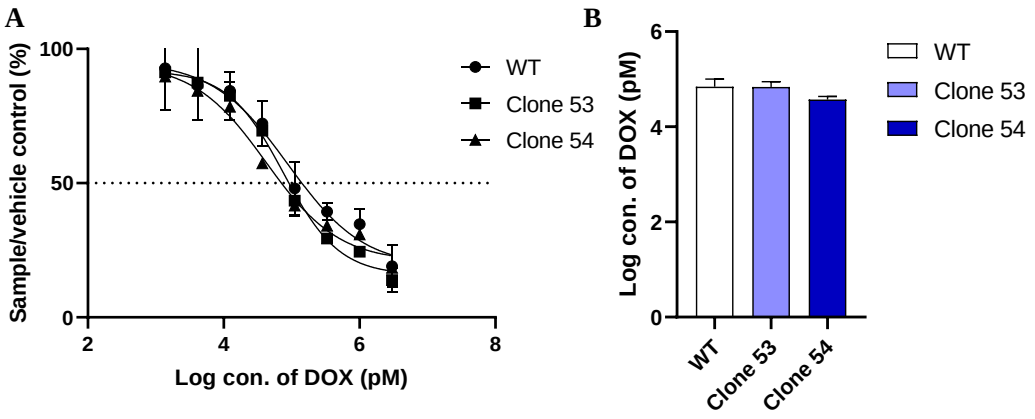

Figure 4.10 The doxorubicin-induced growth inhibition in MDA-MB-231 wild-type cells and heterozygous knockout clones. A. Growth inhibition curve. Results were plotted as % of cell viability from vehicle control vs. log concentration of doxorubicin. Data were presented as mean ± SD of three independent experiments, each repeat was run in triplicates. **B.** Comparison of IC_{50} values between MDA-MB-231 WT cells and KO clones. Results were plotted as Log IC_{50} value vs. cell type. Data were presented as mean ± SD of three independent experiments, each repeat was run in triplicates. No significantly different from the IC_{50} value of doxorubicin in MDA-MB-231 WT cells, calculated using one-way ANOVA and Sidak's multiple comparison post-test to compare all clones with WT cells.

To compare ABCC5-mediated doxorubicin sensitivity in heterozygous MDA-MB-231 KO clones, cells were treated with doxorubicin for 4-hr, followed by 4 days incubation with CM. Similar to the MTT results of the HEK293 cell model (section 6.3.3.3), the sensitivity to doxorubicin of MDA-MB-231 heterozygous KO clones did not show a significant difference from WT cells (Figure 4.10). Although clone 54 showed lower IC_{50} than WT cells, the variations were not statistically significant.

In comparison, olaparib-induced growth inhibition was significantly enhanced in MDA-MB-231 and BT549 WT cells compared with heterozygous KO clones (Figure 4.11 and Figure 4.12). IC_{50} values of heterozygous MDA-MB-231 clone 54 and BT549 clone 30 showed about a 2-fold increase compared with WT cells. These results were

in accord with the HEK293 cell model (section 6.3.3.3) that olaparib might be a CS agent against ABCC5-rich cells. However, the sensitivity of MDA-MB-231 clone 53 to olaparib remained at the same level as WT cells. More clones and repetitions are expected to examine whether or not the sensitivity of clone 53 to olaparib is a result of single-cell variability or off-target effect. But this study failed to include more clones and repetitions due to the COVID-19 pandemic and lockdown restrictions. MCF7 KO clones and MDA-MB-231 and BT549 KO clones from the second round of KO were not proceeded to MTT assay due to the COVID-19 pandemic and lockdown restrictions, either.

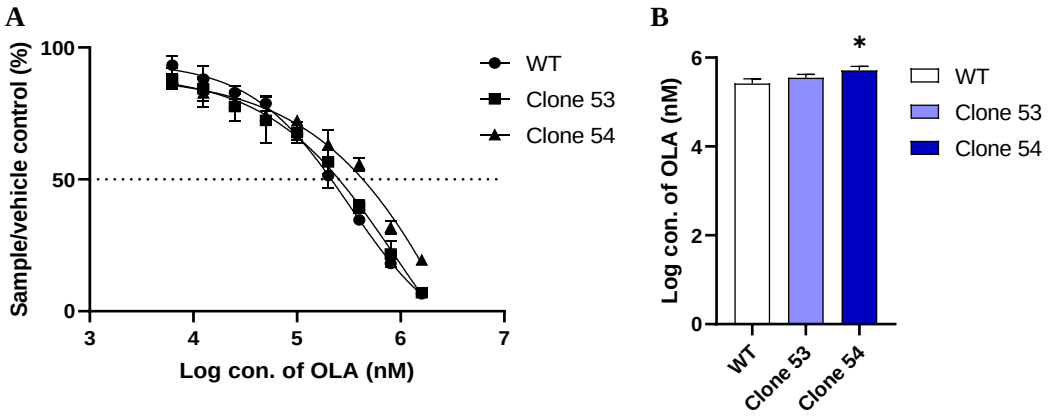

Figure 4.11 The olaparib-induced growth inhibition in MDA-MB-231 wild-type cells and heterozygous knockout clones. A. Growth inhibition curve. Results were plotted as % of cell viability from vehicle control vs. log concentration of olaparib. Data were presented as mean ± SD of triplicates. **B.** Comparison of IC_{50} values between MDA-MB-231 WT cells and KO clones. Results were plotted as Log IC_{50} value vs. cell type. Data were presented as mean ± SD of triplicates. *$P < 0.05$ significantly different from the IC_{50} value of olaparib in MDA-MB-231 WT control, calculated using one-way ANOVA and Sidak's multiple comparison post-test to compare all clones with WT cells.

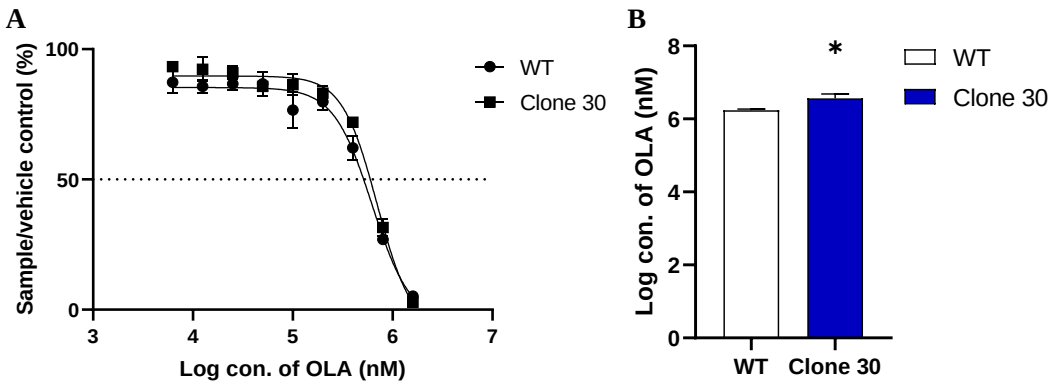

Figure 4.12 The olaparib-induced growth inhibition in BT549 wild-type cells and heterozygous knockout clone. A. Growth inhibition curve. Results were plotted as % of cell viability from vehicle control vs. log concentration of olaparib. Data were presented as mean ± SD of triplicates. **B.** Comparison of Log IC_{50} values between BT549 WT cells and KO clone. Results were plotted as IC_{50} value vs. cell type. Data were presented as mean ± SD of triplicates.

4.3.3 The Synergistic Effect of Olaparib Combined with Doxorubicin in TNBC Cells

4.3.3.1 Determination of IC50 Values for Olaparib and Doxorubicin in MDA-MB-231 and MCF7 Cells

Prior to investigating the synergistic effect of doxorubicin and olaparib in TNBC cells, the antiproliferative effects of these chemodrugs were determined in MDA-MB-231 TNBC cells and MCF7 non-TNBC cells to identify the cytostatic exposure time using MTT assay (section 2.8). These also indicated if ABCC5 overexpression in MDA-MB-231 cells conferred a sensitive phenotype towards olaparib.

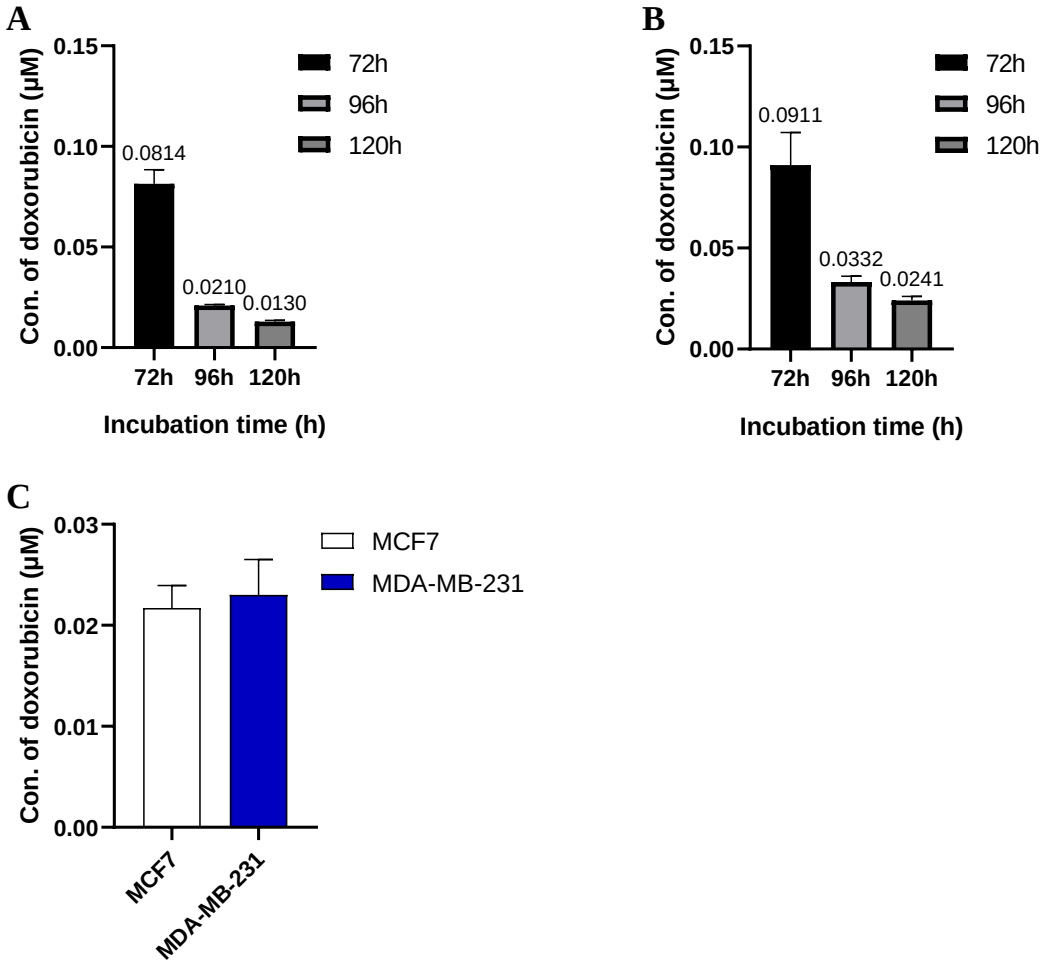

Figure 4.13 Determination of IC_{50} values for doxorubicin in MCF7 (A) and MDA-MB-231 (B) cells. Results were plotted as IC_{50} values for doxorubicin vs. exposure time. Data were presented as mean ± SD of three independent experiments, each repeat was run in triplicates. **C.** Comparison of IC_{50} values in MCF7 and MDA-MB-231 cells after 96-hr treatment with doxorubicin. No significant difference was shown in these two cell lines after 72-, 96- and 120-hr treatment with doxorubicin, calculated using Student's unpaired t-test.

Figure 4.13 shows IC_{50} data of MCF7 and MDA-MB-231 cells after 72-, 96- and 120-hr exposure to increasing concentrations of doxorubicin. The overexpressed ABCC5 in MDA-MB-231 cells was unable to maintain a significantly higher proliferation rate than MCF7 cells over the designated exposure time. The sensitivity to doxorubicin in MDA-MB-231 and MCF7 cells remained at the same level over 72-, 96- and 120-hr exposure time. These data correspond to those obtained in the HEK293 cell model that

doxorubicin cytotoxicity showed no significant difference between HEK-MRP5 and HEK-P cells in section 6.3.3.1.

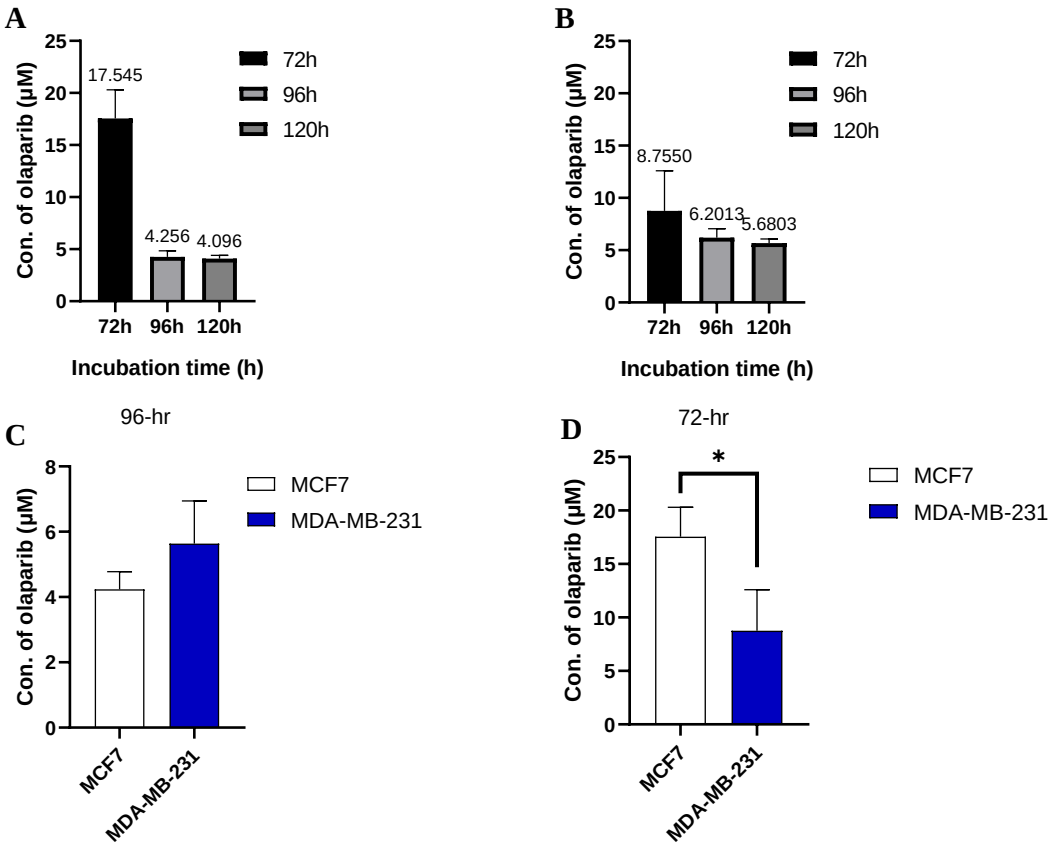

Figure 4.14 Determination of IC_{50} values for olaparib in MCF7 (A) and MDA-MB-231 (B) cells. Results were plotted as IC_{50} values for olaparib vs. exposure time. Data were presented as mean ± SD of three independent experiments, each repeat was run in triplicates. **C.** Comparison of IC_{50} values in MCF7 and MDA-MB-231 cells after 96-hr treatment with olaparib. No significant difference was shown in these two cell lines, calculated using Student's unpaired t-test. **D.** Comparison of IC_{50} values in MCF7 and MDA-MB-231 cells after 72-hr treatment with olaparib. $*P < 0.05$ significantly different from the IC_{50} values in non-TNBC MCF7 cells, calculated using Student's unpaired t-test.

To further investigate the role of ABCC5 in cellular sensitivity to olaparib-induced growth inhibition, MCF7 and MDA-MB-231 cells were exposed to increasing concentrations of olaparib for 72-, 96- and 120-hr. Consistent with results in section

6.3.3.1, the resistance of MCF7 cells to olaparib was 2-fold higher than ABCC5-overexpressing MDA-MB-231 cells after 72-hr exposure with a *P*-value of < 0.05 and remained at the same level after 96 hours exposure (Figure 4.14). In consideration of the nature of combination index (CI) determination, 5 to 9 concentration points are designed to cover ED_{50} and lie in the efficacious concentration range of the drug. At the same time, 96 hours of exposure to olaparib at which the IC_{50} values in different cell lines remained at the same level was used to explore the synergistic effects of olaparib and doxorubicin in breast cancer cells.

4.3.3.2 The Cytotoxicity of Combining Olaparib with Doxorubicin in TNBC Cells

To investigating the synergistic effect of doxorubicin and olaparib in TNBC cells, MDA-MB-231, BT549 and MCF7 cells were treated with increasing concentrations of doxorubicin and olaparib combination at a ratio of 1:200. After 4 days of incubation, the MTT results were analysed by CompuSyn software (Chou, 2006).

Table 4.7, Table 4.8 and Table 4.9 show the CI (combination index) values for the combination of doxorubicin with olaparib. These results demonstrate that a synergistic effect was achievable when around ED_{50} concentrations (CI < 1) were used. However, an antagonism (CI > 1) effect was detected when the concentrations were lower than ED_{30} in all three cell lines. The synergistic effect of doxorubicin and olaparib occurred in both TNBC (MDA-MB-231 and BT549) and non-TNBC (MCF7) cell lines in a consistent manner, indicating a universal synergy between those two drugs in both TNBC and non-TNBC cells.

Table 4.7 CI (combination index) values for the combination of olaparib with doxorubicin in MDA-MB-231 cells. Cells were treated with increasing concentrations of olaparib and doxorubicin at a ratio of 1:200 for 4 days. Data were analysed using CompuSyn software (Chou, 2006) and presented as mean of three independent experiments, each repeat was run in triplicates.

Drug Concentration (μM) Constant ratio of 1:200		ED_X (%)	CI value	
Doxorubicin	**Olaparib**			
0.5	**100**	97	0.21271	Synergy
0.25	**50**	91	0.46208	Synergy
0.125	**25**	84	0.4842	Synergy
0.0625	**12.5**	63	0.96713	Synergy
0.03125	**6.25**	51	0.91877	Synergy
0.01563	**3.12**	47	0.54763	Synergy
0.00781	**1.5625**	31	0.65501	Synergy
0.00391	**0.78125**	11	1.67674	Antagonism
0.00195	**0.39063**	7	1.59696	Antagonism

Table 4.8 CI (combination index) values for the combination of olaparib with doxorubicin in BT549 cells. Cells were treated with increasing concentrations of olaparib and doxorubicin at a ratio of 1:200 for 4 days. Data were analysed using CompuSyn software (Chou, 2006) and presented as mean of three independent experiments, each repeat was run in triplicates.

Drug Concentration (μM) Constant ratio of 1:200		ED_X (%)	CI value	
Doxorubicin	**Olaparib**			
0.5	**100**	99	0.54659	Synergy
0.25	**50**	98	0.74464	Synergy
0.125	**25**	94	1.08504	Antagonism
0.0625	**12.5**	89	1.13298	Antagonism
0.03125	**6.25**	82	0.97479	Synergy
0.01563	**3.12**	80	0.57764	Synergy
0.00781	**1.5625**	65	0.60197	Synergy
0.00391	**0.78125**	32	1.27115	Antagonism
0.00195	**0.39063**	20	1.39668	Antagonism

Table 4.9 CI (combination index) values for the combination of olaparib with doxorubicin in MCF7 cells. Cells were treated with increasing concentrations of olaparib and doxorubicin at a ratio of 1:200 for 4 days. Data were analysed using CompuSyn software (Chou, 2006) and presented as mean of three independent experiments, each repeat was run in triplicates.

Drug Concentration (μM) Constant ratio of 1:200		ED_X (%)	CI value	
Doxorubicin	**Olaparib**			
0.5	**100**	97	0.53015	Synergy
0.25	**50**	95	0.53633	Synergy
0.125	**25**	81	1.17124	Antagonism
0.0625	**12.5**	74	0.89694	Synergy
0.03125	**6.25**	68	0.6118	Synergy
0.01563	**3.12**	51	0.72642	Synergy
0.00781	**1.5625**	31	1.0518	Antagonism
0.00391	**0.78125**	15	1.90877	Antagonism
0.00195	**0.39063**	13	1.1638	Antagonism

4.3.4 Binding Affinity and Hydrogen Bond Interaction of Different Ligands with ABCC5

In the present study, different drugs were analysed through molecular docking study using AutoDock 4.2 software (Morris et al., 2009), and results were evaluated and visualised using Protein-Ligand Interaction Profiler (https://plip-tool.biotec.tu-dresden.de) (Adasme et al., 2021), ProteinsPlus (https://proteins.plus) (Morris et al., 2009; Schoning-Stierand et al., 2020) and LIGPLOT software (Wallace, Laskowski, & Thornton, 1995).

Docking results against receptor molecule from Protein-Ligand Interaction Profiler (https://plip-tool.biotec.tu-dresden.de) (Adasme et al., 2021) showed that all the tested drugs at least formed one hydrogen-bond with ABCC5. The inhibition constant of benzbromarone was evaluated at 21 μM in Figure 4.15. However, 20 μM was found to almost achieve maximum inhibition on ABCC5 in section 3.3.2. The estimated free energy of binding of benzbromarone, pemetrexed, doxorubicin and olaparib are shown

in Figure 4.15 to Figure 4.18. According to the binding energy data, benzbromarone, pemetrexed and olaparib have a higher binding affinity to ABCC5 than doxorubicin. This finding is consistent with the results in section 4.3.2.2 and 6.3.3.1 that ABCC5 was hardly related to doxorubicin translocation and doxorubicin-induced growth inhibition in breast cancer cells and HEK293 cells.

Interestingly, among these four drugs, including ABCC5 substrate pemetrexed, olaparib showed the highest binding affinity to ABCC5 with an inhibition constant at 9.4 μM. But neither the inhibitory effect nor the extracellular translocation of olaparib was found related to ABCC5 in section 6.3.2.3. However, this high binding affinity of olaparib to ABCC5 might partially mirror that the collateral sensitivity to olaparib in breast cancer cells (section 4.3.2.2) and ABCC5-overexpressing HEK293 cells (section 6.3.3.3) might be a result of the non-covalent interactions between olaparib and ABCC5. Future studies may employ microarray assay to analyse the potential downstream effectors underlying these interactions.

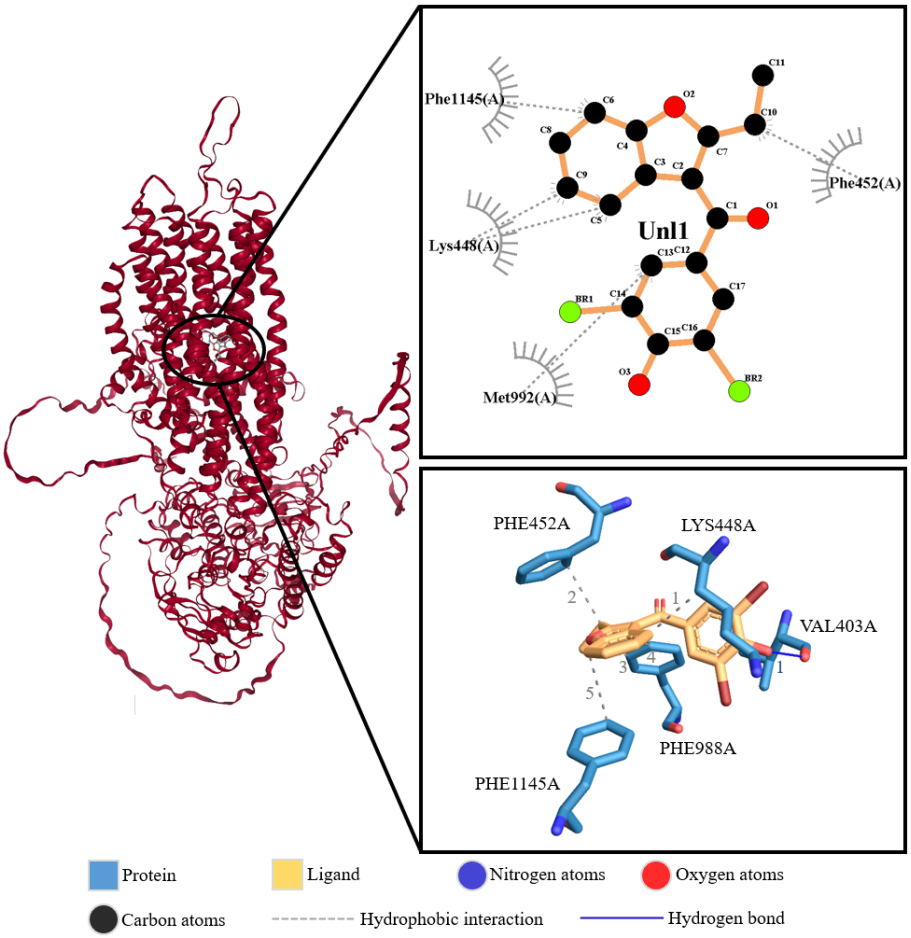

Ligand	Binding energy (kcal/mol)	Inhibition constant (Ki)	
Benzbromarone	-6.38	21 µM	
	Hydrogen bonds interacting residues	**Distance between hydrogen and acceptor atoms**	**Distance between donor and acceptor atoms**
	VAL403A (1)	1.96	2.81
	Hydrophobic interactions	**Distance between interactions carbon atoms**	
	LYS448A (1)	3.59	
	PHE452A (2)	3.74	
	PHE988A (3)	3.96	
	PHE988A (4)	3.95	
	PHE1145A (5)	3.88	

Figure 4.15 Benzbromarone docked on ABCC5 macromolecule. ABCC5 is depicted in red colour in ribbon form. Data were analysed using AutoDock 4.2 software (Morris et al., 2009). Results were visualised using Protein-Ligand Interaction Profiler (https://plip-tool.biotec.tu-dresden.de) (Adasme et al., 2021), ProteinsPlus (https://proteins.plus) (Morris et al., 2009; Schoning-Stierand et al., 2020) and LIGPLOT software (Wallace et al., 1995).

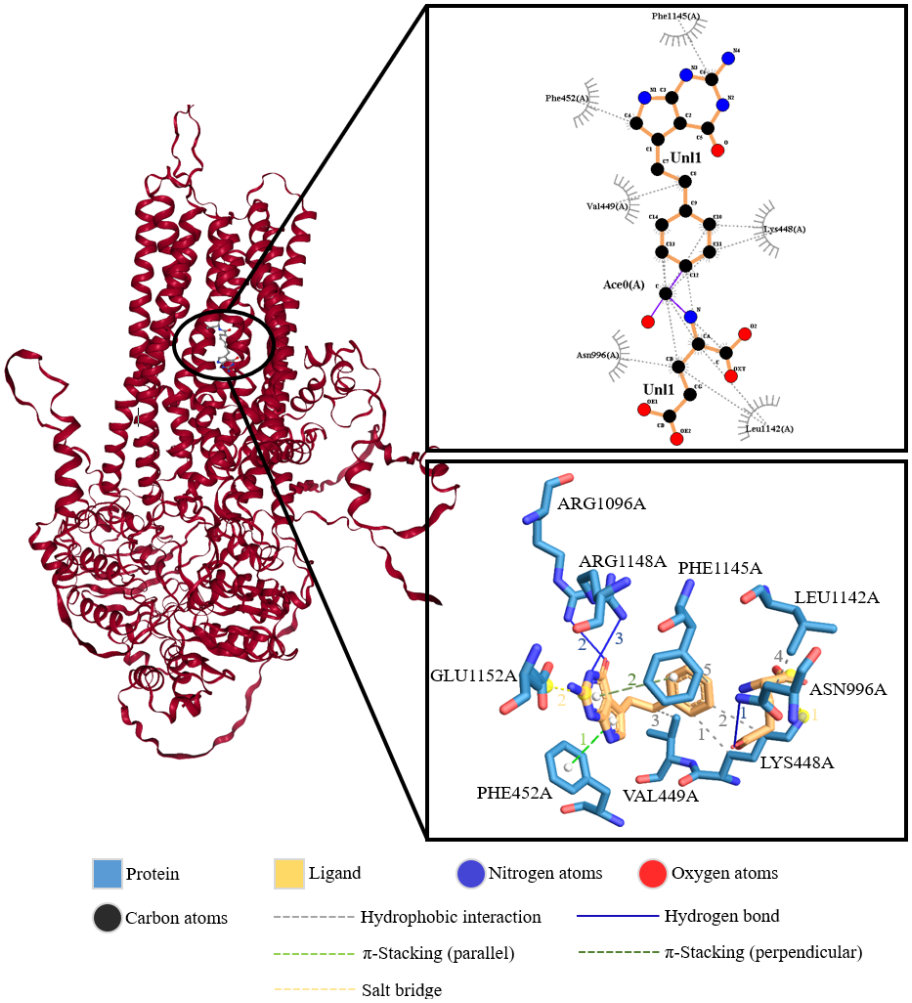

Ligand	Binding energy (kcal/mol)	Inhibition constant (Ki)	
Pemetrexed	-5.04	201.38 μM	
	Hydrogen bonds interacting residues	**Distance between hydrogen and acceptor atoms**	**Distance between donor and acceptor atoms**
	ASN996A (1)	2.72	3.70
	ARG1096A (2)	2.57	3.52
	ARG1148A (3)	3.08	3.78
	Hydrophobic interactions	**Distance between interactions carbon atoms**	
	LYS448A (1)	3.70	
	LYS448A (2)	3.88	
	VAL449A (3)	3.43	
	LEU1142A (4)	3.33	
	PHE1145A (5)	3.99	
	π-Stacking	**Distance between ring centres**	
	PHE452A (1)	4.22	
	PHE1145A (2)	5.04	
	Salt bridge	**Distance between centres of charge**	
	LYS448A (1)	3.05	
	GLU1152A (2)	4.14	

Figure 4.16 Pemetrexed docked on ABCC5 macromolecule. ABCC5 is depicted in red colour in ribbon form. Data were analysed using AutoDock 4.2 software (Morris et al., 2009). Results were visualised using Protein-Ligand Interaction Profiler (https://plip-tool.biotec.tu-dresden.de) (Adasme et al., 2021), ProteinsPlus (https://proteins.plus) (Morris et al., 2009; Schoning-Stierand et al., 2020) and LIGPLOT software (Wallace et al., 1995).

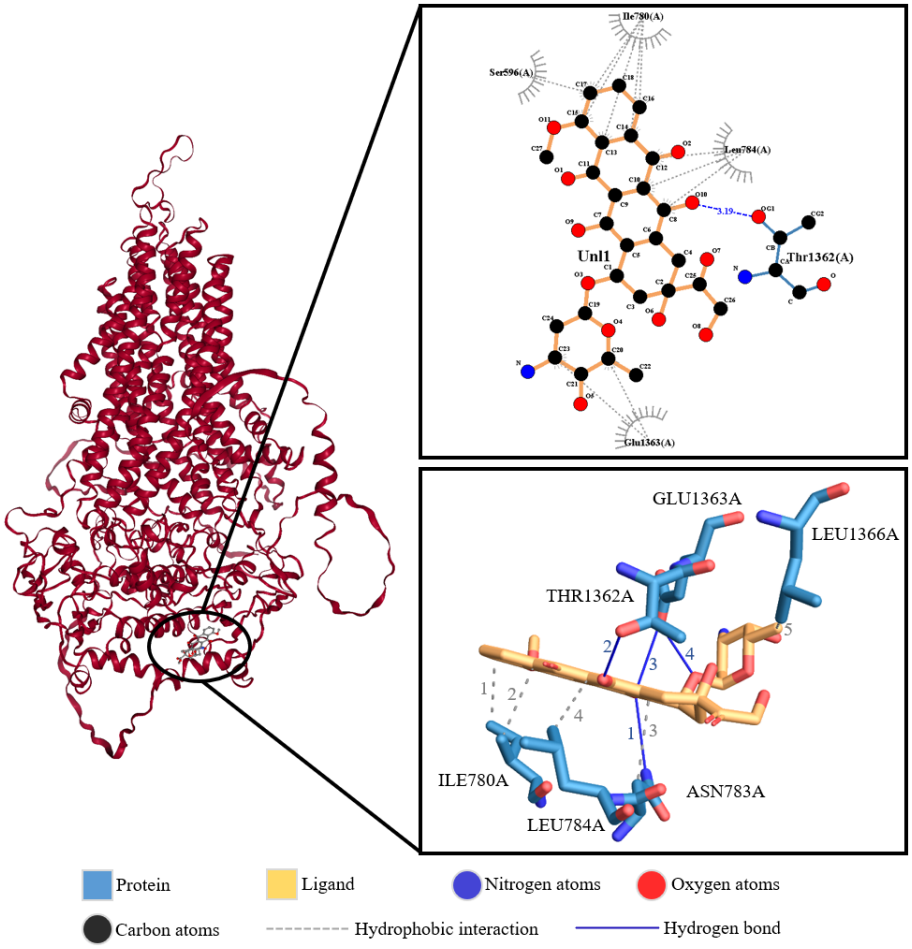

Ligand	Binding energy (kcal/mol)	Inhibition constant (Ki)	
Doxorubicin	-2.86	8.02 mM	
	Hydrogen bonds interacting residues	**Distance between hydrogen and acceptor atoms**	**Distance between donor and acceptor atoms**
	ASN783A (1)	2.81	3.70
	THR1362A (2)	2.66	3.19
	GLU1363A (3)	2.80	3.32
	GLU1363A (4)	2.22	3.06
	Hydrophobic interactions	**Distance between interactions carbon atoms**	
	ILE780A (1)	3.58	
	ILE780A (2)	3.68	
	ASN783A (3)	3.97	
	LEU784A (4)	3.85	
	LEU1366A (5)	3.98	

Figure 4.17 Doxorubicin docked on ABCC5 macromolecule. ABCC5 is depicted in red colour in ribbon form. Data were analysed using AutoDock 4.2 software (Morris et al., 2009). Results were visualised using Protein-Ligand Interaction Profiler (https://plip-tool.biotec.tu-dresden.de) (Adasme et al., 2021), ProteinsPlus (https://proteins.plus) (Morris et al., 2009; Schoning-Stierand et al., 2020) and LIGPLOT software (Wallace et al., 1995).

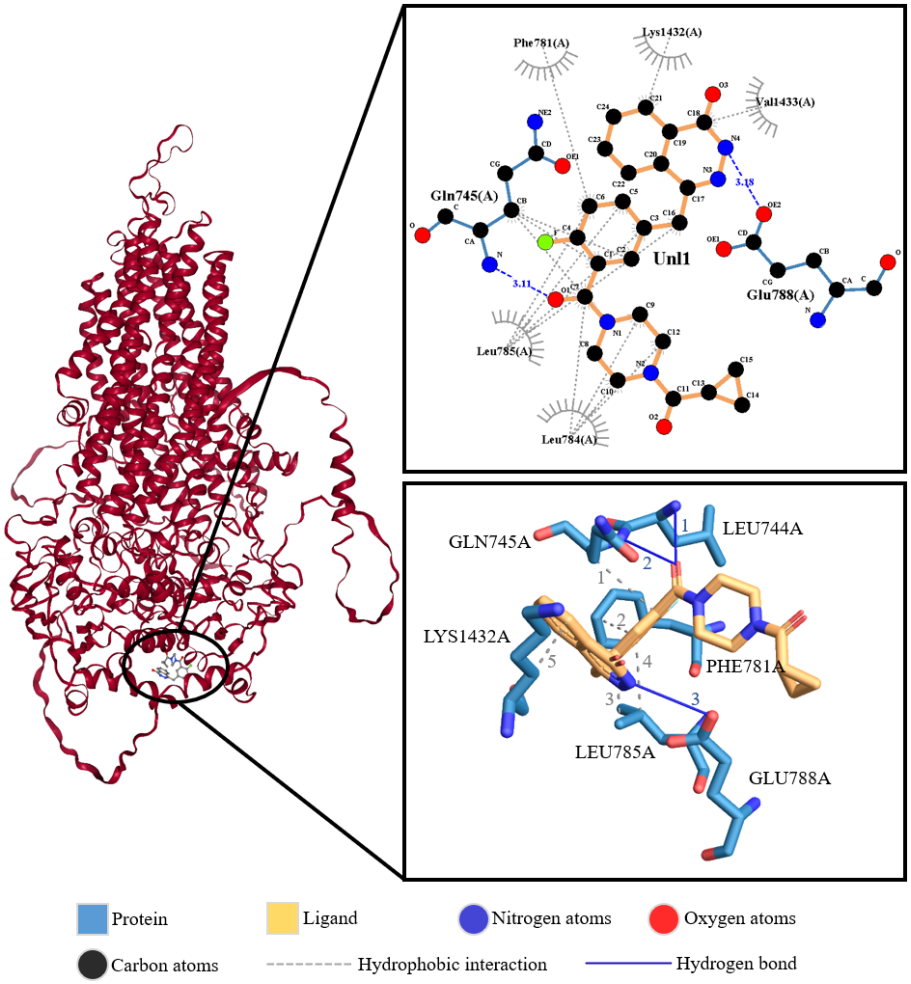

Ligand	Binding energy (kcal/mol)	Inhibition constant (Ki)	
Olaparib	-6.86	9.40 µM	
	Hydrogen bonds interacting residues	**Distance between hydrogen and acceptor atoms**	**Distance between donor and acceptor atoms**
	LEU744A (1)	2.83	3.20
	GLN745A (2)	2.17	3.11
	GLU788A (3)	2.76	3.66
	Hydrophobic interactions	**Distance between interactions carbon atoms**	
	GLN745A (1)	3.66	
	PHE781A (2)	3.65	
	LEU785A (3)	3.20	
	LEU785A (4)	3.73	
	LYS1432A (5)	3.61	

Figure 4.18 Olaparib docked on ABCC5 macromolecule. ABCC5 is depicted in red colour in ribbon form. Data were analysed using AutoDock 4.2 software (Morris et al., 2009). Results were visualised using Protein-Ligand Interaction Profiler (https://plip-tool.biotec.tu-dresden.de) (Adasme et al., 2021), ProteinsPlus (https://proteins.plus) (Morris et al., 2009; Schoning-Stierand et al., 2020) and LIGPLOT software (Wallace et al., 1995).

4.4 Discussion

The studies described in this chapter firstly aimed to assess *ABCC5* expression and

ABCC5-related breast cancer clinical outcomes using ONCOMINE datasets. ABCC5 expression showed more significant overexpression analyses than significant downregulation analyses, especially in breast and lung cancer. These results indicate that ABCC5 tends to be overexpressed in breast cancer compared with normal breast tissue. Given that TNBC is more biologically aggressive than other breast cancer subtypes, the Finak Breast dataset from ONCOMINE, including 59 patients with invasive breast carcinoma, were extracted and analysed. ABCC5 expression was significantly elevated in invasive breast carcinoma by comparing normal and cancerous samples with a *P*-value of < 0.05. These results were consistent with our findings in Chapter 3 that ABCC5 was overexpressed in MDA-MB-231 and BT549 TNBC breast cancer cell lines. Furthermore, ABCC5 expression was not correlated with breast cancer metastasis, recurrence and chemodrug response by comparing different breast cancer patients, but it might impact the overall survival of breast cancer patients. In contrast, some ABC transporters were found to regulate breast cancer metastasis through various pathways, as we previously reviewed (He et al., 2021). Besides, the meta-analysis of Finak Breast and TCGA Breast datasets revealed that *SPAG5*, *KISS1* and *KISS1R* might be coexpressed with *ABCC5* with P-values of 0.005, 0.0000006 and 0.042, respectively. These results indicate that ABCC5 might be a potential downstream effector regulated by SPAG5- and/or KISS1&KISS1R-related signalling pathways. The SPAG5-regulated ABCC5 expression was determined in Chapter 5 in this study.

With regard to the sensitivity to pemetrexed- and doxorubicin-induced growth-inhibition, MDA-MB-231 *ABCC5* KO cells remained at the same level as WT cells. Pemetrexed was employed as a positive control to study ABCC5-related drug sensitivity (Kobayashi et al., 2013). The opposite results obtained in the present study might be because the lowered expression of ABCC5 in heterozygous MDA-MB-231

KO clones was not sufficient to alter the sensitivity to pemetrexed. Of note, a previous study demonstrated that ABCC5 could mediate pemetrexed-resistance in MCF7 breast cancer cells in *ABCC5* knockdown and overexpressing cell models (J. Chen et al., 2021). A 2.3-fold difference in pemetrexed sensitivity was observed between HEK-P and HEK-MRP5 cells in Chapter 6 in the present study. These findings may mirror that the dominant pemetrexed-resistance pathways might be different in different cell lines. The lowered expression of ABCC5-induced sensitive phenotype might be compensated by other signalling pathways that could regulate pemetrexed-resistance in heterozygous MDA-MB-231 KO clones, such as the *solute carrier family 19 member 1 (SLC19A1)* (Tanino et al., 2018) and Hedgehog (HH) pathway (Y. Liu et al., 2020). Similarly, MDA-MB-231 *ABCC5* KO cells did not show elevated sensitivity to doxorubicin than WT cells. As discussed in Chapter 6, the role of ABCC5 in mediating doxorubicin resistance is controversial. Although doxorubicin was regarded as a weak substrate of ABCC5 in HEK293 cell model in present study, the minor difference in doxorubicin accumulation between HEK-MRP5 and HEK-P cells was unable to induce significantly altered resistance. Molecular docking study also confirmed that doxorubicin exhibited low binding affinity to ABCC5. In consideration of the much lower expression level of ABCC5 in breast cancer cells than HEK-MRP5 cells, it is reasonable that MDA-MB-231 *ABCC5* KO cells exhibit a doxorubicin-resistant phenotype as WT cells, especially when only heterozygous KO cells were analysed.

In terms of the sensitivity to olaparib-induced growth-inhibition, MDA-MB-231 and BT549 *ABCC5* KO cells showed resistant phenotype compared with WT cells. Olaparib-induced growth inhibition was about 2-fold enhanced in MDA-MB-231 and BT549 WT cells than heterozygous KO clones. Results in Chapter 6 revealed that olaparib was not a substrate nor an inhibitor of ABCC5. HEK-MRP5 cells showed 3.4-

fold more sensitivity to olaparib-induced growth inhibition than HEK-P cells. These consistent findings in HEK293 and *ABCC5* gene KO cell models indicate that olaparib might be a CS (collateral sensitivity) agent (Hall et al., 2009) against ABCC5-overexpressing cells. The underlying mechanisms are still unclear. Some potentially involved pathways are discussed in Chapter 6. Of note, molecular docking analysis in the present study showed that the binding affinity of olaparib to ABCC5 was even greater than pemetrexed (ABCC5 substrate) and benzbromarone (ABCC5 inhibitor). Also, previous studies reported that olaparib might play a role in mediating membrane transporters *in vitro*, such as ABCB1, ABCG2, OATP1B1, OCT1, OCT2, OAT3, MATE1 and MATE2 (McCormick & Swaisland, 2017; McCormick et al., 2018). These findings may mirror that the collateral sensitivity to olaparib in ABCC5-rich cells might result from the non-covalent interactions between olaparib and ABCC5.

Moreover, a synergistic effect was found between doxorubicin and olaparib in breast cancer cells. This synergistic effect between doxorubicin and olaparib can be explained by their mechanism of action. The potential pharmacodynamics of doxorubicin and olaparib was reviewed in section 1.2. Doxorubicin can induce DNA damage by inhibiting topoisomerase II and generating ROS (Rossi, 2013; Tacar et al., 2013). In the presence of PARP inhibitor olaparib, the PARP-regulated DNA repair pathways are blocked. Although cancer cells have other DNA repair routes, the blocked PARP function, to some extent, prevents the doxorubicin-induced DNA damage from getting repaired and thus cause cell apoptosis. Besides, olaparib was reported to inhibit ABCB1 and ABCG2 and enhance the cellular accumulation of their substrates, such as doxorubicin (McCormick & Swaisland, 2017; McCormick et al., 2018). The elevated intracellular accumulation of doxorubicin definitely improves the pharmacodynamics of doxorubicin. However, the cell death caused by doxorubicin was found to rely on the

hyperactivation of PARP1-induced autophagy and necrosis (Tacar et al., 2013). Doxorubicin-mediated hyperactivation of PARP1 can cause cellular energy collapse and thus trigger autophagy and necrosis, ultimately resulting in apoptosis. Doxorubicin at moderately high concentrations is unable to induce cell death in PARP1-deficient cells. Therefore, in the presence of PARP inhibitor olaparib, to what extent the blocked PARP activity influences the potency of doxorubicin remained to be investigated.

In conclusion, these studies showed olaparib might be a CS agent that selectively targets ABCC5-overexpressing cells. This finding makes ABCC5 a promising target to overcome drug resistance in breast cancer cells. However, the molecular mechanisms underlying this phenomenon are unknown but probably relate to interactions between ABCC5 and olaparib. Future studies may employ microarray assay to analyse the potential downstream effectors underlying these interactions. The collateral sensitivity to olaparib can be enhanced by cotreatment with DNA-damaging drug doxorubicin.

Chapter 5. SPAG5: The Potential Upstream Regulators of ABCC5

5.1 Introduction

Sperm-associated antigen 5 (SPAG5) is a mitotic spindle protein involved in various intracellular processes that regulate tumour initiation and progression, in addition to counteracting the cytotoxic effects of many chemotherapies as we previously reviewed in a review article "SPAG5: An Emerging Oncogene" (He et al., 2020). SPAG5 can confer resistance to olaparib in TNBC cells through c-MYC signalling and regulate gene transcription and protein expression through multiple pathways (He et al., 2020). Here we hypothesise that SPAG5 promotes the expression of ABCC5 in TNBC cells. Thus, *SPAG5* gene knockout probably influences olaparib sensitivity in TNBC cells through mediating ABCC5 expression.

This proposed study aims to: (i) establish *SPAG5* knockout cell lines; (ii) identify the role of SPAG5 in functional expression of ABCC5 in TNBC cell lines; (iii) investigate the role of SPAG5 in olaparib sensitivity in TNBC cell lines.

5.2 Material and Method

The details of chemicals and experimental methods are shown in Chapter 2.

5.3 Results

5.3.1 Validation of Morphology of Cell Lines

To validate the BT549 TNBC cell line and the SKBR3, MCF7 and T47D non-TNBC cell lines, cell morphology was visualized by using Zeiss Primovert Compact Inverted Microscope (Carl Zeiss AG) and compared with the supplier's schematic illustration from ATCC (Cryosite Ltd, NSW, AU). The morphology of BT549 and MCF7 cells are shown in section 3.3.1. Figure 5.1 further indicates the morphology of SKBR3 and T47D non-TNBC cells.

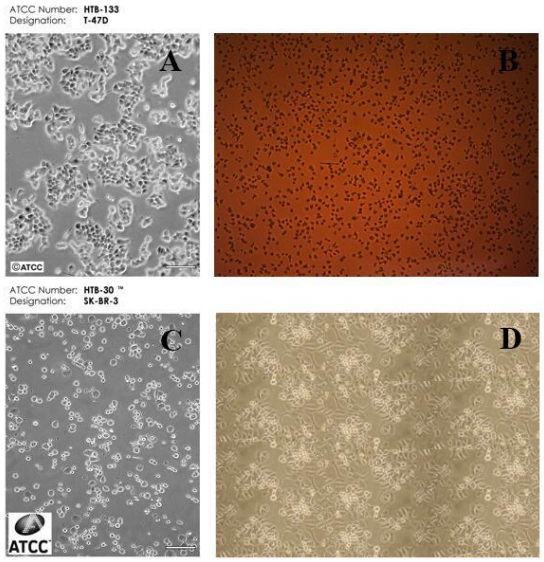

Figure 5.1 Morphology of T47D and SKBR3 cells. Images for T47D cells in Panel A and SKBR3 cells in Panel C were obtained from ATCC (Cryosite Ltd, NSW, AU). Images for T47D cells in Panel B and SKBR3 cells in Panel D were taken using Zeiss Primovert Compact Inverted Microscope (Carl Zeiss AG) and cells were cultured in Applied Sciences Laboratory in AUT.

5.3.2 Validation of SPAG5 Expression in Breast Cancer Cells

Before investigating the role of SPAG5 in human breast cancer cells, western blotting (section 2.9) was adopted to confirm the expression of SPAG5 in these cell lines.

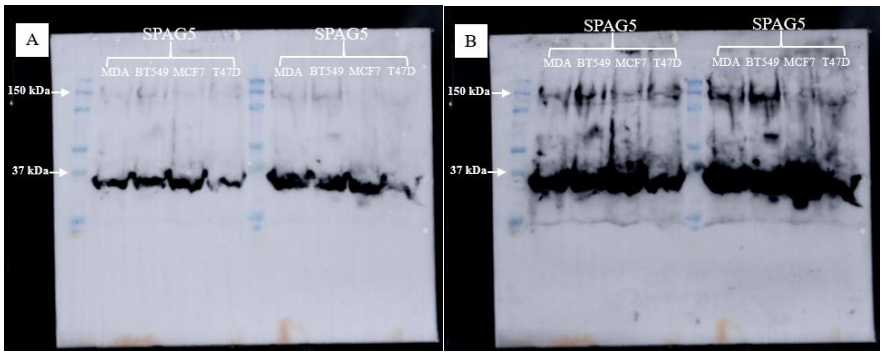

Figure 5.2 Immunoblot of SPAG5 protein from MDA-MB-231, BT549, T47D, and MCF7 cells. The membrane was immunoblotted using SPAG5 Mouse Monoclonal Antibody and Anti-Mouse IgG (whole molecule) – Peroxidase antibody produced in rabbit. Each cell lysate was done in duplicates. **A.** Automatic exposure. **B.** 2 min exposure.

In Figure 5.2, after staining with SPAG5 Mouse Monoclonal Antibody and Anti-Mouse IgG (whole molecule) – Peroxidase antibody produced in rabbit, two bands of around 150 kDa and 30 kDa in size were detected in all of the four tested WT cells. However, the 150 kDa bands were faint even with increased exposure time. The protein concentration of the cell lysate was not measured. 50 µL of cell lysate (maximum volume of the gel) was loaded into each well. According to the manufacturer's demonstration, the 150 kDa band was not detected in KO cells compared with WT, while the 30 kDa band was significantly fainter in KO cells than WT (Figure 5.3). Thus, western blotting could be adopted to validate SPAG5 expression in KO clones.

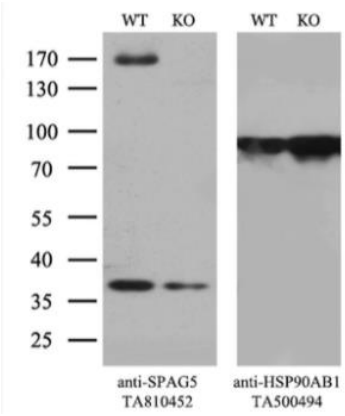

Figure 5.3 Demonstration of SPAG5 Mouse Monoclonal Antibody provided by the manufacturer.

5.3.3 Validation of Self-Prepared DNA Extraction Buffer and Puromycin Concentration for Antibiotic Selection

5.3.3.1 Validation of Self-Prepared DNA Extraction Buffer

Extraction of DNA using QIAamp DNA Mini Kit (QIAGEN, Germany) was complicated and time-consuming, which was not suitable for high-throughput screening of KO clones. Thus, different recipes of extraction buffer (lysis buffer) were tested in this study, including TE buffer containing 0.1% Triton X-100, TE buffer containing 0.1% Tween 20, Tris/glycine buffer containing 0.1% Triton X-100, Tris/glycine buffer containing 0.1% Tween 20, Tris/HCl buffer containing 0.1% Triton X-100, Tris/HCl buffer containing 0.1% Tween 20, lysis buffer from QIAamp DNA Mini Kit (QIAGEN, Germany), and hypotonic buffer (0.5mM Na_2HPO_4 + 0.5mM NaH_2PO_4). The cell lysate was mixed with proteinase K and heated using a thermal cycler as the method shown in section 2.5. Four recipes were found to work well on DNA extraction (Figure 5.4). TE buffer containing 0.1% Tween 20 was used to screen KO clones considering the availability and cost-effectiveness of the reagents.

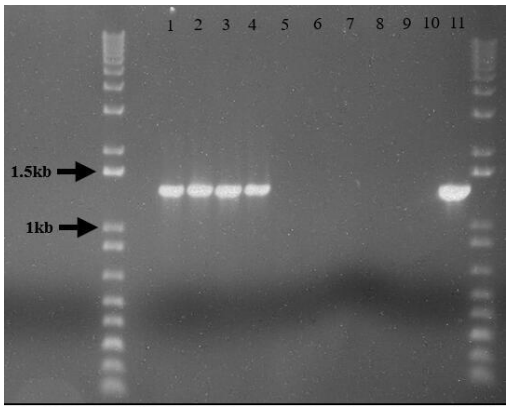

SPAG5F6 + SPAG5R3

1. TE + 0.1% Triton
2. TE + 0.1% Tween 20
3. Tris/glycine + Triton
4. Tris/glycine + Tween 20
5. Tris/HCL + 0.1% Triton
6. Tris/HCL + 0.1% Tween 20
7. Lysis buffer in kit
8. Lysis buffer in kit
9. Hypotonic buffer
10. Hypotonic buffer
11. Positive control

Figure 5.4 Test of self-prepared DNA extraction buffer. The genomic DNA of BT549 WT cells were extracted using the tested lysis buffers and PCR amplified using SPAG5F6-fwd and SPAG5R3-rev primers. A band of 1385 bp in size was expected.

5.3.3.2 Cytotoxicity of Puromycin to Breast Cancer Cells

The cytotoxicity of puromycin to breast cancer cell lines was tested before antibiotic selection. BT549, MCF7, and T47D WT cells were treated with 0.5 μg/mL puromycin for up to 8 days. CM containing puromycin was changed every 4 days. In Figure 5.5, 0.5 μg/mL puromycin (recommended concentration from manufacturer) could effectively induce cell death. In consideration of the cytotoxicity of high concentration puromycin to KO clones, a concentration of 0.4 μg/mL puromycin was adopted to select KO clones for safe. If this concentration were insufficient to kill WT cells in the pooled population, puromycin concentration would be gradually increased to 0.5 μg/mL.

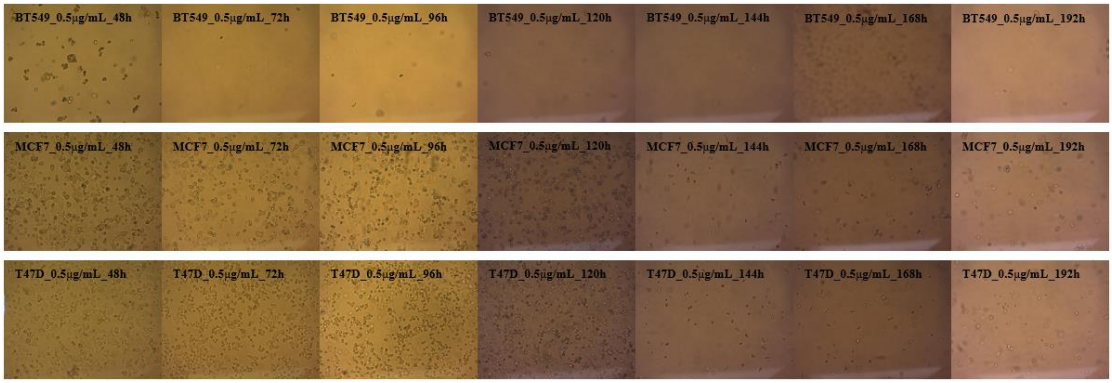

Figure 5.5 Cytotoxicity of puromycin to WT breast cancer cells. BT549, MCF7, and T47D WT cells were treated with 0.5 μg/mL puromycin for up to 8 days. CM containing puromycin was changed every 4 days. The cultures were imaged every 24 hours.

5.3.4 Establishment of *SPAG5* Gene Knockout Clones

5.3.4.1 Preparation of Plasmids Containing gRNA Sequence

After heat shock bacterial transformation (section 2.3.2.1), the plasmid DNA from transformed JM109 competent cells were extracted and purified by using QIAGEN Plasmid Maxi Kit (QIAGEN, Germany). The concentration and quality of two types of plasmids containing different gRNA target sequences are shown in Figure 5.6. Normally, an A260/A280 ratio between 1.8 and 2.0 was considered as DNA samples and an A260/A280 ratio higher than 2 as RNA samples, as well as protein samples with an A260/A280 ratio lower than 2. An A260/A230 ratio between 2.3 and 2.4 was associated with relatively pure dsDNA, and a ratio between 2.1 and 2.3 was RNA. The two plasmids used in this study both showed an A260/A280 ratio at around 1.8 and an A260/A230 ratio at about 2.4. This means that these plasmids were relatively pure dsDNA samples.

A **B**

Figure 5.6 Determination of the quality and concentration of plasmids containing gRNA sequence. An A260/A280 ratio between 1.8 and 2.0 and an A260/A230 ratio higher than 2.3 were considered as relatively pure dsDNA.

To check the accuracy of amplified plasmid DNA, two separate sets of restriction enzyme digestion were employed to cleave the pre-designed cleavage sites in the plasmid. The cleaved bands (1123 bp for EcoR1 and 1574 bp for Not1) were separated and visualized by subsequent agarose gel electrophoresis (section 2.4.3). In Figure 5.7, both plasmids containing gRNA1 and gRNA2 sequence show cleaved bands at 1123 bp after EcoR1 digestion, indicating the correct nucleotide sequence in both plasmids. For Not1 digestion, no bands were observed, probably due to the loss of bioactivity of the enzyme after long-term storage.

The luciferase-puromycin and GFP-neomycin donor plasmids were kindly prepared and tested by one of our colleagues Jiawei Li.

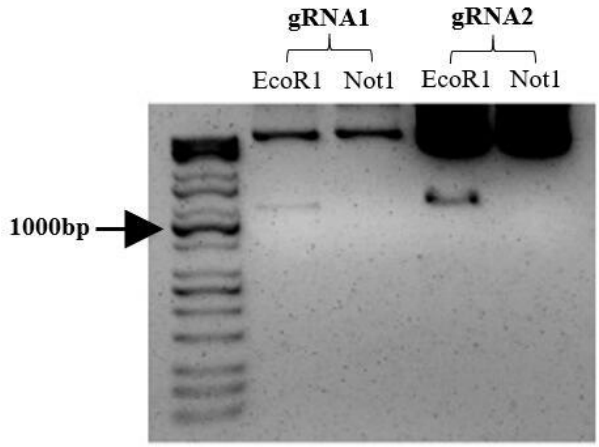

Figure 5.7 Determination of the accuracy of plasmids containing gRNA sequence. The expected length of cleaved bands after EcoR1 and Not1 digestion were 1123 bp and 1574 bp.

5.3.4.2 Screening of *SPAG5* Gene KO Clones

After transfection, the pooled KO population was proceeded to puromycin selection to isolate knockout monoclonal cells. To screen the single-cell colonies, the genomic DNA was extracted and purified using QIAamp DNA Mini Kit (QIAGEN, Germany) and PCR amplified using designated primers. A forward primer Puro5 targeting the sequence of the puromycin-resistant gene in donor plasmid and a reverse primer SPAG5R3 in *SPAG5* gene genomic sequence downstream from gRNA cleavage site were used to select the cell colonies containing donor sequence (Figure 5.8).

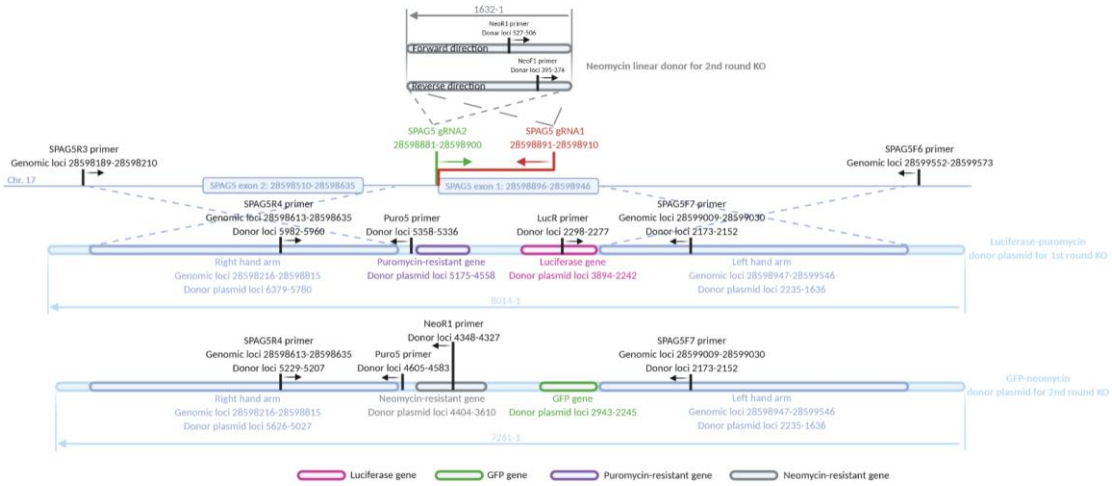

Figure 5.8 SPAG5 forward and reverse primers used in this study. *Created with BioRender.com.*

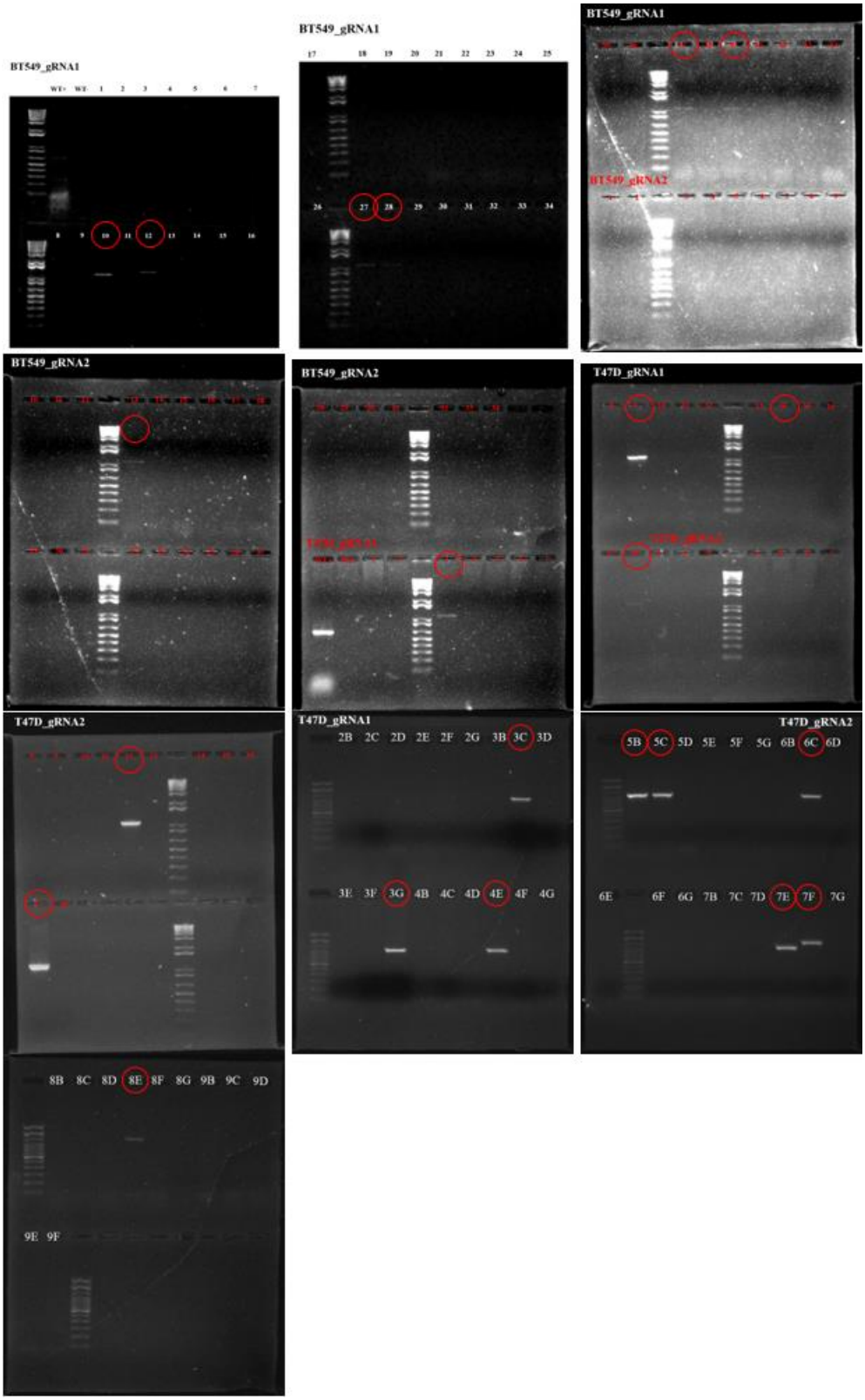

Figure 5.9 Isolation of *SPAG5* gene KO clones. The genomic DNA of single cell colonies were PCR amplified using Puro5-fwd and SPAG5R3-rev primers to examine the on-target integration of donor sequence. A band around 1071 bp was expected in KO clones. The cell colonies with donor sequence were marked by red circle.

BT549 and T47D cell colonies obtained after antibiotic selection (0.4 μg/mL puromycin) were PCR amplified using forward primer Puro5 and reverse primer SPAG5R3. No SKBR3 and MCF7 cell colonies were obtained after antibiotic selection. Future studies are warranted to select these two cell lines using a lower concentration of puromycin. In Figure 5.9, the cell colonies containing the puromycin-resistant gene were marked by red circles. However, the cell colonies may be either homozygous or heterozygous KO cells. Thus, a pair of primers (SPAG5F6-fwd and SPAG5R3-rev) flanking the cleavage site of gRNA were used to hybridize the *SPAG5* genomic sequence to examine the existence of WT allele in the selected single-cell colonies (Figure 5.8). All the selected single-cell colonies were considered as heterozygous KO cells with a WT allele, as shown in Figure 5.10.

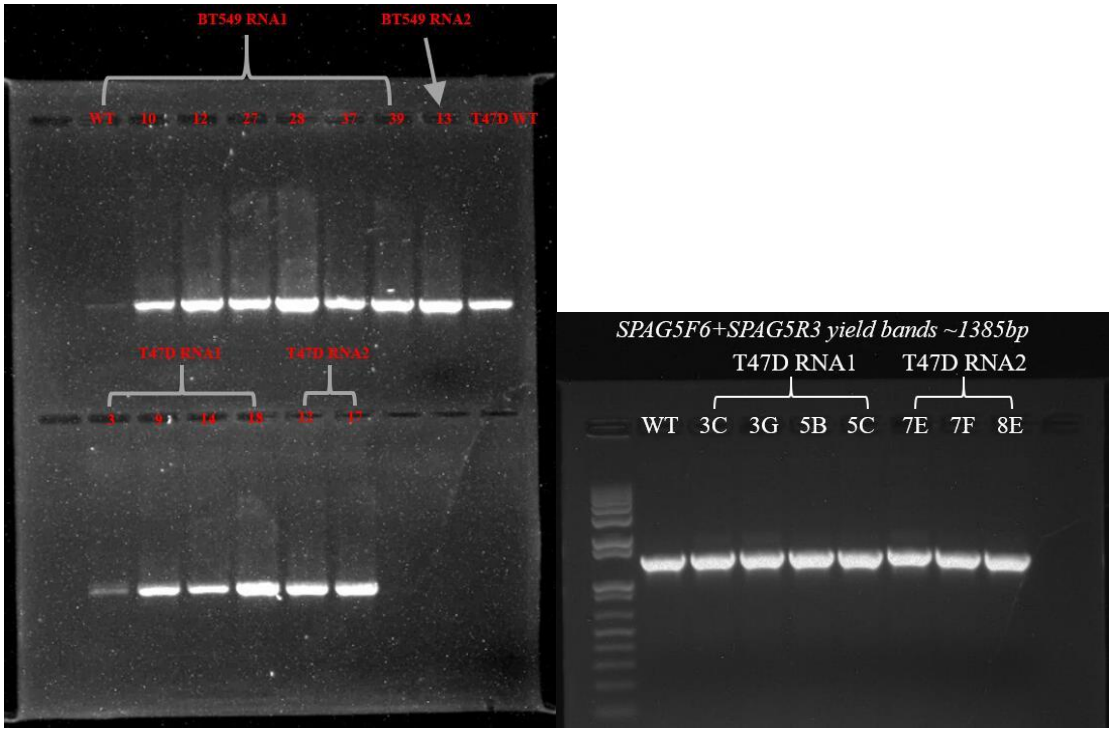

Figure 5.10 Isolation of *SPAG5* gene homozygous KO clones. The genomic DNA of single cell colonies were PCR amplified using SPAG5F6-fwd and SPAG5R3-rev primers to examine the existence of WT allele. A band of around 1385 bp was expected in the presence of WT allele. All the selected cell colonies with donor sequence were heterozygous KO cells.

The existence of luciferase gene sequence in the selected clones was further examined using a forward primer SPAG5F6 in *SPAG5* gene genomic sequence upstream from the gRNA cleavage site and a reverse primer LucR targeting the sequence of the luciferase gene in the donor (Figure 5.8). BT549-gRNA1 single-cell colony 2, 3, 4, 5, 6, BT549-gRNA2 colony 1, T47D-gRNA1 colony 1, 2, and T47D-gRNA2 colony 1 were considered with the integration of luciferase gene as shown in Figure 5.11. The second round of *SPAG5* gene knockout targeting the WT allele was thus done in some of these single cell clones.

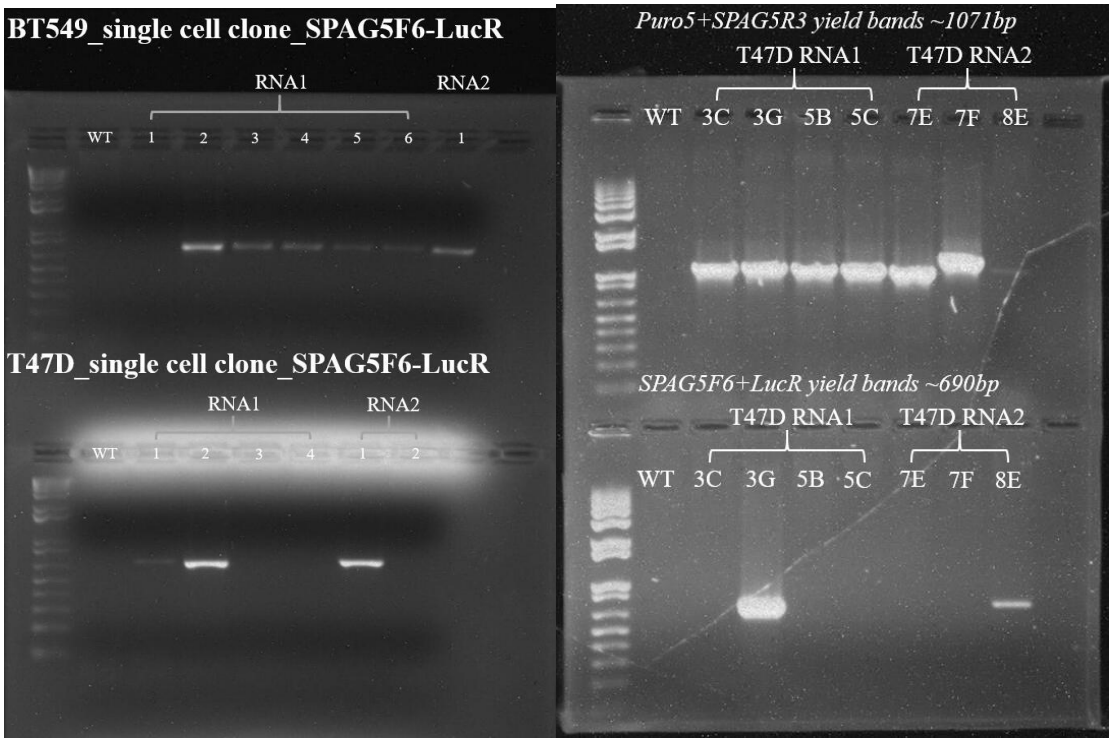

Figure 5.11 Examination of the luciferase gene in selected cell clones. The genomic DNA of single cell colonies were PCR amplified using SPAG5F6-fwd and LucR-rev primers to examine the existence of the luciferase gene. A band of around 690 bp was expected. The colonies were re-numbered based on the original order.

5.3.4.3 PCR Amplicon Sequencing

The allele without donor sequence in the above heterozygous clones might also be cleaved and repaired by NHEJ pathway, which means that one allele was replaced by the donor sequence and the other allele was either intact or indel. However, the latter probably shifted the gRNA target sequence, making those clones unsuitable for the second round of *SPAG5* gene knockout targeting the WT allele. Since the cutting site (3 bp upstream PAM) of gRNA1 was 3 bp downstream from *SPAG5* exon 1, and the cutting site of gRNA2 was just located in *SPAG5* exon 1, the frameshift of the indel allele might affect the transcription of *SPAG5*. However, in order to generate KO clones with biallelic integration of donor sequence, the second round of transfection was done in the heterozygous clones with a WT allele and a donor-integrated allele. The sequence

of the previously selected BT549 and T47D single-cell clones was shown in Figure 5.12 and Figure 5.13, respectively. The primer-flanking sequence of BT549 WT cells was matched with the data from BLAST® (https://blast.ncbi.nlm.nih.gov/Blast.cgi), indicating the homozygosity of non-mutated target sequence in this cell line. The sequencing result of T47D WT cells was not readable, so T47D KO clones were compared with data from BLAST® (https://blast.ncbi.nlm.nih.gov/Blast.cgi) directly.

BT549-gRNA1 clone 2 had an insertion of "T" in the indel allele (3 bp downstream from *SPAG5* exon 1). BT549-gRNA1 clone 4 and BT549-gRNA2 clone 1 were considered as ideal clones with WT allele for the second round of transfection (Figure 5.12). The sequence of other unlisted BT549 clones was unreadable, which might be mixed with other KO cells in antibiotic selection.

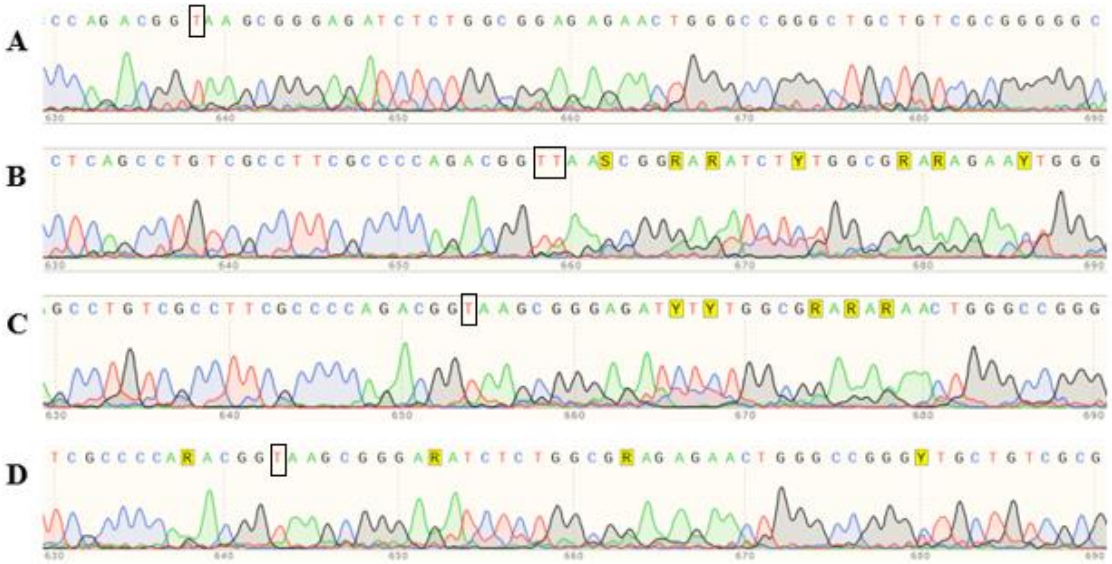

Figure 5.12 Sequencing results of BT549 WT and KO single-cell clones. A. WT; **B.** BT549-gRNA1 clone 2; **C.** BT549-gRNA1 clone 4; **D.** BT549-gRNA2 clone 1.

In terms of T47D clones, T47D-gRNA1 clone 2, 5B and 5C and T47D-gRNA2 clone

7E and 7F had an insertion of “T” in the indel allele (3 bp downstream from *SPAG5* exon 1). T47D-gRNA1 clone 3C and 3G and T47D-gRNA2 clone 6C and 8E contained unknown indel. The sequence of other unlisted T47D clones was unreadable, which might be mixed with other KO cells in antibiotic selection. Thus, all of the T47D KO clones were not suitable for the second round of transfection.

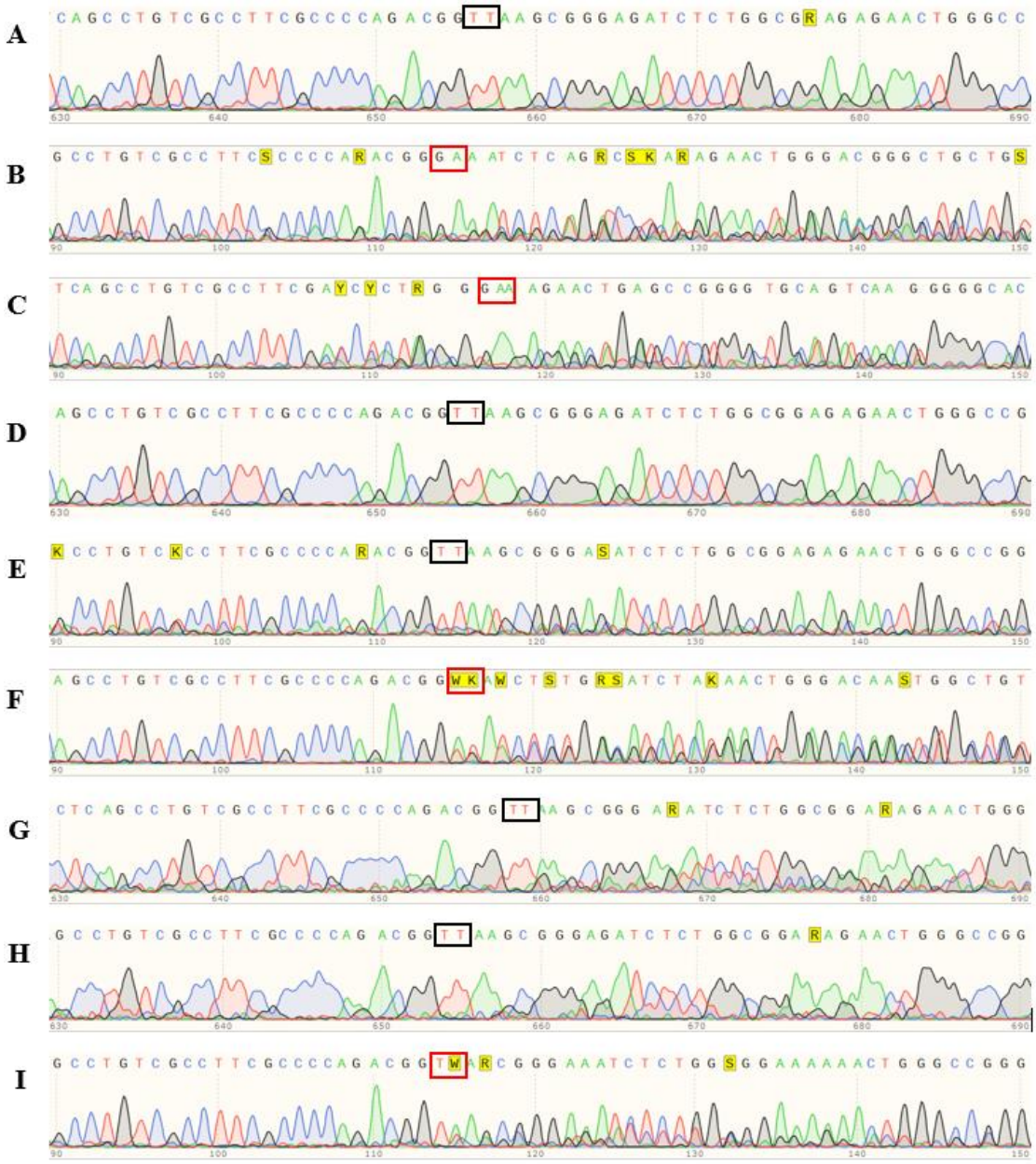

Figure 5.13 Sequencing results of T47D KO single-cell clones. A. T47D-gRNA1 clone 2; **B.** T47D-gRNA1 clone 3C; **C.** T47D-gRNA1 clone 3G; **D.** T47D-gRNA1 clone 5B; **E.** T47D-gRNA1 clone 5C; **F.** T47D-gRNA2 clone 6C; **G.** T47D-gRNA2 clone 7E; **H.** T47D-gRNA2 clone 7F; **I.** T47D-gRNA2 clone 8E.

5.3.4.4 Knockout of Wild-Type Allele in Heterozygous KO Clones

To knock out the WT allele in heterozygous BT549 KO clones, a linear Neomycin-resistant gene (1632 bp) as donor sequence was introduced in this study. The transfected cells were thus selected using 400 μg/mL neomycin. To screen single cell colonies, the

genomic DNA of single cell clones was extracted using self-prepared extraction buffer and PCR amplified using designated primers (section 2.5). A forward primer SPAG5F7 and a reverse primer SPAG5R4 in *SPAG5* gene genomic sequence surrounding the gRNA cleavage site were used to select the cell colonies containing donor sequence (Figure 5.8). Theoretically, a PCR product of around 418 bp and 2050 bp were expected after 2nd round of KO in non-edited and edited cells, respectively.

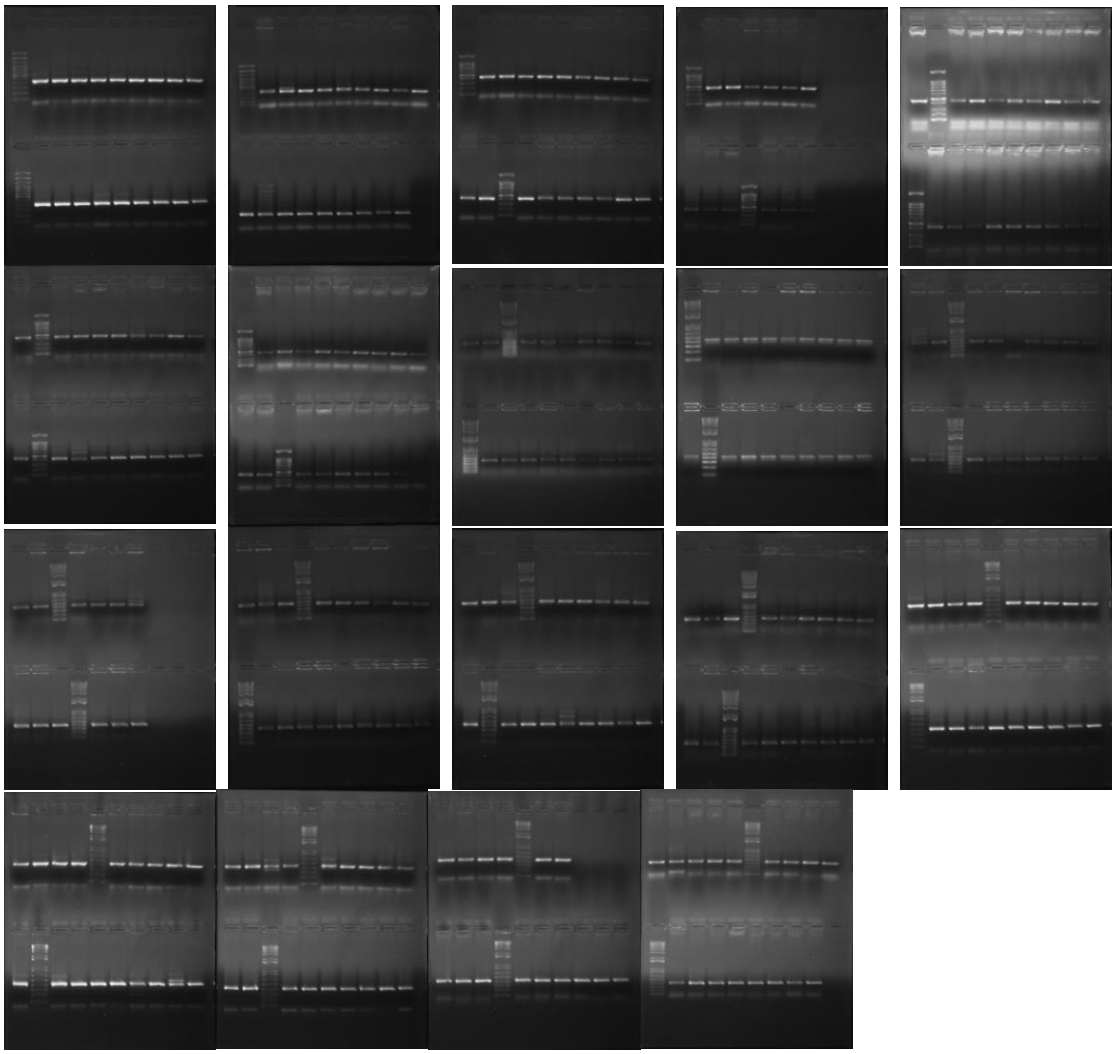

Figure 5.14 Isolation of *SPAG5* gene homozygous KO clones. The genomic DNA of single cell colonies were PCR amplified using SPAG5F7-fwd and SPAG5R4-rev primers to examine the existence of donor sequence. A band of around 418 bp for WT allele and 2050 bp for edited allele were expected after the 2nd round of KO.

In Figure 5.14, all of the clones after 2nd round transfection with linear Neomycin-resistant gene (1632 bp) as donor sequence showed bands around 418 bp, representing the existence of WT allele. A possible reason was all of the clones were pooled population rather than single-cell clones. This might be caused by the high off-target rate of linear Neomycin-resistant DNA that could be randomly integrated into the genomic sequence and facilitate the generation of Neomycin-resistance in cancer cells. The large majority of cells were survived after Neomycin selection and getting clustered when colonies were picked up. Apart from the 418 bp band representing the WT allele, the 2050 bp bands relating to the successful integration of the linear Neomycin-resistant gene were not observed in all clones. To further investigate the integration of the Neomycin-resistant gene, a three-primer PCR strategy (Pekhletski & Hampson, 1996) was used to examine the existence of the forward or reverse inserted Neomycin sequence by using primers including SPAG5F7-fwd, NeoR1-rev and NeoF1-rev (Figure 5.8). Thus, about 660 bp and 528 bp bands were obtained if the linear Neomycin-resistant sequence was integrated with a forward and reverse direction, respectively.

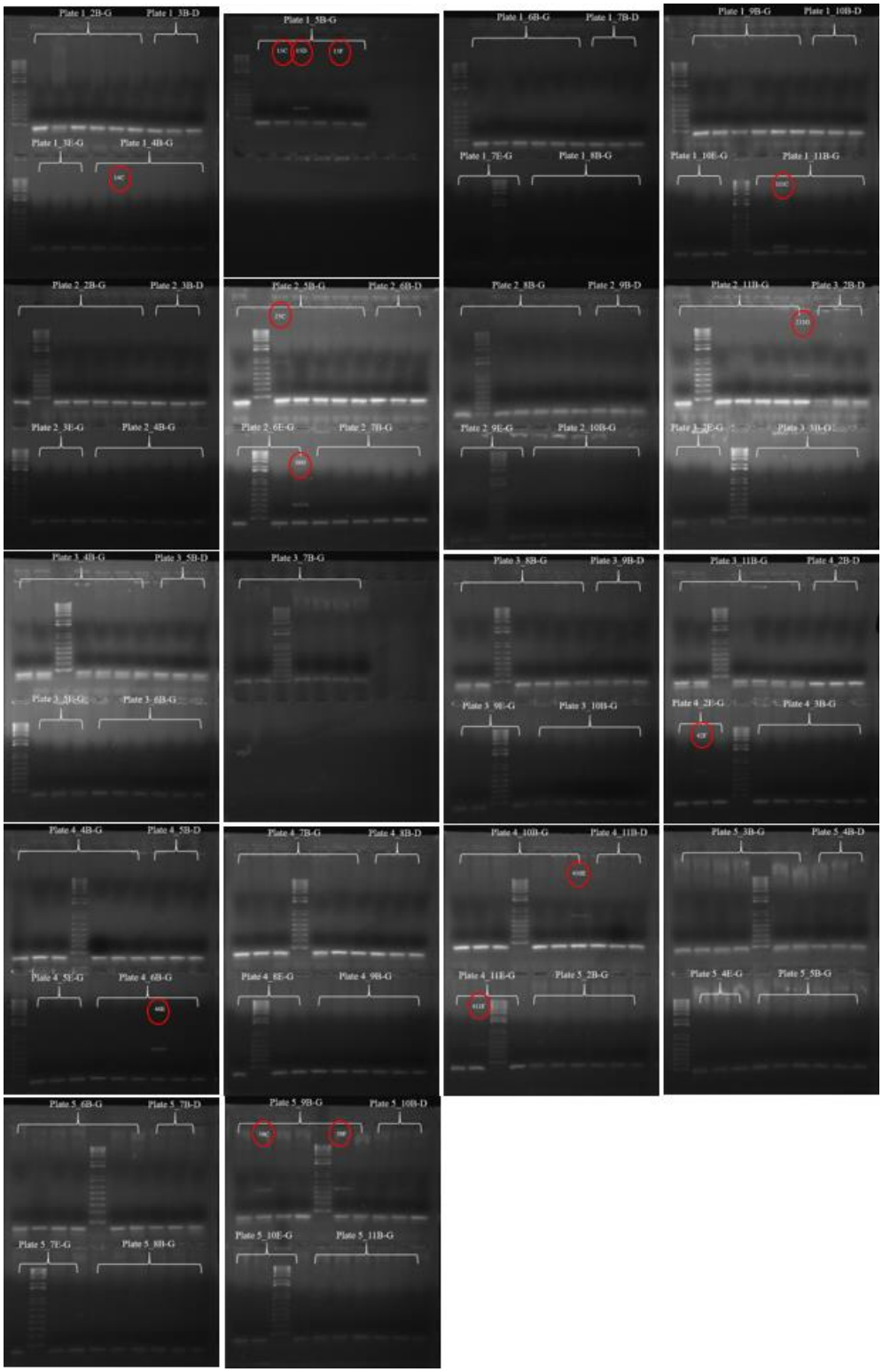

Figure 5.15 Isolation of *SPAG5* gene homozygous KO clones. The genomic DNA of single cell colonies were PCR amplified using SPAG5F7-fwd, NeoF1-rev and NeoR1-rev to examine the existence of donor sequence. A band of around 660 bp or 528 bp for the linear Neomycin-resistant gene in a forward or reverse direction was expected after 2nd round of KO**,** respectively. The cell colonies with donor sequence were marked by red circle.

In Figure 5.15, the linear Neomycin-resistant gene was integrated into some clones. However, due to the heterogeneity of the clones as mentioned above, the 2nd round KO was repeated using traditional plasmid donor with Neomycin-resistant gene and homologous arms to minimize off-target effects.

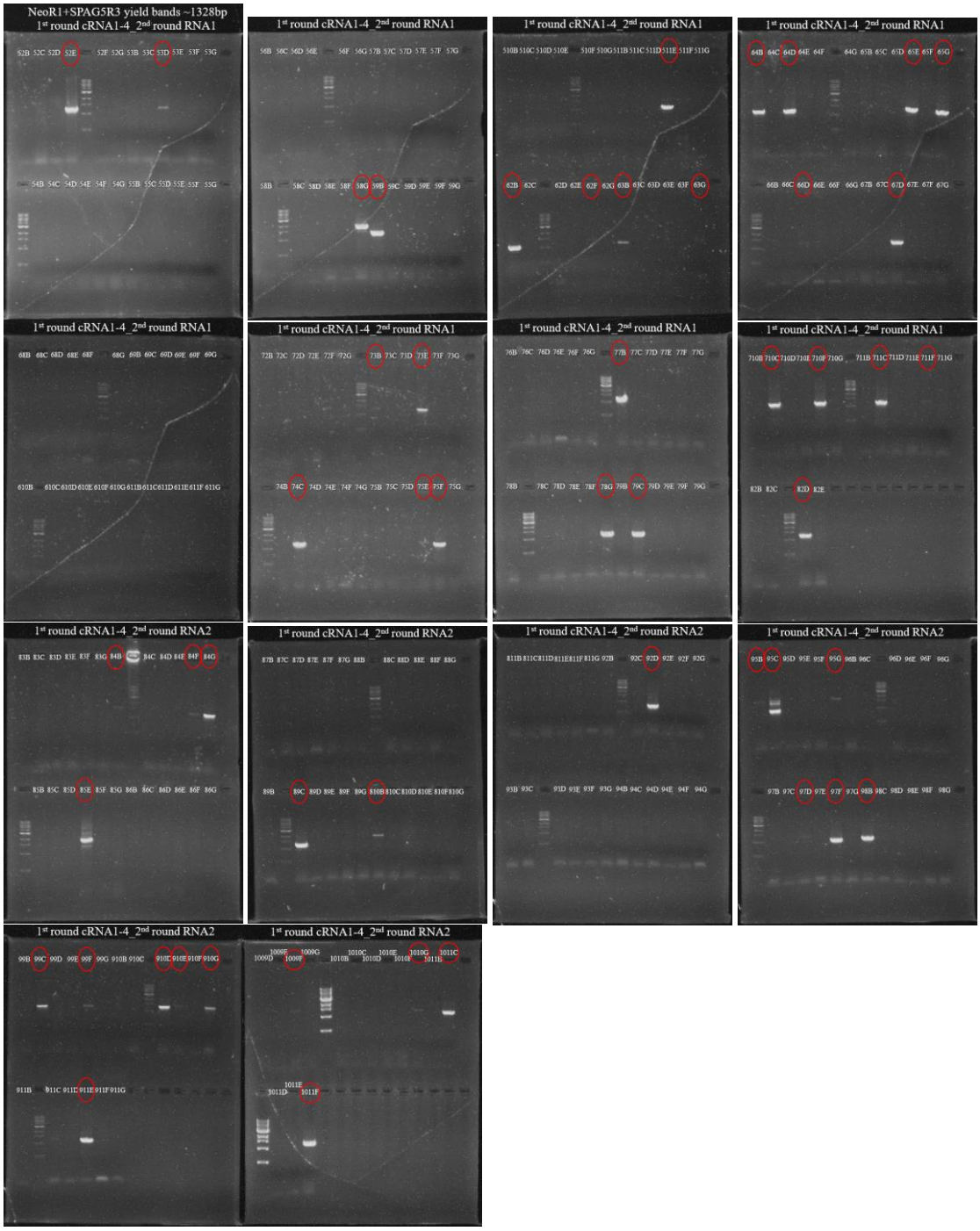

Figure 5.16 Isolation of *SPAG5* gene homozygous KO clones (BT549-gRNA1 clone 4). The genomic DNA of single cell colonies were PCR amplified using NeoR1-fwd and SPAG5R3-rev to examine the existence of donor sequence. A band of around 1328 bp was expected after 2nd round of KO. The cell colonies with donor sequence were marked by red circle.

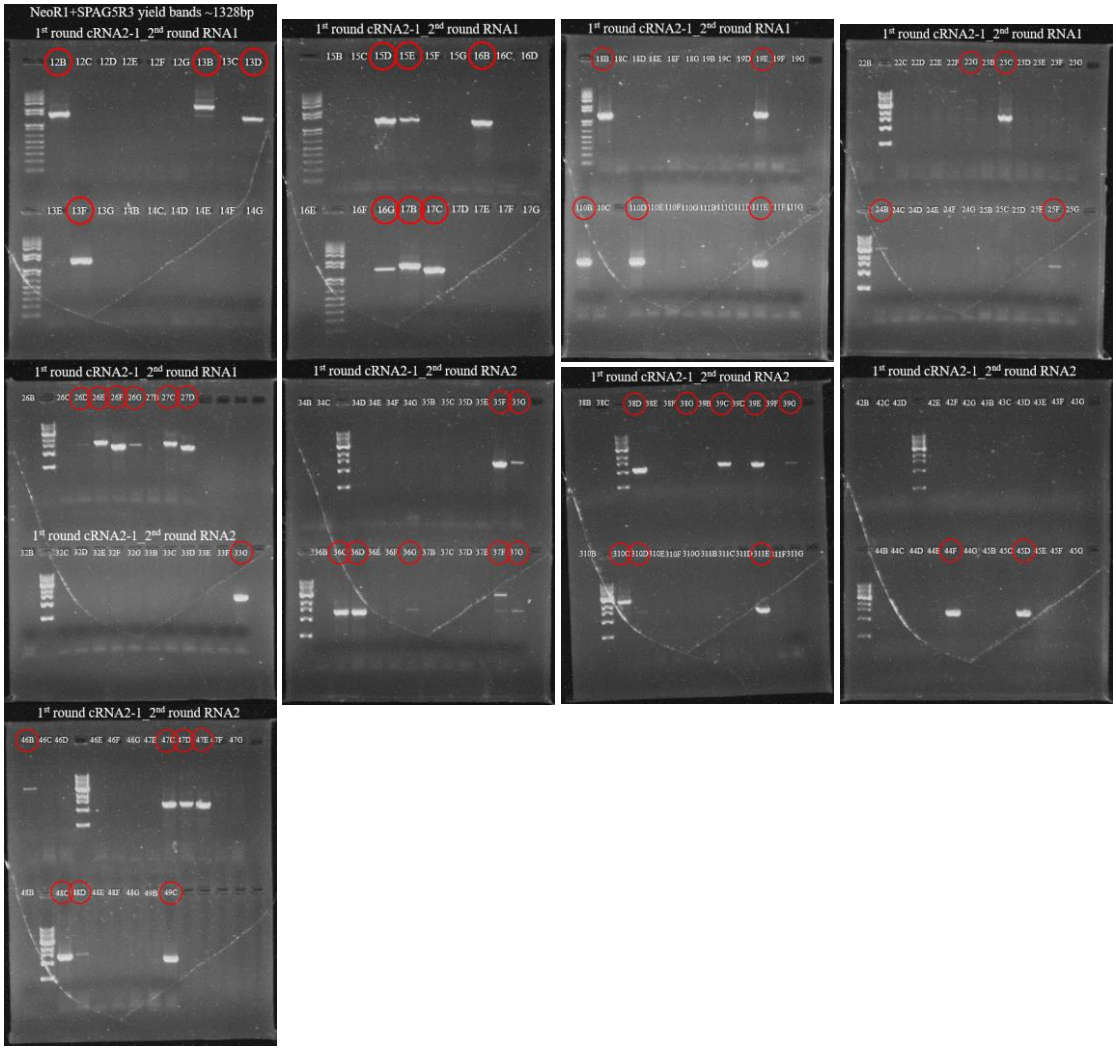

Figure 5.17 Isolation of *SPAG5* gene homozygous KO clones (BT549-gRNA2 clone 1). The genomic DNA of single cell colonies were PCR amplified using NeoR1-fwd and SPAG5R3-rev to examine the existence of donor sequence. A band of around 1328 bp was expected after 2nd round of KO. The cell colonies with donor sequence were marked by red circle.

BT549-gRNA1 clone 4 and BT549-gRNA2 clone 1 were transfected with gRNA1 or gRNA2 accompanied by GFP-neomycin donor plasmid to knock out the WT allele (Figure 5.8). The single-cell clones from 2nd round of KO were screened using NeoR1-fwd and SPAG5R3-rev primers (Figure 5.8). In Figure 5.16 and Figure 5.17, BT549-gRNA1 clone 4 and BT549-gRNA2 clone 1 underwent 2nd round of transfection, respectively, followed by neomycin selection (400 μg/mL). The cell colonies containing the neomycin-resistant gene were marked by red circle. Unfortunately, some of the

clones were dead after subculture. This might be caused by the plasmid donor used in this study; since the antibiotic-resistant gene in the donor plasmid contained PGK promoter, the plasmid donor DNA that was not genomically integrated also provided antibiotics resistance. The approximate lifespan of the plasmid donor was 2-3 weeks in cells. Thus, in the false-positive clones, the random floating plasmid donor in the cytoplasm might provide antibiotics resistance in its lifespan. Also, in some clones with the integration of antibiotics resistant genes, rearrangements might occur at the target site simultaneously, which led to the loss of antibiotics resistance. These clones were eventually dead after the episomal plasmid donor was diluted out. The various sizes of antibiotics resistant genes in Figure 5.16 and Figure 5.17 might be a piece of evidence to prove this hypothesis.

To check the homozygosity of the viable positive clones, the genomic DNA of cells was extracted using QIAamp DNA Mini Kit (QIAGEN, Germany) (section 2.5) and PCR amplified using SPAG5F7-fwd and SPAG5R4-rev primers. Unfortunately, all of the tested clones contained WT allele, indicating the heterozygosity of these clones (Figure 5.18). Similar to *ABCC5* KO clones (Chapter 3), the CNV of *SPAG5* gene might also happen in breast cancer cell lines. Thus, CNV made it virtually impossible to knock out these genes entirely.

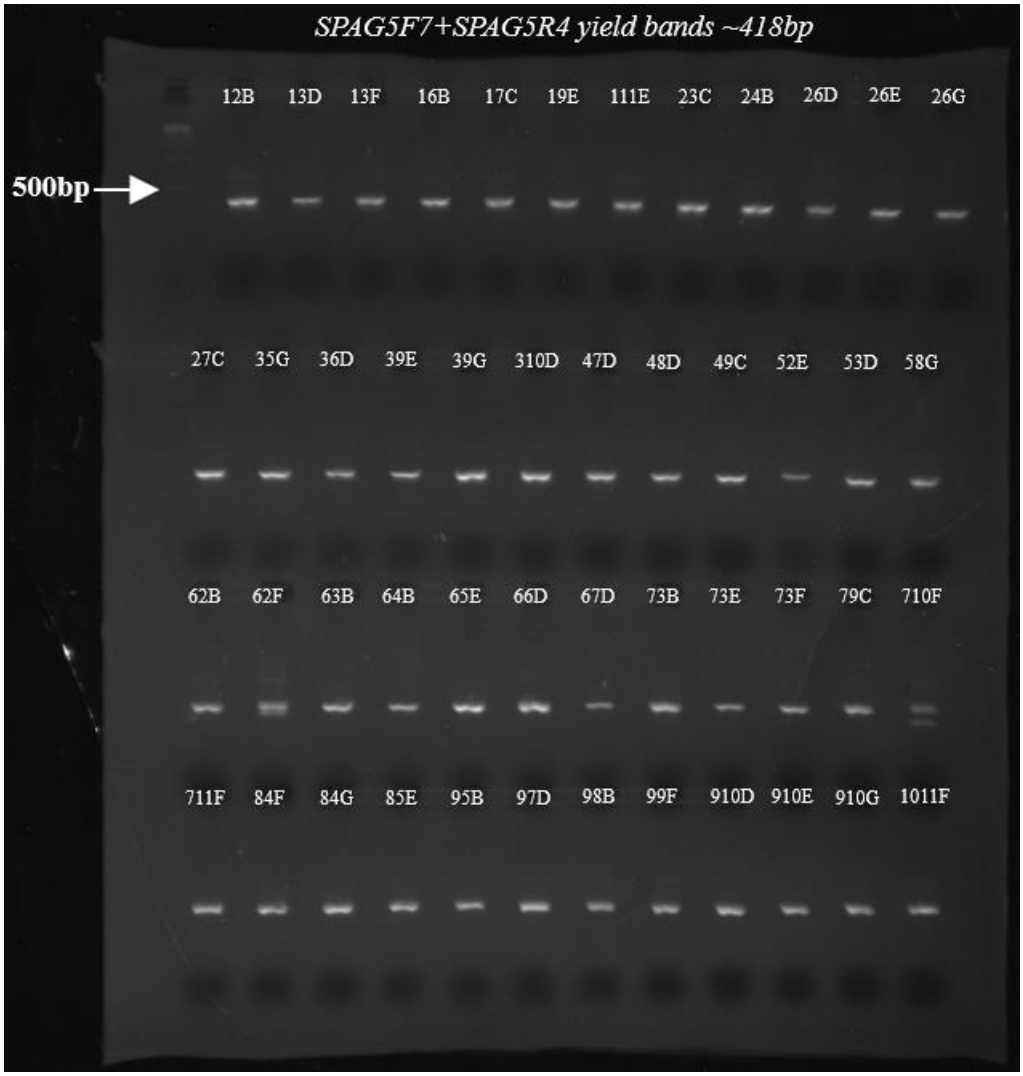

Figure 5.18 Isolation of *SPAG5* gene homozygous KO clones. The genomic DNA of single cell colonies were PCR amplified using SPAG5F7-fwd and SPAG5R4-rev to examine the existence of WT allele. A band of around 418 bp represents the existence of WT allele.

5.3.4.5 Examination of SPAG5 Expression in Knockout Clones

Since no clones with biallelic integration of donor sequence were obtained in the 2nd round of KO, the 1st round KO clones with a donor allele and an indel allele were tested for SPAG5 expression. The indel allele probably shifted the gRNA target sequence. The frameshift might affect the transcription of *SPAG5*. Western blotting was adopted to examine SPAG5 expression in these clones. SPAG5 protein was blotted with SPAG5

Mouse Monoclonal Antibody and Anti-Mouse IgG (whole molecule) – Peroxidase antibody produced in rabbit. The SPAG5 blots were validated with total protein stain and beta-actin blots. Theoretically, the band at 150 kDa in size was not detectable in KO clones, while the 30 kDa band was fainter in KO clones.

In Figure 5.19, T47D KO clone 1-2, 1-5B, 1-5C, 2-6C, 2-7E and 2-7F, and BT549 clone 1-2 showed no SPAG5 expression. The 30 kDa bands of KO clones were not fainter than WT cells. This might be a result of the different post-transcriptional modifications in breast cancer cell lines used in this study compared with the HEK293T cells in the manufacturer's instruction. To confirm these findings, proteins were re-extracted and re-blotted, as shown in Figure 5.20. Except for T47D clone 2-6C, all the KO clones without SPAG5 expression had an indel allele with a "T" insertion no matter which gRNA was used. Although this "T" insertion was located at 3 bp downstream from *SPAG5* exon 1, the SPAG5 expression was interrupted in these clones.

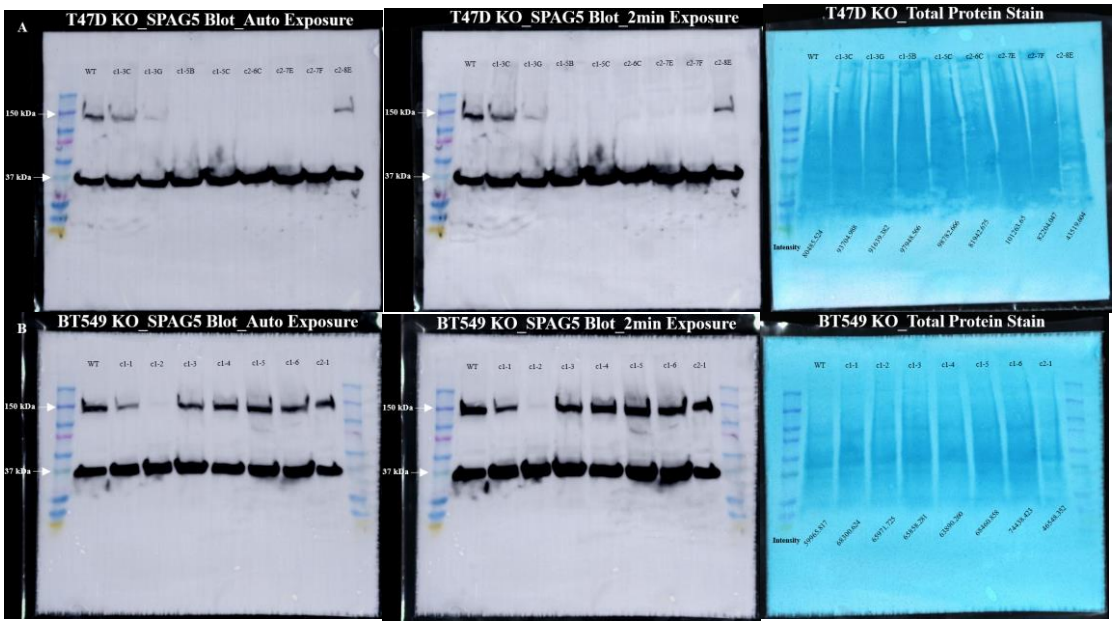

Figure 5.19 Immunoblot of SPAG5 protein from BT549 and T47D KO cells. The membrane was immunoblotted using SPAG5 Mouse Monoclonal Antibody and Anti-Mouse IgG (whole molecule) – Peroxidase antibody produced in rabbit. SPAG5 blots were validated with total protein stain. **A.** T47D KO clones. **B.** BT549 KO clones.

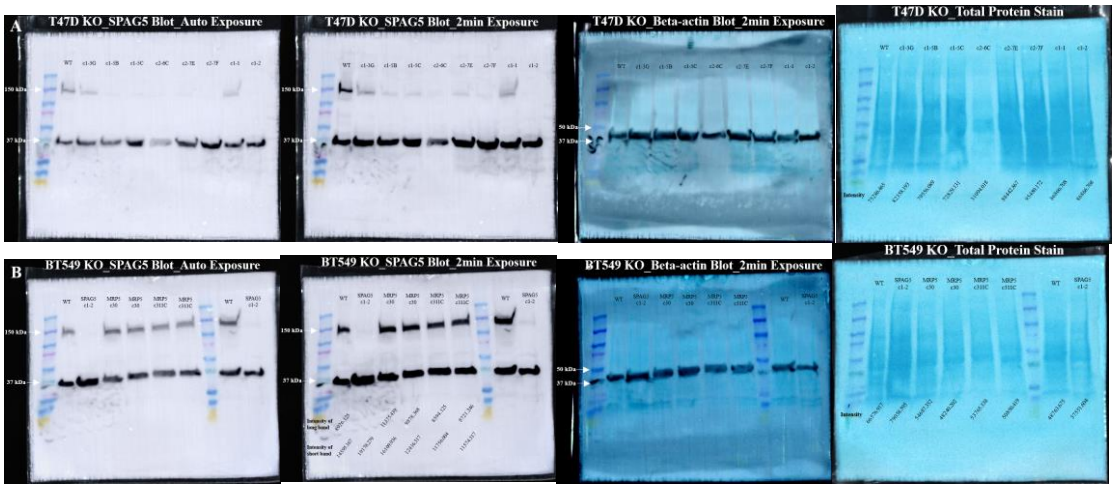

Figure 5.20 Immunoblot of SPAG5 protein from BT549 and T47D KO cells. The membrane was immunoblotted using SPAG5 Mouse Monoclonal Antibody and Anti-Mouse IgG (whole molecule) – Peroxidase antibody produced in rabbit. SPAG5 blots were validated with total protein stain and beta-actin blots. **A.** T47D KO clones. **B.** BT549 KO clones.

5.3.5 The Role of SPAG5 in ABCC5 Functional Expression in Breast Cancer Cells

Because of COVID-19 pandemic and lockdown restrictions, this study failed to evaluate the role of SPAG5 in olaparib sensitivity in TNBC cells and the ABCC5 functional expression in homozygous *SPAG5* KO clones. The SPAG5 expression in heterozygous *ABCC5* KO clones was examined using Western blotting (section 2.9).

Figure 5.21 shows the immunoblots of SPAG5 in BT549 heterozygous *ABCC5* KO clone 30 (from 1st round KO) and 311C (from 2nd round KO). The signal intensity was measured using ImageJ software. The SPAG5 expression in BT549 heterozygous *ABCC5* KO clones remained at the same level as WT cells, indicating that this membrane protein is not involved in SPAG5 expression. However, SPAG5 can regulate gene transcription and protein expression through multiple pathways, as we previously reviewed (He et al., 2020). Future studies are warranted to explore the functional expression of ABCC5 in homozygous *SPAG5* KO TNBC cells.

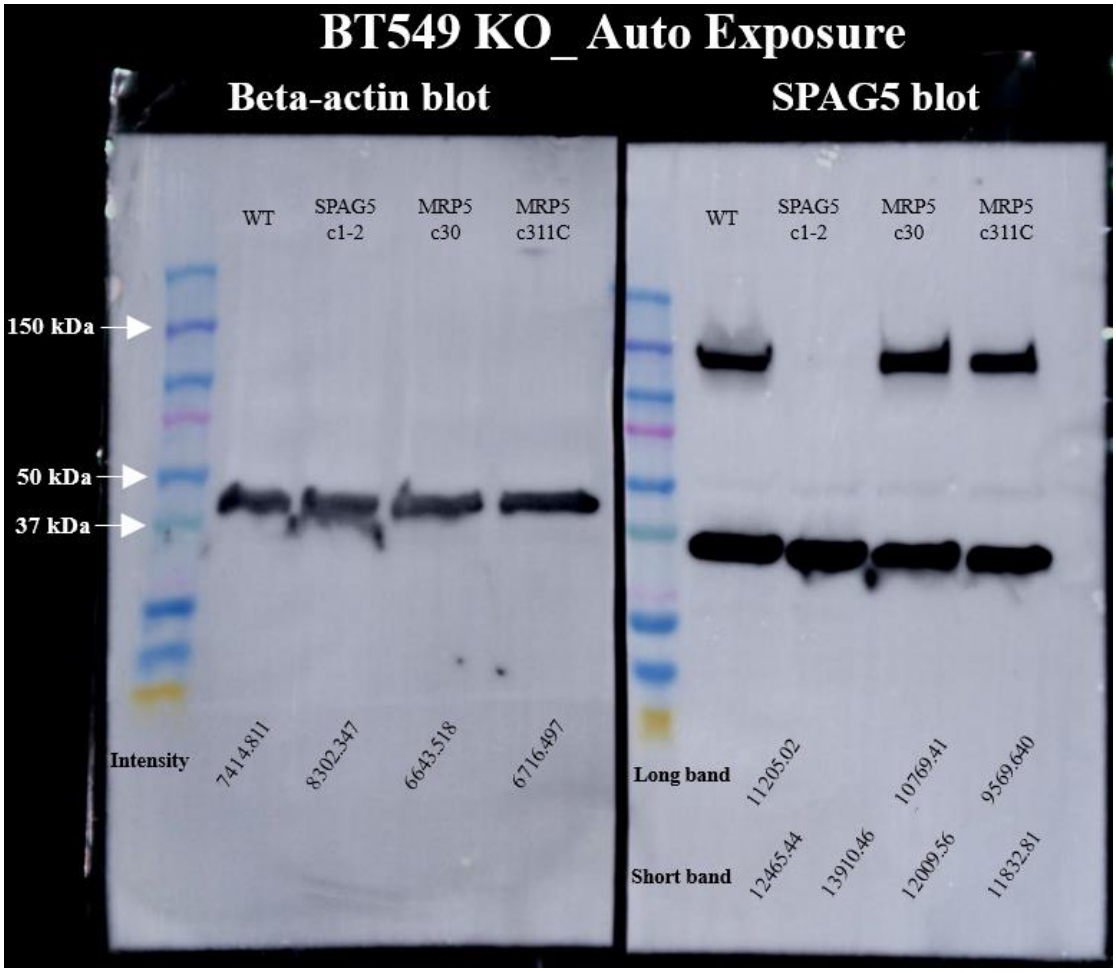

Figure 5.21 SPAG5 expression in BT549 heterozygous *ABCC5* KO clones. The membrane was immunoblotted using SPAG5 Mouse Monoclonal Antibody and Anti-Mouse IgG (whole molecule) – Peroxidase antibody produced in rabbit. SPAG5 blots were validated with beta-actin blots. The intensity was measured using ImageJ software.

5.4 Discussion

The aim of the studies presented in this chapter was to establish homozygous *SPAG5* breast cancer cell lines and examine the role of this protein in functional expression of ABCC5.

SPAG5 KO was accomplished by transfecting different lines with plasmids encoding gRNA and Cas9 protein and donor plasmids. The KO clones were screened and validated at both gene and protein levels.

Before commencing these studies, the expression of SPAG5 was determined in the three cell lines used in *SPAG5* gene KO studies. All the four tested cell lines (i.e., MDA-MB-231, BT549, MCF7 and T47D) were found to express SPAG5 protein. The cytotoxicity of puromycin to BT549, MCF7, and T47D breast cancer cell lines was tested before antibiotic selection. Although the manufacturer's recommended concentration of puromycin at 0.5 μg/mL was working well on these cell lines, a puromycin concentration of 0.4 μg/mL was adopted in this study to secure the survival of KO cells.

To establish *SPAG5* gene knockout cell lines, a CRISPR-Cas9-based gene editing method was applied in a TNBC cell line (i.e., BT549) and three non-TNBC cell lines (i.e., T47D, MCF7 and SKBR3) in this study. The specific plasmids containing the sequence encoding the pre-designed gRNA and Cas9 protein and luciferase-puromycin donor plasmids were delivered into cells through endocytosis. The target site was cleaved by Cas9 protein. The DSBs were repaired by homology-directed repair (HDR) with the integration of donor sequence. After transfection, the pooled KO population was immediately proceeded to puromycin selection. The single-cell colonies were picked up with the aid of a pipettor and microscope. Unfortunately, all the survived BT549 and T47D KO clones were considered as heterozygous at a gene level with a donor-integrated allele and a WT or indel allele. No clones with biallelic integration of donor sequence were screened out in present study. No SKBR3 and MCF7 cell colonies were obtained after antibiotic selection. Future studies may apply a lower concentration of puromycin to these two cell lines. Inevitably, the allele without donor sequence integrated in heterozygous clones might also be cleaved and repaired by NHEJ pathway, which means that one allele was replaced by the donor sequence and the other allele was either intact or indel. The latter probably shifted the gRNA target sequence. This frameshift might affect the transcription of the *SPAG5* gene because the cutting site (3

bp upstream PAM) of gRNA1 was located at 3 bp downstream from *SPAG5* exon 1, and the cutting site of gRNA2 was just situated in *SPAG5* exon 1. In most cases, rather than damage to intronic regulatory elements, loss of the exon was likely to cause eliminated expression of target protein (Kosicki et al., 2018). Interestingly, no matter gRNA1 or gRNA2 was used, a "T" insertion seemed to be a prevalent genotype after NHEJ repair route. As discussed in section 3.4, different edited alleles are supposed to contain different indels because the random base-pair insertion and/or deletion are regarded as a hallmark of NHEJ. The identical "T" insertion in different clones after NHEJ repair route is thus of interest to be investigated. Although this phenomenon might be as simple as a misreading during Sanger Sequencing Service, the potential crosstalk between DNA repair pathways and gene rearrangements, as discussed in section 3.4, might play a role in this process.

Another phenomenon that remained to be investigated was that no clones with biallelic integration of donor sequence were screened out in present study. Undoubtedly, this phenomenon might be partially caused by some common operational errors, such as degradation of plasmids after successive rounds of freeze-thaw cycle and unexpected DNase contamination in transfection complex during manipulation, which resulted in decreased intracellular accumulation of plasmids and thus decreased potency of gRNA and Cas9. However, some other more complicated reasons might play a major role in this phenomenon. The mechanisms of different repair pathways might be such a player. In mammalian cells, DSBs are primarily repaired through competing non-homologous end joining (NHEJ) pathways instead of through homology-directed repair (HDR) (Janssen et al., 2019). HDR is commonly restricted to the G2-S phases of the cell cycle, when sister chromatid sequence become available (Janssen et al., 2019). In contrast, although NHEJ activity peaks in G2/M, it takes place throughout the various stages of

the cell cycle (Z. Mao, Bozzella, Seluanov, & Gorbunova, 2008). The DSBs could thus be repaired by the error-prone NHEJ route even in the presence of episomal donor templates, and in most cases, HDR takes place much less frequently than NHEJ (Janssen et al., 2019). Thus, it is crucial to understand the parameters governing these two DNA repair pathways. Apparently, cell type and cell differentiation stages can influence the relative frequencies of gene-editing endpoints due to different cellular contexts. But these parameters seemed not to be the dominant factors, because the organismal development and cellular differentiation were given in the breast cancer cell lines used in this study.

The chromosomal topologies were found to affect the balance between HDR and NHEJ, as previously reviewed in section 3.4. It was reported that the frequencies of long double-stranded donors-based HDR were higher at heterochromatin compared with euchromatin (Janssen et al., 2019). In contrast, NHEJ frequencies were higher in euchromatin (Janssen et al., 2019). In addition to this chromatin state-induced pathway choice, DSB end resection-related cellular components appear to be another regulator. Specifically, HDR requires extensive DSB end resection, whereas NHEJ requires little or no resection (Heyer, 2015). Mammalian CtIP is such a cell-cycle-dependent kinase in the end resection machinery, which cooperates with MRE11/RAD50/NBS1 complex to provide the initial resection of DSBs (Heyer, 2015). Other regulating factors include extensive chromatin remodelling, histone modifications, Fanconi pathway, the Ku70-80 heterodimer, the checkpoint adaptor 53BP1, Nej1, and RIF1 (Heyer, 2015). Nevertheless, the lifetime of DSBs is poorly understood and may influence the choice of DNA repair pathways. The blocking lesions can be tolerated, and the gap repaired postreplicationally by specialised DNA polymerases performing translesion DNA synthesis (Heyer, 2015). In addition, different types of donor DNA structures, such as

integrase-defective lentiviral vector genomes, conventional recombinant plasmids, and chemically synthesized single-stranded oligodeoxyribonucleotides (ODNs) with both polarities (i.e., sense and antisense), also impose impact on HDR frequencies (Janssen et al., 2019).

However, NHEJ is always present and serves as a major repair route in cells despite various HDR frequencies underlying different chromosome states (Janssen et al., 2019). Indeed, chromatin remodelling agents (e.g., programmable trans-activators, histone deacetylase inhibitors, and DNA methyltransferase inhibitors) that can influence relative proportions of gene-editing endpoints might not benefit the HDR ratio. This is because chromatin remodelling also affects target sequence accessibility, as previously reviewed in section 3.4. NHEJ activity can be increased with HDR due to enhanced physical and temporal exposure of target alleles to Cas9 protein, especially during the cell phases in which HDR is not operative (Janssen et al., 2019). Therefore, to generate homozygous KO with biallelic integration of donor template, future studies may introduce chemical or genetic inhibition of NHEJ and activation of HDR to enhance HDR signalling during transfection (Devkota, 2018). Also, manipulation of cell cycle and stimulation of DSB end resection by mediating the related protein activity may collectively improve the outcomes. Furthermore, covalent linkage of the donor DNA template to Cas9 complex was found to increase HDR efficiency for up to 24-fold through an increase of donor template concentration in the nucleus (Savic et al., 2018). Alternatively, the plasmid donor template could be replaced with single-stranded oligodeoxyribonucleotides (ODNs) donor template. Unlike the above mentioned elevated plasmid-based HDR frequencies at heterochromatin, ODNs showed a higher frequency of HDR at euchromatin (Janssen et al., 2019). Notably, the broken chromosome was extruded from the heterochromatic subcompartment (Heyer, 2015).

This phenomenon may make ODNs a better template than the heterochromatin-dependent conventional recombinant plasmid. However, a question with regard to increasing HDR efficiency is that to what extent DSBs are repaired through exogenous donor templates instead of through sister chromatid or homologous chromosomes. As aforementioned in section 3.4, HDR could re-ligate DNA lesions with high fidelity using either sister chromatid or homologous chromosome as a template. How exogenous donor template competes with sister chromatid or homologous chromosome during HDR and whether there is a threshold remained to be investigated. Also, it is unknown that whether the allele repaired by HDR is randomly selected or selected based on some rules in KO cells with a donor allele and an indel allele.

Furthermore, the common germline mutations of HDR-related genes, such as *BRCA1/2*, in certain breast cancer cells may influence the integration of donor templates. As we previously reviewed, BRCA1/2 can control HDR repair route by regulating RAD51 (He et al., 2020). In the presence of wild-type BRCA1/2, cells could faithfully repair DSB damages by HDR. However, mutations in *BRCA1/2* gene may lead to loss of HDR activity and promote genomic instability. *BRCA1/2* mutations were quite common among breast cancer patients. A total of 19.5% of TNBC patients have been shown to carry *BRCA1/2* mutations (Jhan & Andrechek, 2017). Thus, the mutation status of *BRCA1/2* in the breast cancer cell strains used in present study needs to be further examined.

Since no homozygous KO clones with biallelic integration of donor template were isolated in 1st round of KO, the 2nd round of KO was conducted using the same gRNAs and neomycin-GFP plasmid donor in the heterozygous clones (i.e., BT549 gRNA1 clone 4 and BT549 gRNA2 clone 1) with a WT allele and a donor allele. Theoretically, the WT allele was replaced with neomycin-GFP sequence after 2nd round of KO.

Unfortunately, all the KO clones after 2nd round of transfection were tested as heterozygous again at a gene level. WT allele was still detectable in these clones. No matter in 1st or 2nd round of KO, only around one-tenth of the survived clones after antibiotic selection were validated with on-target editing. In other words, 90% of the survived clones were false-positive without editing in the target *SPAG5* gene. This might be caused by the random integration of donor plasmids into the genome, which provided antibiotics resistance to these clones. Nevertheless, it was found that when introducing conventional recombinant plasmids into cells, the loading of intracellularly synthesised sgRNA into Cas9 protein could be affected by other non-specific RNAs (Mekler, Minakhin, Semenova, Kuznedelov, & Severinov, 2016). Particularly, non-specific RNAs imposed greater inhibitory effects on the formation of Cas9 complexes with sgRNAs bearing shortened 3'-terminal segments (Mekler et al., 2016). Thus, whether or not the formation of noise RNA-Cas9 complexes could induce off-target effects in the KO cells in present study remained to be examined.

KO clones' heterozygosity even after the 2nd round of transfection might be derived from *SPAG5* copy number variation (CNV), chromosomal mosaicism, and the potential crosstalk between Cas9-induced DSBs, gene repair routes, and gene rearrangements as discussed in section 3.4. CNV and chromosomal mosaicism could make Cas9 insufficient to cleave all the copies of *SPAG5* gene. The potential crosstalk might induce the formation of *SPAG5* gene copies after KO and high-fidelity HDR repair according to the wild-type sister chromatid or homologous chromosome. However, in the 1st round of KO, some clones were validated with a donor allele and an indel allele with a "T" insertion. If the copy number of *SPAG5* gene were aberrant, after NHEJ repair, there would be different indels in different *SPAG5* copies in these clones. This might induce the sequencing date unreadable. Thus, the copy number of *SPAG5* gene in WT cell lines

used in this study might be standard (diploid), and CNV of *SPAG5* gene probably occurred after KO. The unreadable sequencing data of the indel allele of some clones (from 1st round of KO) might just indicate the occurrence of extra copies of *SPAG5* gene. The indel allele/alleles and the WT *SPAG5* gene copies generated after transfection collectively made the sequencing data unreadable. Similarly, in the clones with a donor allele and a WT allele used for the 2nd round of KO, the *SPAG5* gene copy number might be altered in both the 1st and 2nd round of transfection, which made WT allele detectable even after the 2nd round of KO. But these speculations remained to be examined. Thus, multiple rounds of transfection might not be an ideal method to generate KO cell lines. A sgRNA targeting exon loci of *SPAG5* gene might be a better choice. In this case, although only one allele is probably replaced with the donor, the indel-induced exon frameshift in the other allele may disrupt SPAG5 protein synthesis.

Since no clones with biallelic integration of donor sequence were obtained even after 2nd round of transfection, the SPAG5 expression was examined in the clones with a donor allele and an indel allele. Some of the clones were tested without SPAG5 expression. The majority of the clones obtained from 1st round KO were with a "T" insertion in the indel allele. However, this "T" insertion was located at 3 bp downstream *SPAG5* exon 1. Fortunately, the location of the inserted "T" could disrupt the GT/AG mRNA processing rule, which led to ineffective splicing of the pre-mRNA. Undoubtedly, SPAG5 isoforms might still be synthesised in these clones due to translation reinitiation. Future *SPAG5* KO studies may recruit high-resolution mass spectrometry and protein sequencing to examine the presence of truncated SPAG5 isoforms and their exact amino acid sequence.

Unfortunately, because of COVID-19 pandemic and immediacy of lockdown restrictions, we have not evaluated the role of SPAG5 in olaparib sensitivity in TNBC

cells and the ABCC5 functional expression in homozygous *SPAG5* KO clones. We only tested the SPAG5 expression in heterozygous *ABCC5* KO clones using Western blotting. But the SPAG5 expression in BT549 heterozygous *ABCC5* KO clones remained at the same level as WT cells, indicating that ABCC5 could not regulate SPAG5 expression. However, as we previously reviewed, SPAG5 can confer resistance to olaparib in TNBC cells through c-MYC signalling and regulate gene transcription and protein expression through multiple pathways (He et al., 2020). In combination with the findings in the present study, olaparib might be a CS agent against ABCC5. If SPAG5 could up-regulate ABCC5 expression in TNBC cells, exploring what phenotype SPAG5 KO cells exhibit will be of interest. To be specific, *SPAG5* KO can make TNBC cells sensitive to olaparib through down-regulation of c-MYC signalling. However, the SPAG5 KO-induced downregulation of ABCC5 can also result in increased resistance to olaparib. How do these two pathways compete is of interest to be explored. On the other hand, if SPAG5 could inhibit ABCC5 expression in TNBC cells, SPAG5 KO might increase olaparib sensitivity by both down-regulation of c-MYC signalling and up-regulation of ABCC5 expression. Targeting SPAG5 may thus be a promising strategy to improve the collateral sensitivity to olaparib in TNBC cells. Future studies are warranted to clarify the relation between SPAG5 and ABCC5 expression in TNBC cells.

Chapter 6. Paired Isogenic HEK293 Cell Model

6.1 Introduction

In the previous chapter, studies of ABCC5 KO and control TNBC cells were described demonstrating the CS of olaparib associated with ABCC5. However, the effect of ABCC5 overexpression on olaparib sensitivity was unclear. HEK293 (human embryonic kidney cell) cell model has been extensively investigated as an excellent platform to study the function of a target gene/protein due to high transfection efficiency, functional expression of target proteins, excellent in vitro-in vivo correlation, and standardized protocol of growth and maintenance. Accumulating evidence suggests cell-based models can be used to study the functional expression of drug transporters. Compared with the drug selected cancer resistant cell lines, HEK293 cells genetically modified to over-express membrane transporter genes give investigators an opportunity to study the activities of the transporter of interest with experimental controls excluding propounding factors other than drug transporters. This cell model pair in this study includes an ABCC5-overexpressing line (HEK-MRP5) and an isogenic parental line (HEK-P). ABCC5-overexpressing HEK293 cell model has been used in previous *in vitro* studies to examine the role of ABCC5 in pharmacology of anti-cancer drugs (Y. Li, Revalde, Reid, & Paxton, 2011; Pratt et al., 2005). This cell model is of significance for studying drug transport mechanisms and cellular sensitivity to anti-cancer drugs. In current study, HEK293 cells genetically modified to overexpress ABCC5 transporter typically contributes to the determination of cellular accumulation of doxorubicin and olaparib and the cell sensitivity to these drugs.

The main aim of this chapter is to investigate the role of ABCC5 in cellular accumulation and cell sensitivity to doxorubicin and olaparib in an ABCC5-

overexpressing cell model. The functional overexpression of ABCC5 was studied initially, followed by comparing HEK-MRP5 and HEK-P cells for their accumulation of doxorubicin and olaparib and sensitivity to these drugs-induced growth inhibitions.

6.2 Material and Methods

The details of the chemicals and experimental methods are shown in Chapter 2.

6.3 Results

6.3.1 Validation of Cell Morphology

To validate the HEK293 cell line, cell morphology was visualized by using Zeiss Primovert Compact Inverted Microscope (Carl Zeiss AG) and compared with the supplier's schematic illustration from ATCC (Cryosite Ltd, NSW, AU) (Figure 6.1).

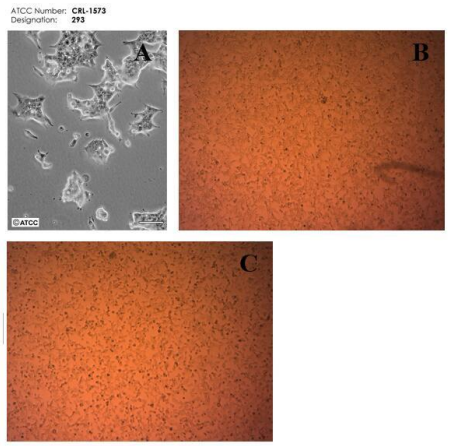

Figure 6.1 Morphology of HEK-MRP5 and HEK-P cells. Image for HEK293 cells in Panel A was obtained from ATCC (Cryosite Ltd, NSW, AU). Images for HEK-P cells in Panel B and HEK-MRP5 cells in Panel C were taken using Zeiss Primovert Compact Inverted Microscope (Carl Zeiss AG) and cells were cultured in Applied Sciences Laboratory in AUT.

6.3.2 Functional Expression of ABCC5 in HEK-MRP5 Cells and Its Role in Doxorubicin and Olaparib Cellular Accumulation

6.3.2.1 The Time-Dependent Accumulation of BCECF and the Reversal Effect of ABCC5 Inhibitors

Before confirming the functional expression of ABCC5 in HEK293 cells, validation of experimental conditions for the flow-cytometry-based cell uptake study (section 2.7.2.1) in HEK-MRP5 cells compared with isogenic control HEK-P cells was conducted. The concentration-dependent BCECF accumulation was done by one of our colleagues, Piyush, in his previous work in which a 0.25 μM BCECF-AM dissolved in DMSO (0.1% DMSO in uptake medium) showed the best uptake rate. Thus, a time-dependent BCECF accumulation was done here to determine the rate-limiting effect of ABCC5 and the steady-state accumulation of BCECF.

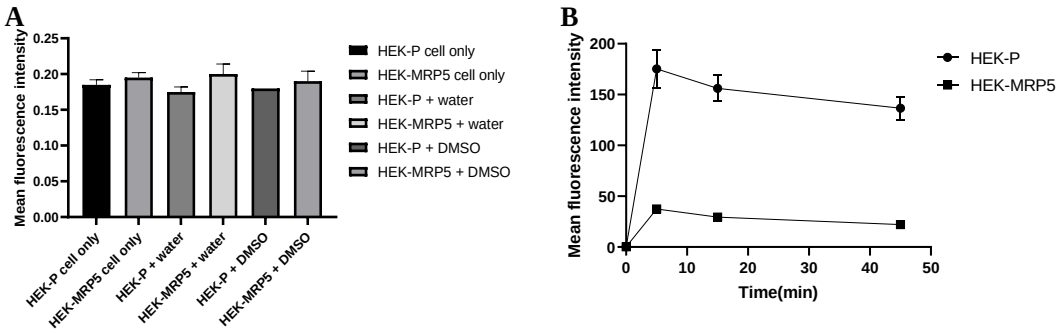

Figure 6.2 The time-dependent accumulation of BCECF in HEK-MRP5 and HEK-P cells determined using flow-cytometry-based cell uptake study. A. The influence of cell autofluorescence and reagent solvents on fluorescence determination. Data were presented as mean ± SD of duplicates. **B.** The BCECF accumulation reached steady-state at around 15 min incubation. Data were presented as mean ± SD of triplicates.

Figure 6.2A shows the influence of cell autofluorescence and reagent solvents on fluorescence determination using MoFlo^{TM} XDP flow cytometer (Beckman Coulter, Inc., CA). The data of the cell uptake study onwards were thus calculated by subtracting the fluorescent intensity of blank control (cells plus reagent solvents) from the fluorescent intensity of samples. ABCC5 apparently limited the accumulation rate of BCECF in HEK-MRP5 cells (Figure 6.2B) compared with isogenic control HEK-P cells, and the BCECF accumulation shows a time-dependent manner that it achieved steady-state after around 15 min exposure time. Thus, a 15 min incubation time with BCECF-AM was considered optimal in the subsequent experiments.

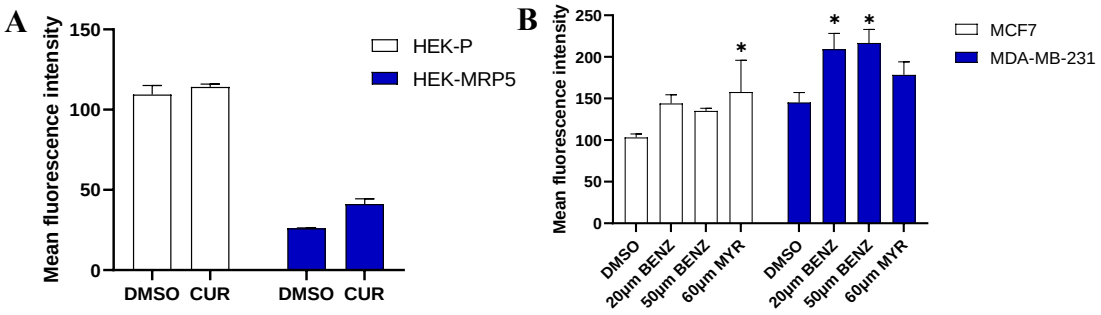

Figure 6.3 Validation of ABCC5 inhibitors. A. The cellular accumulation of BCECF in HEK-P and HEK-MRP5 cells with 30 min pre-incubation of 20 μM curcumin. Results were plotted as average fluorescence vs. cell type. Data were presented as mean ± SD of duplicates. No significant difference in the BCECF accumulation was shown between HEK-MRP5 cells pre-treated with 20 μM curcumin and HEK-MRP5 DMSO control group, calculated using Student's unpaired t-test. **B.** The cellular accumulation of BCECF in MDA-MB-231 and MCF7 cells with 30 min pre-incubation of 20 μM benzbromarone, 50 μM benzbromarone and 60 μM myricetin, respectively. Results were plotted as average fluorescence vs. cell type. Data were presented as mean ± SD of two independent experiments, each repeat was run in duplicates. *P<0.05 significantly different from the BCECF accumulation in corresponding DMSO control groups, calculated using Student's unpaired t-test.

Figure 6.3 shows the BCECF accumulation status in MDA-MB-231, MCF7 or HEK-

MRP5 cells pre-treated with 20 μM curcumin, 20 μM benzbromarone, 50 μM benzbromarone and 60 μM myricetin, respectively. The test of curcumin intrinsic fluorescence is shown in Figure 0.1 in appendix. No significant difference in the BCECF accumulation was shown between HEK-MRP5 cells pre-treated with 20 μM curcumin and HEK-MRP5 DMSO control group, calculated using two-way ANOVA and Sidak's multiple comparison post-test to compare all treatment groups with the DMSO control group (Figure 6.3A). Moreover, the accumulated BCECF in MDA-MB-231 cells pre-treated with 20 μM and 50 μM benzbromarone was significantly higher than that in negative control DMSO (the solvent of benzbromarone) group with *P* values of < 0.01 and < 0.001 respectively (Figure 6.3C). 60 μM myricetin showed no major reversal effect on BCECF accumulation in MDA-MB-231 cells. However, an opposite result was shown in MCF7 cells, where 60 μM myricetin significantly increased the BCECF accumulation ($P < 0.01$) rather than different concentrations of benzbromarone. These data suggest that benzbromarone and myricetin might be ideal ABCC5 inhibitors in BCECF accumulation study. Given the well-documented inhibitory effect of benzbromarone on ABCC5 in previous studies (J. Wijnholds et al., 2000) and in TNBC cells in this study and the degradation of chemicals in long-term storage, 50 μM benzbromarone was used in the subsequent experiments.

6.3.2.2 Validation of ABCC5 Functional Expression in HEK-MRP5 Cells

The isogenic parental HEK-P cells and ABCC5-overexpressing HEK-MRP5 cells were used to study the role of ABCC5 in olaparib and doxorubicin transport at a cellular level, as well as pemetrexed as a positive control. The consistent expression of ABCC5 in HEK-MRP5 cells was confirmed by using flow-cytometry-based cell uptake study (section 2.7.2.1) every 1 to 2 months. Before investigating the ABCC5-mediated

resistance to olaparib and doxorubicin, the cell uptake study (section 2.7.2) and western blotting (section 2.9) were confirmed the functional expression of ABCC5 in HEK-MRP5 cells compared with isogenic parental HEK-P cells.

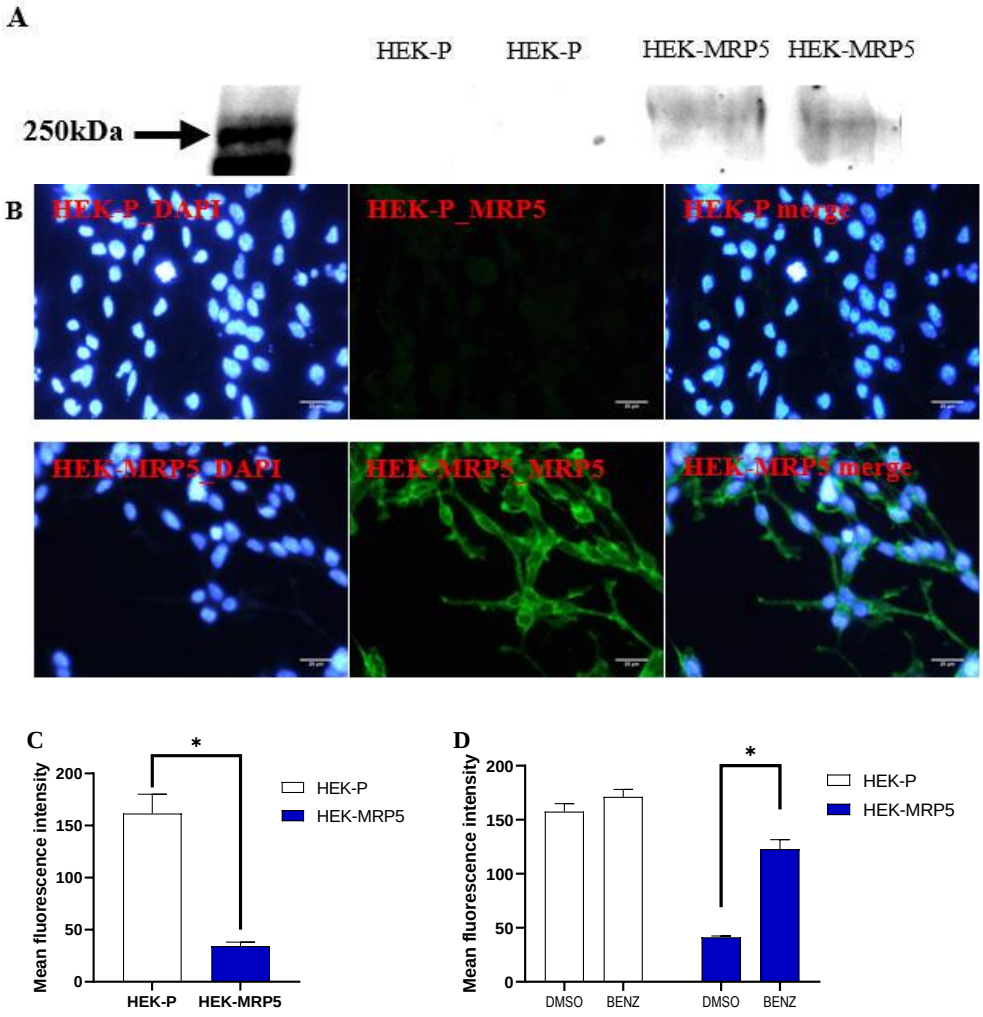

Figure 6.4 Validation of ABCC5 expression in HEK-MRP5 cells compared with the isogenic control HEK-P cells. A. Immunoblot of membrane fractions from HEK-MRP5 and HEK-P cells using MRP5 Monoclonal Antibody and Goat anti-Rabbit IgG (H+L) Secondary Antibody, HRP. **B.** Immunocytochemistry of HEK-MRP5 and HEK-P cells. Cells were stained with MRP5 Monoclonal Antibody and Goat Anti-Rat IgG H&L (DyLight® 488) secondary antibody. **C.** The cellular accumulation of BCECF in HEK-P and HEK-MRP5 cells. Results were plotted as average fluorescence vs. cell type. Data were presented as mean ± SD of three independent experiments, each repeat was run in duplicates. *P<0.05 significantly different from the BCECF accumulation in HEK-P control cell line, calculated using Student's unpaired t-test. **D.** Benzbromarone reversed the function of ABCC5 in HEK-MRP5 cells. Data were presented as mean ± SD of triplicates. *P<0.05 significantly different from the BCECF

accumulation in HEK-MRP5 control cells treated with DMSO, calculated using Student's unpaired t-test.

Figure 6.4A shows an immunoblot demonstrating the expression level of ABCC5 in HEK-MRP5 and HEK-P cells. After staining with MRP5 Monoclonal Antibody and Goat Anti-Rat IgG H&L (DyLight® 488) secondary antibody, ABCC5 bands only appeared in the lane loaded with HEK-MRP5 cell lysate, without any signal in the negative control HEK-P cell lysate. The detected bands correspond to the BCECF accumulation status in HEK-MRP5 and HEK-P cells in Figure 6.4B. A *P*-value of < 0.05 demonstrates that the accumulated BCECF in negative control HEK-P cells was significantly (nearly 5-fold) higher than HEK-MRP5 cells. This ABCC5-mediated rate-limiting effect on BCECF accumulation could be reversed by pre-incubating the cells with 50 μM benzbromarone (Figure 6.4C), a well-documented ABCC5 inhibitor (J. Wijnholds et al., 2000). A *P*-value of < 0.05 elucidates that the accumulated BCECF in HEK-MRP5 cells pre-treated with benzbromarone was significantly higher than that in negative control HEK-MRP5 cells pre-treated with the same volume of DMSO (the solvent of benzbromarone). These results suggest that ABCC5 was functionally overexpressed in HEK-MRP5 cells compared to the HEK-P cells without ABCC5 expression. The subsequent cytotoxicity studies in HEK-MRP5 and HEK-P cells are based on the ABCC5 expression and function to evaluate the role of this membrane transporter in doxorubicin and olaparib sensitivity.

6.3.2.3 The Role of ABCC5 in Doxorubicin and Olaparib Cellular Accumulation

To investigate the role of ABCC5 in the transport of doxorubicin and olaparib, HEK-

MRP5 and HEK-P cells were incubated with doxorubicin and olaparib for designated time points, followed by measurement of fluorescence intensity using MoFlo^{TM} XDP flow cytometer (Beckman Coulter, Inc., CA).

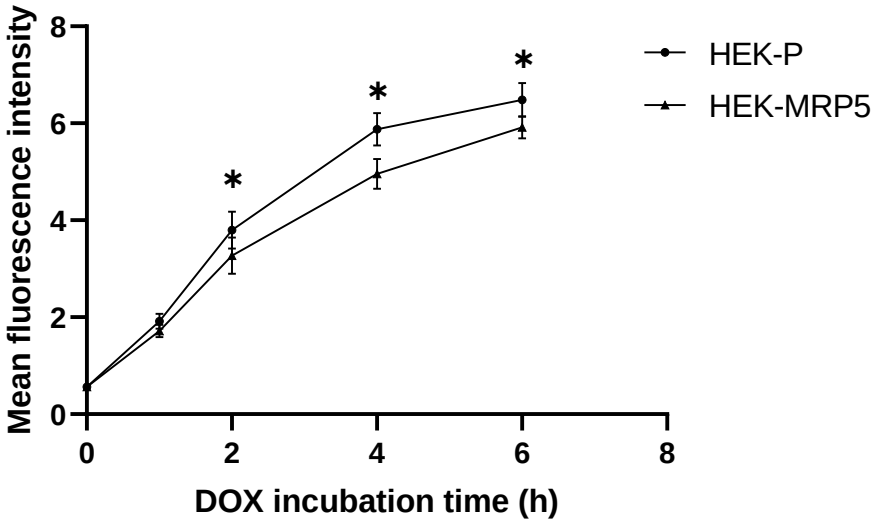

Figure 6.5 The time-dependent accumulation of 6 μM doxorubicin in HEK-MRP5 and isogenic HEK-P cells. Results were plotted as average fluorescence vs. incubation time. Data were presented as mean ± SD of three independent experiments, each repeat was run in duplicates. *P<0.05 significantly different from the doxorubicin accumulation in corresponding HEK-P control groups at the same incubation time point, calculated using Student's unpaired t-test.

Doxorubicin has intrinsic fluorescence with an emission signal at 595 nm upon excitation with a 470 nm laser. A concentration of 6 μM doxorubicin was applied to cells according to the analysis of a previous study (Durand & Olive, 1981). HEK-MRP5 and its isogenic HEK-P cells were incubated with 6 μM doxorubicin for up to 6 hours. In Figure 6.5, the accumulation of doxorubicin was significantly higher in HEK-MRP5 cells compared with the isogenic parental HEK-P cell at the same time points from 2- to 6-hr incubation. The rate-limiting effect of ABCC5 on doxorubicin accumulation in

HEK-MRP5 cells peaked after 4-hr exposure to doxorubicin, at which the fluorescence of HEK-P cells was 1.2-fold higher than HEK-MRP5 cells. In comparison, after 6-hr incubation, the ABCC5-mediated transport of doxorubicin appeared to be decreased, probably due to the cytotoxicity of doxorubicin. Given the approximately 5-fold difference in BCECF accumulation between HEK-MRP5 and HEK-P cells (Figure 6.4C), the 1.2-fold difference in doxorubicin accumulation at 4-hr exposure time may indicate that ABCC5 could regulate the export of doxorubicin but with a low efflux capability.

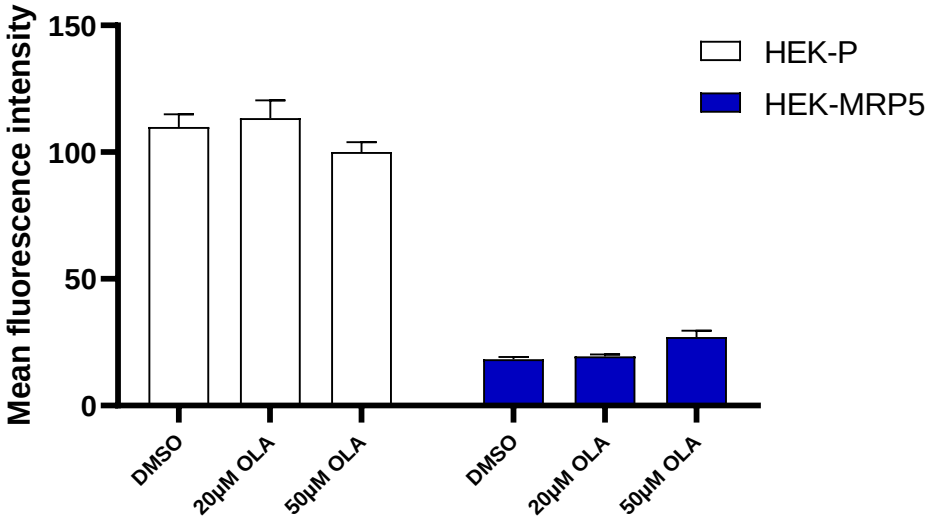

Figure 6.6 Competitive efflux of olaparib with BCECF. Results were plotted as average fluorescence vs. cell type. Data were presented as mean ± SD of triplicates. No significant difference of the BCECF accumulation was shown between HEK-MRP5 cells pre-treated with different concentrations of olaparib and HEK-MRP5 DMSO control group, calculated using one-way ANOVA and Sidak's multiple comparison post-test to compare all treatment groups with the DMSO control group.

Unlike doxorubicin, olaparib has no intrinsic fluorescence. Thus, the olaparib transportability of ABCC5 was determined by an indirect method that if olaparib is a

substrate of ABCC5, it would competitively decrease the ABCC5-mediated BCECF efflux. In other words, the BCECF accumulation is considered elevated in HEK-MRP5 cells pre-treated with olaparib compared to the negative control without pre-treatment. HEK-MRP5 and HEK-P cells were pre-treated with 20 μM, 50 μM olaparib and DMSO as a blank control for 30 min, followed by a 15 min incubation with BCECF. Figure 6.6 shows that the BCECF accumulation in HEK-MRP5 cells pre-treated with olaparib remained at the same level as the DMSO control group. This demonstrates that the ABCC5-mediated BCECF efflux was not impeded by exposure to olaparib. Thus, olaparib may not be a substrate of ABCC5 and has a minor impact upon ABCC5 function.

6.3.3 The Cytotoxicity of Doxorubicin and Olaparib in HEK-MRP5 and HEK-P cells

6.3.3.1 The Time-Dependent Cytotoxicity of Doxorubicin and Olaparib in HEK-MRP5 and HEK-P Cells

Before investigating the cytotoxicity of doxorubicin and olaparib, the antiproliferative effects of these chemodrugs were determined in HEK-MRP5 and the isogenic parental HEK-P cells to identify non-cytotoxic and cytostatic exposure time using MTT assay (section 2.8). These also indicated if ABCC5 overexpression conferred a resistant phenotype towards doxorubicin and olaparib.

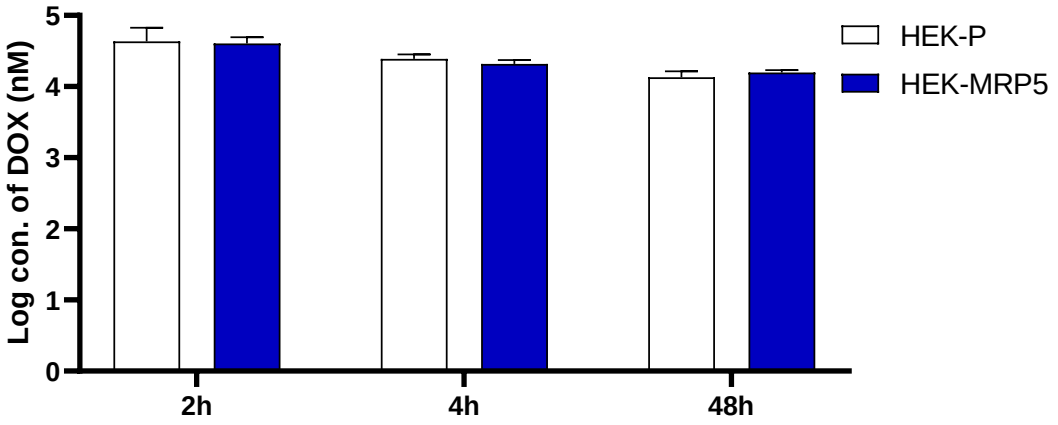

Figure 6.7 The time-dependent cytotoxicity of doxorubicin in HEK-MRP5 and HEK-P cells determined using MTT assay. Results were plotted as Log IC_{50} value vs. exposure time. Data were presented as mean ± SD of triplicates. No significant difference was shown in IC_{50} value between HEK-MRP5 and HEK-P cells after 2-, 4- and 48-hr exposure to doxorubicin.

Figure 6.7 shows IC_{50} data of HEK-MRP5 and HEK-P cells after 2-, 4- and 48-hr exposure to increasing concentrations of doxorubicin, followed by 2 days incubation with CM. The overexpressed ABCC5 in HEK-MRP5 cells was unable to maintain a higher proliferation rate than HEK-P cells over the designated exposure time. The sensitivity to doxorubicin in HEK-MRP5 and HEK-P cells remained at the same level after 2-, 4- and 48-hr exposure. However, data in section 6.3.2.3 demonstrated that ABCC5 could export doxorubicin in HEK-MRP5 cells. This might be because the 1.2-fold difference in doxorubicin accumulation between HEK-MRP5 and HEK-P cells after 4-hr exposure was less and insufficient to affect cell survival.

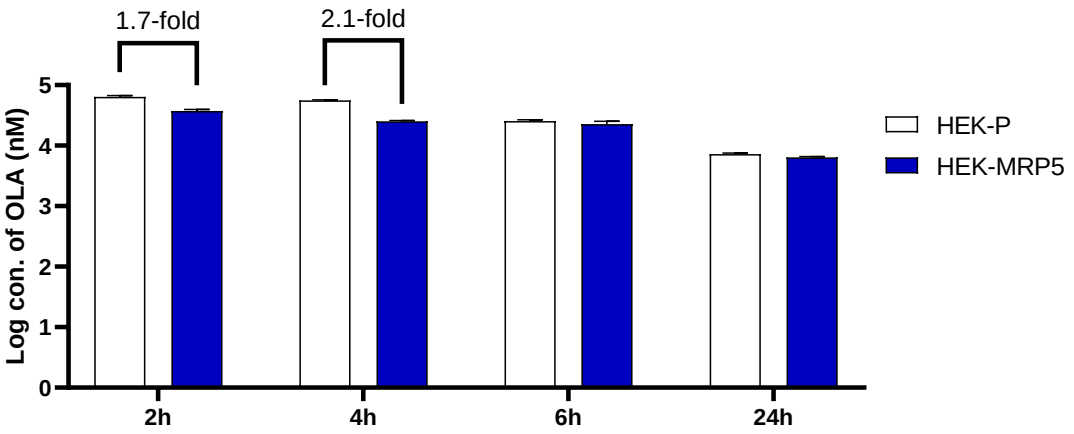

Figure 6.8 The time-dependent cytotoxicity of olaparib in HEK-MRP5 and HEK-P cells determined using MTT assay. Results were plotted as Log IC_{50} value vs. exposure time. Data were presented as mean ± SD of triplicates. Cells were exposed to olaparib for 2-, 4-, 6- and 24-hr, followed by 4 days incubation with fresh CM. The IC_{50} values in HEK-P cells after 2- and 4-hr exposure to olaparib were 1.7- and 2.1-fold higher than HEK-MRP5 cells, respectively.

To further investigate the role of ABCC5 in cellular sensitivity to olaparib-induced growth inhibition, HEK-MRP5 and HEK-P cells were exposed to increasing concentrations of olaparib for 2-, 4-, 6- and 24-hr, followed by 4 days incubation with CM. Interestingly, contrary to our hypothesis, the resistance of HEK-P cells to olaparib was higher than HEK-MRP5 cells at 2- and 4-hr exposure time respectively by increasing IC_{50} values by up to 1.7-fold and 2.1-fold, and remained at the same level with HEK-MRP5 cells after 6 hours exposure to olaparib (Figure 6.8). Compared to HEK-P cells without ABCC5 expression, the overexpressed ABCC5 in HEK-MRP5 cells made the cells more sensitive to olaparib, which peaked at 4-hr exposure (Figure 6.9). 4-hr exposure time to olaparib was thus used in the subsequent experiments.

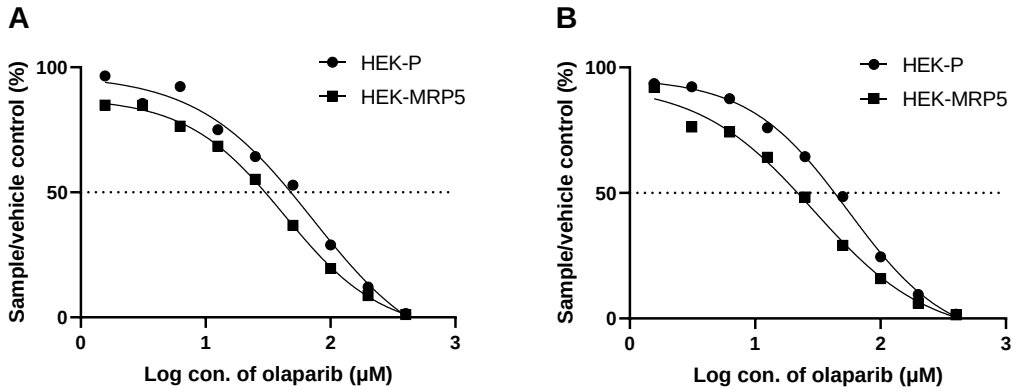

Figure 6.9 Increased olaparib-induced growth inhibition in HEK-MRP5 cells compared with the isogenic parental HEK-P cells after 2- (A) and 4-hr (B) exposure. Results were plotted as % of cell viability from vehicle control vs. Log concentration of olaparib. Data were presented as mean of triplicates.

6.3.3.2 Reversal of ABCC5-Mediated Sensitivity to Olaparib

The previously identified ABCC5 inhibitor, benzbromarone (section 6.3.2.2), was tested for its cytotoxicity on HEK-P, HEK-MRP5, MDA-MB-231, BT549 and MCF7 cells. Cells were treated with serially diluted benzbromarone for 4-hr, followed by 4 days incubation with fresh CM. IC_{50} values for benzbromarone-induced growth inhibition remained at the same level in these tested cell lines (approximately 200 μM) (Figure 6.10). For more accurate estimation of IC_{50}, further study may include additional concentrations of benzbromarone between 200- and 300-μM. Although 20- and 50-μM benzbromarone only reduced cell viability by around 15% in all tested cell lines, the data were still statistically significant (*$P < 0.05$) (Figure 6.10D). Thus, the impact of benzbromarone on cell viability should be taken into account when determining its inhibitory effect on ABCC5 function in cell viability assay. This impact was minor in uptake study, considering the much shorter incubation time.

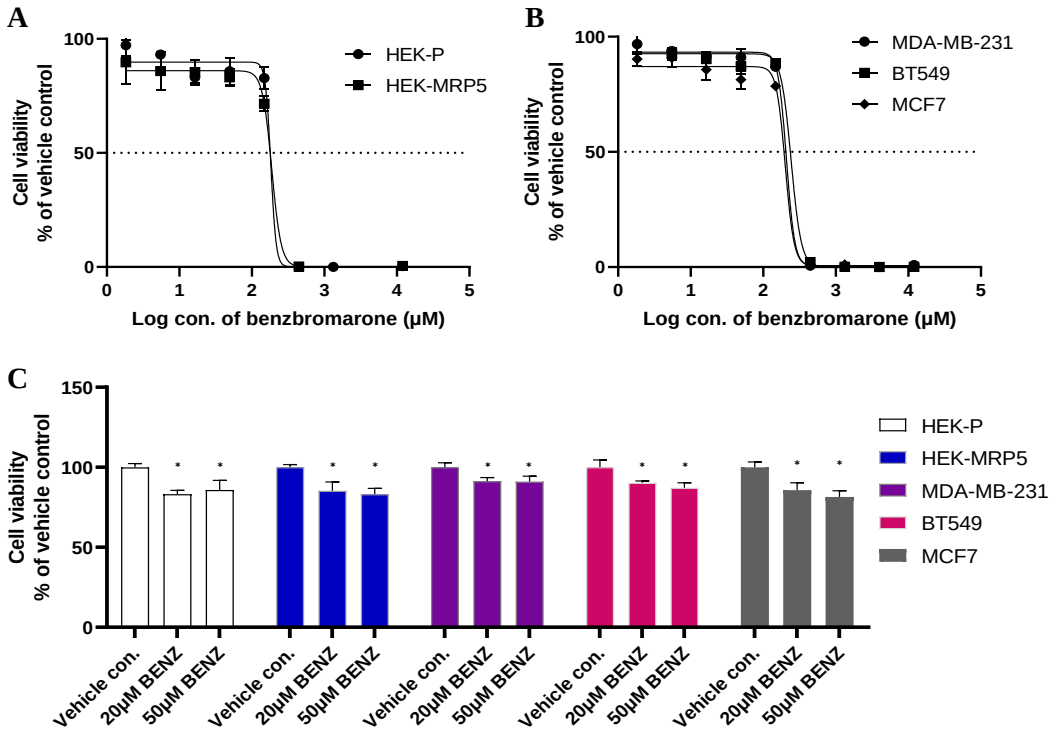

Figure 6.10 The cytotoxicity of benzbromarone on HEK293 and breast cancer cells. **A.** Growth inhibition curve of HEK-P and HEK-MRP5 cells. Results were plotted as % of cell viability from vehicle control vs. log concentration of benzbromarone. Data were presented as mean ± SD of triplicates. **B.** Growth inhibition curve of MDA-MB-231, BT549 and MCF7 cells. Results were plotted as % of cell viability from vehicle control vs. log concentration of benzbromarone. Data were presented as mean ± SD of triplicates. **C.** The cytotoxicity of 20 μM and 50 μM benzbromarone on tested cell lines. Results were plotted as % of cell viability from vehicle control vs. cell type. Data were presented as mean ± SD of triplicates. **P* < 0.05 significantly different from the cell viability of corresponding vehicle control, calculated using one-way ANOVA and Sidak's multiple comparison post-test to compare all treatment groups with the corresponding vehicle control.

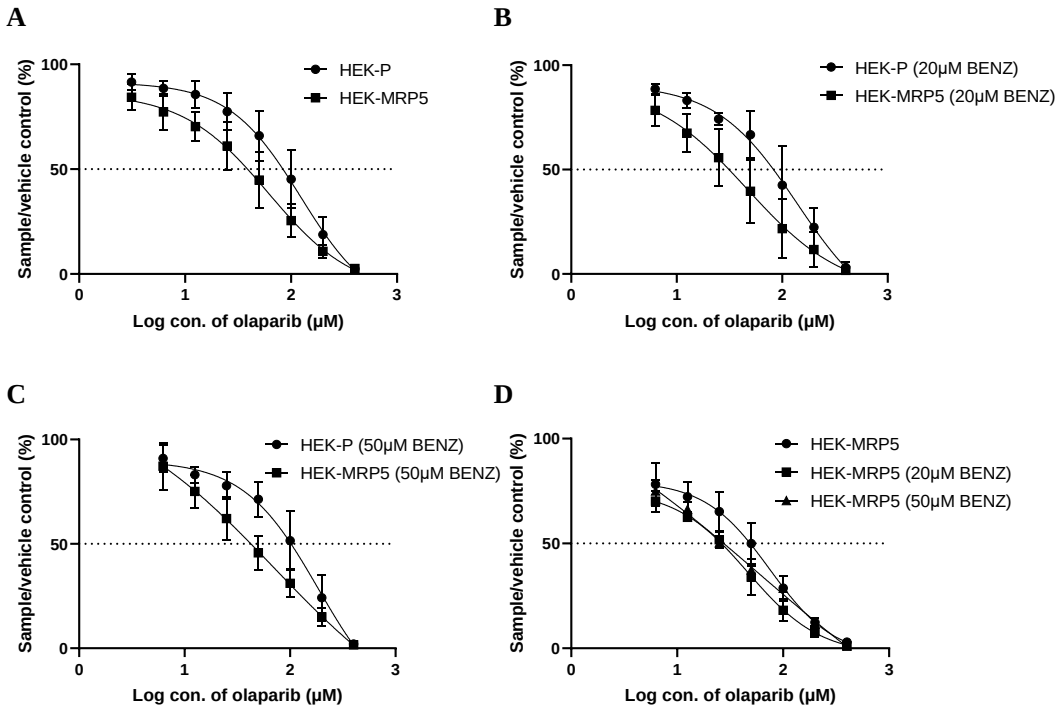

Figure 6.11 Reversal of ABCC5-mediated sensitivity to olaparib in HEK-MRP5 and HEK-P cells. Cells were pre-treated CM **(A)**, 20 μM **(B)** and 50 μM **(C)** benzbromarone and exposed to olaparib for 4-hr, followed by 4 days incubation with fresh CM. Results were plotted as % of cell viability from vehicle control vs. log concentration of olaparib. Data were presented as mean ± SD of three independent experiments, each repeat was run in triplicates. **D.** Comparison of ABCC5-mediated sensitivity to olaparib after pre-treatment with CM, 20 μM and 50 μM benzbromarone in HEK-MRP5 cells. Results were plotted as % of cell viability from vehicle control vs. log concentration of olaparib. Data were presented as mean ± SD of three independent experiments, each repeat was run in triplicates.

The ability of benzbromarone to reverse ABCC5-mediated cellular sensitivity in HEK-MRP5 cells was examined. Figure 6.11D shows that neither 20 μM nor 50 μM benzbromarone reduced the sensitivity of HEK-MRP5 cells to olaparib. The negative control, HEK-MRP5 cells pre-treated with CM for 30 min, even showed higher cell viability.

Due to the cytotoxicity of benzbromarone (Kobayashi et al., 2013) and the potential synergistic effect of benzbromarone in combination with olaparib, the reversal effect of

benzbromarone on ABCC5-mediated sensitivity to olaparib might be compromised by its cytotoxicity. Figure 6.12 shows the IC_{50} values of olaparib in HEK-MRP5 and HEK-P cells pre-treated with benzbromarone. The IC_{50} values were decreased with the increase of benzbromarone concentration in HEK-MRP5 cells and remained stable in HEK-P cells. The treatment of benzbromarone did not restore resistance to olaparib in HEK-MRP5 cells compared with the HEK-P control group. Given that HEK-P cells were previously tested without ABCC5 expression (section 6.3.2.2), the decreased cell viability over increasing concentrations of benzbromarone in HEK-MRP5 was probably derived from the synergistic cytotoxicity of benzbromarone mixed with olaparib, which could selectively target ABCC5-overexpressing cells. Also, the cytotoxicity of ABC transporter inhibitors is such a main obstacle to clinical application, as previously reviewed in section 1.7.

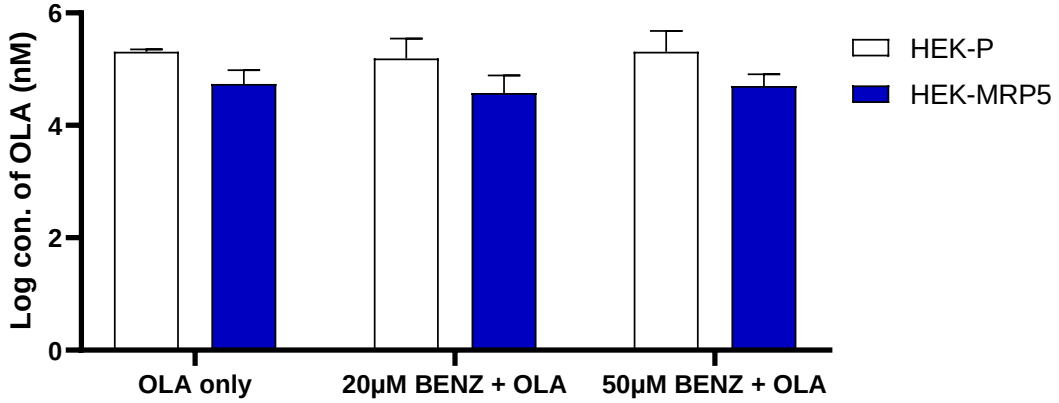

Figure 6.12 The IC_{50} value of 4-hr exposure to olaparib in HEK-MRP5 and HEK-P cells determined using MTT assay. Cells were pre-treated CM, 20 μM, and 50 μM benzbromarone. Results were plotted as Log IC_{50} value vs. cell type. Data were presented as mean ± SD of three independent experiments, each repeat was run in triplicates.

6.3.3.3 The ABCC5-Mediated Sensitivity to Olaparib

Since the reversal of ABCC5-mediated sensitivity to olaparib by benzbromarone was failed (section 6.3.3.2), an antifolate chemodrug pemetrexed that is a well-documented ABCC5 substrate (Kobayashi et al., 2013) was employed as a positive control to study the ABCC5-related olaparib sensitivity.

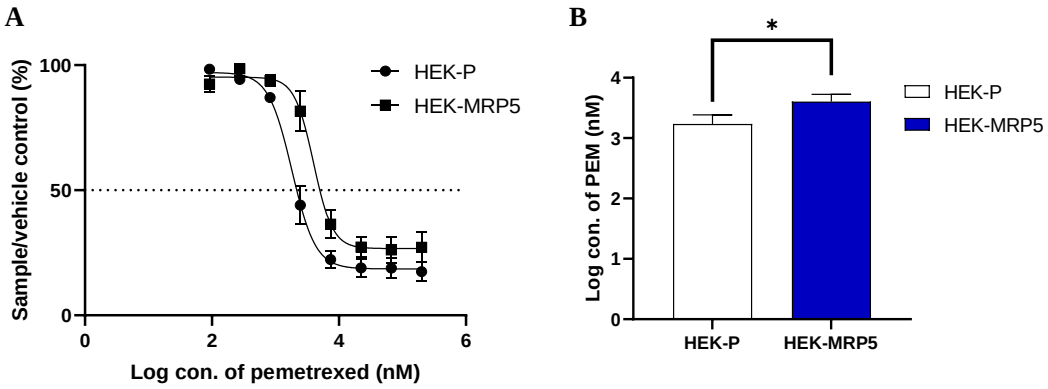

Figure 6.13 Increased pemetrexed-induced growth inhibition in HEK-P cells but not in HEK-MRP5 cells. A. Growth inhibition curve. Results were plotted as % of cell viability from vehicle control vs. log concentration of pemetrexed. Data were presented as mean ± SD of two independent experiments, each repeat was run in triplicates. **B.** Comparison of IC_{50} values between HEK-MPR5 and HEK-P cells. Results were plotted as Log IC_{50} value vs. cell type. Data were presented as mean ± SD of two independent experiments, each repeat was run in triplicates. *$P < 0.05$ significantly different from the IC_{50} value of pemetrexed in HEK-P control cell line, calculated using Student's unpaired t-test.

To compare ABCC5-mediated pemetrexed sensitivity in HEK-MRP5 and HEK-P cells, cells were treated with pemetrexed for 4-hr, followed by 4 days incubation with CM. The ABCC5 expression in HEK-MRP5 cells decreased pemetrexed-induced growth inhibition compared with HEK-P cells (Figure 6.13A). IC_{50} values for pemetrexed-induced growth inhibition were up to 2.3-fold higher in HEK-MRP5 cells than HEK-P cells with a *P*-value of < 0.05 (Figure 6.13B and Table 6.1). Compared to HEK-P cells,

HEK-MRP5 cells with overexpression of ABCC5 were considered more resistant to pemetrexed.

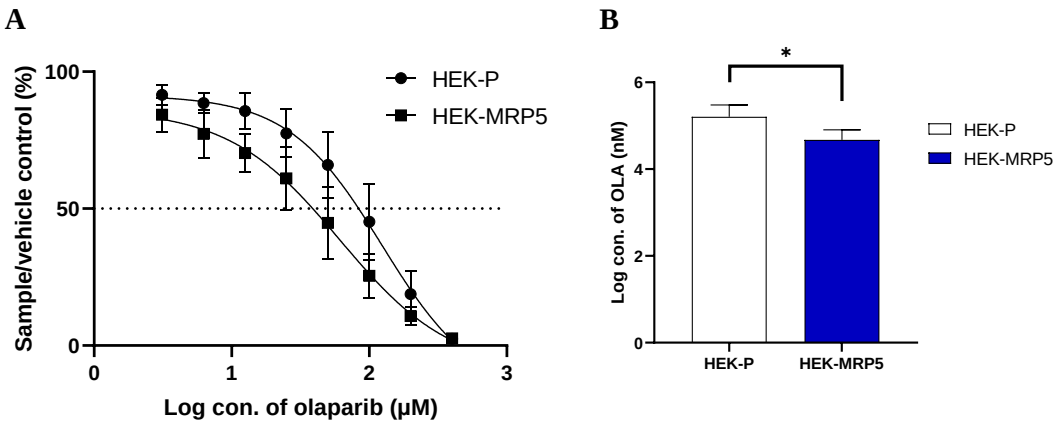

Figure 6.14 Increased olaparib-induced growth inhibition in HEK-MRP5 cells but not in HEK-P cells. A. Growth inhibition curve. Results were plotted as % of cell viability from vehicle control vs. log concentration of olaparib. Data were presented as mean ± SD of five independent experiments, each repeat was run in triplicates. **B.** Comparison of IC_{50} values between HEK-MPR5 and HEK-P cells. Results were plotted as Log IC_{50} value vs. cell type. Data were presented as mean ± SD of five independent experiments, each repeat was run in triplicates. *$P < 0.05$ significantly different from the IC_{50} value of olaparib in HEK-P control cell line, calculated using Student's unpaired t-test.

In comparison, opposite results were shown in HEK-MRP5 and HEK-P cells treated with olaparib. Figure 6.14A shows that the ABCC5 expression in HEK-MRP5 cells enhanced olaparib-induced growth inhibition compared with HEK-P cells. This elevated growth inhibition of olaparib selectively lowered the cell viability of HEK-MRP5 cells throughout the designated olaparib concentration range. Olaparib is thus considered as a CS (collateral sensitivity) agent against ABCC5-overexpressing cells. In the case of CS, at least a two-fold effect is probably required to be regarded as significant (Hall et al., 2009). The IC_{50} values for olaparib-induced growth inhibition

showed an up to 3.4-fold difference in HEK-MRP5 cells compared to HEK-P cells with a *P*-value of < 0.05 (Figure 6.14B and Table 6.1). These results suggest that olaparib might be a CS agent that is able to selectively induce cell death in an ABCC5-overexpressing HEK293 cell model. Further gene knockout and knockdown studies are warranted in order to prove this hypothesis.

Table 6.1 The IC_{50} values for olaparib- and pemetrexed-induced growth inhibition in HEK-MRP5 and HEK-P cells. Data were presented as mean ± SD of five or two independent experiments, each repeat was run in triplicates.

	Olaparib	Pemetrexed
HEK-P	182.004 ± 80.726	1.803 ± 0.661
HEK-MRP5	53.042 ± 29.286	4.141 ± 1.083

6.4 Discussion

The studies described in this chapter firstly aimed to confirm the phenotype of HEK-MRP5 cells that were stably transfected to overexpress ABCC5 protein in comparison to a non-transfected parental line. HEK-MRP5 cells showed greater ABCC5 protein expression than HEK-P cells. The efflux of ABCC5 substrate BCECF in HEK-MRP5 cells was 5-fold higher than HEK-P cells, while this significant difference could be reversed by ABCC5 inhibitor benzbromarone (J. Wijnholds et al., 2000). The 5-fold differences in BCECF accumulation between HEK-MRP5 and HEK-P cells were similar to the data reported by other studies (Y. Li et al., 2011; C. P. Wu, Calcagno, Hladky, Ambudkar, & Barrand, 2005). The sensitivity of HEK-MRP5 cells to the known ABCC5 substrate drug pemetrexed was 2.3-fold less than the parental line. The 2.3-fold differences in pemetrexed sensitivity between HEK-MRP5 and HEK-P cells were smaller than the data reported by other studies (Pratt et al., 2005) but were still

statistically significant. These results indicate that HEK-MRP5 cells showed stable functional overexpression of ABCC5 protein that altered the efficacy of its substrate drugs in an extracellular translocation-dependent manner compared to HEK-P cells. Thus, HEK-MRP5 cell line is considered as a valid ABCC5-overexpressing cell model for downstream functional studies.

With regard to the accumulation of doxorubicin and sensitivity to doxorubicin-induced growth-inhibition, HEK-MRP5 cells accumulated up to 1.2-fold less doxorubicin after 4 hours exposure compared to HEK-P cells. However, the 1.2-fold differences in doxorubicin accumulation between HEK-MRP5 and HEK-P cells were unable to result in altered growth inhibitory effects in these cells. In fact, the role of ABCC5 in mediating doxorubicin efflux was controversial in previous studies. For example, Pratt et al. (2005) reported that HEK-MRP5 cells were about 2-fold more resistant to doxorubicin compared with the parental line. In contrast, another study demonstrated that no elevated resistance to doxorubicin was detected in two tested HEK-MRP5 clones (J. Wijnholds et al., 2000). The contradictory findings in different studies, including current study, might be derived from many reasons, such as single-cell variability (Eberwine & Kim, 2015; Smith & Grima, 2018), ABCC5 polymorphisms (Lal et al., 2017), unexpected interruption of other genes after the integration of plasmid, and brand and batch differences of doxorubicin. Single-cell variability could result in various expressions of doxorubicin-resistance-related protein networks in different HEK-MRP5 clones after antibiotic selection. This variation in transcriptome thus led to different findings in different studies. Similarly, ABCC5 polymorphisms may result in different substrate drug specificity and transportability. For instance, Lal et al. (2017) reported that the pharmacokinetics of doxorubicin and doxorubicinol was significantly influenced by the *ABCC5* g.*+7161G>A* (rs1533682) and *ABCC5* g.*-1679T>A*

polymorphisms, respectively. The potential genetic or epigenetic changes in different HEK293 strains in different labs might lead to ABCC5 polymorphism variations. Furthermore, the randomly integrated plasmids that were delivered into cells might interrupt the expression of other doxorubicin-resistance-related genes, as we previously reviewed (He et al., 2021). Taken together, given the approximately 5-fold difference in BCECF accumulation between HEK-MRP5 and HEK-P cells, the 1.2-fold difference in doxorubicin accumulation might indicate that ABCC5 could regulate the export of doxorubicin. But, in consideration of the limited resistance of HEK-MRP5 cells to doxorubicin and the controversial results in previous studies, the specificity and efflux capability of ABCC5 to doxorubicin might be weak. On the basis of these results, ABCC5 might not affect doxorubicin-resistance in breast cancer cells considering their much lower ABCC5 expression than HEK-MRP5 cells.

To further investigate the role of ABCC5 in determining olaparib accumulation and cytotoxicity, HEK-MRP5 and HEK-P cells were treated with serially diluted olaparib for different time courses. Since olaparib has no autofluorescence, the cellular accumulation of olaparib was evaluated by concurrent incubation of cells with olaparib and BCECF-AM. Olaparib was thought to competitively decrease the ABCC5-mediated BCECF efflux in HEK-MRP5 cells. Concurrent treatment of HEK-MRP5 cells with olaparib and BCECF-AM did not alter the cellular accumulation of BCECF, indicating that olaparib might not be a substrate of ABCC5 and had a minor impact upon ABCC5 function. In contrast, HEK-MRP5 cells were about 3.4-fold more sensitive to olaparib-induced growth inhibition compared to HEK-P cells. In other words, olaparib might be a CS (collateral sensitivity) agent (Hall et al., 2009) against ABCC5-overexpressing cells. However, the elevated sensitivity of HEK-MRP5 cells to olaparib was not reversed by ABCC5 inhibitor benzbromarone. This might result from

the cytotoxicity of benzbromarone (Kobayashi et al., 2013) and the potential synergistic effect of benzbromarone in combination with olaparib that could compromise the reversal effect of benzbromarone on ABCC5-mediated sensitivity to olaparib. Besides, there was still a possibility that the elevated expression of ABCC5 in HEK-MRP5 cells might induce hyperactivation or overexpression of a set of transcriptional activators (He et al., 2021). Rather than targeting ABCC5, olaparib might interact with the proteins in this network, making HEK-MRP5 cells more sensitive to olaparib. Apart from the above aspects, the metabolites of olaparib might also play a role in the altered sensitivity of HEK-MRP5 cells to olaparib. Olaparib was mainly metabolised by the action of CYP3A4/5 enzymes as previously reviewed in section 1.2.2.3. To complicate matters, CYP3A4/5 enzymes were detected to express in normal kidney (Murray et al., 1999) and a considerable portion of breast cancer tissues (van Eijk, Boosman, Schinkel, Huitema, & Beijnen, 2019). Thus, some of the intracellular accumulated olaparib might be converted to metabolites within the given time course and exerted an impact on cancer cells. In fact, up to 20, 37 and 20 metabolites were detected in plasma, urine, and faeces, respectively; but, unfortunately, the pharmacodynamic activity of these metabolites is unknown (Paul & Montoya, 2020).

In conclusion, these studies showed that pemetrexed was a typical substrate of ABCC5 in HEK293 cell model, compared to doxorubicin as a weak substrate. However, olaparib might be a CS agent that selectively targets ABCC5-overexpressing HEK-MRP5 cells. Inhibition of ABCC5 protein did not reverse the elevated cytotoxicity of olaparib in HEK-MRP5 cells. The molecular mechanisms underlying this phenomenon are unknown. But based on the findings in Chapter 4, olaparib-induced growth inhibitory effects in ABCC5-rich cells might be derived from the interactions between olaparib and ABCC5.

Chapter 7. General Discussion

7.1 Summary of the Findings

In this final chapter, the critical findings of this thesis were summarised and discussed. The first topic of discussion concerns the establishment of gene KO cell models using CRISPR-Cas9 technology, which highlighted the contributions of this study to current knowledge, the issues that arose in our practice, and future directions of CRISPR-Cas9 technology. The pharmacodynamics of olaparib in ABCC5-rich TNBC cells was then elaborated, followed by a discussion on the potential mechanisms underlying the ABCC5-related collateral sensitivity to olaparib. Finally, directions for future studies in investigating ABCC5-related collateral sensitivity were considered.

Five genetically modified cell models, including heterozygous *ABCC5* gene KO MDA-MB-231 cells, heterozygous *ABCC5* gene KO BT549 cells, heterozygous *ABCC5* gene KO MCF7 cells, homozygous *SPAG5* gene KO BT549 cells, homozygous *SPAG5* gene KO T47D cells, were established to study the ABCC5-associated collateral sensitivity to olaparib. An ABCC5-overexpressing HEK293 cell model was further adopted to confirm these findings.

Pemetrexed was confirmed as an ABCC5 substrate by using paired isogenic HEK293 cell models but there were no differences in its sensitivity between wildtype and heterozygous *ABCC5* gene KO MDA-MB-231 cells. Doxorubicin was a very weak substrate of ABCC5 in both HEK239 and heterozygous *ABCC5* gene KO MDA-MB-231 cell models.

ABCC5 was related to the collateral sensitivity to olaparib in HEK293, heterozygous

ABCC5 gene KO MDA-MB-231 and heterozygous *ABCC5* gene KO BT549 cell models. Inhibiting ABCC5 by benzbromarone did not alter the sensitive phenotype of HEK-P cells. This ABCC5-related collateral sensitivity to olaparib implicated in interactions between ABCC5 and olaparib in molecular docking studies. However, in the analysis using ONCOMINE datasets, although *ABCC5* was found to overexpress in invasive breast carcinoma, *ABCC5* expression was not correlated with breast cancer metastasis, recurrence and overall clinical outcomes.

Of note, in the meta-analysis using ONCOMINE datasets, *SPAG5* expression was found significantly associated with *ABCC5* expression in breast carcinoma. However, SPAG5 has not been tested for its role in ABCC5 expression. But ABCC5 was unable to alter SPAG5 expression in the heterozygous *ABCC5* gene KO BT549 cell model.

7.2 Establishment of Knockout Cell Lines Using CRISPR-Cas9 Technology

7.2.1 Contributions of This Study to Knowledge

The KO studies demonstrated that both RNP- and recombinant plasmid-based CRISPR-Cas9 technology were able to modify target genes in breast cancer cells. But the CNV of target genes might remain an obstacle to obtain homozygous KO cell lines. This study first proposed that potential crosstalk between Cas9-induced DSBs, gene repair routes and gene rearrangements might be involved in certain gene KO processes. This makes multiple rounds of transfection aiming at eliminating all copies of the target gene impracticable. To complicate matters, the repair route employed by cells may not simply depend on whether episomal donor templates exist. The RNP-induced DSBs

may be repaired by high-fidelity HDR route in the absence of donor templates according to the wild-type sister chromatid or homologous chromosome, which may be regulated by chromosomal topologies (Janssen et al., 2019) and DSB ends resection-related cellular components (Heyer, 2015). To be exact, in the absence of donor templates, the RNP-induced DSB in the first allele may be repaired by NHEJ, while the DSB in the second allele may be repaired by HDR according to the first repaired allele. This speculation explains why the mutated gene in a given KO clone only showed a single sequence in some studies (Binda et al., 2020; Kawamura et al., 2015).

For the conventional plasmid-based CRISPR-Cas9 technology, the homozygous KO cells were more likely dependent on both high-fidelity HDR repair and error-prone NHEJ repair, rather than a single HDR repair route. This means that even in the presence of episomal homologous double-stranded donor templates, only one allele can be re-ligated by HDR. Cells tend to employ NHEJ to repair the DSB in the other allele. As a consequence, when designing gRNA for plasmid-based CRISPR-Cas9 technology, the target loci should be located in exons. Thus, the NHEJ-induced frameshift can interrupt the transcription of the target gene. Alternatively, this study first found that targeting locus 3 bp downstream from exons could also interrupt gene expression. The mutation in the immediate vicinity of exons breaks the GT/AG mRNA processing rule, leading to ineffective splicing of the pre-mRNA. Meanwhile, this study first found that the indel generated by NHEJ repair in this circumstance might not follow the random insertion and/or deletion rule. A fixed “T” insertion was found in virtually all the positive clones, irrespective of gRNA and cell line.

7.2.2 Limitations of CRISPR/Cas9 systems in this thesis

As discussed in Chapter 3, targeting the sequence embedded in more relaxed chromatin structure and low nucleosome occupancy regions may increase the accumulation of Cas9-mediated mutagenesis. But lack of a proper database and molecular modelling tool to examine the chromosomal state of the target gene and the loci of the target DNA sequence in the nucleosome makes it challenging to improve cleavage efficiency by this method.

Besides, it was reported that Cas9-induced mutagenesis benefited from the orientation of sgRNA (Verkuijl & Rots, 2019) and the dynamic R-loop structure between target DNA and sgRNA (Xu et al., 2017). But to what extent the orientation of sgRNA influences cleavage efficiency and how to bend the R-loop structure into the most effective shape remained to be investigated.

Moreover, chromosomal mosaicism and germline CNVs of the target gene might dramatically decrease cleavage efficiency and make it virtually impossible to delete all the copies. To complicate matters, cancer cells in culture might acquire genomic CNVs that were not present in the starting material (Pollex & Hegele, 2007). K. J. Woodward et al. (2005) and J. A. Lee et al. (2006) proposed that one of the broken ends of a single DSB in one strand could invade and copy from the sister chromatid and result in duplication. This duplication might influence chromosomal topologies, which were found to control gene-editing outcomes by changing the balance between different DNA repair pathways that are recruited during DNA lesions occur (Janssen et al., 2019). Meanwhile, the lifetime of DSBs is poorly understood and may influence the choice of DNA repair pathways. The blocking lesions can be tolerated, and the gap repaired postreplicationally by specialized DNA polymerases performing translesion DNA

synthesis (Heyer, 2015). Therefore, potential crosstalk between RNP-induced DSBs, gene repair routes, and gene rearrangements was proposed in this study but remained to be determined. Similarly, the CNV of the *ABCC5* gene generated either endogenously in wild-type cells or exogenously by RNPs might induce chromatin conformational changes and thus influence repair route choices. Whether the RNP-induced DSB in one strand of *ABCC5* gene could be repaired precisely according to the other allele *via* repair routes other than NHEJ, such as HDR and MMEJ, was of interest to be explored.

Furthermore, the screening of KO clones in present study was limited to the immediate vicinity of the cleavage site and loss-of-function screens. There was a possibility that clones with Cas9-induced large-scale gene rearrangements, chromosomal translocations and gene inversions were misclassified as wild-type despite the fact that ABCC5 expression in these cases might not be affected. Similarly, whether the indel allele in some clones was lost due to loss of heterozygosity (LOH), a common genetic event in cancer cells (Thiagalingam et al., 2001), remained to be investigated.

In addition, the production of truncated protein isoforms due to translation reinitiation or skipping of the edited exon might result in failure in generating KO cell lines. These truncated protein isoforms could remain cellular function and presumably involve other unknown roles, as we previously reviewed (He et al., 2021). The genetically validated homozygous MCF7 *ABCC5* KO clone 28E was still detected with ABCC5 expression, probably due to this phenomenon. However, the amino acids encoded by the deleted DNA sequence overlapped with the target epitope sequence of the ABCC5 primary antibody used in this study. Theoretically, the ABCC5 primary antibody could not bind to homozygous KO clones that lack the DNA sequence encoding the target epitope. Whether this phenomenon is a result of cross-reactions or other unknown mechanisms

remained to be elucidated.

Additionally, in homozygous *SPAG5* gene KO cell models, a “T” insertion seemed to be a prevalent genotype in the allele repaired by NHEJ, irrespective of gRNA and cell lines. Whether this phenomenon is related to the potential crosstalk between DNA repair pathways and gene rearrangements remained to be explored.

Further, a question with regard to increasing HDR efficiency is that to what extent DSBs are repaired through exogenous donor templates instead of through sister chromatid or homologous chromosomes. How exogenous donor template competes with sister chromatid or homologous chromosome during HDR and whether there is a threshold remained to be investigated. Also, it is unknown that whether the allele repaired by HDR in diploid cells is randomly selected or selected based on some rules.

Also, when screening homozygous *SPAG5* gene KO clones, only around one-tenth of the survived clones after antibiotic selection were validated with on-target editing, no matter in the 1st or 2nd round of KO. Nearly 90% of the survived clones were false-positive without editing in the target *SPAG5* gene. This might be caused by the random integration of donor plasmids into the genome, which provided antibiotic resistance to these clones. Nevertheless, whether or not the formation of noise RNA-Cas9 complexes (Mekler et al., 2016) could induce off-target effects in the KO cells in present study remained to be examined.

7.2.3 Future Directions for CRISPR-Cas9 Technology

Based on the limitations presented in the section above, some reasonable and feasible improvements were concluded.

Firstly, in consideration of the potential CNVs of the target gene and the considerable impact of CNVs on gene KO study, future attempts to establish gene KO cell lines may start with examining CNV using technologies, such as Microarray, Next Generation Sequencing (NGS), Fluorescence In Situ Hybridization (FISH), Southern Blotting and qPCR.

Secondly, a comprehensive database and molecular modelling tool involve the chromosomal state of the target gene, the loci of the target DNA sequence in the nucleosome, genomic CNV map is in urgent demand.

Thirdly, to improve KO efficiency, future gene KO studies may employ chromatin remodelling agents (e.g., programmable trans-activators, histone deacetylase inhibitors, and DNA methyltransferase inhibitors) to modify the chromosomal state. Similarly, siRNA-mediated inhibition against the silencing protein SuZ12 relating to heterochromatin may represent a reliable strategy to enhance Cas9 function (Daer et al., 2017). An increase in the amount of sgRNA and Cas9 protein and a prolonged transfection time course may also help improve cleavage efficiency.

Fourthly, the screening of KO clones in present study was limited to the immediate vicinity of the cleavage site and loss-of-function screens. These methods are unable to examine large-scale gene rearrangements, chromosomal translocations, gene inversions and production of truncated protein isoforms due to translation reinitiation or skipping of the edited exon. Thus, future gene KO studies may recruit high-throughput and high-fidelity large-scale gene and protein screening methods, such as Next Generation Sequencing (NGS) and high-resolution mass spectrometry (LC-MS/MS). But these methods were limited by their cost-effectiveness.

Sixthly, to generate homozygous KO cells with biallelic integration of donor template,

future studies may start with examining the common germline mutations of HDR-related genes that influence the integration of donor templates, such as *BRCA1/2*, as we previously reviewed (He et al., 2020). Similarly, future studies may introduce chemical or genetic inhibition of NHEJ and activation of HDR to enhance HDR signalling during transfection (Devkota, 2018). Also, manipulation of cell cycle and stimulation of DSB end resection by mediating the related protein activity may collectively improve the outcomes. But the cytotoxicity of these agents needs to be considered. Alternatively, covalent linkage of the donor DNA template to Cas9 complex was found to increase HDR efficiency for up to 24-fold through an increase of donor template concentration in the nucleus (Savic et al., 2018). The single-stranded oligodeoxyribonucleotides (ODNs) might also represent a promising donor template, which exhibited a higher frequency of HDR at euchromatin (Janssen et al., 2019).

Seventhly, data in the present study suggested that the current CRISPR-Cas9 systems might not be suitable for clinical use considering the unacceptable off-target effects. Any mutations in off-target sites may cause irreparable damage and thus poor clinical outcomes.

7.3 Collateral Sensitivity to Olaparib Associated with ABCC5 in TNBC Cells

The most essential and brilliant finding of this research was the ABCC5-associated collateral sensitivity to olaparib, which was confirmed in both ABCC5-overexpressing HEK293 and *ABCC5* gene KO cell models. Cell accumulation studies based on HEK-MRP5 cells suggested that olaparib was not a substrate nor an inhibitor of ABCC5. Although ABCC5 inhibitor benzbromarone could not reverse the sensitive phenotype

of HEK-MRP5 cells to olaparib, HEK-MRP5 cells were about 3.4-fold more sensitive to olaparib-induced growth inhibition compared to HEK-P cells. This collateral sensitivity of olaparib against ABCC5-rich HEK-MRP5 cells was compared with ABCC5 substrate drug pemetrexed-induced growth inhibition. The sensitivity of HEK-MRP5 cells to pemetrexed was 2.3-fold less than the parental line. In heterozygous *ABCC5* gene KO MDA-MB-231 and BT549 cell models, olaparib-induced growth inhibition was about 2-fold greater in MDA-MB-231 and BT549 WT cells than heterozygous KO clones. Notably, the above cell models may be limited by off-target effects-induced genetic or epigenetic changes and single-cell variability. The potential genetic or epigenetic changes and single-cell variability could result in various expressions of olaparib-resistance-related protein networks in different cell strains and even in different clones of a given cell line. This variation in transcriptome thus led to different findings.

The mechanisms underlying the ABCC5-related collateral sensitivity to olaparib was unknown. Some potential speculations were concluded as follow. First, molecular docking analysis in the present study suggested that ABCC5 might directly bind and interact with olaparib. These interactions might then mediate some cell survival signalling pathways. Second, the elevated ABCC5 expression in ABCC5-rich cells might induce hyperactivation or overexpression of a set of transcriptional activators. Rather than targeting ABCC5, olaparib might interact with the proteins in this network and make ABCC5-rich cells more sensitive to olaparib. Third, the metabolites of olaparib might play a role in the altered sensitivity of ABCC5-rich cells to olaparib. Olaparib was mainly metabolised by the action of CYP3A4/5 enzymes, which was detected to express in normal kidney (Murray et al., 1999) and a considerable portion of breast cancer tissues (van Eijk et al., 2019). The cell lines used in this study were just

isolated from these tissues. Although it was not assessed in the present study, the potential CYP3A4/5 expression might accelerate intracellular olaparib metabolism within the given time course and exerted an impact on ABCC5-rich cells. But unfortunately, the pharmacodynamic activity of olaparib metabolites is unknown.

Besides, a synergistic effect was found between doxorubicin and olaparib in MDA-MB-231, BT549 and MCF7 breast cancer cells. In other words, doxorubicin might improve the collateral sensitivity of olaparib against ABCC5-rich cells. The potential mechanisms were concluded as follow. First, the blocked PARP function by olaparib might partially prevent doxorubicin-induced DNA damage from getting repaired and thus cause cell apoptosis. Second, olaparib might enhance the cellular accumulation of doxorubicin by inhibiting ABCB1 and ABCG2. However, doxorubicin-induced cell death was reported to rely on the hyperactivation of PARP1-induced autophagy and necrosis (Tacar et al., 2013). Therefore, in the presence of PARP inhibitor olaparib, to what extent the blocked PARP activity influences the potency of doxorubicin remained to be investigated. Whether the blocked PARP activity-induced decreased doxorubicin potency was compensated by ABCC5-associated collateral sensitivity was of interest to be explored.

7.4 Future Directions for Collateral Sensitivity to Olaparib

The above findings suggested that ABCC5 might be a promising biomarker for breast carcinoma and a target to overcome drug resistance in breast cancer cells by being a protein associated with collateral sensitivity. A broader and better understanding of the functions and roles of ABCC5 in breast cancer biology will potentially contribute to stratifying patients for precision regimens and promote the development of novel

therapies. This study failed to include more functional studies to help fully understand the molecular mechanisms underlying ABCC5-associated collateral sensitivity due to COVID-19 pandemic and lockdown restrictions.

Therefore, future research is warranted to involve an in-depth pharmacological study to fully investigate the role of ABCC5 in the collateral sensitivity of olaparib using both ABCC5-overexpressing HEK293 and *ABCC5* gene KO cell models. Assays that need to be carried out include LC-MS/MS, qRT-PCR assay, cell proliferation MTT assay, apoptotic cell death assay, cell cycle assay, wound healing assay, transwell assay, colony formation assay and *in vitro* tumour growth in 3D Matrigel. To be specific, LC-MS/MS helps to determine the cellular accumulation of olaparib in gene KO cell models, given that olaparib has no autofluorescence. qRT-PCR examines the expression of *ABCC5* and its potential downstream effecters at transcription level. Cell cycle assay examines the influence of olaparib and ABCC5 on mitosis. Wound healing assay, transwell assay and colony formation assay are used to determine the role of olaparib and ABCC5 in cell motility, migration, invasion and clonogenicity. Furthermore, future research should also focus on the modulation of ABCC5 in breast tumour xenograft mouse models. This can be established by injecting WT breast cancer cells and *ABCC5* gene KO/KD cells, respectively. These mouse models provide valuable *in vivo* data concerning the pharmacodynamics of olaparib and/or drug combinations.

7.5 Final Conclusions

In conclusion, the experimental work described in this thesis has demonstrated that ABCC5 is associated with the collateral sensitivity to a novel drug olaparib in TNBC cells. Our studies have provided *in vitro* evidence that olaparib may be not only a PARP

inhibitor but also an agent selectively targeting ABCC5. The clinical inhibition of ABC transporter to overcome MDR has been disappointing, as we previously reviewed (He et al., 2021). However, given that ABCC5 overexpression is a feature of breast cancer stem cells contributing to chemotherapeutic resistance in breast cancers (Zhu et al, 2011), the *in vitro* evidence in the present study suggests ABC transporters, especially ABCC5, could be exploited as a promising biomarker for breast carcinoma and a target to overcome MDR in breast cancer patients. Better understanding of the roles of ABCC5 and its associated signalling pathways in evolutionary breast cancer hallmarks may facilitate the design and discovery of highly selective and potent CS agents. Together with genomic profiling-based patient stratification, we propose such novel therapeutics could prevent and/or reverse MDR in patients with breast cancers.

Publications Arising from This Thesis

1. He, J., Green, A. R., Li, Y., Chan, S., & Liu, D. X. (2020). SPAG5: An Emerging Oncogene. *Trends in cancer*, *6*(7), 543–547. https://doi.org/10.1016/j.trecan.2020.03.006.
2. He, J., Fortunati, E., Liu, D. X., & Li, Y. (2021). Pleiotropic Roles of ABC Transporters in Breast Cancer. *International journal of molecular sciences*, *22*(6), 3199. https://doi.org/10.3390/ijms22063199.
3. He, J., Biswas, R., Bugde, P., Li, J., Liu, D. X., & Li, Y. (2022). Application of CRISPR-Cas9 system to study biological barriers to drug delivery. *Pharmaceutics*.

Reference

Adasme, M. F., Linnemann, K. L., Bolz, S. N., Kaiser, F., Salentin, S., Haupt, V. J., & Schroeder, M. (2021). PLIP 2021: expanding the scope of the protein-ligand interaction profiler to DNA and RNA. *Nucleic Acids Res, 49*(W1), W530-W534. doi:10.1093/nar/gkab294

Al-Eitan, L. N., Rababa'h, D. M., Alghamdi, M. A., & Khasawneh, R. H. (2019). Role of Four ABC Transporter Genes in Pharmacogenetic Susceptibility to Breast Cancer in Jordanian Patients. *J Oncol, 2019*, 6425708. doi:10.1155/2019/6425708

Allikmets, R., Gerrard, B., Hutchinson, A., & Dean, M. (1996). Characterization of the human ABC superfamily: isolation and mapping of 21 new genes using the expressed sequence tags database. *Hum Mol Genet, 5*(10), 1649-1655.

Ambudkar, S. V., Dey, S., Hrycyna, C. A., Ramachandra, M., Pastan, I., & Gottesman, M. M. (1999). Biochemical, cellular, and pharmacological aspects of the multidrug transporter. *Annual review of pharmacology and toxicology, 39*(1), 361-398.

Ambudkar, S. V., Kimchi-Sarfaty, C., Sauna, Z. E., & Gottesman, M. M. (2003). P-glycoprotein: from genomics to mechanism. *Oncogene, 22*(47), 7468. doi:DOI: 10.1038/sj.onc.1206948

American Cancer Society. (2013). Breast Cancer Survival Rates Retrieved from https://www.cancer.org/cancer/breast-cancer/understanding-a-breast-cancer-diagnosis/breast-cancer-survival-rates.html

Ames, B. N., Shigenaga, M. K., & Hagen, T. M. (1993). Oxidants, antioxidants, and the degenerative diseases of aging. *Proceedings of the National Academy of Sciences, 90*(17), 7915-7922.

Anders, C. K., & Carey, L. A. (2009). Biology, metastatic patterns, and treatment of patients with triple-negative breast cancer. *Clinical breast cancer, 9*, S73-S81.

Andreopoulou, E., Kelly, C. M., & McDaid, H. M. (2017). Therapeutic Advances and New Directions for Triple-Negative Breast Cancer. *Breast Care (Basel), 12*(1), 21-28. doi:10.1159/000455821

Ashley, N., & Poulton, J. (2009). Mitochondrial DNA is a direct target of anti-cancer anthracycline drugs. *Biochem Biophys Res Commun, 378*(3), 450-455. doi:10.1016/j.bbrc.2008.11.059

Auner, V., Sehouli, J., Oskay-Oezcelik, G., Horvat, R., Speiser, P., & Zeillinger, R. (2010). ABC transporter gene expression in benign and malignant ovarian tissue. *Gynecologic Oncology, 117*(2), 198-201. doi:10.1016/j.ygyno.2009.10.077

Balaji, S. A., Udupa, N., Chamallamudi, M. R., Gupta, V., & Rangarajan, A. (2016). Role of the Drug Transporter ABCC3 in Breast Cancer Chemoresistance. *PLoS One, 11*(5), e0155013. doi:DOI: 10.1371/journal.pone.0155013

Baltimore, D., Berg, P., Botchan, M., Carroll, D., Charo, R. A., Church, G., . . . Fenner, M. (2015). A prudent path forward for genomic engineering and germline gene modification. *Science, 348*(6230), 36-38.

Barrangou, R., Fremaux, C., Deveau, H., Richards, M., Boyaval, P., Moineau, S., . . . Horvath, P. (2007). CRISPR provides acquired resistance against viruses in

prokaryotes. *Science, 315*(5819), 1709-1712.
Beroukhim, R., Mermel, C. H., Porter, D., Wei, G., Raychaudhuri, S., Donovan, J., . . . Meyerson, M. (2010). The landscape of somatic copy-number alteration across human cancers. *Nature, 463*(7283), 899-905. doi:10.1038/nature08822
Bhaya, D., Davison, M., & Barrangou, R. (2011). CRISPR-Cas systems in bacteria and archaea: versatile small RNAs for adaptive defense and regulation. *Annual review of genetics, 45*, 273-297.
Binda, C. S., Klaver, B., Berkhout, B., & Das, A. T. (2020). CRISPR-Cas9 Dual-gRNA Attack Causes Mutation, Excision and Inversion of the HIV-1 Proviral DNA. *Viruses, 12*(3). doi:10.3390/v12030330
Biswas, R., Bugde, P., He, J., Merien, F., Lu, J., Liu, D. X., . . . Li, Y. (2019). Transport-Mediated Oxaliplatin Resistance Associated with Endogenous Overexpression of MRP2 in Caco-2 and PANC-1 Cells. *Cancers (Basel), 11*(9). doi:10.3390/cancers11091330
Blake, A., Dragan, M., Tirona, R. G., Hardy, D. B., Brackstone, M., Tuck, A. B., . . . Bhattacharya, M. (2017). G protein-coupled KISS1 receptor is overexpressed in triple negative breast cancer and promotes drug resistance. *Sci Rep, 7*.
Bodley, A., Liu, L. F., Israel, M., Seshadri, R., Koseki, Y., Giuliani, F. C., . . . Potmesil, M. (1989). DNA topoisomerase II-mediated interaction of doxorubicin and daunorubicin congeners with DNA. *Cancer research, 49*(21), 5969-5978.
Borst, P., de Wolf, C., & van de Wetering, K. (2007). Multidrug resistance-associated proteins 3, 4, and 5. *Pflugers Arch, 453*(5), 661-673. doi:10.1007/s00424-006-0054-9
Borst, P., Evers, R., Kool, M., & Wijnholds, J. (1999). The multidrug resistance protein family. *Biochimica et Biophysica Acta (BBA)-Biomembranes, 1461*(2), 347-357.
Borst, P., Evers, R., Kool, M., & Wijnholds, J. (2000). A family of drug transporters: the multidrug resistance-associated proteins. *Journal Of The National Cancer Institute, 92*(16), 1295-1302.
Bosch, I., & Croop, J. (1996). P-glycoprotein multidrug resistance and cancer. *Biochimica et Biophysica Acta (BBA)-Reviews on Cancer, 1288*(2), F37-F54.
Braasch, D. A., Jensen, S., Liu, Y., Kaur, K., Arar, K., White, M. A., & Corey, D. R. (2003). RNA interference in mammalian cells by chemically-modified RNA. *Biochemistry, 42*(26), 7967-7975.
Brenton, J. D., Carey, L. A., Ahmed, A. A., & Caldas, C. (2005). Molecular classification and molecular forecasting of breast cancer: ready for clinical application? *Journal of clinical oncology, 23*(29), 7350-7360.
Büchler, M., König, J., Brom, M., Kartenbeck, J., Spring, H., Horie, T., & Keppler, D. (1996). cDNA cloning of the hepatocyte canalicular isoform of the multidrug resistance protein, cMrp, reveals a novel conjugate export pump deficient in hyperbilirubinemic mutant rats. *Journal of Biological Chemistry, 271*(25), 15091-15098.
Bugde, P., Biswas, R., Merien, F., Lu, J., Liu, D.-X., Chen, M., . . . Li, Y. (2017). The therapeutic potential of targeting ABC transporters to combat multi-drug resistance. *Expert opinion on therapeutic targets, 21*(5), 511-530.
Burger, H., Foekens, J. A., Look, M. P., Meijer-van Gelder, M. E., Klijn, J. G., Wiemer, E. A., . . . Nooter, K. (2003). RNA expression of breast cancer resistance protein, lung resistance-related protein, multidrug resistance-associated proteins 1 and 2, and multidrug resistance gene 1 in breast cancer: correlation with chemotherapeutic response. *Clin Cancer Res, 9*(2), 827-836.
Burgess, D. J., Doles, J., Zender, L., Xue, W., Ma, B., McCombie, W. R., . . . Hemann,

M. T. (2008). Topoisomerase levels determine chemotherapy response in vitro and in vivo. *Proc Natl Acad Sci U S A, 105*(26), 9053-9058. doi:10.1073/pnas.0803513105

Carroll, D. (2014). Genome engineering with targetable nucleases. *Annual review of biochemistry, 83*, 409-439.

Caulfield, S. E., Davis, C. C., & Byers, K. F. (2019). Olaparib: A Novel Therapy for Metastatic Breast Cancer in Patients With a BRCA1/2 Mutation. *J Adv Pract Oncol, 10*(2), 167-174.

Cervera, L., Gutiérrez, S., Gòdia, F., & Segura, M. M. (2011). Optimization of HEK 293 cell growth by addition of non-animal derived components using design of experiments. *BMC Proc, 5 Suppl 8*(Suppl 8), P126. doi:10.1186/1753-6561-5-s8-p126

Chen, B. W., Chen, W., Liang, H., Liu, H., Liang, C., Zhi, X., . . . Liang, T. B. (2015). Inhibition of mTORC2 Induces Cell-Cycle Arrest and Enhances the Cytotoxicity of Doxorubicin by Suppressing MDR1 Expression in HCC Cells. *Mol Cancer Ther, 14*(8), 1805-1815. doi:10.1158/1535-7163.Mct-15-0029

Chen, C.-j., Chin, J. E., Ueda, K., Clark, D. P., Pastan, I., Gottesman, M. M., & Roninson, I. B. (1986). Internal duplication and homology with bacterial transport proteins in the mdr1 (P-glycoprotein) gene from multidrug-resistant human cells. *Cell, 47*(3), 381-389.

Chen, F., Pruett-Miller, S. M., Huang, Y., Gjoka, M., Duda, K., Taunton, J., . . . Davis, G. D. (2011). High-frequency genome editing using ssDNA oligonucleotides with zinc-finger nucleases. *Nature methods, 8*(9), 753.

Chen, J., Wang, Z., Gao, S., Wu, K., Bai, F., Zhang, Q., . . . Liu, Y. (2021). Human drug efflux transporter ABCC5 confers acquired resistance to pemetrexed in breast cancer. *Cancer Cell Int, 21*(1), 136. doi:10.1186/s12935-021-01842-x

Chen, L., Gu, J., Xu, L., Qu, C., Zhang, Y., & Zhang, W. (2014). RNAi-mediated silencing of ATP-binding cassette C4 protein inhibits cell growth in MGC80-3 gastric cancer cell lines. *Cell Mol Biol (Noisy-le-grand), 60*(1), 1-5.

Chen, L., Manautou, J. E., Rasmussen, T. P., & Zhong, X. B. (2019). Development of precision medicine approaches based on inter-individual variability of BCRP/ABCG2. *Acta Pharm Sin B, 9*(4), 659-674. doi:10.1016/j.apsb.2019.01.007

Chen, S., Sanjana, N. E., Zheng, K., Shalem, O., Lee, K., Shi, X., . . . Weissleder, R. (2015). Genome-wide CRISPR screen in a mouse model of tumor growth and metastasis. *cell, 160*(6), 1246-1260.

Chen, Z., Liu, F., Ren, Q., Zhao, Q., Ren, H., Lu, S., . . . Han, Z. (2010). Suppression of ABCG2 inhibits cancer cell proliferation. *Int J Cancer, 126*(4), 841-851. doi:10.1002/ijc.24796

Chiu, Y.-L., & Rana, T. M. (2003). siRNA function in RNAi: a chemical modification analysis. *Rna, 9*(9), 1034-1048.

Choi, C.-H. (2005). ABC transporters as multidrug resistance mechanisms and the development of chemosensitizers for their reversal. *Cancer cell international, 5*(1), 30.

Choi, H. K., Yang, J. W., Roh, S. H., Han, C. Y., & Kang, K. W. (2007). Induction of multidrug resistance associated protein 2 in tamoxifen-resistant breast cancer cells. *Endocr Relat Cancer, 14*(2), 293-303. doi:10.1677/erc-06-0016

Chou, T. C. (2006). Theoretical basis, experimental design, and computerized simulation of synergism and antagonism in drug combination studies. *Pharmacol Rev, 58*(3), 621-681. doi:10.1124/pr.58.3.10

Cole, S., Bhardwaj, G., Gerlach, J., Mackie, J., Grant, C., Almquist, K., . . . Deeley, R. (1992). Overexpression of a transporter gene in a multidrug-resistant human lung cancer cell line. *Science, 258*(5088), 1650-1654.

Cole, S. P., Sparks, K. E., Fraser, K., Loe, D. W., Grant, C. E., Wilson, G. M., & Deeley, R. G. (1994). Pharmacological characterization of multidrug resistant MRP-transfected human tumor cells. *Cancer research, 54*(22), 5902-5910.

Colone, M., Calcabrini, A., Toccacieli, L., Bozzuto, G., Stringaro, A., Gentile, M., . . . Molinari, A. (2008). The multidrug transporter P-glycoprotein: a mediator of melanoma invasion? *J Invest Dermatol, 128*(4), 957-971. doi:10.1038/sj.jid.5701082

Cong, L., Ran, F. A., Cox, D., Lin, S., Barretto, R., Habib, N., . . . Marraffini, L. (2013). Multiplex genome engineering using CRISPR/Cas systems. *Science*, 1231143.

Cooray, H. C., Blackmore, C. G., Maskell, L., & Barrand, M. A. (2002). Localisation of breast cancer resistance protein in microvessel endothelium of human brain. *Neuroreport, 13*(16), 2059-2063.

Cordon-Cardo, C., O'brien, J., Boccia, J., Casals, D., Bertino, J., & Melamed, M. (1990). Expression of the multidrug resistance gene product (P-glycoprotein) in human normal and tumor tissues. *Journal of Histochemistry & Cytochemistry, 38*(9), 1277-1287.

Cordon-Cardo, C., O'Brien, J. P., Casals, D., Rittman-Grauer, L., Biedler, J. L., Melamed, M. R., & Bertino, J. R. (1989). Multidrug-resistance gene (P-glycoprotein) is expressed by endothelial cells at blood-brain barrier sites. *Proceedings of the National Academy of Sciences, 86*(2), 695-698.

Cortés-Funes, H., & Coronado, C. (2007). Role of anthracyclines in the era of targeted therapy. *Cardiovascular toxicology, 7*(2), 56-60.

Daer, R. M., Cutts, J. P., Brafman, D. A., & Haynes, K. A. (2017). The Impact of Chromatin Dynamics on Cas9-Mediated Genome Editing in Human Cells. *ACS Synth Biol, 6*(3), 428-438. doi:10.1021/acssynbio.5b00299

Dantzic, D., Noel, P., Merien, F., Liu, D.-X., Lu, J., Han, H., . . . Li, Y. (2018). The Effects of Synthetically Modified Natural Compounds on ABC Transporters. *Pharmaceutics, 10*(3), 127.

Davies, G., Lobanova, L., Dawicki, W., Groot, G., Gordon, J. R., Bowen, M., . . . Arnason, T. (2017). Metformin inhibits the development, and promotes the resensitization, of treatment-resistant breast cancer. *PLoS One, 12*(12), e0187191. doi:10.1371/journal.pone.0187191

De Laurentiis, M., Cancello, G., D'Agostino, D., Giuliano, M., Giordano, A., Montagna, E., . . . Silvestro, L. (2008). Taxane-based combinations as adjuvant chemotherapy of early breast cancer: a meta-analysis of randomized trials. *Journal of clinical oncology, 26*(1), 44-53.

Dean, M., Hamon, Y., & Chimini, G. (2001). The human ATP-binding cassette (ABC) transporter superfamily. *Journal of lipid research, 42*(7), 1007-1017.

Deeley, R. G., Westlake, C., & Cole, S. P. (2006). Transmembrane transport of endo- and xenobiotics by mammalian ATP-binding cassette multidrug resistance proteins. *Physiological reviews, 86*(3), 849-899.

Del Vecchio, S., Ciarmiello, A., Potena, M. I., Carriero, M. V., Mainolfi, C., Botti, G., . . . Tsuruo, T. (1997). In vivo detection of multidrug-resistant (MDR1) phenotype by technetium-99m sestamibi scan in untreated breast cancer patients. *European journal of nuclear medicine, 24*(2), 150-159.

Devkota, S. (2018). The road less traveled: strategies to enhance the frequency of homology-directed repair (HDR) for increased efficiency of CRISPR/Cas-

mediated transgenesis. *BMB Rep, 51*(9), 437-443.
Donner, M. G., & Keppler, D. (2001). Up-regulation of basolateral multidrug resistance protein 3 (Mrp3) in cholestatic rat liver. *Hepatology, 34*(2), 351-359. doi:10.1053/jhep.2001.26213
Doyle, L. A., & Ross, D. D. (2003). Multidrug resistance mediated by the breast cancer resistance protein BCRP (ABCG2). *Oncogene, 22*(47), 7340.
Doyle, L. A., Yang, W., Abruzzo, L. V., Krogmann, T., Gao, Y., Rishi, A. K., & Ross, D. D. (1998). A multidrug resistance transporter from human MCF-7 breast cancer cells. *Proceedings of the National Academy of Sciences, 95*(26), 15665-15670.
Durand, R. E., & Olive, P. L. (1981). Flow cytometry studies of intracellular adriamycin in single cells in vitro. *Cancer Res, 41*(9 Pt 1), 3489-3494.
Dziadkowiec, K. N., Gasiorowska, E., Nowak-Markwitz, E., & Jankowska, A. (2016). PARP inhibitors: review of mechanisms of action and BRCA1/2 mutation targeting. *Prz Menopauzalny, 15*(4), 215-219. doi:10.5114/pm.2016.65667
Eaton, S. L., Roche, S. L., Llavero Hurtado, M., Oldknow, K. J., Farquharson, C., Gillingwater, T. H., & Wishart, T. M. (2013). Total protein analysis as a reliable loading control for quantitative fluorescent Western blotting. *PLoS One, 8*(8), e72457. doi:10.1371/journal.pone.0072457
Eberwine, J., & Kim, J. (2015). Cellular Deconstruction: Finding Meaning in Individual Cell Variation. *Trends Cell Biol, 25*(10), 569-578. doi:10.1016/j.tcb.2015.07.004
Esser, L., Zhou, F., Pluchino, K. M., Shiloach, J., Ma, J., Tang, W.-k., . . . Madigan, J. P. (2017). Structures of the multidrug transporter P-glycoprotein reveal asymmetric ATP binding and the mechanism of polyspecificity. *Journal of Biological Chemistry, 292*(2), 446-461.
Evers, R., Zaman, G., van Deemter, L., Jansen, H., Calafat, J., Oomen, L., . . . Schinkel, A. H. (1996). Basolateral localization and export activity of the human multidrug resistance-associated protein in polarized pig kidney cells. *The Journal of clinical investigation, 97*(5), 1211-1218.
Faneyte, I. F., Kristel, P. M., & van de Vijver, M. J. (2004). Multidrug resistance associated genes MRP1, MRP2 and MRP3 in primary and anthracycline exposed breast cancer. *Anticancer Res, 24*(5a), 2931-2939.
Fletcher, J. I., Haber, M., Henderson, M. J., & Norris, M. D. (2010). ABC transporters in cancer: more than just drug efflux pumps. *Nat Rev Cancer, 10*(2), 147-156. doi:10.1038/nrc2789
Fletcher, J. I., Williams, R. T., Henderson, M. J., Norris, M. D., & Haber, M. (2016). ABC transporters as mediators of drug resistance and contributors to cancer cell biology. *Drug Resist Updat, 26*, 1-9. doi:10.1016/j.drup.2016.03.001
Fu, Y., Foden, J. A., Khayter, C., Maeder, M. L., Reyon, D., Joung, J. K., & Sander, J. D. (2013). High-frequency off-target mutagenesis induced by CRISPR-Cas nucleases in human cells. *Nature biotechnology, 31*(9), 822.
Gerlach, J., Kartner, N., Bell, D., & Ling, V. (1986). Multidrug resistance. *Cancer Surveys, 5*(1), 25-46.
Ghafouri, H., Ghaderi, B., Amini, S., Nikkhoo, B., Abdi, M., & Hoseini, A. (2016). Association of ABCB1 and ABCG2 single nucleotide polymorphisms with clinical findings and response to chemotherapy treatments in Kurdish patients with breast cancer. *Tumour Biol, 37*(6), 7901-7906. doi:10.1007/s13277-015-4679-1
Gottesman, M. M., Fojo, T., & Bates, S. E. (2002). Multidrug resistance in cancer: role

of ATP–dependent transporters. *Nature Reviews Cancer, 2*(1), 48.

Gros, P., CROoP, J., Roninson, I., Varshavsky, A., & Housman, D. E. (1986). Isolation and characterization of DNA sequences amplified in multidrug-resistant hamster cells. *Proceedings of the National Academy of Sciences, 83*(2), 337-341.

Gu, W., Zhang, F., & Lupski, J. R. (2008). Mechanisms for human genomic rearrangements. *Pathogenetics, 1*(1), 4. doi:10.1186/1755-8417-1-4

Gupta, S. K., Garg, A., Bar, C., Chatterjee, S., Foinquinos, A., Milting, H., . . . Thum, T. (2018). Quaking Inhibits Doxorubicin-Mediated Cardiotoxicity Through Regulation of Cardiac Circular RNA Expression. *Circ Res, 122*(2), 246-254. doi:10.1161/circresaha.117.311335

Hall, M. D., Handley, M. D., & Gottesman, M. M. (2009). Is resistance useless? Multidrug resistance and collateral sensitivity. *Trends Pharmacol Sci, 30*(10), 546-556. doi:DOI: 10.1016/j.tips.2009.07.003

He, J., Fortunati, E., Liu, D. X., & Li, Y. (2021). Pleiotropic Roles of ABC Transporters in Breast Cancer. *Int J Mol Sci, 22*(6). doi:10.3390/ijms22063199

He, J., Green, A. R., Li, Y., Chan, S. Y. T., & Liu, D. X. (2020). SPAG5: An Emerging Oncogene. *Trends Cancer*. doi:10.1016/j.trecan.2020.03.006

Henderson, M. J., Haber, M., Porro, A., Munoz, M. A., Iraci, N., Xue, C., . . . Norris, M. D. (2011). ABCC multidrug transporters in childhood neuroblastoma: clinical and biological effects independent of cytotoxic drug efflux. *J Natl Cancer Inst, 103*(16), 1236-1251. doi:10.1093/jnci/djr256

Heo, Y. A., & Dhillon, S. (2018). Olaparib Tablet: A Review in Ovarian Cancer Maintenance Therapy. *Target Oncol, 13*(6), 801-808. doi:10.1007/s11523-018-0606-x

Heyer, W. D. (2015). Regulation of recombination and genomic maintenance. *Cold Spring Harb Perspect Biol, 7*(8), a016501. doi:10.1101/cshperspect.a016501

Hlaváč, V., Brynychová, V., Václavíková, R., Ehrlichová, M., Vrána, D., Pecha, V., . . . Kopperová, D. (2013). The expression profile of ATP-binding cassette transporter genes in breast carcinoma. *Pharmacogenomics, 14*(5), 515-529. doi:DOI: 10.2217/pgs.13.26

Ho, L. L., Kench, J. G., Handelsman, D. J., Scheffer, G. L., Stricker, P. D., Grygiel, J. G., . . . Horvath, L. G. (2008). Androgen regulation of multidrug resistance-associated protein 4 (MRP4/ABCC4) in prostate cancer. *Prostate, 68*(13), 1421-1429. doi:10.1002/pros.20809

Hollenstein, K., Dawson, R. J., & Locher, K. P. (2007). Structure and mechanism of ABC transporter proteins. *Current opinion in structural biology, 17*(4), 412-418.

Holohan, C., Van Schaeybroeck, S., Longley, D. B., & Johnston, P. G. (2013). Cancer drug resistance: an evolving paradigm. *Nature Reviews Cancer, 13*(10), 714.

Howerton, S. B., Nagpal, A., & Dean Williams, L. (2003). Surprising roles of electrostatic interactions in DNA–ligand complexes. *Biopolymers: Original Research on Biomolecules, 69*(1), 87-99.

Hsu, P. D., Scott, D. A., Weinstein, J. A., Ran, F. A., Konermann, S., Agarwala, V., . . . Shalem, O. (2013). DNA targeting specificity of RNA-guided Cas9 nucleases. *Nature biotechnology, 31*(9), 827.

Hsu, P. D., Scott, D. A., Weinstein, J. A., Ran, F. A., Konermann, S., Agarwala, V., . . . Zhang, F. (2013). DNA targeting specificity of RNA-guided Cas9 nucleases. *Nat Biotechnol, 31*(9), 827-832. doi:10.1038/nbt.2647

Huang, J., Liu, K., Yu, Y., Xie, M., Kang, R., Vernon, P., . . . Ni, J. (2012). Targeting HMGB1-mediated autophagy as a novel therapeutic strategy for osteosarcoma. *Autophagy, 8*(2), 275-277. doi:10.4161/auto.8.2.18940

Iafrate, A. J., Feuk, L., Rivera, M. N., Listewnik, M. L., Donahoe, P. K., Qi, Y., . . . Lee, C. (2004). Detection of large-scale variation in the human genome. *Nat Genet, 36*(9), 949-951. doi:10.1038/ng1416

Ito, K., Olsen, S. L., Qiu, W., Deeley, R. G., & Cole, S. P. (2001). Mutation of a single conserved tryptophan in multidrug resistance protein 1 (MRP1/ABCC1) results in loss of drug resistance and selective loss of organic anion transport. *J Biol Chem, 276*(19), 15616-15624. doi:10.1074/jbc.M011246200

Janssen, J. M., Chen, X., Liu, J., & Goncalves, M. (2019). The Chromatin Structure of CRISPR-Cas9 Target DNA Controls the Balance between Mutagenic and Homology-Directed Gene-Editing Events. *Mol Ther Nucleic Acids, 16*, 141-154. doi:10.1016/j.omtn.2019.02.009

Jedlitschky, G., Cattaneo, M., Lubenow, L. E., Rosskopf, D., Lecchi, A., Artoni, A., . . . Greinacher, A. (2010). Role of MRP4 (ABCC4) in platelet adenine nucleotide-storage: evidence from patients with delta-storage pool deficiencies. *Am J Pathol, 176*(3), 1097-1103. doi:10.2353/ajpath.2010.090425

Jhan, J.-R., & Andrechek, E. R. (2017). Triple-negative breast cancer and the potential for targeted therapy. *Pharmacogenomics, 18*(17), 1595-1609.

Ji Yeon, Y., Seon-Ah, H., Yun-Sik, Y., & Jin Woo, K. (2010). p-Glycoprotein ABCB5 and YB-1 expression plays arole in increased heterogeneity of breast cancercells: correlations with cell fusion and doxorubicinresistance. *BMC Cancer, 10*, 388.

Jinek, M., Chylinski, K., Fonfara, I., Hauer, M., Doudna, J. A., & Charpentier, E. (2012). A programmable dual-RNA–guided DNA endonuclease in adaptive bacterial immunity. *Science*, 1225829.

Johnson, Z. L., & Chen, J. (2017). Structural basis of substrate recognition by the multidrug resistance protein MRP1. *Cell, 168*(6), 1075-1085. e1079. doi:DOI: 10.1016/j.cell.2017.01.041

Jonker, J. W., Merino, G., Musters, S., van Herwaarden, A. E., Bolscher, E., Wagenaar, E., . . . Schinkel, A. H. (2005). The breast cancer resistance protein BCRP (ABCG2) concentrates drugs and carcinogenic xenotoxins into milk. *Nat Med, 11*(2), 127-129. doi:10.1038/nm1186

Jonker, J. W., Smit, J. W., Brinkhuis, R. F., Maliepaard, M., Beijnen, J. H., Schellens, J. H., & Schinkel, A. H. (2000). Role of breast cancer resistance protein in the bioavailability and fetal penetration of topotecan. *Journal Of The National Cancer Institute, 92*(20), 1651-1656.

Juliano, R. L., & Ling, V. (1976). A surface glycoprotein modulating drug permeability in Chinese hamster ovary cell mutants. *Biochimica et Biophysica Acta (BBA)-Biomembranes, 455*(1), 152-162.

Kao, C.-H., Tsai, S.-C., Liu, T.-J., Ho, Y.-J., Wang, J.-J., Ho, S.-T., & ChangLai, S.-P. (2001). P-Glycoprotein and multidrug resistance-related protein expressions in relation to technetium-99m methoxyisobutylisonitrile scintimammography findings. *Cancer research, 61*(4), 1412-1414.

Karwatsky, J., Lincoln, M. C., & Georges, E. (2003). A mechanism for P-glycoprotein-mediated apoptosis as revealed by verapamil hypersensitivity. *Biochemistry, 42*(42), 12163-12173. doi:10.1021/bi034149+

Kataja, V., & Castiglione, M. (2008). Locally recurrent or metastatic breast cancer: ESMO clinical recommendations for diagnosis, treatment and follow-up. *Annals of oncology, 19*(suppl_2), ii11-ii13.

Katoh, S. Y., Ueno, M., & Takakura, N. (2008). Involvement of MDR1 function in proliferation of tumour cells. *J Biochem, 143*(4), 517-524. doi:10.1093/jb/mvm242

Kawamura, N., Nimura, K., Nagano, H., Yamaguchi, S., Nonomura, N., & Kaneda, Y. (2015). CRISPR/Cas9-mediated gene knockout of NANOG and NANOGP8 decreases the malignant potential of prostate cancer cells. *Oncotarget, 6*(26), 22361-22374. doi:10.18632/oncotarget.4293

Keppler, D., & Konig, J. (1997). Hepatic canalicular membrane 5: Expression and localization of the conjugate export pump encoded by the MRP2 (cMRP/cMOAT) gene in liver. *Faseb j, 11*(7), 509-516.

Khunweeraphong, N., Stockner, T., & Kuchler, K. (2017). The structure of the human ABC transporter ABCG2 reveals a novel mechanism for drug extrusion. *Sci Rep, 7*(1), 13767. doi:10.1038/s41598-017-11794-w

Kiyomiya, K.-i., Matsuo, S., & Kurebe, M. (2001). Mechanism of specific nuclear transport of adriamycin: the mode of nuclear translocation of adriamycin-proteasome complex. *Cancer research, 61*(6), 2467-2471.

Kiyotani, K., Mushiroda, T., Imamura, C. K., Hosono, N., Tsunoda, T., Kubo, M., . . . Zembutsu, H. (2010). Significant effect of polymorphisms in CYP2D6 and ABCC2 on clinical outcomes of adjuvant tamoxifen therapy for breast cancer patients. *J Clin Oncol, 28*(8), 1287-1293. doi:10.1200/jco.2009.25.7246

Kobayashi, K., Kajiwara, E., Ishikawa, M., Mimura, H., Oka, H., Ejiri, Y., . . . Chiba, K. (2013). Cytotoxic effects of benzbromarone and its 1'-hydroxy metabolite in human hepatocarcinoma FLC4 cells cultured on micro-space cell culture plates. *Drug Metab Pharmacokinet, 28*(3), 265-268. doi:10.2133/dmpk.dmpk-12-nt-105

Kolber, M. A., Quinones, R. R., Gress, R. E., & Henkert, P. A. (1988). Measurement of cytotoxicity by target cell release and retention of the fluorescent dye bis-carboxyethyl-carboxyfluorescein (BCECF). *Journal of immunological methods, 108*(1-2), 255-264.

Konig, J., Nies, A. T., Cui, Y., Leier, I., & Keppler, D. (1999). Conjugate export pumps of the multidrug resistance protein (MRP) family: localization, substrate specificity, and MRP2-mediated drug resistance. *Biochim Biophys Acta, 1461*(2), 377-394.

König, J., Nies, A. T., Cui, Y., Leier, I., & Keppler, D. (1999). Conjugate export pumps of the multidrug resistance protein (MRP) family: localization, substrate specificity, and MRP2-mediated drug resistance. *Biochimica et Biophysica Acta (BBA)-Biomembranes, 1461*(2), 377-394.

Kool, M., de Haas, M., Scheffer, G. L., Scheper, R. J., van Eijk, M. J., Juijn, J. A., . . . Borst, P. (1997). Analysis of expression of cMOAT (MRP2), MRP3, MRP4, and MRP5, homologues of the multidrug resistance-associated protein gene (MRP1), in human cancer cell lines. *Cancer research, 57*(16), 3537-3547.

Kool, M., van der Linden, M., de Haas, M., Scheffer, G. L., de Vree, J. M., Smith, A. J., . . . Borst, P. (1999). MRP3, an organic anion transporter able to transport anti-cancer drugs. *Proc Natl Acad Sci U S A, 96*(12), 6914-6919.

Kosicki, M., Tomberg, K., & Bradley, A. (2018). Repair of double-strand breaks induced by CRISPR–Cas9 leads to large deletions and complex rearrangements. *Nature biotechnology*.

Kruh, G. D., & Belinsky, M. G. (2003). The MRP family of drug efflux pumps. *Oncogene, 22*(47), 7537.

Kruijtzer, C. M., Beijnen, J. H., Rosing, H., ten Bokkel Huinink, W. W., Schot, M., Jewell, R. C., . . . Schellens, J. H. (2002). Increased oral bioavailability of topotecan in combination with the breast cancer resistance protein and P-glycoprotein inhibitor GF120918. *J Clin Oncol, 20*(13), 2943-2950.

doi:10.1200/jco.2002.12.116

Kumaran, M., Cass, C. E., Graham, K., Mackey, J. R., Hubaux, R., Lam, W., . . . Damaraju, S. (2017). Germline copy number variations are associated with breast cancer risk and prognosis. *Sci Rep, 7*(1), 14621. doi:10.1038/s41598-017-14799-7

Kuscu, C., Arslan, S., Singh, R., Thorpe, J., & Adli, M. (2014). Genome-wide analysis reveals characteristics of off-target sites bound by the Cas9 endonuclease. *Nature biotechnology, 32*(7), 677.

Kuss, B. J., Corbo, M., Lau, W. M., Fennell, D. A., Dean, N. M., & Cotter, F. E. (2002). In vitro and in vivo downregulation of MRP1 by antisense oligonucleotides: a potential role in neuroblastoma therapy. *Int J Cancer, 98*(1), 128-133.

Lal, S., Mahajan, A., Chen, W. N., & Chowbay, B. (2010). Pharmacogenetics of target genes across doxorubicin disposition pathway: a review. *Curr Drug Metab, 11*(1), 115-128. doi:10.2174/138920010791110890

Lal, S., Sutiman, N., Ooi, L. L., Wong, Z. W., Wong, N. S., Ang, P. C. S., & Chowbay, B. (2017). Pharmacogenetics of ABCB5, ABCC5 and RLIP76 and doxorubicin pharmacokinetics in Asian breast cancer patients. *Pharmacogenomics J, 17*(4), 337-343. doi:10.1038/tpj.2016.17

Lal, S., Wong, Z. W., Sandanaraj, E., Xiang, X., Ang, P. C., Lee, E. J., & Chowbay, B. (2008). Influence of ABCB1 and ABCG2 polymorphisms on doxorubicin disposition in Asian breast cancer patients. *Cancer Sci, 99*(4), 816-823. doi:10.1111/j.1349-7006.2008.00744.x

Lang, T., Hitzl, M., Burk, O., Mornhinweg, E., Keil, A., Kerb, R., . . . Fromm, M. F. (2004). Genetic polymorphisms in the multidrug resistance-associated protein 3 (ABCC3, MRP3) gene and relationship to its mRNA and protein expression in human liver. *Pharmacogenetics, 14*(3), 155-164.

Lee, J. A., Inoue, K., Cheung, S. W., Shaw, C. A., Stankiewicz, P., & Lupski, J. R. (2006). Role of genomic architecture in PLP1 duplication causing Pelizaeus-Merzbacher disease. *Hum Mol Genet, 15*(14), 2250-2265. doi:10.1093/hmg/ddl150

Lee, K., Klein-Szanto, A. J., & Kruh, G. D. (2000). Analysis of the MRP4 drug resistance profile in transfected NIH3T3 cells. *J Natl Cancer Inst, 92*(23), 1934-1940.

Leggas, M., Adachi, M., Scheffer, G. L., Sun, D., Wielinga, P., Du, G., . . . Schuetz, J. D. (2004). Mrp4 confers resistance to topotecan and protects the brain from chemotherapy. *Mol Cell Biol, 24*(17), 7612-7621. doi:10.1128/mcb.24.17.7612-7621.2004

Leier, I., Jedlitschky, G., Buchholz, U., Cole, S., Deeley, R. G., & Keppler, D. (1994). The MRP gene encodes an ATP-dependent export pump for leukotriene C4 and structurally related conjugates. *Journal of Biological Chemistry, 269*(45), 27807-27810.

Levy, B., Hoffmann, E. R., McCoy, R. C., & Grati, F. R. (2021). Chromosomal mosaicism: Origins and clinical implications in preimplantation and prenatal diagnosis. *Prenat Diagn, 41*(5), 631-641. doi:10.1002/pd.5931

Li, J., Xu, L. Z., He, K. L., Guo, W. J., Zheng, Y. H., Xia, P., & Chen, Y. (2001). Reversal effects of nomegestrol acetate on multidrug resistance in adriamycin-resistant MCF7 breast cancer cell line. *Breast Cancer Res, 3*(4), 253-263.

Li, W., Jia, M., Qin, X., Hu, J., Zhang, X., & Zhou, G. (2013). Harmful effect of ERbeta on BCRP-mediated drug resistance and cell proliferation in ERalpha/PR-negative breast cancer. *Febs j, 280*(23), 6128-6140. doi:10.1111/febs.12533

Li, Y., Revalde, J. L., Reid, G., & Paxton, J. W. (2011). Modulatory effects of curcumin on multi-drug resistance-associated protein 5 in pancreatic cancer cells. *Cancer Chemother Pharmacol, 68*(3), 603-610. doi:10.1007/s00280-010-1515-6

Liang, X., Potter, J., Kumar, S., Zou, Y., Quintanilla, R., Sridharan, M., . . . Chesnut, J. D. (2015). Rapid and highly efficient mammalian cell engineering via Cas9 protein transfection. *J Biotechnol, 208*, 44-53. doi:10.1016/j.jbiotec.2015.04.024

Lieber, M. R., Gu, J., Lu, H., Shimazaki, N., & Tsai, A. G. (2010). Nonhomologous DNA end joining (NHEJ) and chromosomal translocations in humans. *Subcell Biochem, 50*, 279-296. doi:10.1007/978-90-481-3471-7_14

Liedtke, C., Mazouni, C., Hess, K. R., André, F., Tordai, A., Mejia, J. A., . . . Green, M. (2008). Response to neoadjuvant therapy and long-term survival in patients with triple-negative breast cancer. *Journal of clinical oncology, 26*(8), 1275-1281.

Lin, S., Staahl, B. T., Alla, R. K., & Doudna, J. A. (2014). Enhanced homology-directed human genome engineering by controlled timing of CRISPR/Cas9 delivery. *Elife, 3*.

Lipscomb, L. A., Peek, M. E., Zhou, F. X., Bertrand, J. A., VanDerveer, D., & Williams, L. D. (1994). Water ring structure at DNA interfaces: hydration and dynamics of DNA-anthracycline complexes. *Biochemistry, 33*(12), 3649-3659.

Liu, X., Homma, A., Sayadi, J., Yang, S., Ohashi, J., & Takumi, T. (2016). Sequence features associated with the cleavage efficiency of CRISPR/Cas9 system. *Sci Rep, 6*, 19675. doi:10.1038/srep19675

Liu, Y., Huber, R. M., Kiefl, R., Tufman, A., & Kauffmann-Guerrero, D. (2020). Hedgehog Pathway Activation Might Mediate Pemetrexed Resistance in NSCLC Cells. *Anticancer Res, 40*(3), 1451-1458. doi:10.21873/anticanres.14087

Liu, Y., Peng, H., & Zhang, J. T. (2005). Expression profiling of ABC transporters in a drug-resistant breast cancer cell line using AmpArray. In (Vol. 68, pp. 430-438).

Liu, Y. Y., Hill, R. A., & Li, Y. T. (2013). Ceramide glycosylation catalyzed by glucosylceramide synthase and cancer drug resistance. *Adv Cancer Res, 117*, 59-89. doi:10.1016/b978-0-12-394274-6.00003-0

Liu, Y. Y., Yu, J. Y., Yin, D., Patwardhan, G. A., Gupta, V., Hirabayashi, Y., . . . Cabot, M. C. (2008). A role for ceramide in driving cancer cell resistance to doxorubicin. *Faseb j, 22*(7), 2541-2551. doi:10.1096/fj.07-092981

Loe, D. W., Almquist, K. C., Cole, S. P., & Deeley, R. G. (1996). ATP-dependent 17-Estradiol 17-(-D-Glucuronide) Transport by Multidrug Resistance Protein (MRP) INHIBITION BY CHOLESTATIC STEROIDS. *Journal of Biological Chemistry, 271*(16), 9683-9689.

Loe, D. W., Deeley, R. G., & Cole, S. P. (1998). Characterization of vincristine transport by the Mr 190,000 multidrug resistance protein (MRP): evidence for cotransport with reduced glutathione. *Cancer research, 58*(22), 5130-5136.

Loi, S., Pommey, S., Haibe-Kains, B., Beavis, P. A., Darcy, P. K., Smyth, M. J., & Stagg, J. (2013). CD73 promotes anthracycline resistance and poor prognosis in triple negative breast cancer. *Proc Natl Acad Sci U S A, 110*(27), 11091-11096. doi:10.1073/pnas.1222251110

Maciejczyk, A., Jagoda, E., Wysocka, T., Matkowski, R., Gyorffy, B., Lage, H., & Surowiak, P. (2012). ABCC2 (MRP2, cMOAT) localized in the nuclear envelope of breast carcinoma cells correlates with poor clinical outcome. *Pathol Oncol Res, 18*(2), 331-342. doi:10.1007/s12253-011-9449-9

Makarova, K. S., Haft, D. H., Barrangou, R., Brouns, S. J., Charpentier, E., Horvath,

P., . . . Yakunin, A. F. (2011). Evolution and classification of the CRISPR–Cas systems. *Nature Reviews Microbiology, 9*(6), 467.

Mali, P., Yang, L., Esvelt, K. M., Aach, J., Guell, M., DiCarlo, J. E., . . . Church, G. M. (2013). RNA-guided human genome engineering via Cas9. *Science, 339*(6121), 823-826.

Maliepaard, M., Scheffer, G. L., Faneyte, I. F., van Gastelen, M. A., Pijnenborg, A. C., Schinkel, A. H., . . . Schellens, J. H. (2001). Subcellular localization and distribution of the breast cancer resistance protein transporter in normal human tissues. *Cancer research, 61*(8), 3458-3464.

Mao, Q., & Unadkat, J. D. (2015). Role of the breast cancer resistance protein (BCRP/ABCG2) in drug transport—an update. *The AAPS journal, 17*(1), 65-82.

Mao, Z., Bozzella, M., Seluanov, A., & Gorbunova, V. (2008). DNA repair by nonhomologous end joining and homologous recombination during cell cycle in human cells. *Cell Cycle, 7*(18), 2902-2906. doi:10.4161/cc.7.18.6679

Mateo, J., Moreno, V., Gupta, A., Kaye, S. B., Dean, E., Middleton, M. R., . . . Molife, L. R. (2016). An Adaptive Study to Determine the Optimal Dose of the Tablet Formulation of the PARP Inhibitor Olaparib. *Target Oncol, 11*(3), 401-415. doi:10.1007/s11523-016-0435-8

Matys, V., Fricke, E., Geffers, R., Gößling, E., Haubrock, M., Hehl, R., . . . Kel-Margoulis, O. V. (2003). TRANSFAC®: transcriptional regulation, from patterns to profiles. *Nucleic acids research, 31*(1), 374-378.

McCormick, A., & Swaisland, H. (2017). In vitro assessment of the roles of drug transporters in the disposition and drug-drug interaction potential of olaparib. *Xenobiotica, 47*(10), 903-915. doi:10.1080/00498254.2016.1241449

McCormick, A., Swaisland, H., Reddy, V. P., Learoyd, M., & Scarfe, G. (2018). In vitro evaluation of the inhibition and induction potential of olaparib, a potent poly(ADP-ribose) polymerase inhibitor, on cytochrome P450. *Xenobiotica, 48*(6), 555-564. doi:10.1080/00498254.2017.1346332

Mean, R. J., Pierides, A., Deltas, C. C., & Koptides, M. (2004). Modification of the enzyme mismatch cleavage method using T7 endonuclease I and silver staining. *Biotechniques, 36*(5), 758-760. doi:10.2144/04365BM01

Mechetner, E., Kyshtoobayeva, A., Zonis, S., Kim, H., Stroup, R., Garcia, R., . . . Fruehauf, J. P. (1998). Levels of multidrug resistance (MDR1) P-glycoprotein expression by human breast cancer correlate with in vitro resistance to taxol and doxorubicin. *Clin Cancer Res, 4*(2), 389-398.

Mekler, V., Minakhin, L., Semenova, E., Kuznedelov, K., & Severinov, K. (2016). Kinetics of the CRISPR-Cas9 effector complex assembly and the role of 3'-terminal segment of guide RNA. *Nucleic Acids Res, 44*(6), 2837-2845. doi:10.1093/nar/gkw138

Mickley, L. A., Lee, J.-S., Weng, Z., Zhan, Z., Alvarez, M., Wilson, W., . . . Fojo, T. (1998). Genetic polymorphism in MDR-1: a tool for examining allelic expression in normal cells, unselected and drug-selected cell lines, and human tumors. *Blood, 91*(5), 1749-1756.

Miletti-Gonzalez, K. E., Chen, S., Muthukumaran, N., Saglimbeni, G. N., Wu, X., Yang, J., . . . Rodriguez-Rodriguez, L. (2005). The CD44 receptor interacts with P-glycoprotein to promote cell migration and invasion in cancer. *Cancer Res, 65*(15), 6660-6667. doi:10.1158/0008-5472.Can-04-3478

Min, A., & Im, S. A. (2020). PARP Inhibitors as Therapeutics: Beyond Modulation of PARylation. *Cancers (Basel), 12*(2). doi:10.3390/cancers12020394

Minotti, G. (1989). Reactions of adriamycin with microsomal iron and lipids. *Free*

radical research communications, 7(3-6), 143-148.

Mochida, Y., Taguchi, K.-i., Taniguchi, S., Tsuneyoshi, M., Kuwano, H., Tsuzuki, T., . . . Wada, M. (2003). The role of P-glycoprotein in intestinal tumorigenesis: disruption of mdr1a suppresses polyp formation in Apc Min/+ mice. *Carcinogenesis, 24*(7), 1219-1224. doi:DOI: 10.1093/carcin/bgg073

Moreno-Aspitia, A., & Perez, E. A. (2009). *Treatment options for breast cancer resistant to anthracycline and taxane.* Paper presented at the Mayo Clinic Proceedings.

Morris, G. M., Huey, R., Lindstrom, W., Sanner, M. F., Belew, R. K., Goodsell, D. S., & Olson, A. J. (2009). AutoDock4 and AutoDockTools4: Automated docking with selective receptor flexibility. *J Comput Chem, 30*(16), 2785-2791. doi:10.1002/jcc.21256

Mosaffa, F., Lage, H., Afshari, J. T., & Behravan, J. (2009). Interleukin-1 beta and tumor necrosis factor-alpha increase ABCG2 expression in MCF-7 breast carcinoma cell line and its mitoxantrone-resistant derivative, MCF-7/MX. *Inflamm Res, 58*(10), 669-676. doi:10.1007/s00011-009-0034-6

Mourskaia, A. A., Amir, E., Dong, Z., Tiedemann, K., Cory, S., Omeroglu, A., . . . Siegel, P. M. (2012). ABCC5 supports osteoclast formation and promotes breast cancer metastasis to bone. *Breast Cancer Res, 14*(6), R149. doi:10.1186/bcr3361

Müller, M., Meijer, C., Zaman, G., Borst, P., Scheper, R. J., Mulder, N. H., . . . Jansen, P. (1994). Overexpression of the gene encoding the multidrug resistance-associated protein results in increased ATP-dependent glutathione S-conjugate transport. *Proceedings of the National Academy of Sciences, 91*(26), 13033-13037.

Murray, G. I., McFadyen, M. C., Mitchell, R. T., Cheung, Y. L., Kerr, A. C., & Melvin, W. T. (1999). Cytochrome P450 CYP3A in human renal cell cancer. *Br J Cancer, 79*(11-12), 1836-1842. doi:10.1038/sj.bjc.6690292

Myint, K., Biswas, R., Li, Y., Jong, N., Jamieson, S., Liu, J., . . . McKeage, M. (2019). Identification of MRP2 as a targetable factor limiting oxaliplatin accumulation and response in gastrointestinal cancer. *Sci Rep, 9*(1), 2245. doi:10.1038/s41598-019-38667-8

Natarajan, K., Xie, Y., Baer, M. R., & Ross, D. D. (2012). Role of breast cancer resistance protein (BCRP/ABCG2) in cancer drug resistance. *Biochem Pharmacol, 83*(8), 1084-1103. doi:10.1016/j.bcp.2012.01.002

Nemcova-Furstova, V., Kopperova, D., Balusikova, K., Ehrlichova, M., Brynychova, V., Vaclavikova, R., . . . Kovar, J. (2016). Characterization of acquired paclitaxel resistance of breast cancer cells and involvement of ABC transporters. *Toxicol Appl Pharmacol, 310*, 215-228. doi:10.1016/j.taap.2016.09.020

New Zealand Ministry of Health. (2016a). *Cancer: New registrations and deaths 2013*. Retrieved from https://www.health.govt.nz/

New Zealand Ministry of Health. (2016b). *New cancer registrations 2016*. Retrieved from https://www.health.govt.nz/

Nies, A., Jedlitschky, G., König, J., Herold-Mende, C., Steiner, H., Schmitt, H.-P., & Keppler, D. (2004). Expression and immunolocalization of the multidrug resistance proteins, MRP1–MRP6 (ABCC1–ABCC6), in human brain. *Neuroscience, 129*(2), 349-360.

Nies, A. T., & Keppler, D. (2007). The apical conjugate efflux pump ABCC2 (MRP2). *Pflugers Arch, 453*(5), 643-659. doi:10.1007/s00424-006-0109-y

Nooter, K., De La Riviere, G. B., Look, M., Van Wingerden, K., Henzen-Logmans, S., Scheper, R., . . . Foekens, J. (1997). The prognostic significance of expression

of the multidrug resistance-associated protein (MRP) in primary breast cancer. *British journal of cancer, 76*(4), 486.

Nooter, K., Westerman, A. M., Flens, M. J., Zaman, G., Scheper, R. J., Van Wingerden, K., . . . Sonneveld, P. (1995). Expression of the multidrug resistance-associated protein (MRP) gene in human cancers. *Clinical Cancer Research, 1*(11), 1301-1310.

Norris, M. D., Smith, J., Tanabe, K., Tobin, P., Flemming, C., Scheffer, G. L., . . . Haber, M. (2005). Expression of multidrug transporter MRP4/ABCC4 is a marker of poor prognosis in neuroblastoma and confers resistance to irinotecan in vitro. *Mol Cancer Ther, 4*(4), 547-553. doi:10.1158/1535-7163.Mct-04-0161

Oba, T., Izumi, H., & Ito, K. I. (2016). ABCB1 and ABCC11 confer resistance to eribulin in breast cancer cell lines. *Oncotarget, 7*(43), 70011-70027. doi:DOI: 10.18632/oncotarget.11727

Octavia, Y., Tocchetti, C. G., Gabrielson, K. L., Janssens, S., Crijns, H. J., & Moens, A. L. (2012). Doxorubicin-induced cardiomyopathy: from molecular mechanisms to therapeutic strategies. *J Mol Cell Cardiol, 52*(6), 1213-1225. doi:10.1016/j.yjmcc.2012.03.006

Ogawa, Y., Tsuda, H., Hai, E., Tsuji, N., Yamagata, S., Tokunaga, S., . . . Nishiguchi, Y. (2006). Clinical role of ABCF2 expression in breast cancer. *Anticancer Res, 26*(3a), 1809-1814.

Orlando, U. D., Castillo, A. F., Medrano, M. A. R., Solano, A. R., Maloberti, P. M., & Podesta, E. J. (2019). Acyl-CoA synthetase-4 is implicated in drug resistance in breast cancer cell lines involving the regulation of energy-dependent transporter expression. *Biochem Pharmacol, 159*, 52-63. doi:10.1016/j.bcp.2018.11.005

Park, S., Shimizu, C., Shimoyama, T., Takeda, M., Ando, M., Kohno, T., . . . Fujiwara, Y. (2006). Gene expression profiling of ATP-binding cassette (ABC) transporters as a predictor of the pathologic response to neoadjuvant chemotherapy in breast cancer patients. *Breast Cancer Res Treat, 99*(1), 9-17.

Park, S., Shimizu, C., Shimoyama, T., Takeda, M., Ando, M., Kohno, T., . . . Fujiwara, Y. (2006). Gene expression profiling of ATP-binding cassette (ABC) transporters as a predictor of the pathologic response to neoadjuvant chemotherapy in breast cancer patients. *Breast Cancer Res Treat, 99*(1), 9-17. doi:10.1007/s10549-006-9175-2

Partanen, L., Staaf, J., Tanner, M., Tuominen, V. J., Borg, A., & Isola, J. (2012). Amplification and overexpression of the ABCC3 (MRP3) gene in primary breast cancer. *Genes Chromosomes Cancer, 51*(9), 832-840. doi:10.1002/gcc.21967

Pastan, I., & Gottesman, M. (1987). Multiple-drug resistance in human cancer. *New England Journal of Medicine, 316*(22), 1388-1393.

Pattanayak, V., Lin, S., Guilinger, J. P., Ma, E., Doudna, J. A., & Liu, D. R. (2013). High-throughput profiling of off-target DNA cleavage reveals RNA-programmed Cas9 nuclease specificity. *Nature biotechnology, 31*(9), 839.

Paul, B., & Montoya, G. (2020). CRISPR-Cas12a: Functional overview and applications. *Biomed J, 43*(1), 8-17. doi:10.1016/j.bj.2019.10.005

Pekhletski, R., & Hampson, D. R. (1996). Differentiating allele combinations of a transgene using multiple primer PCR. *Biotechniques, 20*(6), 956-958, 960. doi:10.2144/96206bm02

Perez, E. E., Wang, J., Miller, J. C., Jouvenot, Y., Kim, K. A., Liu, O., . . . Lee, Y.-L. (2008). Establishment of HIV-1 resistance in CD4+ T cells by genome editing using zinc-finger nucleases. *Nature biotechnology, 26*(7), 808.

Peto, R., & Group, E. B. C. T. C. (2007). *The worldwide overview: new results for systemic adjuvant therapies.* Paper presented at the San Antonio breast cancer symposium.

Platt, R. J., Chen, S., Zhou, Y., Yim, M. J., Swiech, L., Kempton, H. R., . . . Jovanovic, M. (2014). CRISPR-Cas9 knockin mice for genome editing and cancer modeling. *cell, 159*(2), 440-455.

Pluchino, K. M., Hall, M. D., Goldsborough, A. S., Callaghan, R., & Gottesman, M. M. (2012). Collateral sensitivity as a strategy against cancer multidrug resistance. *Drug Resist Updat, 15*(1-2), 98-105. doi:10.1016/j.drup.2012.03.002

Plummer, R., Swaisland, H., Leunen, K., van Herpen, C. M., Jerusalem, G., De Greve, J., . . . Molife, L. R. (2015). Olaparib tablet formulation: effect of food on the pharmacokinetics after oral dosing in patients with advanced solid tumours. *Cancer Chemother Pharmacol, 76*(4), 723-729. doi:10.1007/s00280-015-2836-2

Poller, B., Drewe, J., Krahenbuhl, S., Huwyler, J., & Gutmann, H. (2010). Regulation of BCRP (ABCG2) and P-glycoprotein (ABCB1) by cytokines in a model of the human blood-brain barrier. *Cell Mol Neurobiol, 30*(1), 63-70. doi:10.1007/s10571-009-9431-1

Pollex, R. L., & Hegele, R. A. (2007). Copy number variation in the human genome and its implications for cardiovascular disease. *Circulation, 115*(24), 3130-3138. doi:10.1161/CIRCULATIONAHA.106.677591

Pradhan, M., Bembinster, L. A., Baumgarten, S. C., & Frasor, J. (2010). Proinflammatory cytokines enhance estrogen-dependent expression of the multidrug transporter gene ABCG2 through estrogen receptor and NF{kappa}B cooperativity at adjacent response elements. *J Biol Chem, 285*(41), 31100-31106. doi:10.1074/jbc.M110.155309

Pratt, S., Shepard, R. L., Kandasamy, R. A., Johnston, P. A., Perry, W., 3rd, & Dantzig, A. H. (2005). The multidrug resistance protein 5 (ABCC5) confers resistance to 5-fluorouracil and transports its monophosphorylated metabolites. *Mol Cancer Ther, 4*(5), 855-863. doi:10.1158/1535-7163.Mct-04-0291

Rahdar, M., McMahon, M. A., Prakash, T. P., Swayze, E. E., Bennett, C. F., & Cleveland, D. W. (2015). Synthetic CRISPR RNA-Cas9-guided genome editing in human cells. *Proc Natl Acad Sci U S A, 112*(51), E7110-7117. doi:10.1073/pnas.1520883112

Rahdar, M., McMahon, M. A., Prakash, T. P., Swayze, E. E., Bennett, C. F., & Cleveland, D. W. (2015). Synthetic CRISPR RNA-Cas9–guided genome editing in human cells. *Proceedings of the National Academy of Sciences, 112*(51), E7110-E7117.

Ran, F. A., Cong, L., Yan, W. X., Scott, D. A., Gootenberg, J. S., Kriz, A. J., . . . Makarova, K. S. (2015). In vivo genome editing using Staphylococcus aureus Cas9. *Nature, 520*(7546), 186.

Ran, F. A., Cong, L., Yan, W. X., Scott, D. A., Gootenberg, J. S., Kriz, A. J., . . . Zhang, F. (2015). In vivo genome editing using Staphylococcus aureus Cas9. *Nature, 520*(7546), 186-191. doi:10.1038/nature14299

Rao, V. V., Dahlheimer, J. L., Bardgett, M. E., Snyder, A. Z., Finch, R. A., Sartorelli, A. C., & Piwnica-Worms, D. (1999). Choroid plexus epithelial expression of MDR1 P glycoprotein and multidrug resistance-associated protein contribute to the blood–cerebrospinal-fluid drug-permeability barrier. *Proceedings of the National Academy of Sciences, 96*(7), 3900-3905.

Rappa, G., Lorico, A., Flavell, R. A., & Sartorelli, A. C. (1997). Evidence that the multidrug resistance protein (MRP) functions as a co-transporter of glutathione

and natural product toxins. *Cancer research, 57*(23), 5232-5237.

Rhodes, D. R., Kalyana-Sundaram, S., Mahavisno, V., Varambally, R., Yu, J., Briggs, B. B., . . . Chinnaiyan, A. M. (2007). Oncomine 3.0: genes, pathways, and networks in a collection of 18,000 cancer gene expression profiles. *Neoplasia, 9*(2), 166-180. doi:10.1593/neo.07112

Rhodes, D. R., Yu, J., Shanker, K., Deshpande, N., Varambally, R., Ghosh, D., . . . Chinnaiyan, A. M. (2004). ONCOMINE: a cancer microarray database and integrated data-mining platform. *Neoplasia, 6*(1), 1-6. doi:10.1016/s1476-5586(04)80047-2

Rius, M., Hummel-Eisenbeiss, J., Hofmann, A. F., & Keppler, D. (2006). Substrate specificity of human ABCC4 (MRP4)-mediated cotransport of bile acids and reduced glutathione. *Am J Physiol Gastrointest Liver Physiol, 290*(4), G640-649. doi:10.1152/ajpgi.00354.2005

Rius, M., Nies, A. T., Hummel-Eisenbeiss, J., Jedlitschky, G., & Keppler, D. (2003). Cotransport of reduced glutathione with bile salts by MRP4 (ABCC4) localized to the basolateral hepatocyte membrane. *Hepatology, 38*(2), 374-384. doi:10.1053/jhep.2003.50331

Robey, R. W., Pluchino, K. M., Hall, M. D., Fojo, A. T., Bates, S. E., & Gottesman, M. M. (2018). Revisiting the role of ABC transporters in multidrug-resistant cancer. *Nature Reviews Cancer*, 1.

Robey, R. W., Polgar, O., Deeken, J., To, K. W., & Bates, S. E. (2007). ABCG2: determining its relevance in clinical drug resistance. *Cancer Metastasis Rev, 26*(1), 39-57. doi:10.1007/s10555-007-9042-6

Roninson, I. B., Chin, J. E., Choi, K. G., Gros, P., Housman, D. E., Fojo, A., . . . Pastan, I. (1986). Isolation of human mdr DNA sequences amplified in multidrug-resistant KB carcinoma cells. *Proceedings of the National Academy of Sciences, 83*(12), 4538-4542.

Rossi, S. (2013). *Australian Medicines Handbook (2013 ed.). Adelaide: The Australian Medicines Handbook Unit Trust*. Retrieved from

Russel, F. G., Koenderink, J. B., & Masereeuw, R. (2008). Multidrug resistance protein 4 (MRP4/ABCC4): a versatile efflux transporter for drugs and signalling molecules. *Trends Pharmacol Sci, 29*(4), 200-207. doi:10.1016/j.tips.2008.01.006

Sakuma, T., Nishikawa, A., Kume, S., Chayama, K., & Yamamoto, T. (2014). Multiplex genome engineering in human cells using all-in-one CRISPR/Cas9 vector system. *Sci Rep, 4*, 5400. doi:10.1038/srep05400

Saleh-Gohari, N., & Helleday, T. (2004). Conservative homologous recombination preferentially repairs DNA double-strand breaks in the S phase of the cell cycle in human cells. *Nucleic acids research, 32*(12), 3683-3688.

Sarkadi, B., Homolya, L., Szakács, G., & Váradi, A. (2006). Human multidrug resistance ABCB and ABCG transporters: participation in a chemoimmunity defense system. *Physiological reviews, 86*(4), 1179-1236.

Sassi, Y., Lipskaia, L., Vandecasteele, G., Nikolaev, V. O., Hatem, S. N., Cohen Aubart, F., . . . Hulot, J. S. (2008). Multidrug resistance-associated protein 4 regulates cAMP-dependent signaling pathways and controls human and rat SMC proliferation. *J Clin Invest, 118*(8), 2747-2757. doi:10.1172/jci35067

Savic, N., Ringnalda, F. C., Lindsay, H., Berk, C., Bargsten, K., Li, Y., . . . Schwank, G. (2018). Covalent linkage of the DNA repair template to the CRISPR-Cas9 nuclease enhances homology-directed repair. *Elife, 7*. doi:10.7554/eLife.33761

Scheffer, G. L., Kool, M., de Haas, M., de Vree, J. M., Pijnenborg, A. C., Bosman, D.

K., . . . Scheper, R. J. (2002). Tissue distribution and induction of human multidrug resistant protein 3. *Lab Invest, 82*(2), 193-201.

Scheffer, G. L., Kool, M., Heijn, M., de Haas, M., Pijnenborg, A. C., Wijnholds, J., . . . Mol, C. A. (2000). Specific detection of multidrug resistance proteins MRP1, MRP2, MRP3, MRP5, and MDR3 P-glycoprotein with a panel of monoclonal antibodies. *Cancer research, 60*(18), 5269-5277.

Schinkel, A. H., & Jonker, J. W. (2012). Mammalian drug efflux transporters of the ATP binding cassette (ABC) family: an overview. *Advanced drug delivery reviews, 64*, 138-153.

Schinkel, A. H., Mayer, U., Wagenaar, E., Mol, C. A., Van Deemter, L., Smit, J. J., . . . Van Tellingen, O. (1997). Normal viability and altered pharmacokinetics in mice lacking mdr1-type (drug-transporting) P-glycoproteins. *Proceedings of the National Academy of Sciences, 94*(8), 4028-4033.

Schoning-Stierand, K., Diedrich, K., Fahrrolfes, R., Flachsenberg, F., Meyder, A., Nittinger, E., . . . Rarey, M. (2020). ProteinsPlus: interactive analysis of protein-ligand binding interfaces. *Nucleic Acids Res, 48*(W1), W48-W53. doi:10.1093/nar/gkaa235

Sebat, J., Lakshmi, B., Troge, J., Alexander, J., Young, J., Lundin, P., . . . Wigler, M. (2004). Large-scale copy number polymorphism in the human genome. *Science, 305*(5683), 525-528. doi:10.1126/science.1098918

Sedlakova, I., Laco, J., Tosner, J., Caltova, K., Cervinka, M., Rezac, A., . . . Skapinec, P. (2012). [Proteins of resistance and drug resistance in ovarian carcinoma patients]. *Klin Onkol, 25*(6), 457-463.

Shagufta, & Ahmad, I. (2018). Tamoxifen a pioneering drug: An update on the therapeutic potential of tamoxifen derivatives. *Eur J Med Chem, 143*, 515-531. doi:10.1016/j.ejmech.2017.11.056

Shao, X., Lv, N., Liao, J., Long, J., Xue, R., Ai, N., . . . Fan, X. (2019). Copy number variation is highly correlated with differential gene expression: a pan-cancer study. *BMC Med Genet, 20*(1), 175. doi:10.1186/s12881-019-0909-5

Shlien, A., & Malkin, D. (2009). Copy number variations and cancer. *Genome Med, 1*(6), 62. doi:10.1186/gm62

Shukla, S., Chen, Z.-S., & Ambudkar, S. V. (2012). Tyrosine kinase inhibitors as modulators of ABC transporter-mediated drug resistance. *Drug resistance updates, 15*(1-2), 70-80.

Silver, D. P., Richardson, A. L., Eklund, A. C., Wang, Z. C., Szallasi, Z., Li, Q., . . . Buraimoh, A. (2010). Efficacy of neoadjuvant Cisplatin in triple-negative breast cancer. *Journal of clinical oncology, 28*(7), 1145.

Slastnikova, T. A., Ulasov, A. V., Rosenkranz, A. A., & Sobolev, A. S. (2018). Targeted Intracellular Delivery of Antibodies: The State of the Art. *Front Pharmacol, 9*, 1208. doi:10.3389/fphar.2018.01208

Slot, A. J., Molinski, S. V., & Cole, S. P. (2011). Mammalian multidrug-resistance proteins (MRPs). *Essays in biochemistry, 50*, 179-207.

Smith, S., & Grima, R. (2018). Single-cell variability in multicellular organisms. *Nat Commun, 9*(1), 345. doi:10.1038/s41467-017-02710-x

Smitherman, P. K., Townsend, A. J., Kute, T. E., & Morrow, C. S. (2004). Role of Multidrug Resistance Protein 2 (MRP2, ABCC2) in Alkylating Agent Detoxification: MRP2 Potentiates Glutathione S-Transferase A1-1-Mediated Resistance to Chlorambucil Cytotoxicity. *Journal of Pharmacology and Experimental Therapeutics, 308*(1), 260-267. doi:10.1124/jpet.103.057729

Smits, A. H., Ziebell, F., Joberty, G., Zinn, N., Mueller, W. F., Clauder-Munster, S., . . .

Huber, W. (2019). Biological plasticity rescues target activity in CRISPR knock outs. *Nat Methods, 16*(11), 1087-1093. doi:DOI: 10.1038/s41592-019-0614-5

Sparreboom, A., Loos, W. J., Burger, H., Sissung, T. M., Verweij, J., Figg, W. D., . . . Gelderblom, H. (2005). Effect of ABCG2 genotype on the oral bioavailability of topotecan. *Cancer Biol Ther, 4*(6), 650-658.

Sparreboom, A., Van Asperen, J., Mayer, U., Schinkel, A. H., Smit, J. W., Meijer, D. K., . . . Van Tellingen, O. (1997). Limited oral bioavailability and active epithelial excretion of paclitaxel (Taxol) caused by P-glycoprotein in the intestine. *Proceedings of the National Academy of Sciences, 94*(5), 2031-2035.

St-Pierre, M., Serrano, M., Macias, R., Dubs, U., Hoechli, M., Lauper, U., . . . Marin, J. (2000). Expression of members of the multidrug resistance protein family in human term placenta. *American Journal of Physiology-Regulatory, Integrative and Comparative Physiology, 279*(4), R1495-R1503.

Sun, S.-S., Hsieh, J.-F., Tsai, S.-C., Ho, Y.-J., Lee, J.-K., & Kao, C.-H. (2000). Expression of mediated P-glycoprotein multidrug resistance related to Tc-99m MIBI scintimammography results. *Cancer letters, 153*(1-2), 95-100.

Szakács, G., Paterson, J. K., Ludwig, J. A., Booth-Genthe, C., & Gottesman, M. M. (2006). Targeting multidrug resistance in cancer. *Nature reviews Drug discovery, 5*(3), 219.

Szybalski, W., & Bryson, V. (1952). Genetic studies on microbial cross resistance to toxic agents. I. Cross resistance of Escherichia coli to fifteen antibiotics. *J Bacteriol, 64*(4), 489-499. doi:DOI: 10.1128/JB.64.4.489-499.1952

Tacar, O., Sriamornsak, P., & Dass, C. R. (2013). Doxorubicin: an update on anticancer molecular action, toxicity and novel drug delivery systems. *J Pharm Pharmacol, 65*(2), 157-170. doi:10.1111/j.2042-7158.2012.01567.x

Tang, P., & Tse, G. M. (2016). Immunohistochemical Surrogates for Molecular Classification of Breast Carcinoma: A 2015 Update. *Arch Pathol Lab Med, 140*(8), 806-814. doi:10.5858/arpa.2015-0133-RA

Tanino, R., Tsubata, Y., Harashima, N., Harada, M., & Isobe, T. (2018). Novel drug-resistance mechanisms of pemetrexed-treated non-small cell lung cancer. *Oncotarget, 9*(24), 16807-16821. doi:10.18632/oncotarget.24704

Taylor, N. M., Manolaridis, I., Jackson, S. M., Kowal, J., Stahlberg, H., & Locher, K. P. (2017). Structure of the human multidrug transporter ABCG2. *Nature, 546*(7659), 504. doi:DOI: 10.1038/nature22345

Terns, M. P., & Terns, R. M. (2011). CRISPR-based adaptive immune systems. *Current opinion in microbiology, 14*(3), 321-327.

Tewey, K., Rowe, T., Yang, L., Halligan, B., & Liu, L. (1984). Adriamycin-induced DNA damage mediated by mammalian DNA topoisomerase II. *Science, 226*(4673), 466-468.

Thiagalingam, S., Laken, S., Willson, J. K., Markowitz, S. D., Kinzler, K. W., Vogelstein, B., & Lengauer, C. (2001). Mechanisms underlying losses of heterozygosity in human colorectal cancers. *Proc Natl Acad Sci U S A, 98*(5), 2698-2702. doi:10.1073/pnas.051625398

Thiebaut, F., Tsuruo, T., Hamada, H., Gottesman, M. M., Pastan, I., & Willingham, M. C. (1987). Cellular localization of the multidrug-resistance gene product P-glycoprotein in normal human tissues. *Proceedings of the National Academy of Sciences, 84*(21), 7735-7738.

Thomas, H., & Coley, H. M. (2003). Overcoming multidrug resistance in cancer: an update on the clinical strategy of inhibiting p-glycoprotein. *Cancer control, 10*(2), 159-165. doi:DOI: 10.1177/107327480301000207

Thompson, S. L., & Compton, D. A. (2011). Chromosomes and cancer cells. *Chromosome Res, 19*(3), 433-444. doi:10.1007/s10577-010-9179-y

Thorn, C. F., Oshiro, C., Marsh, S., Hernandez-Boussard, T., McLeod, H., Klein, T. E., & Altman, R. B. (2011). Doxorubicin pathways: pharmacodynamics and adverse effects. *Pharmacogenet Genomics, 21*(7), 440-446. doi:10.1097/FPC.0b013e32833ffb56

Triller, N., Korošec, P., Kern, I., Košnik, M., & Debeljak, A. (2006). Multidrug resistance in small cell lung cancer: expression of P-glycoprotein, multidrug resistance protein 1 and lung resistance protein in chemo-naive patients and in relapsed disease. *Lung cancer, 54*(2), 235-240.

Trock, B. J., Leonessa, F., & Clarke, R. (1997). Multidrug resistance in breast cancer: a meta-analysis of MDR1/gp170 expression and its possible functional significance. *Journal Of The National Cancer Institute, 89*(13), 917-931.

Tsai, S. Q., Zheng, Z., Nguyen, N. T., Liebers, M., Topkar, V. V., Thapar, V., . . . Le, L. P. (2015). GUIDE-seq enables genome-wide profiling of off-target cleavage by CRISPR-Cas nucleases. *Nature biotechnology, 33*(2), 187.

Ueda, K., Cornwell, M. M., Gottesman, M. M., Pastan, I., Roninson, I. B., Ling, V., & Riordan, J. R. (1986). The mdrl gene, responsible for multidrug-resistance, codes for P-glycoprotein. *Biochem Biophys Res Commun, 141*(3), 956-962.

van de Ven, R., Scheffer, G. L., Scheper, R. J., & de Gruijl, T. D. (2009). The ABC of dendritic cell development and function. *Trends Immunol, 30*(9), 421-429. doi:10.1016/j.it.2009.06.004

van Eijk, M., Boosman, R. J., Schinkel, A. H., Huitema, A. D. R., & Beijnen, J. H. (2019). Cytochrome P450 3A4, 3A5, and 2C8 expression in breast, prostate, lung, endometrial, and ovarian tumors: relevance for resistance to taxanes. *Cancer Chemother Pharmacol, 84*(3), 487-499. doi:10.1007/s00280-019-03905-3

van Overbeek, M., Capurso, D., Carter, M. M., Thompson, M. S., Frias, E., Russ, C., . . . May, A. P. (2016). DNA Repair Profiling Reveals Nonrandom Outcomes at Cas9-Mediated Breaks. *Mol Cell, 63*(4), 633-646. doi:10.1016/j.molcel.2016.06.037

Verkuijl, S. A., & Rots, M. G. (2019). The influence of eukaryotic chromatin state on CRISPR-Cas9 editing efficiencies. *Curr Opin Biotechnol, 55*, 68-73. doi:10.1016/j.copbio.2018.07.005

Vouillot, L., Thelie, A., & Pollet, N. (2015). Comparison of T7E1 and surveyor mismatch cleavage assays to detect mutations triggered by engineered nucleases. *G3 (Bethesda), 5*(3), 407-415. doi:10.1534/g3.114.015834

Vu, T., & Claret, F. X. (2012). Trastuzumab: updated mechanisms of action and resistance in breast cancer. *Front Oncol, 2*, 62. doi:10.3389/fonc.2012.00062

Vulsteke, C., Lambrechts, D., Dieudonne, A., Hatse, S., Brouwers, B., van Brussel, T., . . . Wildiers, H. (2013). Genetic variability in the multidrug resistance associated protein-1 (ABCC1/MRP1) predicts hematological toxicity in breast cancer patients receiving (neo-)adjuvant chemotherapy with 5-fluorouracil, epirubicin and cyclophosphamide (FEC). *Ann Oncol, 24*(6), 1513-1525. doi:10.1093/annonc/mdt008

Wallace, A. C., Laskowski, R. A., & Thornton, J. M. (1995). LIGPLOT: a program to generate schematic diagrams of protein-ligand interactions. *Protein Eng, 8*(2), 127-134. doi:10.1093/protein/8.2.127

Wang, H., Yang, H., Shivalila, C. S., Dawlaty, M. M., Cheng, A. W., Zhang, F., & Jaenisch, R. (2013). One-step generation of mice carrying mutations in multiple

genes by CRISPR/Cas-mediated genome engineering. *cell, 153*(4), 910-918.

Wang, X., Wu, X., Wang, C., Zhang, W., Ouyang, Y., Yu, Y., & He, Z. (2010). Transcriptional suppression of breast cancer resistance protein (BCRP) by wild-type p53 through the NF-kappaB pathway in MCF-7 cells. *FEBS Lett, 584*(15), 3392-3397. doi:10.1016/j.febslet.2010.06.033

Ween, M., Armstrong, M., Oehler, M., & Ricciardelli, C. (2015). The role of ABC transporters in ovarian cancer progression and chemoresistance. *Critical reviews in oncology/hematology, 96*(2), 220-256.

Weiss, R. B. (1992). *The anthracyclines: will we ever find a better doxorubicin?* Paper presented at the Seminars in oncology.

Wen, S. H., Su, S. C., Liou, B. H., Lin, C. H., & Lee, K. R. (2018). Sulbactam-enhanced cytotoxicity of doxorubicin in breast cancer cells. *Cancer Cell Int, 18*, 128. doi:10.1186/s12935-018-0625-9

Wiedenheft, B., Sternberg, S. H., & Doudna, J. A. (2012). RNA-guided genetic silencing systems in bacteria and archaea. *Nature, 482*(7385), 331.

Wijnholds, J., Mol, C. A., van Deemter, L., de Haas, M., Scheffer, G. L., Baas, F., . . . De Clercq, E. (2000). Multidrug-resistance protein 5 is a multispecific organic anion transporter able to transport nucleotide analogs. *Proceedings of the National Academy of Sciences, 97*(13), 7476-7481.

Wijnholds, J., Mol, C. A., van Deemter, L., de Haas, M., Scheffer, G. L., Baas, F., . . . Borst, P. (2000). Multidrug-resistance protein 5 is a multispecific organic anion transporter able to transport nucleotide analogs. *Proc Natl Acad Sci U S A, 97*(13), 7476-7481. doi:10.1073/pnas.120159197

Woodward, K. J., Cundall, M., Sperle, K., Sistermans, E. A., Ross, M., Howell, G., . . . Hobson, G. M. (2005). Heterogeneous duplications in patients with Pelizaeus-Merzbacher disease suggest a mechanism of coupled homologous and nonhomologous recombination. *Am J Hum Genet, 77*(6), 966-987. doi:10.1086/498048

Woodward, O. M., Kottgen, A., Coresh, J., Boerwinkle, E., Guggino, W. B., & Kottgen, M. (2009). Identification of a urate transporter, ABCG2, with a common functional polymorphism causing gout. *Proc Natl Acad Sci U S A, 106*(25), 10338-10342. doi:10.1073/pnas.0901249106

World Health Organization. (2018, 12.09.2018). Cancer. Retrieved from https://www.who.int/news-room/fact-sheets/detail/cancer

Wu, C. P., Calcagno, A. M., Hladky, S. B., Ambudkar, S. V., & Barrand, M. A. (2005). Modulatory effects of plant phenols on human multidrug-resistance proteins 1, 4 and 5 (ABCC1, 4 and 5). *Febs j, 272*(18), 4725-4740. doi:10.1111/j.1742-4658.2005.04888.x

Wu, H., Liu, Y., Kang, H., Xiao, Q., Yao, W., Zhao, H., . . . Wei, M. (2015). Genetic Variations in ABCG2 Gene Predict Breast Carcinoma Susceptibility and Clinical Outcomes after Treatment with Anthracycline-Based Chemotherapy. *Biomed Res Int, 2015*, 279109. doi:10.1155/2015/279109

Wu, X., Zhang, X., Sun, L., Zhang, H., Li, L., Wang, X., . . . Zhou, G. (2013). Progesterone negatively regulates BCRP in progesterone receptor-positive human breast cancer cells. *Cell Physiol Biochem, 32*(2), 344-354. doi:10.1159/000354442

Xiang, L., Su, P., Xia, S., Liu, Z., Wang, Y., Gao, P., & Zhou, G. (2011). ABCG2 is associated with HER-2 expression, lymph node metastasis and clinical stage in breast invasive ductal carcinoma. *Diagn Pathol, 6*, 90. doi:10.1186/1746-1596-6-90

Xie, C., Jiang, X. H., Zhang, J. T., Sun, T. T., Dong, J. D., Sanders, A. J., . . . Chan, H. C. (2013). CFTR suppresses tumor progression through miR-193b targeting urokinase plasminogen activator (uPA) in prostate cancer. *Oncogene, 32*(18), 2282-2291, 2291.e2281-2287. doi:10.1038/onc.2012.251

Xiong, H., Callaghan, D., Jones, A., Bai, J., Rasquinha, I., Smith, C., . . . Zhang, W. (2009). ABCG2 is upregulated in Alzheimer's brain with cerebral amyloid angiopathy and may act as a gatekeeper at the blood-brain barrier for Abeta(1-40) peptides. *J Neurosci, 29*(17), 5463-5475. doi:10.1523/jneurosci.5103-08.2009

Xu, X., Duan, D., & Chen, S. J. (2017). CRISPR-Cas9 cleavage efficiency correlates strongly with target-sgRNA folding stability: from physical mechanism to off-target assessment. *Sci Rep, 7*(1), 143. doi:10.1038/s41598-017-00180-1

Yamada, A., Nagahashi, M., Aoyagi, T., Huang, W. C., Lima, S., Hait, N. C., . . . Takabe, K. (2018). ABCC1-Exported Sphingosine-1-phosphate, Produced by Sphingosine Kinase 1, Shortens Survival of Mice and Patients with Breast Cancer. *Mol Cancer Res, 16*(6), 1059-1070. doi:10.1158/1541-7786.Mcr-17-0353

Yang, F., Kemp, C. J., & Henikoff, S. (2013). Doxorubicin enhances nucleosome turnover around promoters. *Curr Biol, 23*(9), 782-787. doi:10.1016/j.cub.2013.03.043

Yang, F., Teves, S. S., Kemp, C. J., & Henikoff, S. (2014). Doxorubicin, DNA torsion, and chromatin dynamics. *Biochim Biophys Acta, 1845*(1), 84-89. doi:10.1016/j.bbcan.2013.12.002

Yang, Y. J., Wang, Y., Li, Z. F., Gong, Y., Zhang, P., Hu, W. C., . . . Li, Y. Z. (2017). Increasing on-target cleavage efficiency for CRISPR/Cas9-induced large fragment deletion in Myxococcus xanthus. *Microb Cell Fact, 16*(1), 142. doi:10.1186/s12934-017-0758-x

Yi, M., Dong, B., Qin, S., Chu, Q., Wu, K., & Luo, S. (2019). Advances and perspectives of PARP inhibitors. *Exp Hematol Oncol, 8*, 29. doi:10.1186/s40164-019-0154-9

Yoshida, M., Suzuki, T., Komiya, T., Hatashita, E., Nishio, K., Kazuhiko, N., & Fukuoka, M. (2001). Induction of MRP5 and SMRP mRNA by adriamycin exposure and its overexpression in human lung cancer cells resistant to adriamycin. *Int J Cancer, 94*(3), 432-437. doi:10.1002/ijc.1490

Yu, D., & Hung, M.-C. (2009). *Breast cancer chemosensitivity* (Vol. 608). Basel, Switzerland: Springer Science & Business Media.

Yuen, G., Khan, F. J., Gao, S., Stommel, J. M., Batchelor, E., Wu, X., & Luo, J. (2017). CRISPR/Cas9-mediated gene knockout is insensitive to target copy number but is dependent on guide RNA potency and Cas9/sgRNA threshold expression level. *Nucleic Acids Res, 45*(20), 12039-12053. doi:10.1093/nar/gkx843

Zalcberg, J., Hu, X., Slater, A., Parisot, J., El-Osta, S., Kantharidis, P., . . . Parkin, J. (2000). MRP1 not MDR1 gene expression is the predominant mechanism of acquired multidrug resistance in two prostate carcinoma cell lines. *Prostate cancer and prostatic diseases, 3*(2), 66.

Zander, S. A., Kersbergen, A., Sol, W., Gonggrijp, M., van de Wetering, K., Jonkers, J., . . . Rottenberg, S. (2012). Lack of ABCG2 shortens latency of BRCA1-deficient mammary tumors and this is not affected by genistein or resveratrol. *Cancer Prevention Research, 5*(8), 1053-1060.

Zelcer, N., Saeki, T., Reid, G., Beijnen, J. H., & Borst, P. (2001). Characterization of drug transport by the human multidrug resistance protein 3 (ABCC3). *J Biol*

Chem, 276(49), 46400-46407. doi:10.1074/jbc.M107041200

Zeng, H., Bain, L. J., Belinsky, M. G., & Kruh, G. D. (1999). Expression of multidrug resistance protein-3 (multispecific organic anion transporter-D) in human embryonic kidney 293 cells confers resistance to anticancer agents. *Cancer research, 59*(23), 5964-5967.

Zetsche, B., Gootenberg, J. S., Abudayyeh, O. O., Slaymaker, I. M., Makarova, K. S., Essletzbichler, P., . . . Zhang, F. (2015). Cpf1 is a single RNA-guided endonuclease of a class 2 CRISPR-Cas system. *Cell, 163*(3), 759-771. doi:10.1016/j.cell.2015.09.038

Zhang, F., Gu, W., Hurles, M. E., & Lupski, J. R. (2009). Copy number variation in human health, disease, and evolution. *Annu Rev Genomics Hum Genet, 10*, 451-481. doi:10.1146/annurev.genom.9.081307.164217

Zhang, J. T., Jiang, X. H., Xie, C., Cheng, H., Da Dong, J., Wang, Y., . . . Chan, H. C. (2013). Downregulation of CFTR promotes epithelial-to-mesenchymal transition and is associated with poor prognosis of breast cancer. *Biochim Biophys Acta, 1833*(12), 2961-2969. doi:10.1016/j.bbamcr.2013.07.021

Zhang, Y., Schuetz, J. D., Elmquist, W. F., & Miller, D. W. (2004). Plasma membrane localization of multidrug resistance-associated protein homologs in brain capillary endothelial cells. *J Pharmacol Exp Ther, 311*(2), 449-455. doi:10.1124/jpet.104.068528

Zhang, Z., Wang, J., Shen, B., Peng, C., & Zheng, M. (2012). The ABCC4 gene is a promising target for pancreatic cancer therapy. *Gene, 491*(2), 194-199. doi:10.1016/j.gene.2011.09.029

Zhao, X., Guo, Y., Yue, W., Zhang, L., Gu, M., & Wang, Y. (2014). ABCC4 is required for cell proliferation and tumorigenesis in non-small cell lung cancer. *Onco Targets Ther, 7*, 343-351. doi:10.2147/ott.S56029

Zhou, S., Schuetz, J. D., Bunting, K. D., Colapietro, A.-M., Sampath, J., Morris, J. J., . . . Nakauchi, H. (2001). The ABC transporter Bcrp1/ABCG2 is expressed in a wide variety of stem cells and is a molecular determinant of the side-population phenotype. *Nature medicine, 7*(9), 1028.

Zhu, X., Chen, L., Huang, B., Wang, Y., Ji, L., Wu, J., . . . Wang, Z. (2020). The prognostic and predictive potential of Ki-67 in triple-negative breast cancer. *Sci Rep, 10*(1), 225. doi:10.1038/s41598-019-57094-3

Zhu, Y., Yu, F., Jiao, Y., Feng, J., Tang, W., Yao, H., . . . Zhang, Y. (2011). Reduced miR-128 in breast tumor–initiating cells induces chemotherapeutic resistance via Bmi-1 and ABCC5. *Clinical Cancer Research*.

Zochbauer-Muller, S., Filipits, M., Rudas, M., Brunner, R., Krajnik, G., Suchomel, R., . . . Pirker, R. (2001). P-glycoprotein and MRP1 expression in axillary lymph node metastases of breast cancer patients. *Anticancer Res, 21*(1a), 119-124.

Appendix

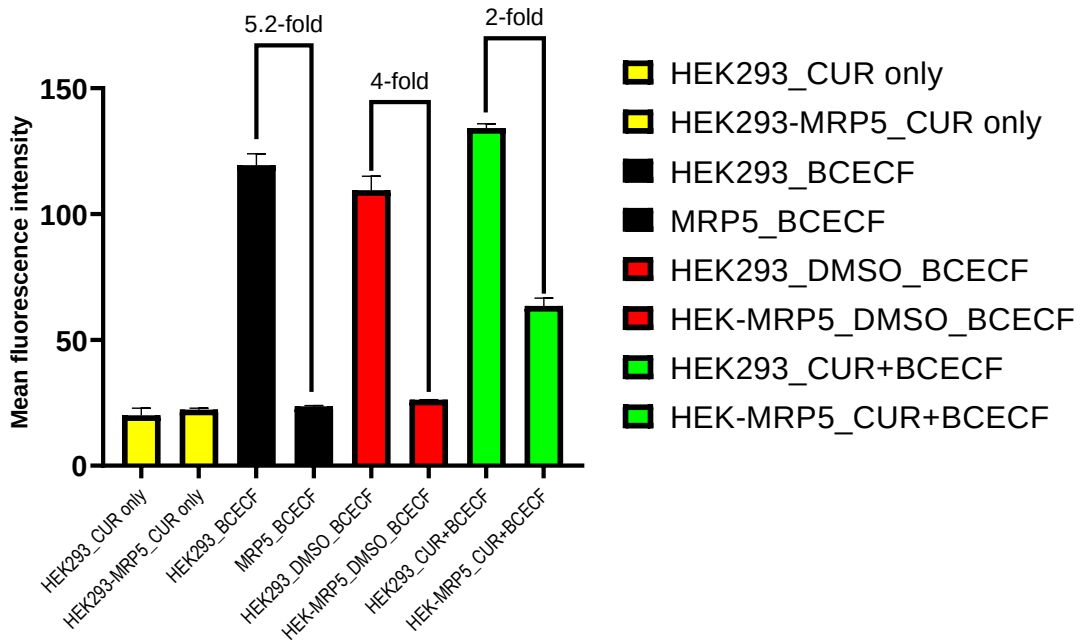

Figure 0.1 The detection of curcumin intrinsic fluorescence using cell uptake study. Supplement of Figure 6.3A in section 6.3.2.1. Data were presented as mean ± SD of duplicates.

Figure 0.2 Global alignment using BLAST®. The primer-flanking sequence of MDA-MB-231 WT cells compared with data from BLAST® (https://blast.ncbi.nlm.nih.gov/Blast.cgi). The sgRNA targeting sequence is labelled in red colour.

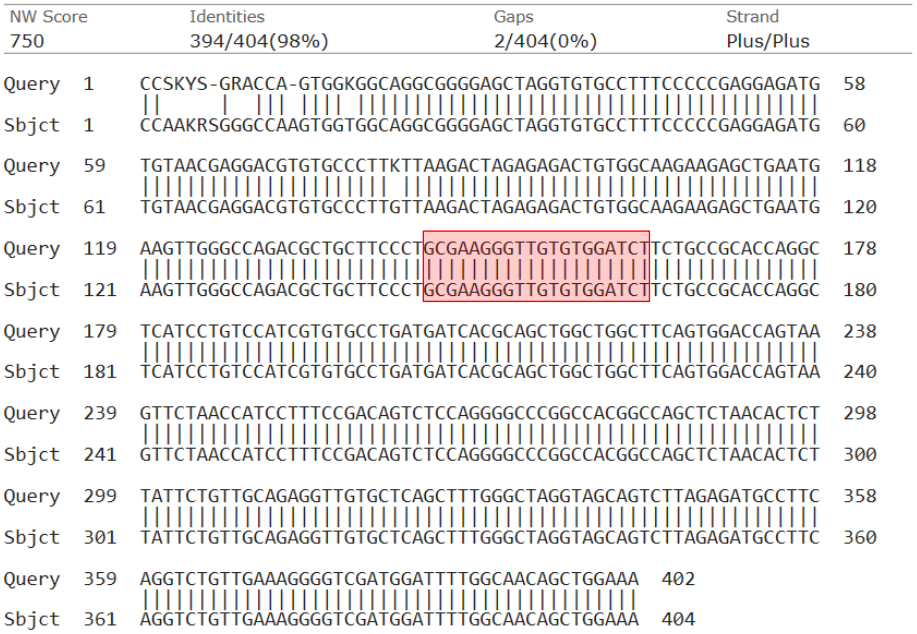

Figure 0.3 Global alignment using BLAST®. The primer-flanking sequence of MDA-MB-231 RNA only group compared with WT cells. The sgRNA targeting sequence is labelled in red colour.

Figure 0.4 Global alignment using BLAST®. The primer-flanking sequence of MDA-MB-231 Cas9 only group compared with WT cells. The sgRNA targeting sequence is labelled in red colour.

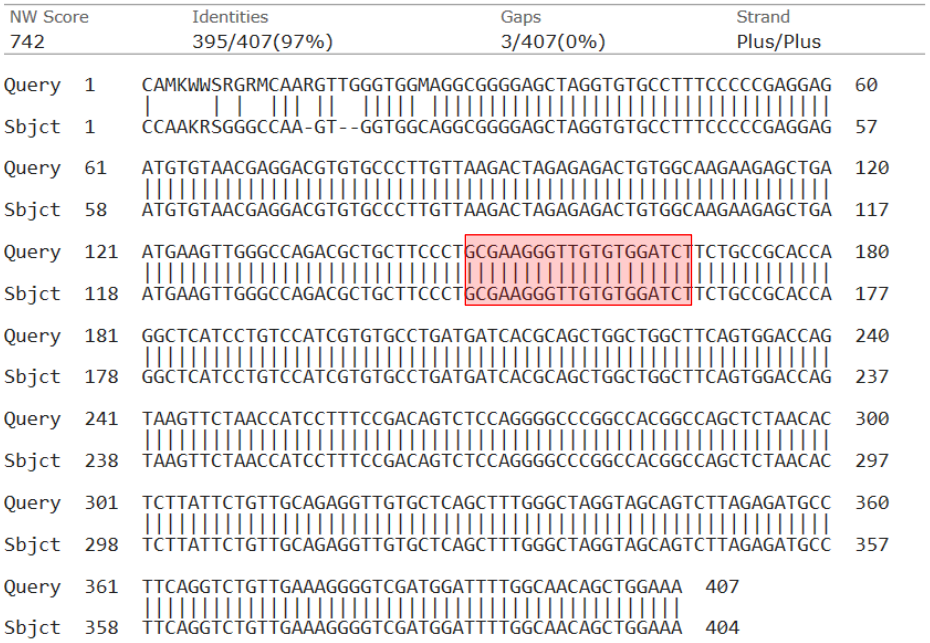

Figure 0.5 Global alignment using BLAST®. The primer-flanking sequence of MDA-MB-231 KO clone 39 compared with WT cells. The sgRNA targeting sequence is labelled in red colour.

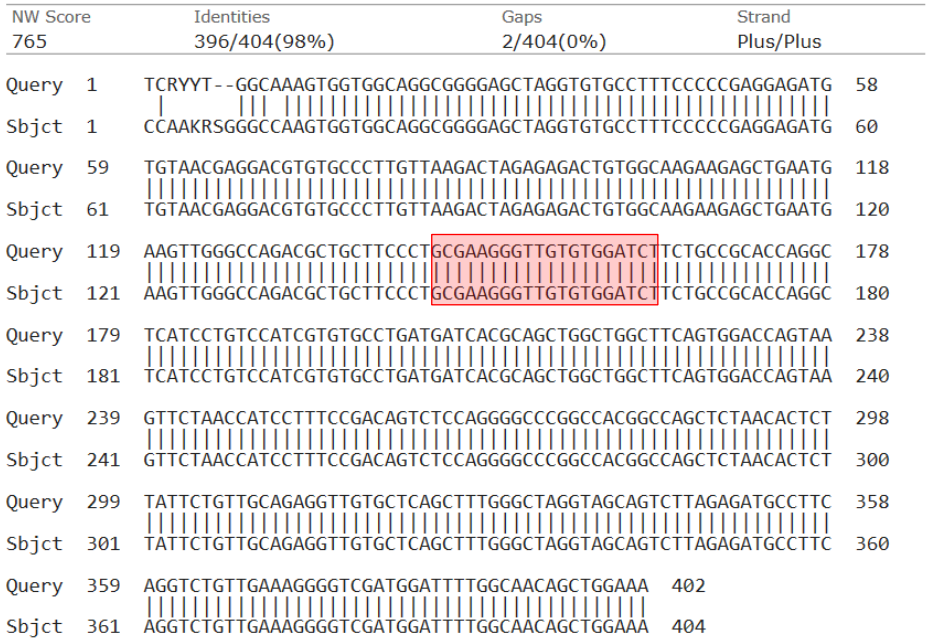

Figure 0.6 Global alignment using BLAST®. The primer-flanking sequence of MDA-MB-231 KO clone 42 compared with WT cells. The sgRNA targeting sequence is labelled in red colour.

Figure 0.7 Global alignment using BLAST®. The primer-flanking sequence of MDA-MB-231 KO clone 43 compared with WT cells. The sgRNA targeting sequence is labelled in red colour.

NW Score	Identities	Gaps	Strand
575	359/404(89%)	2/404(0%)	Plus/Plus

```
Query   1    CCMSKS--GGACAAGTGGTGGCAGGCGGGGAGCTAGGTGTGCCTTTCCCCCGAGGAGATG  58
Sbjct   1    CCAAKRSGGGCCAAGTGGTGGCAGGCGGGGAGCTAGGTGTGCCTTTCCCCCGAGGAGATG  60

Query   59   TGTAACGAGGACGTGTGCCCTTGTTAAKACTAKAGAGACTGTGGCAAGAAKAGCTGAATG  118
Sbjct   61   TGTAACGAGGACGTGTGCCCTTGTTAAGACTAGAGAGACTGTGGCAAGAAGAGCTGAATG  120

Query   119  AAGTTGGGCCARACGCTGCTTCCCTGCGAAGGGTTGKGTGRATCTTCKGCCSCACCAGGC  178
Sbjct   121  AAGTTGGGCCAGACGCTGCTTCCCTGCGAAGGGTTGTGTGGATCTTCTGCCGCACCAGGC  180

Query   179  TCATCCTGTCCATCKGGTGCCTGATGATCACSCASCTGGCTGGCTTCRKTGGACCAKTAA  238
Sbjct   181  TCATCCTGTCCATCGTGTGCCTGATGATCACGCAGCTGGCTGGCTTCAGTGGACCAGTAA  240

Query   239  KTTCTAACCWTCCTTTCCAACRKTCTCCRGGGGCCCGGCCMCGGCCASCTCTAAMACTCT  298
Sbjct   241  GTTCTAACCATCCTTTCCGACAGTCTCCAGGGGCCCGGCCACGGCCAGCTCTAACACTCT  300

Query   299  TATTCTGTTGCAAAGGTTGTGCTCASCTTTGGGCTAGGTASCAKTCTTAAAAATGCCTTC  358
Sbjct   301  TATTCTGTTGCAGAGGTTGTGCTCAGCTTTGGGCTAGGTAGCAGTCTTAGAGATGCCTTC  360

Query   359  AGGTCKGTTRAARGGGGTCAATGGATTTTGSCAMCRSCTGRAAA  402
Sbjct   361  AGGTCTGTTGAAAGGGGTCGATGGATTTTGGCAACAGCTGGAAA  404
```

Figure 0.8 Global alignment using BLAST®. The primer-flanking sequence of MDA-MB-231 KO clone 49 compared with WT cells. The sgRNA targeting sequence is labelled in red colour.

NW Score	Identities	Gaps	Strand
527	351/405(87%)	2/405(0%)	Plus/Plus

```
Query   1    CSKWWCSGRSC-AAKTGGTTGGCAGGCGGGGAGCTAGGTGTGCCTTTCCCCCGAGGAGAT  59
Sbjct   1    CCAAKRSGGGCCAAGTGGT-GGCAGGCGGGGAGCTAGGTGTGCCTTTCCCCCGAGGAGAT  59

Query   60   GTGTAACGAGGACGTGTGCCCTTGTTAAGACTAGAGAGACTGTGGCAAGAAGAGCTGAAT  119
Sbjct   60   GTGTAACGAGGACGTGTGCCCTTGTTAAGACTAGAGAGACTGTGGCAAGAAGAGCTGAAT  119

Query   120  GAAGTTGGGCCAGASKCTGCTTCCCTGCCAASGGTTGYGTGGATCTTCTGCCSCWCCAGG  179
Sbjct   120  GAAGTTGGGCCAGACGCTGCTTCCCTGCGAAGGGTTGTGTGGATCTTCTGCCGCACCAGG  179

Query   180  STCATCCTGTCCMTCRKGTGCCTGATGATCACGCACCTGGMTGGYTTCASYGGACCTTYA  239
Sbjct   180  CTCATCCTGTCCATCGTGTGCCTGATGATCACGCAGCTGGCTGGCTTCAGTGGACCAGTA  239

Query   240  AATTCTAACCATCCTTTCCGACAGKCTCCRSGGGCCCGGYCWCRGYCAGYTCTAAAACTC  299
Sbjct   240  AGTTCTAACCATCCTTTCCGACAGTCTCCAGGGGCCCGGCCACGGCCAGCTCTAACACTC  299

Query   300  TTATTCTGTTGYRGASGWTGTGCTCAKCTTTGGGMTASGTASCAGTCTTAKARATGCCTT  359
Sbjct   300  TTATTCTGTTGCAGAGGTTGTGCTCAGCTTTGGGCTAGGTAGCAGTCTTAGAGATGCCTT  359

Query   360  CRAGKCTGTTGAAAGGGGKCKATGGATTTTGGCAACAGCTGGAAA  404
Sbjct   360  CAGGTCTGTTGAAAGGGGTCGATGGATTTTGGCAACAGCTGGAAA  404
```

Figure 0.9 Global alignment using BLAST®. The primer-flanking sequence of MDA-MB-231 KO clone 53 compared with WT cells. The sgRNA targeting sequence is labelled in red colour. The 19 bp deleted was labelled in purple colour.

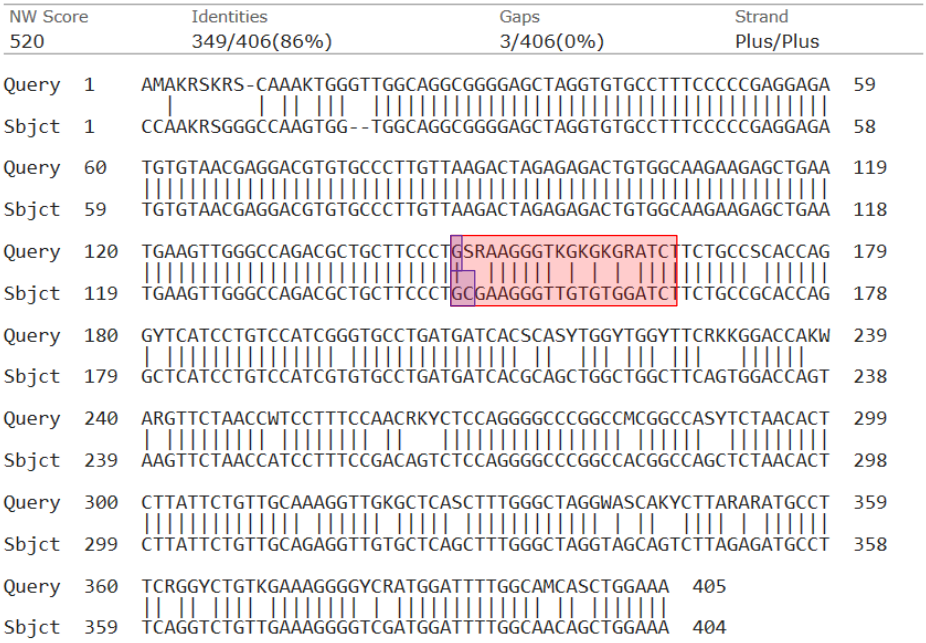

Figure 0.10 Global alignment using BLAST®. The primer-flanking sequence of MDA-MB-231 KO clone 54 compared with WT cells. The sgRNA targeting sequence is labelled in red colour. The replacement of "GC" with "T" was labelled in purple colour.

Figure 0.11 Global alignment using BLAST®. The primer-flanking sequence of BT549 WT cells compared with data from BLAST® (https://blast.ncbi.nlm.nih.gov/Blast.cgi). The sgRNA targeting sequence is labelled in red colour.

NW Score	Identities	Gaps	Strand
746	395/405(98%)	1/405(0%)	Plus/Plus

```
Query  1    CMKKSSGRASCCAAGGTGGTGGCAGGCGGGGAGCTAGGTGTGCCTTTCCCCCGAGGAGAT  60
Sbjct  1    ASAWGSGRS-CAAAGTGGGTGGCAGGCGGGGAGCTAGGTGTGCCTTTCCCCCGAGGAGAT  59
Query  61   GTGTAACGAGGACGTGTGCCCTTGTTAAGACTAGAGAGACTGTGGCAAGAAGAGCTGAAT  120
Sbjct  60   GTGTAACGAGGACGTGTGCCCTTGTTAAGACTAGAGAGACTGTGGCAAGAAGAGCTGAAT  119
Query  121  GAAGTTGGGCCAGACGCTGCTTCCCTGCGAAGGGTTGTGTGGATCTTCTGCCGCACCAGG  180
Sbjct  120  GAAGTTGGGCCAGACGCTGCTTCCCTGCGAAGGGTTGTGTGGATCTTCTGCCGCACCAGG  179
Query  181  CTCATCCTGTCCATCGTGTGCCTGATGATCACGCAGCTGGCTGGCTTCAGTGGACCAGTA  240
Sbjct  180  CTCATCCTGTCCATCGTGTGCCTGATGATCACGCAGCTGGCTGGCTTCAGTGGACCAGTA  239
Query  241  AGTTCTAACCATCCTTTCCGACAGTCTCCAGGGGCCCGGCCACGGCCAGCTCTAACACTC  300
Sbjct  240  AGTTCTAACCATCCTTTCCGACAGTCTCCAGGGGCCCGGCCACGGCCAGCTCTAACACTC  299
Query  301  TTATTCTGTTGCAGAGGTTGTGCTCAGCTTTGGGCTAGGTAGCAGTCTTAGAGATGCCTT  360
Sbjct  300  TTATTCTGTTGCAGAGGTTGTGCTCAGCTTTGGGCTAGGTAGCAGTCTTAGAGATGCCTT  359
Query  361  CAGGTCTGTTGAAAGGGGTCGATGGATTTTGGCAACAGCTGGAAA  405
Sbjct  360  CAGGTCTGTTGAAAGGGGTCGATGGATTTTGGCAACAGCTGGAAA  404
```

Figure 0.12 Global alignment using BLAST®. The primer-flanking sequence of BT549 RNA only group compared with WT cells. The sgRNA targeting sequence is labelled in red colour.

NW Score	Identities	Gaps	Strand
768	397/404(98%)	0/404(0%)	Plus/Plus

```
Query  1    CSSKWGGGGCAAAGTGGGTGGCAGGCGGGGAGCTAGGTGTGCCTTTCCCCCGAGGAGATG  60
Sbjct  1    ASAWGSGRSCAAAGTGGGTGGCAGGCGGGGAGCTAGGTGTGCCTTTCCCCCGAGGAGATG  60
Query  61   TGTAACGAGGACGTGTGCCCTTGTTAAGACTAGAGAGACTGTGGCAAGAAGAGCTGAATG  120
Sbjct  61   TGTAACGAGGACGTGTGCCCTTGTTAAGACTAGAGAGACTGTGGCAAGAAGAGCTGAATG  120
Query  121  AAGTTGGGCCAGACGCTGCTTCCCTGCGAAGGGTTGTGTGGATCTTCTGCCGCACCAGGC  180
Sbjct  121  AAGTTGGGCCAGACGCTGCTTCCCTGCGAAGGGTTGTGTGGATCTTCTGCCGCACCAGGC  180
Query  181  TCATCCTGTCCATCGTGTGCCTGATGATCACGCAGCTGGCTGGCTTCAGTGGACCAGTAA  240
Sbjct  181  TCATCCTGTCCATCGTGTGCCTGATGATCACGCAGCTGGCTGGCTTCAGTGGACCAGTAA  240
Query  241  GTTCTAACCATCCTTTCCGACAGTCTCCAGGGGCCCGGCCACGGCCAGCTCTAACACTCT  300
Sbjct  241  GTTCTAACCATCCTTTCCGACAGTCTCCAGGGGCCCGGCCACGGCCAGCTCTAACACTCT  300
Query  301  TATTCTGTTGCAGAGGTTGTGCTCAGCTTTGGGCTAGGTAGCAGTCTTAGAGATGCCTTC  360
Sbjct  301  TATTCTGTTGCAGAGGTTGTGCTCAGCTTTGGGCTAGGTAGCAGTCTTAGAGATGCCTTC  360
Query  361  AGGTCTGTTGAAAGGGGTCGATGGATTTTGGCAACAGCTGGAAA  404
Sbjct  361  AGGTCTGTTGAAAGGGGTCGATGGATTTTGGCAACAGCTGGAAA  404
```

Figure 0.13 Global alignment using BLAST®. The primer-flanking sequence of BT549 Cas9 only group compared with WT cells. The sgRNA targeting sequence is labelled in red colour.

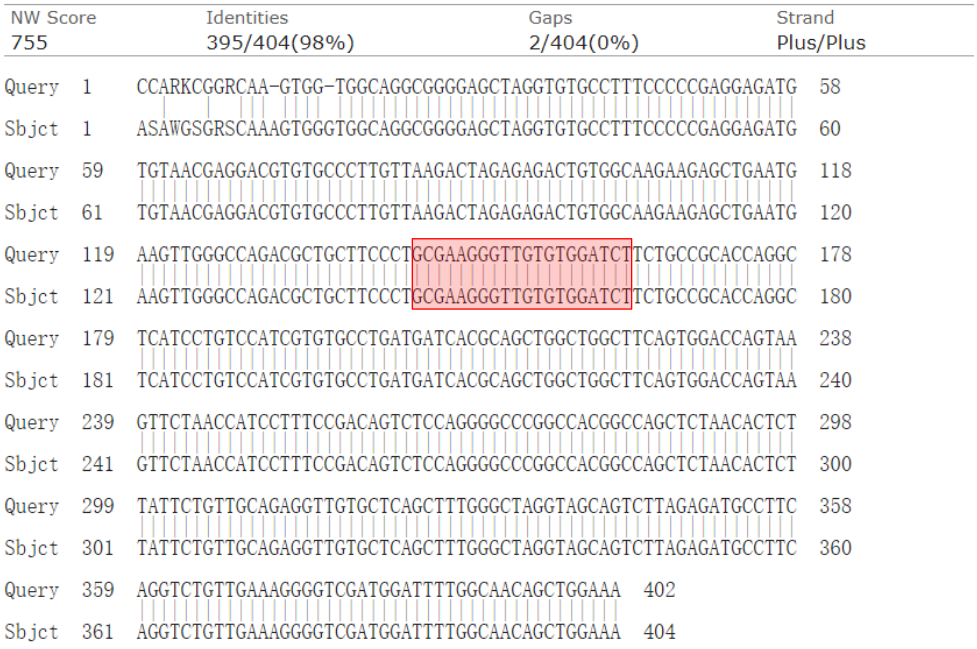

Figure 0.14 Global alignment using BLAST®. The primer-flanking sequence of BT549 KO clone 26 compared with WT cells. The sgRNA targeting sequence is labelled in red colour.

Figure 0.15 Global alignment using BLAST®. The primer-flanking sequence of BT549 KO clone 29 compared with WT cells. The sgRNA targeting sequence is labelled in red colour.

NW Score	Identities	Gaps	Strand
457	337/404(83%)	4/404(0%)	Plus/Plus

```
Query  1    CCSYKGGG-CAA-GTGG-TGGCAGGCGGGGAGCTAGGTGTGCCTTTCCCCCGAGGAGATG  57
Sbjct  1    ASAWGSGRSCAAAGTGGGTGGCAGGCGGGGAGCTAGGTGTGCCTTTCCCCCGAGGAGATG  60
Query  58   TGTAACGAGGACGTGTGCCCTTGTTAAGACTAGAGAGACTGTGGCAAGAAGAGCTGAATG  117
Sbjct  61   TGTAACGAGGACGTGTGCCCTTGTTAAGACTAGAGAGACTGTGGCAAGAAGAGCTGAATG  120
Query  118  AAGTTGGGCCAGACGCTGCTTCCCTGCGARGGKTKGKGKGRATCTTCTGCCSCACCRGGC  177
Sbjct  121  AAGTTGGGCCAGACGCTGCTTCCCTGCGAAGGGTTGTGTGGATCTTCTGCCGCACCAGGC  180
Query  178  TCATCCGGTCCATCKGGGGCCTGATGATCACSCRSCTGGTTGGTTTCRKGGAACCAKWAR  237
Sbjct  181  TCATCCTGTCCATCGTGTGCCTGATGATCACGCAGCTGGCTGGCTTCAGTGGACCAGTAA  240
Query  238  KTTCTAACCATCCTTTCCAACRKYCTCCRGGGGCCCGGCCACGGCCASTTCTAACACTCT  297
Sbjct  241  GTTCTAACCATCCTTTCCGACAGTCTCCAGGGGCCCGGCCACGGCCAGCTCTAACACTCT  300
Query  298  TATTCGGTTGCAAAGGTTGTGCTCASCTTTGGSCTAGGWASMAKYCTTAAAAATGCCTTC  357
Sbjct  301  TATTCTGTTGCAGAGGTTGTGCTCAGCTTTGGGCTAGGTAGCAGTCTTAGAGATGCCTTC  360
Query  358  RGGYCKGTTGAARGGGGYCAATGGATTTTGSCAMRSYK-GRAAA  400
Sbjct  361  AGGTCTGTTGAAAGGGGTCGATGGATTTTGGCAACAGCTGGAAA  404
```

Figure 0.16 Global alignment using BLAST®. The primer-flanking sequence of BT549 KO clone 30 compared with WT cells. The sgRNA targeting sequence is labelled in red colour. The "A" deletion was labelled in purple colour.

NW Score	Identities	Gaps	Strand
742	393/404(97%)	4/404(0%)	Plus/Plus

```
Query  1    CCSKYGG--CAA-GTGG-TGGCAGGCGGGGAGCTAGGTGTGCCTTTCCCCCGAGGAGATG  56
Sbjct  1    ASAWGSGRSCAAAGTGGGTGGCAGGCGGGGAGCTAGGTGTGCCTTTCCCCCGAGGAGATG  60
Query  57   TGTAACGAGGACGTGTGCCCTTGTTAAGACTAGAGAGACTGTGGCAAGAAGAGCTGAATG  116
Sbjct  61   TGTAACGAGGACGTGTGCCCTTGTTAAGACTAGAGAGACTGTGGCAAGAAGAGCTGAATG  120
Query  117  AAGTTGGGCCAGACGCTGCTTCCCTGCGAAGGGTTGTGTGGATCTTCTGCCGCACCAGGC  176
Sbjct  121  AAGTTGGGCCAGACGCTGCTTCCCTGCGAAGGGTTGTGTGGATCTTCTGCCGCACCAGGC  180
Query  177  TCATCCTGTCCATCGTGTGCCTGATGATCACGCAGCTGGCTGGCTTCAGTGGACCAGTAA  236
Sbjct  181  TCATCCTGTCCATCGTGTGCCTGATGATCACGCAGCTGGCTGGCTTCAGTGGACCAGTAA  240
Query  237  GTTCTAACCATCCTTTCCGACAGTCTCCAGGGGCCCGGCCACGGCCAGCTCTAACACTCT  296
Sbjct  241  GTTCTAACCATCCTTTCCGACAGTCTCCAGGGGCCCGGCCACGGCCAGCTCTAACACTCT  300
Query  297  TATTCTGTTGCAGAGGTTGTGCTCAGCTTTGGGCTAGGTAGCAGTCTTAGAGATGCCTTC  356
Sbjct  301  TATTCTGTTGCAGAGGTTGTGCTCAGCTTTGGGCTAGGTAGCAGTCTTAGAGATGCCTTC  360
Query  357  AGGTCTGTTGAAAGGGGTCGATGGATTTTGGCAMCAGCTGGAAA  400
Sbjct  361  AGGTCTGTTGAAAGGGGTCGATGGATTTTGGCAACAGCTGGAAA  404
```

Figure 0.17 Global alignment using BLAST®. The primer-flanking sequence of BT549 KO clone 32 compared with WT cells. The sgRNA targeting sequence is labelled in red colour.

NW Score	Identities	Gaps	Strand
639	372/406(92%)	2/406(0%)	Plus/Plus

```
Query  1    TCCWASSRMACCAARGKGGGTGGCAGGCGGGGAGCTAGGTGTGCCTTTCCCCCGAGGAGA  60
Sbjct  1    AS--AWGSGRSCAAAGTGGGTGGCAGGCGGGGAGCTAGGTGTGCCTTTCCCCCGAGGAGA  58
Query  61   TGTGTAACGAGGACGTGTGCCCTTGTTAAGACTAGAGAGACTGTGGCAAGAAGAGCTGAA  120
Sbjct  59   TGTGTAACGAGGACGTGTGCCCTTGTTAAGACTAGAGAGACTGTGGCAAGAAGAGCTGAA  118
Query  121  TGAAGTTGGGCCAGACSCTGCTTCCCTGCGARGGGTTGTGKGGATCTTCTGCCGCAMCRR  180
Sbjct  119  TGAAGTTGGGCCAGACGCTGCTTCCCTGCGAAGGGTTGTGTGGATCTTCTGCCGCACCAG  178
Query  181  GCTCATCCTGKCCATCGTGTGCCTGATGATCACGCWKCTGGCTGGCTTCMGTGGACCAGT  240
Sbjct  179  GCTCATCCTGTCCATCGTGTGCCTGATGATCACGCAGCTGGCTGGCTTCAGTGGACCAGT  238
Query  241  AAGTTCTMACCMTCCTTTCCGACMGTCTCCAGGGGCCCGGCCACGGMCAGCTCTAACACT  300
Sbjct  239  AAGTTCTAACCATCCTTTCCGACAGTCTCCAGGGGCCCGGCCACGGCCAGCTCTAACACT  298
Query  301  CTTATTCTGTTGCASAGGTTGTGCTCAGCTTTGGGCTAKGTAGCARTCTTASARATGCCT  360
Sbjct  299  CTTATTCTGTTGCAGAGGTTGTGCTCAGCTTTGGGCTAGGTAGCAGTCTTAGAGATGCCT  358
Query  361  TCRGGTCTGTTGAAAGGGGTCGATGGATTTTGGCMACAGCTGRAAA  406
Sbjct  359  TCAGGTCTGTTGAAAGGGGTCGATGGATTTTGGCAACAGCTGGAAA  404
```

Figure 0.18 Global alignment using BLAST®. The primer-flanking sequence of BT549 KO clone 39 compared with WT cells. The sgRNA targeting sequence is labelled in red colour.

NW Score	Identities	Gaps	Strand
746	394/404(98%)	3/404(0%)	Plus/Plus

```
Query  1    CMWWKGG--CAT-GTGGGTGGCAGGCGGGGAGCTAGGTGTGCCTTTCCCCCGAGGAGATG  57
Sbjct  1    ASAWGSGRSCAAAGTGGGTGGCAGGCGGGGAGCTAGGTGTGCCTTTCCCCCGAGGAGATG  60
Query  58   TGTAACGAGGACGTGTGCCCTTGTTAAGACTAGAGAGACTGTGGCAAGAAGAGCTGAATG  117
Sbjct  61   TGTAACGAGGACGTGTGCCCTTGTTAAGACTAGAGAGACTGTGGCAAGAAGAGCTGAATG  120
Query  118  AAGTTGGGCCAGACGCTGCTTCCCTGCGAAGGGTTGTGTGGATCTTCTGCCGCACCAGGC  177
Sbjct  121  AAGTTGGGCCAGACGCTGCTTCCCTGCGAAGGGTTGTGTGGATCTTCTGCCGCACCAGGC  180
Query  178  TCATCCTGTCCATCGTGTGCCTGATGATCACGCAGCTGGCTGGCTTCAGTGGACCAGTAA  237
Sbjct  181  TCATCCTGTCCATCGTGTGCCTGATGATCACGCAGCTGGCTGGCTTCAGTGGACCAGTAA  240
Query  238  GTTCTAACCATCCTTTCCGACAGTCTCCAGGGGCCCGGCCACGGCCAGCTCTAACACTCT  297
Sbjct  241  GTTCTAACCATCCTTTCCGACAGTCTCCAGGGGCCCGGCCACGGCCAGCTCTAACACTCT  300
Query  298  TATTCTGTTGCAGAGGTTGTGCTCAGCTTTGGGCTAGGTAGCAGTCTTAGAGATGCCTTC  357
Sbjct  301  TATTCTGTTGCAGAGGTTGTGCTCAGCTTTGGGCTAGGTAGCAGTCTTAGAGATGCCTTC  360
Query  358  AGGTCTGTTGAAAGGGGTCGATGGATTTTGGCACCAGCTGGAAA  401
Sbjct  361  AGGTCTGTTGAAAGGGGTCGATGGATTTTGGCAACAGCTGGAAA  404
```

Figure 0.19 Global alignment using BLAST®. The primer-flanking sequence of BT549 KO clone 45 compared with WT cells. The sgRNA targeting sequence is labelled in red colour.

NW Score	Identities	Gaps	Strand
557	356/405(88%)	2/405(0%)	Plus/Plus

```
Query  1    CMRKWYYGGCCAAAGTGG-TGGCAGGCGGGGAGCTAGGTGTGCCTTTCCCCCGAGGAGAT  59
Sbjct  1    ASAWGS-GRSCAAAGTGGGTGGCAGGCGGGGAGCTAGGTGTGCCTTTCCCCCGAGGAGAT  59
Query  60   GTGTAACGAGGACGTGTGCCCTTGTTAAGACTAGAGAGACTGTGGCAAGAAGAGCTGAAT  119
Sbjct  60   GTGTAACGAGGACGTGTGCCCTTGTTAAGACTAGAGAGACTGTGGCAAGAAGAGCTGAAT  119
Query  120  GAAGTTGGGCCAGACRCTGCTTCCCTGCGAAGGGTTGTGKGGATCTTCTGCCGCMCCAGG  179
Sbjct  120  GAAGTTGGGCCAGACGCTGCTTCCCTGCGAAGGGTTGTGTGGATCTTCTGCCGCACCAGG  179
Query  180  MTCATCCTGYCCATCGGGTGCCTGATGATCACSCRKTTGGYTGGYTTCWKKGGACCAKTA  239
Sbjct  180  CTCATCCTGTCCATCGTGTGCCTGATGATCACGCAGCTGGCTGGCTTCAGTGGACCAGTA  239
Query  240  AKTTCTAMCCATCCTTTCCRACATYCTCCAGGGGCCCGGCCACGGCCAGSTCTAACWCTC  299
Sbjct  240  AGTTCTAACCATCCTTTCCGACAGTCTCCAGGGGCCCGGCCACGGCCAGCTCTAACACTC  299
Query  300  TTATTCGGTTGSAAAGGTTGTGCTCRRTTTTGGGCTAGGTAKCARWCTTAGARATGCCTT  359
Sbjct  300  TTATTCTGTTGCAGAGGTTGTGCTCAGCTTTGGGCTAGGTAGCAGTCTTAGAGATGCCTT  359
Query  360  CWGGTCTGTTGAAGGGGATCRATGGATTTTGGCAACASCTGRAAA  404
Sbjct  360  CAGGTCTGTTGAAAGGGGTCGATGGATTTTGGCAACAGCTGGAAA  404
```

Figure 0.20 Global alignment using BLAST®. The primer-flanking sequence of BT549 KO clone 46 compared with WT cells. The sgRNA targeting sequence is labelled in red colour.

NW Score	Identities	Gaps	Strand
749	393/404(97%)	1/404(0%)	Plus/Plus

```
Query  1    CCCRYYGGGGCAAGTGG-TGGCAGGCGGGGAGCTAGGTGTGCCTTTCCCCCGAGGAGATG  59
Sbjct  1    ASAWGSGRSCAAAGTGGGTGGCAGGCGGGGAGCTAGGTGTGCCTTTCCCCCGAGGAGATG  60
Query  60   TGTAACGAGGACGTGTGCCCTTGTTAAGACTAGAGAGACTGTGGCAAGAAGAGCTGAATG  119
Sbjct  61   TGTAACGAGGACGTGTGCCCTTGTTAAGACTAGAGAGACTGTGGCAAGAAGAGCTGAATG  120
Query  120  AAGTTGGGCCAGACGCTGCTTCCCTGCGAAGGGTTGTGTGGATCTTCTGCCGCACCAGGC  179
Sbjct  121  AAGTTGGGCCAGACGCTGCTTCCCTGCGAAGGGTTGTGTGGATCTTCTGCCGCACCAGGC  180
Query  180  TCATCCTGTCCATCGTGTGCCTGATGATCACGCAGCTGGCTGGCTTCAGTGGACCAGTAA  239
Sbjct  181  TCATCCTGTCCATCGTGTGCCTGATGATCACGCAGCTGGCTGGCTTCAGTGGACCAGTAA  240
Query  240  GTTCTAACCATCCTTTCCGACAGTCTCCAGGGGCCCGGCCACGGCCAGCTCTAACACTCT  299
Sbjct  241  GTTCTAACCATCCTTTCCGACAGTCTCCAGGGGCCCGGCCACGGCCAGCTCTAACACTCT  300
Query  300  TATTCTGTTGCAGAGGTTGTGCTCAGCTTTGGGCTAGGTAGCAGTCTTAGAGATGCCTTC  359
Sbjct  301  TATTCTGTTGCAGAGGTTGTGCTCAGCTTTGGGCTAGGTAGCAGTCTTAGAGATGCCTTC  360
Query  360  AGGTCTGTTGAAAGGGGTCGATGGATTTTGGCAACAGCTGGAAA  403
Sbjct  361  AGGTCTGTTGAAAGGGGTCGATGGATTTTGGCAACAGCTGGAAA  404
```

Figure 0.21 Global alignment using BLAST®. The primer-flanking sequence of BT549 KO clone 48 compared with WT cells. The sgRNA targeting sequence is labelled in red colour.

NW Score	Identities	Gaps	Strand
754	394/404(98%)	1/404(0%)	Plus/Plus

```
Query   1    CMAAKWTGGCAAGGTGG-TGGCAGGCGGGGAGCTAGGTGTGCCTTTCCCCCGAGGAGATG   59
Sbjct   1    ASAWGSGRSCAAAGTGGGTGGCAGGCGGGGAGCTAGGTGTGCCTTTCCCCCGAGGAGATG   60
Query   60   TGTAACGAGGACGTGTGCCCTTGTTAAGACTAGAGAGACTGTGGCAAGAAGAGCTGAATG   119
Sbjct   61   TGTAACGAGGACGTGTGCCCTTGTTAAGACTAGAGAGACTGTGGCAAGAAGAGCTGAATG   120
Query   120  AAGTTGGGCCAGACGCTGCTTCCCTGCGAAGGGTTGTGTGGATCTTCTGCCGCACCAGGC   179
Sbjct   121  AAGTTGGGCCAGACGCTGCTTCCCTGCGAAGGGTTGTGTGGATCTTCTGCCGCACCAGGC   180
Query   180  TCATCCTGTCCATCGTGTGCCTGATGATCACGCAGCTGGCTGGCTTCAGTGGACCAGTAA   239
Sbjct   181  TCATCCTGTCCATCGTGTGCCTGATGATCACGCAGCTGGCTGGCTTCAGTGGACCAGTAA   240
Query   240  GTTCTAACCATCCTTTCCGACAGTCTCCAGGGGCCCGGCCACGGCCAGCTCTAACACTCT   299
Sbjct   241  GTTCTAACCATCCTTTCCGACAGTCTCCAGGGGCCCGGCCACGGCCAGCTCTAACACTCT   300
Query   300  TATTCTGTTGCAGAGGTTGTGCTCAGCTTTGGGCTAGGTAGCAGTCTTAGAGATGCCTTC   359
Sbjct   301  TATTCTGTTGCAGAGGTTGTGCTCAGCTTTGGGCTAGGTAGCAGTCTTAGAGATGCCTTC   360
Query   360  AGGTCTGTTGAAAGGGGTCGATGGATTTTGGCAACAGCTGGAAA   403
Sbjct   361  AGGTCTGTTGAAAGGGGTCGATGGATTTTGGCAACAGCTGGAAA   404
```

Figure 0.22 Global alignment using BLAST®. The primer-flanking sequence of BT549 KO clone 49 compared with WT cells. The sgRNA targeting sequence is labelled in red colour.

NW Score	Identities	Gaps	Strand
759	395/404(98%)	1/404(0%)	Plus/Plus

```
Query   1    CMSKKGGGGCAAAGTGG-TGGCAGGCGGGGAGCTAGGTGTGCCTTTCCCCCGAGGAGATG   59
Sbjct   1    ASAWGSGRSCAAAGTGGGTGGCAGGCGGGGAGCTAGGTGTGCCTTTCCCCCGAGGAGATG   60
Query   60   TGTAACGAGGACGTGTGCCCTTGTTAAGACTAGAGAGACTGTGGCAAGAAGAGCTGAATG   119
Sbjct   61   TGTAACGAGGACGTGTGCCCTTGTTAAGACTAGAGAGACTGTGGCAAGAAGAGCTGAATG   120
Query   120  AAGTTGGGCCAGACGCTGCTTCCCTGCGAAGGGTTGTGTGGATCTTCTGCCGCACCAGGC   179
Sbjct   121  AAGTTGGGCCAGACGCTGCTTCCCTGCGAAGGGTTGTGTGGATCTTCTGCCGCACCAGGC   180
Query   180  TCATCCTGTCCATCGTGTGCCTGATGATCACGCAGCTGGCTGGCTTCAGTGGACCAGTAA   239
Sbjct   181  TCATCCTGTCCATCGTGTGCCTGATGATCACGCAGCTGGCTGGCTTCAGTGGACCAGTAA   240
Query   240  GTTCTAACCATCCTTTCCGACAGTCTCCAGGGGCCCGGCCACGGCCAGCTCTAACACTCT   299
Sbjct   241  GTTCTAACCATCCTTTCCGACAGTCTCCAGGGGCCCGGCCACGGCCAGCTCTAACACTCT   300
Query   300  TATTCTGTTGCAGAGGTTGTGCTCAGCTTTGGGCTAGGTAGCAGTCTTAGAGATGCCTTC   359
Sbjct   301  TATTCTGTTGCAGAGGTTGTGCTCAGCTTTGGGCTAGGTAGCAGTCTTAGAGATGCCTTC   360
Query   360  AGGTCTGTTGAAAGGGGTCGATGGATTTTGGCAACAGCTGGAAA   403
Sbjct   361  AGGTCTGTTGAAAGGGGTCGATGGATTTTGGCAACAGCTGGAAA   404
```

Figure 0.23 Global alignment using BLAST®. The primer-flanking sequence of BT549 KO clone 50 compared with WT cells. The sgRNA targeting sequence is labelled in red colour.

NW Score	Identities	Gaps	Strand
750	394/404(98%)	2/404(0%)	Plus/Plus

```
Query  1    C-ARYKGGGCCTAGTGG-TGGCAGGCGGGGAGCTAGGTGTGCCTTTCCCCCGAGGAGATG  58
Sbjct  1    ASAWGSGRSCAAAGTGGGTGGCAGGCGGGGAGCTAGGTGTGCCTTTCCCCCGAGGAGATG  60
Query  59   TGTAACGAGGACGTGTGCCCTTGTTAAGACTAGAGAGACTGTGGCAAGAAGAGCTGAATG  118
Sbjct  61   TGTAACGAGGACGTGTGCCCTTGTTAAGACTAGAGAGACTGTGGCAAGAAGAGCTGAATG  120
Query  119  AAGTTGGGCCAGACGCTGCTTCCCTGCGAAGGGTTGTGTGGATCTTCTGCCGCACCAGGC  178
Sbjct  121  AAGTTGGGCCAGACGCTGCTTCCCTGCGAAGGGTTGTGTGGATCTTCTGCCGCACCAGGC  180
Query  179  TCATCCTGTCCATCGTGTGCCTGATGATCACGCAGCTGGCTGGCTTCAGTGGACCAGTAA  238
Sbjct  181  TCATCCTGTCCATCGTGTGCCTGATGATCACGCAGCTGGCTGGCTTCAGTGGACCAGTAA  240
Query  239  GTTCTAACCATCCTTTCCGACAGTCTCCAGGGGCCCGGCCACGGCCAGCTCTAACACTCT  298
Sbjct  241  GTTCTAACCATCCTTTCCGACAGTCTCCAGGGGCCCGGCCACGGCCAGCTCTAACACTCT  300
Query  299  TATTCTGTTGCAGAGGTTGTGCTCAGCTTTGGGCTAGGTAGCAGTCTTAGAGATGCCTTC  358
Sbjct  301  TATTCTGTTGCAGAGGTTGTGCTCAGCTTTGGGCTAGGTAGCAGTCTTAGAGATGCCTTC  360
Query  359  AGGTCTGTTGAAAGGGGTCGATGGATTTTGGCAACAGCTGGAAA  402
Sbjct  361  AGGTCTGTTGAAAGGGGTCGATGGATTTTGGCAACAGCTGGAAA  404
```

Figure 0.24 Global alignment using BLAST®. The primer-flanking sequence of BT549 KO clone 53 compared with WT cells. The sgRNA targeting sequence is labelled in red colour.

NW Score	Identities	Gaps	Strand
774	399/404(99%)	1/404(0%)	Plus/Plus

```
Query  1    CCRKKKGGGGC-AAGTGGTGGCAGGCGGGGAGCTAGGTGTGCCTTTCCCCCGAGGAGATG  59
Sbjct  1    CCAAKRSGGGCCAAGTGGTGGCAGGCGGGGAGCTAGGTGTGCCTTTCCCCCGAGGAGATG  60
Query  60   TGTAACGAGGACGTGTGCCCTTGTTAAGACTAGAGAGACTGTGGCAAGAAGAGCTGAATG  119
Sbjct  61   TGTAACGAGGACGTGTGCCCTTGTTAAGACTAGAGAGACTGTGGCAAGAAGAGCTGAATG  120
Query  120  AAGTTGGGCCAGACGCTGCTTCCCTGCGAAGGGTTGTGTGGATCTTCTGCCGCACCAGGC  179
Sbjct  121  AAGTTGGGCCAGACGCTGCTTCCCTGCGAAGGGTTGTGTGGATCTTCTGCCGCACCAGGC  180
Query  180  TCATCCTGTCCATCGTGTGCCTGATGATCACGCAGCTGGCTGGCTTCAGTGGACCAGTAA  239
Sbjct  181  TCATCCTGTCCATCGTGTGCCTGATGATCACGCAGCTGGCTGGCTTCAGTGGACCAGTAA  240
Query  240  GTTCTAACCATCCTTTCCGACAGTCTCCAGGGGCCCGGCCACGGCCAGCTCTAACACTCT  299
Sbjct  241  GTTCTAACCATCCTTTCCGACAGTCTCCAGGGGCCCGGCCACGGCCAGCTCTAACACTCT  300
Query  300  TATTCTGTTGCAGAGGTTGTGCTCAGCTTTGGGCTAGGTAGCAGTCTTAGAGATGCCTTC  359
Sbjct  301  TATTCTGTTGCAGAGGTTGTGCTCAGCTTTGGGCTAGGTAGCAGTCTTAGAGATGCCTTC  360
Query  360  AGGTCTGTTGAAAGGGGTCGATGGATTTTGGCAACAGCTGGAAA  403
Sbjct  361  AGGTCTGTTGAAAGGGGTCGATGGATTTTGGCAACAGCTGGAAA  404
```

Figure 0.25 Global alignment using BLAST®. The primer-flanking sequence of BT549 KO clone 60 compared with WT cells. The sgRNA targeting sequence is labelled in red colour.

Figure 0.26 Global alignment using BLAST®. The primer-flanking sequence of MCF7 WT cells compared with data from BLAST® (https://blast.ncbi.nlm.nih.gov/Blast.cgi). The sgRNA targeting sequence is labelled in red colour.

NW Score	Identities	Gaps	Strand
716	391/405(97%)	6/405(1%)	Plus/Plus

```
Query   1    GSSYYWGRASCAAARTGGGTGGCAGGCGGGGAGCTAGGTGTGCCTTTCCCCCGAGGAGAT   60
Sbjct   1    CCMYYGGGCACG---TGG-TGGCAGGCGGGGAGCTAGGTGTGCCTTTCCCCCGAGGAGAT   56

Query   61   GTGTAACGAGGACGTGTGCCCTTGTTAAGACTAGAGAGACTGTGGCAAGAAGAGCTGAAT   120
Sbjct   57   GTGTAACGAGGACGTGTGCCCTTGTTAAGACTAGAGAGACTGTGGCAAGAAGAGCTGAAT   116

Query   121  GAAGTTGGGCCAGACGCTGCTTCCCTGCGAAGGGTTGTGTGGATCTTCTGCCGCACCAGG   180
Sbjct   117  GAAGTTGGGCCAGACGCTGCTTCCCTGCGAAGGGTTGTGTGGATCTTCTGCCGCACCAGG   176

Query   181  CTCATCCTGTCCATCGTGTGCCTGATGATCACGCAGCTGGCTGGCTTCAGTGGACCAGTA   240
Sbjct   177  CTCATCCTGTCCATCGTGTGCCTGATGATCACGCAGCTGGCTGGCTTCAGTGGACCAGTA   236

Query   241  AGTTCTAACCATCCTTTCCGACAGTCTCCAGGGGCCCGGCCACGGCCAGCTCTAACACTC   300
Sbjct   237  AGTTCTAACCATCCTTTCCGACAGTCTCCAGGGGCCCGGCCACGGCCAGCTCTAACACTC   296

Query   301  TTATTCTGTTGCAGAGGTTGTGCTCAGCTTTGGGCTAGGTAGCAGTCTTAGAGATGCCTT   360
Sbjct   297  TTATTCTGTTGCAGAGGTTGTGCTCAGCTTTGGGCTAGGTAGCAGTCTTAGAGATGCCTT   356

Query   361  CAGGTCTGTTGAAAGGGGTCGATGGATTTTGGCAACAGCTGGAAA   405
Sbjct   357  CAGGTCTGTTGAAAGGGGTCGATGGATTTTGGCA-CAGCTGGAA    399
```

Figure 0.27 Global alignment using BLAST®. The primer-flanking sequence of MCF7 RNA only group compared with WT cells. The sgRNA targeting sequence is labelled in red colour.

NW Score	Identities	Gaps	Strand
738	392/404(97%)	5/404(1%)	Plus/Plus

```
Query   1    CCAWWKGRRSCAAAGTGGTGGCAGGCGGGGAGCTAGGTGTGCCTTTCCCCCGAGGAGATG   60
Sbjct   1    CCMYYGGGCAC---GTGGTGGCAGGCGGGGAGCTAGGTGTGCCTTTCCCCCGAGGAGATG   57

Query   61   TGTAACGAGGACGTGTGCCCTTGTTAAGACTAGAGAGACTGTGGCAAGAAGAGCTGAATG   120
Sbjct   58   TGTAACGAGGACGTGTGCCCTTGTTAAGACTAGAGAGACTGTGGCAAGAAGAGCTGAATG   117

Query   121  AAGTTGGGCCAGACGCTGCTTCCCTGCGAAGGGTTGTGTGGATCTTCTGCCGCACCAGGC   180
Sbjct   118  AAGTTGGGCCAGACGCTGCTTCCCTGCGAAGGGTTGTGTGGATCTTCTGCCGCACCAGGC   177

Query   181  TCATCCTGTCCATCGTGTGCCTGATGATCACGCAGCTGGCTGGCTTCAGTGGACCAGTAA   240
Sbjct   178  TCATCCTGTCCATCGTGTGCCTGATGATCACGCAGCTGGCTGGCTTCAGTGGACCAGTAA   237

Query   241  GTTCTAACCATCCTTTCCGACAGTCTCCAGGGGCCCGGCCACGGCCAGCTCTAACACTCT   300
Sbjct   238  GTTCTAACCATCCTTTCCGACAGTCTCCAGGGGCCCGGCCACGGCCAGCTCTAACACTCT   297

Query   301  TATTCTGTTGCAGAGGTTGTGCTCAGCTTTGGGCTAGGTAGCAGTCTTAGAGATGCCTTC   360
Sbjct   298  TATTCTGTTGCAGAGGTTGTGCTCAGCTTTGGGCTAGGTAGCAGTCTTAGAGATGCCTTC   357

Query   361  AGGTCTGTTGAAAGGGGTCGATGGATTTTGGCAACAGCTGGAAA   404
Sbjct   358  AGGTCTGTTGAAAGGGGTCGATGGATTTTGGCA-CAGCTGGAA    399
```

Figure 0.28 Global alignment using BLAST®. The primer-flanking sequence of MCF7 Cas9 only group compared with WT cells. The sgRNA targeting sequence is labelled in red colour.

NW Score	Identities	Gaps	Strand
750	394/403(98%)	4/403(0%)	Plus/Plus

```
Query  1    CMKWKGGGCCCAAGTGGTGGCAGGCGGGGAGCTAGGTGTGCCTTTCCCCCGAGGAGATGT  60
Sbjct  1    CCMYYGGGCAC--GTGGTGGCAGGCGGGGAGCTAGGTGTGCCTTTCCCCCGAGGAGATGT  58
Query  61   GTAACGAGGACGTGTGCCCTTGTTAAGACTAGAGAGACTGTGGCAAGAAGAGCTGAATGA  120
Sbjct  59   GTAACGAGGACGTGTGCCCTTGTTAAGACTAGAGAGACTGTGGCAAGAAGAGCTGAATGA  118
Query  121  AGTTGGGCCAGACGCTGCTTCCCTGCGAAGGGTTGTGTGGATCTTCTGCCGCACCAGGCT  180
Sbjct  119  AGTTGGGCCAGACGCTGCTTCCCTGCGAAGGGTTGTGTGGATCTTCTGCCGCACCAGGCT  178
Query  181  CATCCTGTCCATCGTGTGCCTGATGATCACGCAGCTGGCTGGCTTCAGTGGACCAGTAAG  240
Sbjct  179  CATCCTGTCCATCGTGTGCCTGATGATCACGCAGCTGGCTGGCTTCAGTGGACCAGTAAG  238
Query  241  TTCTAACCATCCTTTCCGACAGTCTCCAGGGGCCCGGCCACGGCCAGCTCTAACACTCTT  300
Sbjct  239  TTCTAACCATCCTTTCCGACAGTCTCCAGGGGCCCGGCCACGGCCAGCTCTAACACTCTT  298
Query  301  ATTCTGTTGCAGAGGTTGTGCTCAGCTTTGGGCTAGGTAGCAGTCTTAGAGATGCCTTCA  360
Sbjct  299  ATTCTGTTGCAGAGGTTGTGCTCAGCTTTGGGCTAGGTAGCAGTCTTAGAGATGCCTTCA  358
Query  361  GGTCTGTTGAAAGGGGTCGATGGATTTTGGCAACAGCTGGAAA  403
Sbjct  359  GGTCTGTTGAAAGGGGTCGATGGATTTTGGCA-CAGCTGGAA  399
```

Figure 0.29 Global alignment using BLAST®. The primer-flanking sequence of MCF7 KO clone 20 compared with WT cells. The sgRNA targeting sequence is labelled in red colour.

NW Score	Identities	Gaps	Strand
730	392/403(97%)	4/403(0%)	Plus/Plus

```
Query  1    CSKWYWSRRCAARGTGGTGGCAGGCGGGGAGCTAGGTGTGCCTTTCCCCCGAGGAGATGT  60
Sbjct  1    CCMYYGGG-CAC-GTGGTGGCAGGCGGGGAGCTAGGTGTGCCTTTCCCCCGAGGAGATGT  58
Query  61   GTAACGAGGACGTGTGCCCTTGTTAAGACTAGAGAGACTGTGGCAAGAAGAGCTGAATGA  120
Sbjct  59   GTAACGAGGACGTGTGCCCTTGTTAAGACTAGAGAGACTGTGGCAAGAAGAGCTGAATGA  118
Query  121  AGTTGGGCCAGACGCTGCTTCCCTGCGAAGGGTTGTGTGGATCTTCTGCCGCACCAGGCT  180
Sbjct  119  AGTTGGGCCAGACGCTGCTTCCCTGCGAAGGGTTGTGTGGATCTTCTGCCGCACCAGGCT  178
Query  181  CATCCTGTCCATCGTGTGCCTGATGATCACGCAGCTGGCTGGCTTCAGTGGACCAGTAAG  240
Sbjct  179  CATCCTGTCCATCGTGTGCCTGATGATCACGCAGCTGGCTGGCTTCAGTGGACCAGTAAG  238
Query  241  TTCTAACCATCCTTTCCGACAGTCTCCAGGGGCCCGGCCACGGCCAGCTCTAACACTCTT  300
Sbjct  239  TTCTAACCATCCTTTCCGACAGTCTCCAGGGGCCCGGCCACGGCCAGCTCTAACACTCTT  298
Query  301  ATTCTGTTGCAGAGGTTGTGCTCAGCTTTGGGCTAGGTAGCAGTCTTAGAGATGCCTTCA  360
Sbjct  299  ATTCTGTTGCAGAGGTTGTGCTCAGCTTTGGGCTAGGTAGCAGTCTTAGAGATGCCTTCA  358
Query  361  GGTCTGTTGAAAGGGGTCGATGGATTTTGGCAACAGCTGGAAA  403
Sbjct  359  GGTCTGTTGAAAGGGGTCGATGGATTTTGGCA-CAGCTGGAA  399
```

Figure 0.30 Global alignment using BLAST®. The primer-flanking sequence of MCF7 KO clone 23 compared with WT cells. The sgRNA targeting sequence is labelled in red colour.

NW Score	Identities	Gaps	Strand
733	394/404(98%)	5/404(1%)	Plus/Plus

```
Query   1    CMMWWRGGSCAAGGTGGGTGGCAGGCGGGGAGCTAGGTGTGCCTTTCCCCCGAGGAGATG   60
             ||| |||| |||| |||| |||||||||||||||||||||||||||||||||||||||||
Sbjct   1    CCMYYGGG-CACG-TGG-TGGCAGGCGGGGAGCTAGGTGTGCCTTTCCCCCGAGGAGATG   57

Query   61   TGTAACGAGGACGTGTGCCCTTGTTAAGACTAGAGAGACTGTGGCAAGAAGAGCTGAATG   120
             ||||||||||||||||||||||||||||||||||||||||||||||||||||||||||||
Sbjct   58   TGTAACGAGGACGTGTGCCCTTGTTAAGACTAGAGAGACTGTGGCAAGAAGAGCTGAATG   117

Query   121  AAGTTGGGCCAGACGCTGCTTCCCTGCGAAGGGTTGTGTGGATCTTCTGCCGCACCAGGC   180
             ||||||||||||||||||||||||||||||||||||||||||||||||||||||||||||
Sbjct   118  AAGTTGGGCCAGACGCTGCTTCCCTGCGAAGGGTTGTGTGGATCTTCTGCCGCACCAGGC   177

Query   181  TCATCCTGTCCATCGTGTGCCTGATGATCACGCAGCTGGCTGGCTTCAGTGGACCAGTAA   240
             ||||||||||||||||||||||||||||||||||||||||||||||||||||||||||||
Sbjct   178  TCATCCTGTCCATCGTGTGCCTGATGATCACGCAGCTGGCTGGCTTCAGTGGACCAGTAA   237

Query   241  GTTCTAACCATCCTTTCCGACAGTCTCCAGGGGCCCGGCCACGGCCAGCTCTAACACTCT   300
             ||||||||||||||||||||||||||||||||||||||||||||||||||||||||||||
Sbjct   238  GTTCTAACCATCCTTTCCGACAGTCTCCAGGGGCCCGGCCACGGCCAGCTCTAACACTCT   297

Query   301  TATTCTGTTGCAGAGGTTGTGCTCAGCTTTGGGCTAGGTAGCAGTCTTAGAGATGCCTTC   360
             ||||||||||||||||||||||||||||||||||||||||||||||||||||||||||||
Sbjct   298  TATTCTGTTGCAGAGGTTGTGCTCAGCTTTGGGCTAGGTAGCAGTCTTAGAGATGCCTTC   357

Query   361  AGGTCTGTTGAAAGGGGTCGATGGATTTTGGCAACAGCTGGAAA   404
             |||||||||||||||||||||||||||||||||||||||||||
Sbjct   358  AGGTCTGTTGAAAGGGGTCGATGGATTTTGGCA-CAGCTGGAA   399
```

Figure 0.31 Global alignment using BLAST®. The primer-flanking sequence of MCF7 KO clone 24 compared with WT cells. The sgRNA targeting sequence is labelled in red colour.

NW Score	Identities	Gaps	Strand
752	395/402(98%)	3/402(0%)	Plus/Plus

```
Query   1    CCAKYYGGCAAAGTGGTGGCAGGCGGGGAGCTAGGTGTGCCTTTCCCCCGAGGAGATGTG   60
             ||| |||||||||||||||||||||||||||||||||||||||||||||||||||||||||
Sbjct   1    CCMYYGGGCAC-GTGGTGGCAGGCGGGGAGCTAGGTGTGCCTTTCCCCCGAGGAGATGTG   59

Query   61   TAACGAGGACGTGTGCCCTTGTTAAGACTAGAGAGACTGTGGCAAGAAGAGCTGAATGAA   120
             ||||||||||||||||||||||||||||||||||||||||||||||||||||||||||||
Sbjct   60   TAACGAGGACGTGTGCCCTTGTTAAGACTAGAGAGACTGTGGCAAGAAGAGCTGAATGAA   119

Query   121  GTTGGGCCAGACGCTGCTTCCCTGCGAAGGGTTGTGTGGATCTTCTGCCGCACCAGGCTC   180
             ||||||||||||||||||||||||||||||||||||||||||||||||||||||||||||
Sbjct   120  GTTGGGCCAGACGCTGCTTCCCTGCGAAGGGTTGTGTGGATCTTCTGCCGCACCAGGCTC   179

Query   181  ATCCTGTCCATCGTGTGCCTGATGATCACGCAGCTGGCTGGCTTCAGTGGACCAGTAAGT   240
             ||||||||||||||||||||||||||||||||||||||||||||||||||||||||||||
Sbjct   180  ATCCTGTCCATCGTGTGCCTGATGATCACGCAGCTGGCTGGCTTCAGTGGACCAGTAAGT   239

Query   241  TCTAACCATCCTTTCCGACAGTCTCCAGGGGCCCGGCCACGGCCAGCTCTAACACTCTTA   300
             ||||||||||||||||||||||||||||||||||||||||||||||||||||||||||||
Sbjct   240  TCTAACCATCCTTTCCGACAGTCTCCAGGGGCCCGGCCACGGCCAGCTCTAACACTCTTA   299

Query   301  TTCTGTTGCAGAGGTTGTGCTCAGCTTTGGGCTAGGTAGCAGTCTTAGAGATGCCTTCAG   360
             ||||||||||||||||||||||||||||||||||||||||||||||||||||||||||||
Sbjct   300  TTCTGTTGCAGAGGTTGTGCTCAGCTTTGGGCTAGGTAGCAGTCTTAGAGATGCCTTCAG   359

Query   361  GTCTGTTGAAAGGGGTCGATGGATTTTGGCAACAGCTGGAAA   402
             |||||||||||||||||||||||||||||||||||||||||||
Sbjct   360  GTCTGTTGAAAGGGGTCGATGGATTTTGGCA-CAGCTGGAA   399
```

Figure 0.32 Global alignment using BLAST®. The primer-flanking sequence of MCF7 KO clone 59 compared with WT cells. The sgRNA targeting sequence is labelled in red colour.

Appendix

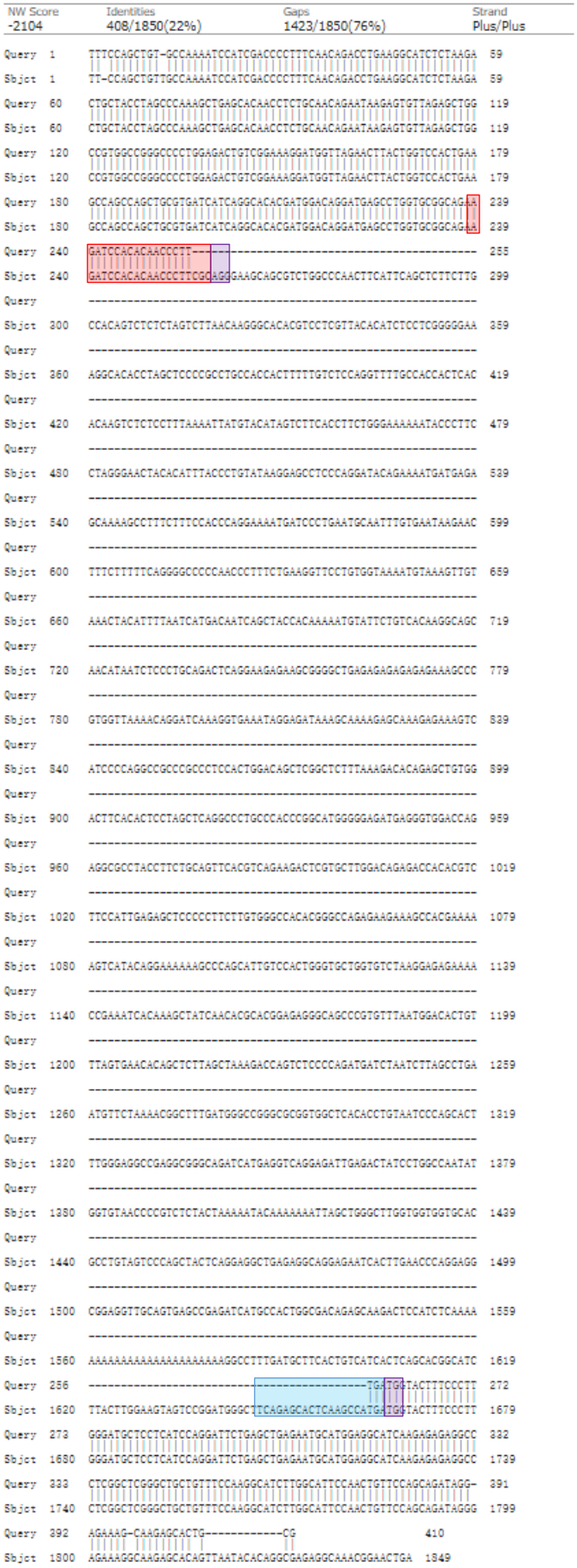
NW Score
-2104
Identities
408/1850(22%)
Gaps
1423/1850(76%)
Strand
Plus/Plus

Figure 0.33 Global alignment using BLAST®. The primer-flanking sequence of MDA-MB-231 KO clone 19E compared with WT cells. The sgRNA targeting sequence is labelled in red (IDT *ABCC5* sgRNA) and blue colour (Thermofisher *ABCC5* sgRNA set1). PAM was labelled in purple colour.

Appendix

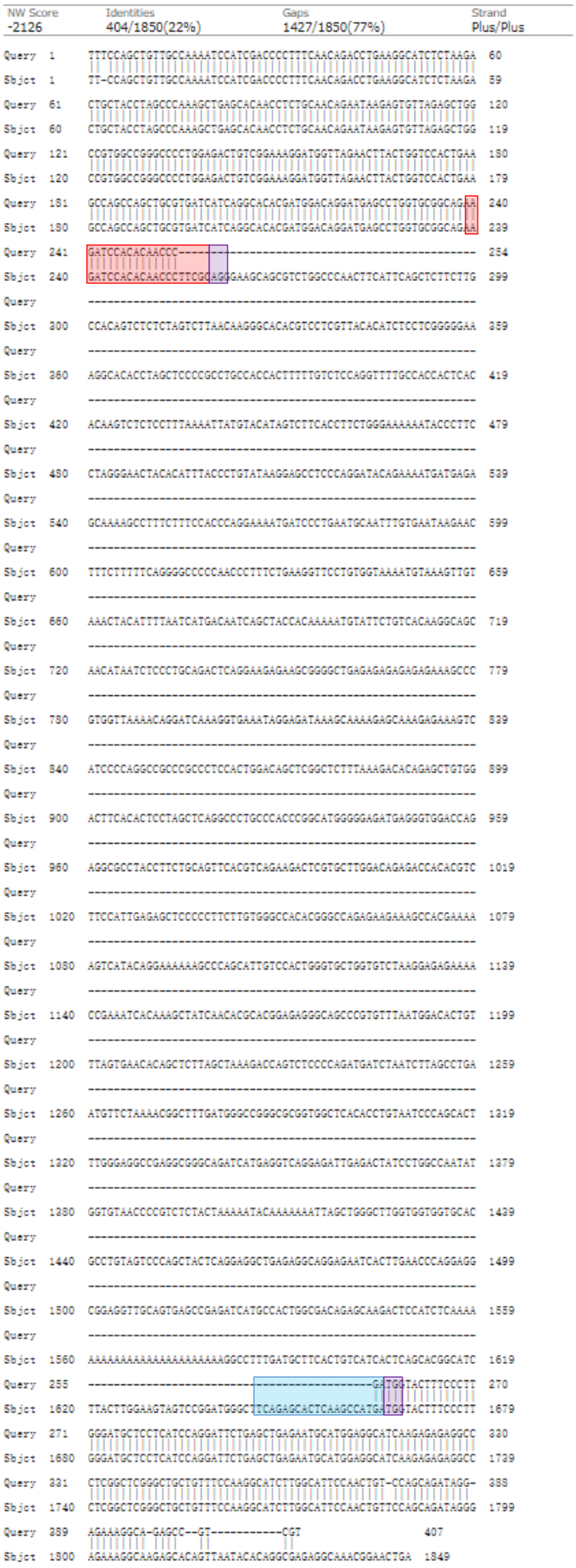
NW Score
-2126
Identities
404/1850(22%)
Gaps
1427/1850(77%)
Strand
Plus/Plus

Figure 0.34 Global alignment using BLAST®. The primer-flanking sequence of MDA-MB-231 KO clone 22B compared with WT cells. The sgRNA targeting sequence is labelled in red (IDT *ABCC5* sgRNA) and blue colour (Thermofisher *ABCC5* sgRNA set1). PAM was labelled in purple colour.

Appendix

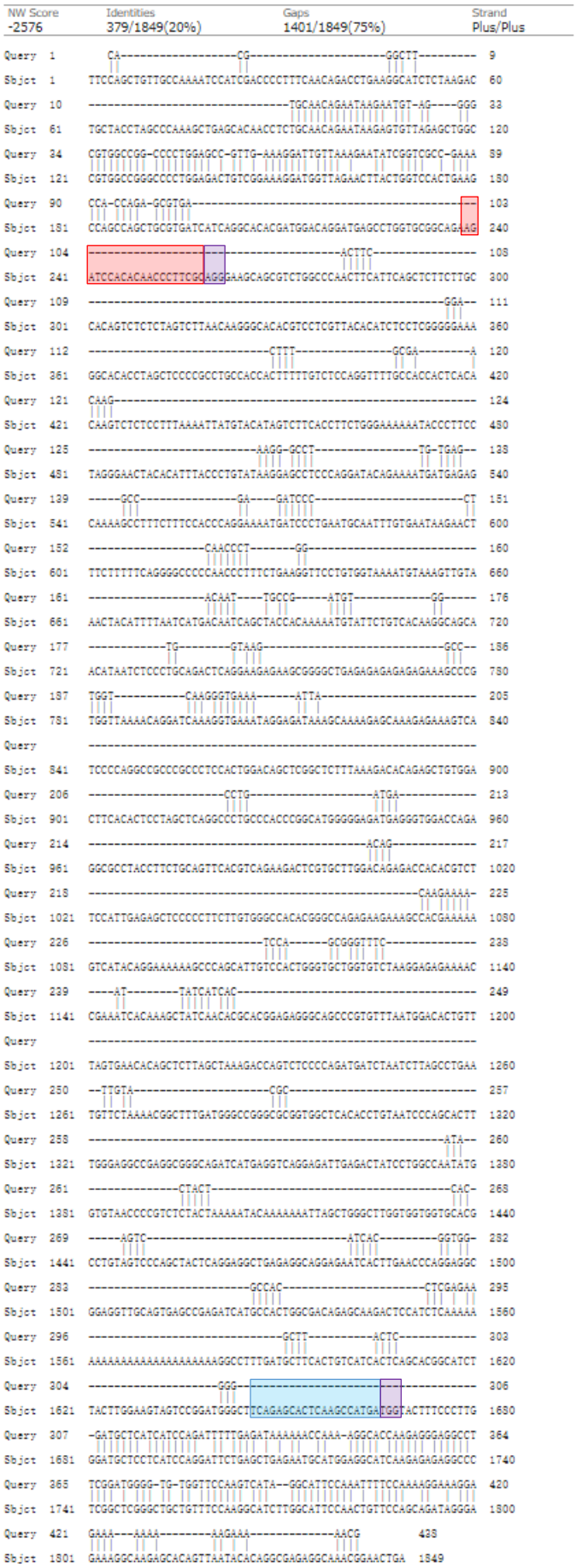
NW Score
-2576
Identities
379/1849(20%)
Gaps
1401/1849(75%)
Strand
Plus/Plus

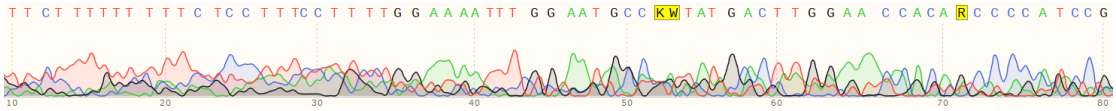

Figure 0.35 Global alignment using BLAST®. The primer-flanking sequence of BT549 KO clone 15F (long band) compared with WT cells. The sgRNA targeting sequence is labelled in red (IDT *ABCC5* sgRNA) and blue colour (Thermofisher *ABCC5* sgRNA set1). PAM was labelled in purple colour.

Appendix

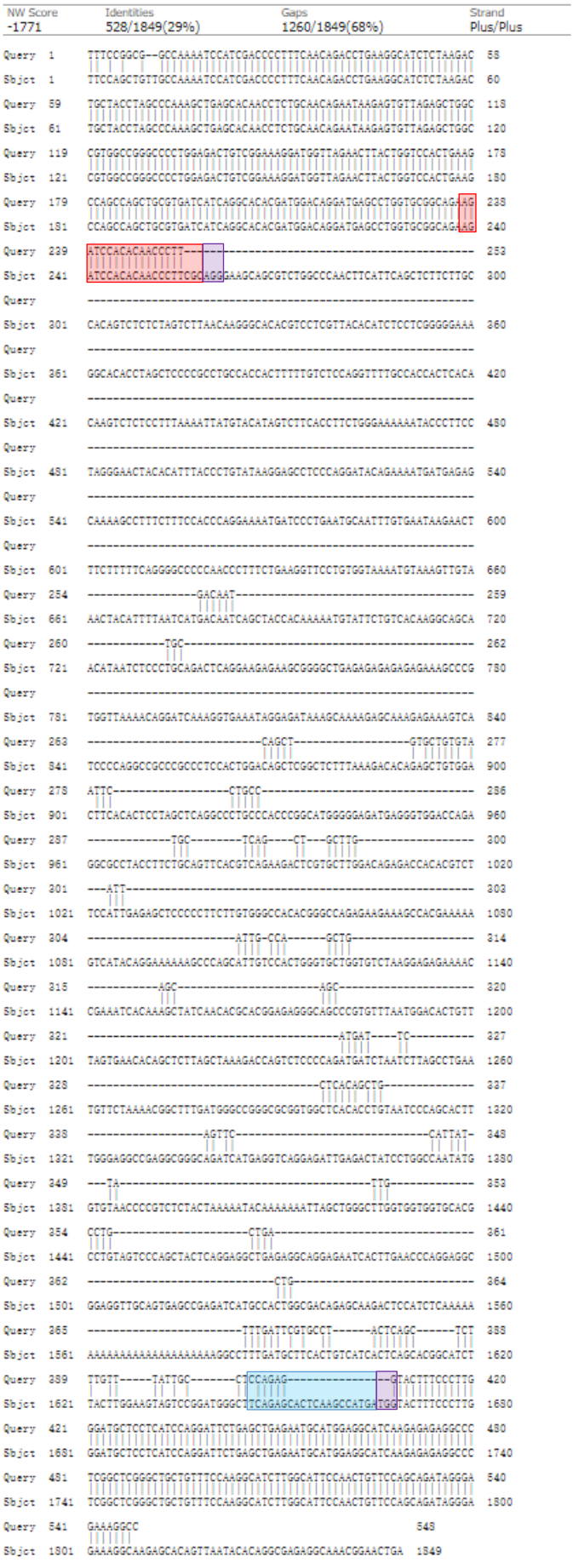
NW Score
-1771
Identities
528/1849(29%)
Gaps
1260/1849(68%)
Strand
Plus/Plus

Figure 0.36 Global alignment using BLAST®. The primer-flanking sequence of BT549 KO clone 15F (short band) compared with WT cells. The sgRNA targeting sequence is labelled in red (IDT *ABCC5* sgRNA) and blue colour (Thermofisher *ABCC5* sgRNA set1). PAM was labelled in purple colour.

Appendix


NW Score
-2130
Identities
401/1850(22%)
Gaps
1415/1850(76%)
Strand
Plus/Plus

Figure 0.37 Global alignment using BLAST®. The primer-flanking sequence of BT549 KO clone 38C compared with WT cells. The sgRNA targeting sequence is labelled in red (IDT *ABCC5* sgRNA) and blue colour (Thermofisher *ABCC5* sgRNA set1). PAM was labelled in purple colour.

Appendix

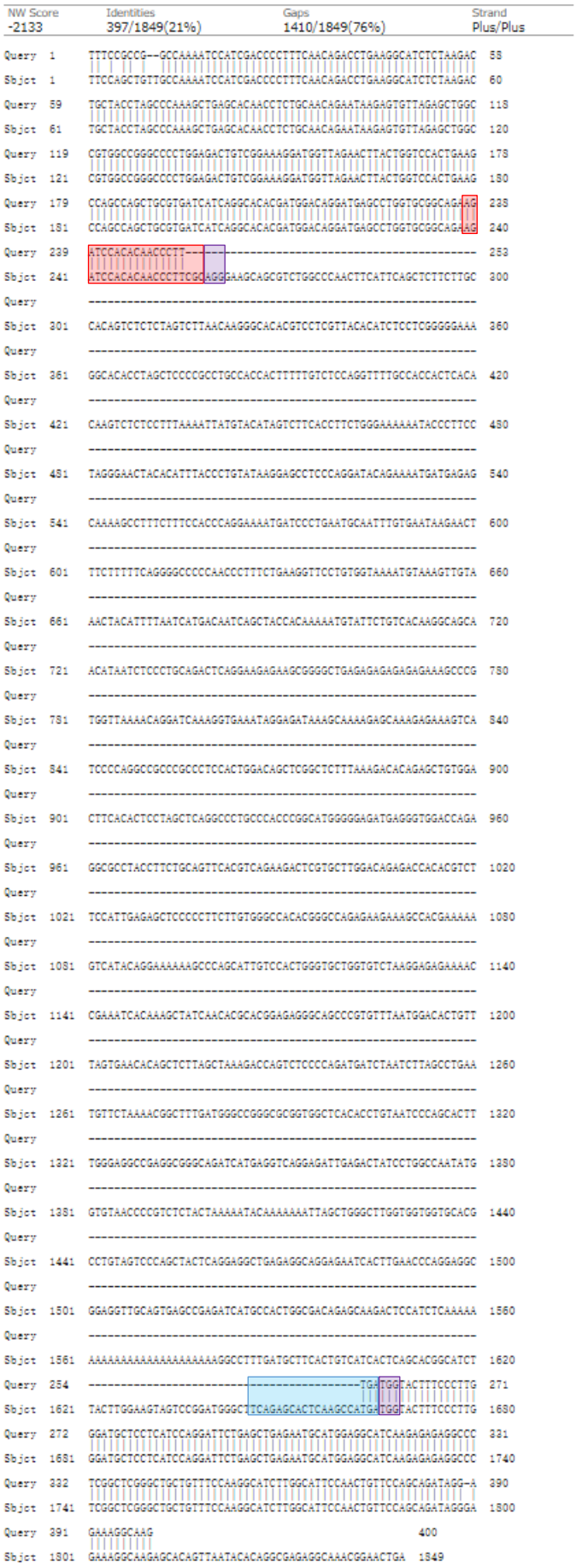
NW Score
-2133
Identities
397/1849(21%)
Gaps
1410/1849(76%)
Strand
Plus/Plus

Figure 0.38 Global alignment using BLAST®. The primer-flanking sequence of BT549 KO clone 311C compared with WT cells. The sgRNA targeting sequence is labelled in red (IDT *ABCC5* sgRNA) and blue colour (Thermofisher *ABCC5* sgRNA set1). PAM was labelled in purple colour.

Appendix

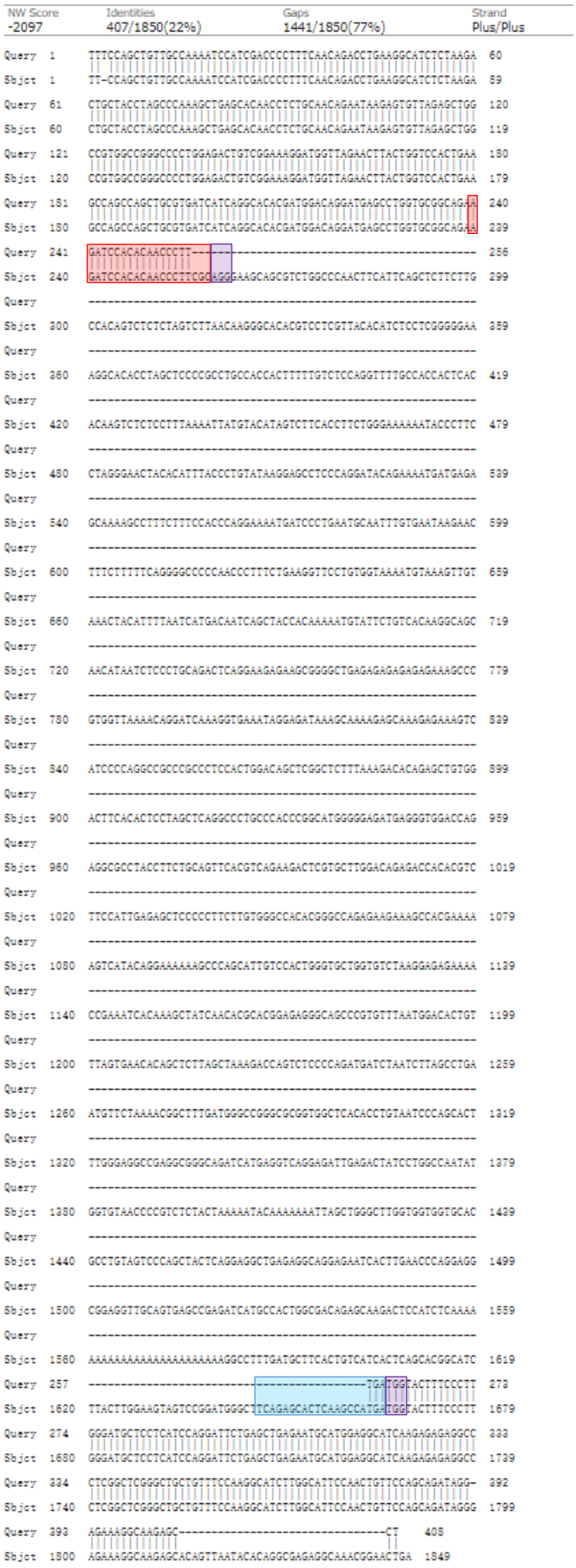
NW Score
-2097
Identities
407/1850(22%)
Gaps
1441/1850(77%)
Strand
Plus/Plus

Figure 0.39 Global alignment using BLAST®. The primer-flanking sequence of BT549 KO clone 43E compared with WT cells. The sgRNA targeting sequence is labelled in red (IDT *ABCC5* sgRNA) and blue colour (Thermofisher *ABCC5* sgRNA set1). PAM was labelled in purple colour.